CHARACTERISATION OF GEOTECHNICAL, GEOCHEMICAL AND METALLURGICAL PROPERTIES FOR MINE-TO-MILL OPTIMISATION AT SANDSLOOT OPEN PIT PLATINUM MINE, SOUTH AFRICA

SHONAGH WALKER

Submitted in fulfilment of the academic
requirements for the degree of
Master of Science in the
School of Geological Sciences,
University of KwaZulu-Natal
Durban

December 2008

ABSTRACT

Sandsloot open pit mine extracts platinum, copper and nickel from the Platreef orebody in the Northern Limb of the Bushveld Complex. At present, it is the world's largest open pit platinum mine, but it is one of the smaller of six pits to be mined in this area by Potgietersrust Platinums Limited (PPRust). As mining progresses and the mine operations expand, sound knowledge of the subsurface ground, the orebody properties and their performance in the processing plant is imperative. An accurately characterised orebody, in terms of its geotechnical, geochemical and metallurgical properties, will facilitate the development of appropriate and cost effective mining practices and processing plant design. It will improve the prediction and performance of materials in each of the steps involved in converting the orebody rock mass into a concentrate /marketable product, which ultimately leads to mine-to-mill optimisation. This dissertation has focused on the geotechnical and metallurgical strength properties of the Platreef orebody at Sandsloot; the geochemical properties of the various lithologies and defined for each orebody rock type the associations and correlations within and between these properties. The petrography of the orebody material was studied to identify and classify the rock types. A rigorous testing programme was conducted and an extensive database of petrographic, geotechnical, geochemical and metallurgical information was assembled. The corresponding results within and across the different studies were grouped together and statistical analysis and interrogation of the data sets were performed. The research identified diverse rock types with contrasting physical properties in the Sandsloot open pit orebody. For each of the rock types the distinguishing characteristics and the variations in properties were identified. Significant differences and relationships between rock types for each property were assessed for predictability in mining. Statistical associations and correlations between the properties of each study were defined and models for predicting strength and rock type were developed.

PREFACE

The experimental work described in this dissertation was carried out in the School of Geological Sciences, University of KwaZulu-Natal, Durban, from July 2005 to December 2008, under the supervision of Professor Colin A. Jermy and Professor Allan H. Wilson.

These studies represent original work by the author and have not otherwise been submitted in any form for any degree or diploma to any tertiary institution. Where use has been made of the work of others it is duly acknowledged in the text.

DECLARATION

I, ...Shonagh Walker... declare that

1. The research reported in this dissertation, except where otherwise indicated, is my original research.

2. This dissertation has not been submitted for any degree or examination at any other university.

3. This dissertation does not contain other persons' data, pictures, graphs or other information, unless specifically acknowledged as being sourced from other persons.

4. This dissertation does not contain other persons' writing, unless specifically acknowledged as being sourced from other researchers. Where other written sources have been quoted, then:
   a. Their words have been re-written but the general information attributed to them has been referenced
   b. Where their exact words have been used, then their writing has been placed in italics and inside quotation marks, and referenced.

5. This dissertation does not contain text, graphics or tables copied and pasted from the Internet, unless specifically acknowledged, and the source being detailed in the thesis and in the References sections.

Signed: ..... Date: ...1 December 2008

ACKNOWLEGEMENTS

Anglo Platinum is thanked for providing the drill core used for this study. Anglo Platinum and THRIP (Technology and Human Resources Industry Programme) are acknowledged for financial support.

I would like to thank and acknowledge the following people:

My supervisors, Professor Colin A. Jermy and Professor Allan H. Wilson, for guidance, advice given and for reading and making improvements to the dissertation.

The technical staff at the University of KwaZulu-Natal and the University of Witwatersrand for their assistance with laboratory apparatus and sample preparation.

PPRust site personnel for organizing the on-site logistics of the project, Datamine ® pictures of Sandsloot open pit, analysis of XRD results with the PPRust *EVA* software and filters and for their encouragement.

Thanks and love to my family and friends for their encouragement throughout this and previous years of study. Finally, to Greg and Diane thank you for your constant support and love.

CONTENTS

Page

ABSTRACT ii
PREFACE iii
DECLARATION iv
ACKNOWLEDGEMENTS v
CONTENTS vi

1 INTRODUCTION 1
1.1 Objectives of Research 1
1.2 Format of Thesis 2
1.3 Area of Study 3
1.4 The Mine-to-Mill Optimisation Concept 5

2 GEOLOGY 8
2.1 Regional Geology 8
2.1.1 Geology of the Bushveld Complex 8
2.1.2 Theories of Emplacement Genesis for the Bushveld Complex 11
2.2 Local Geology 13
2.2.1 Geology of the Potgietersrus Limb, Bushveld Complex 13
2.2.2 Geology of Sandsloot Open Pit 18
2.3 Summary 22

3 MINING OPERATIONS ON THE PLATREEF AND AT SANDSLOOT OPEN PIT 24
3.1 Introduction 24
3.2 History of Mining and Development 24
3.3 Open Pit Mining 26
3.4 Mining Operations at Sandsloot 28

4 PETROGRAPHY 32
4.1 Introduction 32
4.2 Methods of Mineral Identification 32

4.2.1 Transmitted Light Microscopy 32
4.2.2 X-ray Diffraction (XRD) 33
4.3 Sample Selection and Preparation 33
4.4 Testing Procedures 35
4.5 Results 36
4.6 Discussion 52
4.7 Summary and Conclusions 55

5 GEOTECHNICAL INVESTIGATION 57
5.1 Introduction 57
5.2 Methods of Investigation 57
5.2.1 Drill Hole Logging 57
5.2.2 Laboratory Testing 58
5.2.2.1 Moisture Content and Porosity 58
5.2.2.2 Density 59
5.2.2.3 Ultrasonic Velocity 60
5.2.2.4 Point Load Testing 60
5.2.2.5 Brazilian Disc Test 62
5.2.2.6 Unconfined Compressive Strength (UCS) Testing 63
5.3 Sample Selection and Preparation 64
5.4 Testing Procedures 65
5.5 Results and Analysis 65
5.5.1 Moisture Content and Porosity 70
5.5.2 Density 71
5.5.3 Ultrasonic Velocity 73
5.5.4 Point Load Index (PLI) 75
5.5.5 Brazilian Disc Tensile Strength 79
5.5.6 Uniaxial Compressive Strength 82
5.6 Discussion and Correlations 85
5.7 Summary and Conclusions 94

6 GEOCHEMICAL INVESTIGATION 96
6.1 Introduction 96
6.2 Methods of Investigation 96
6.2.1 X-ray Fluorescence Spectroscopy (XRF) 96

6.2.2 Inductively Coupled Plasma Mass Spectrometer (ICP-MS) 97
6.3 Sample Selection and Preparation 98
6.4 Testing Procedures 99
6.5 Results and Analysis 99
6.5.1 Major Element Oxides 101
6.5.2 Base Metal Elements 107
6.5.3 Platinum Group Elements 110
6.5.4 Alkali and Alkali Earth Elements 113
6.5.5 Rare Earth Elements 115
6.5.6 Incompatible Elements 117
6.6 Discussion and Correlations 120
6.6.1 Discriminant Analysis 124
6.7 Summary and Conclusions 129

7 METALLURGICAL INVESTIGATION 132
7.1 Introduction 132
7.2 Methods of Investigation 133
7.2.1 Drop Weight Testing 133
7.2.1.1 Tumbling Test 133
7.2.1.2 Julius Kruttschnitt Drop Weight Test 134
7.2.2 Bond Ball Mill Work Index 136
7.3 Sample Selection and Preparation 137
7.4 Testing Procedures 137
7.5 Results and Analysis 138
7.5.1 Drop Weight Testing 138
7.5.1.1 Drop Weight Tumbling Test 138
7.5.1.2 Julius Kruttschnitt Drop Weight Test 141
7.5.2 Bond Ball Mill Work Index 143
7.6 Discussion and Correlations 145
7.7 Summary and Conclusions 148

8 DISCUSSION 150
8.1 Comparisons between Petrography, Geotechnical, Geochemical and Metallurgical Properties 150
8.2 Geotechnical and Geochemical Relationships 153

8.3 Geotechnical and Metallurgical Relationships 156
8.4 Metallurgical and Geochemical Relationships 163

9 CONCLUSION 168
9.1 Geological and Data Processing Considerations 169
9.2 Petrographic Considerations 170
9.3 Geotechnical Considerations 171
9.4 Geochemical Considerations 172
9.5 Metallurgical Considerations 173
9.6 Comparison of Properties 174
9.7 Further Work and Research Suggestions 176

REFERENCES 178

APPENDICIES
(All Appendix Data is Stored Digitally in the Attached Compact Disk)

APPENDIX A CORE PHOTOGRAPHS AND DIAMOND DRILL HOLE LOGS
APPENDIX B PETROGRAPHY APPENDIX
APPENDIX C GEOTECHNICAL APPENDIX
APPENDIX D GEOCHEMICAL APPENDIX
APPENDIX E METALLURGICAL APPENDIX

Chapter 1

INTRODUCTION

In a mine, greater productivity, which is defined in its simplest form as the increase in the throughput of the processing plant, will increase the revenue and profit of the mine. But throughput cannot be increased without a thorough understanding of the material being processed.

An orebody which is characterised well in terms of its geotechnical, geochemical and metallurgical properties, with respect to the processes between mining and milling, will allow for greater plant throughput through:

- better prediction of the ore material characteristics and variability
- improved production forecast and planning
- calculation of the ore variability impacts on plant performance
- refining the plant design and circuit optimisation

Essentially a well characterised orebody will provide the basis for mine-to-mill optimisation and ultimately will lead to greater productivity of the mine.

1.1 Objectives of Research

The materials that are mined in the Sandsloot open pit comprise numerous rock types of varied geological origins and contrasting physical properties. These properties affect blasting, milling and processing operations, and the extent of their variability makes the prediction of mining and milling conditions difficult.

This research was undertaken to improve the knowledge of the rock properties being mined, transported and processed at Sandsloot open pit mine. The purpose of the study was to characterise the wide range of rock types in the ore zone from all aspects of the physical properties and to determine if these properties could be identified using a few, relatively simple tests. The objective of the study was to provide a foundation of distinguished rock properties for

extended mine-to-mill optimisation at Sandsloot open pit mine. Consequently, these properties could be used as a basis for comparison with the rock properties in subsequent open pit mining operations on the Northern Bushveld Limb, by Potgietersrust Platinums Limited.

The first step towards creating this foundation was to build a database of geotechnical, geochemical and metallurgical properties for the various rock types of the orebody at Sandsloot open pit. This was done by performing geotechnical, geochemical and metallurgical testing on drill core and compiling the data. Thereafter the aim was to use the database to:

- Characterise the orebody rock types by performing standard statistical tests on each of the rock type properties.
- Determine the summary statistical descriptives.
- Qualify the significance of the differences in properties and resultant differences in rock type behaviour statistically.
- Define associations and correlations within and between the geotechnical properties, composition, geochemistry and metallurgical strength for the range of rock types.

The results of this research may be used to confirm, improve and fill in missing data in the existing Potgietersrust Platinums Limited (PPRust) database, which will in turn be used by the mine in the existing 3D geotechnical model and mine-to-mill optimisation. In the future, the PPRust database will be used in the study between material types from Sandsloot open pit and Potgietersrust Platinums Limited North Mining area (PPRust North). The aim of which is to assist with the optimum design of the PPRust plant expansion and to provide an understanding of the expected performance of the PPRust North material in the current plant.

1.2 Format of Thesis

This thesis aims to analyse and evaluate the properties of the orebody at Sandsloot open pit mine. Chapter 2 gives an account of the regional, local and in pit geology. It describes the geological setting, stratigraphy and emplacement of the Bushveld Complex, focusing on the Northern Potgietersrus Limb and the hanging wall/footwall geology, structures, mineralisation and geohydrology of the Sandsloot open pit. The mining history on the Platreef and the processes and operations at Sandsloot open pit are summarised in Chapter 3.

Chapters 4 through to 7 cover the investigation of the orebody properties. There are four studies which respectively examine the mineralogical properties (Chapter 4), the geotechnical properties (Chapter 5), the geochemical properties (Chapter 6) and the metallurgical properties (Chapter 7). Each chapter is a discrete investigation with an individual introduction, methods of investigation, results and analysis section, discussion and conclusion.

The eighth chapter is a final discussion, which draws comparisons and contrasts between the findings and conclusions of the four previous investigations. The chapter defines relationships for the properties which are interdisciplinary and where possible links them with statistical associations or correlations.

The conclusions and deliverables from the thesis are given in Chapter 9.

1.3 Area of Study

Sandsloot open pit mine is situated in the Northern Province of South Africa approximately 250 km north east of Johannesburg and 63 km north-northwest of Mokopane, formerly Potgietersrus. It is located on the northern limb of the Bushveld Complex and was developed to extract the platinum, nickel and copper reserves from the Platreef orebody. Sandsloot open pit was opened in 1992 and was the first of six potential pits to be mined by Potgietersrust Platinums Limited (PPRust), a subsidiary of Anglo Platinum. The mining lease area held by PPRust is shown in Figure 1.1. The farms Knapdaar 234 KR, Tweefontein 238 KR and Rietfontein 240 KR, which are south of the Sandsloot 236 KR and Vaalkop 819 LR farms, are also licensed for mining but at present are not being mined

Sandsloot is the worlds largest open pit platinum mine, with 40 million tonnes of rock material being mined annually and an estimated 400 000 tonnes of ore being processed by its plant in a month. As with most open pits the shape of the orebody controls the length and orientation of the pit walls. The pit strikes north-south and follows the 45˚ westerly dip of the orebody. At present it is on cutback 5 with a length of 1.8 km, a width of 600 m and a depth of 240 m. The final pit, which will be achieved with a sixth cutback, will have the same length and width but will have a depth of 300 m. This is the current economic depth for the pit and to extend deeper, underground mining would be required.

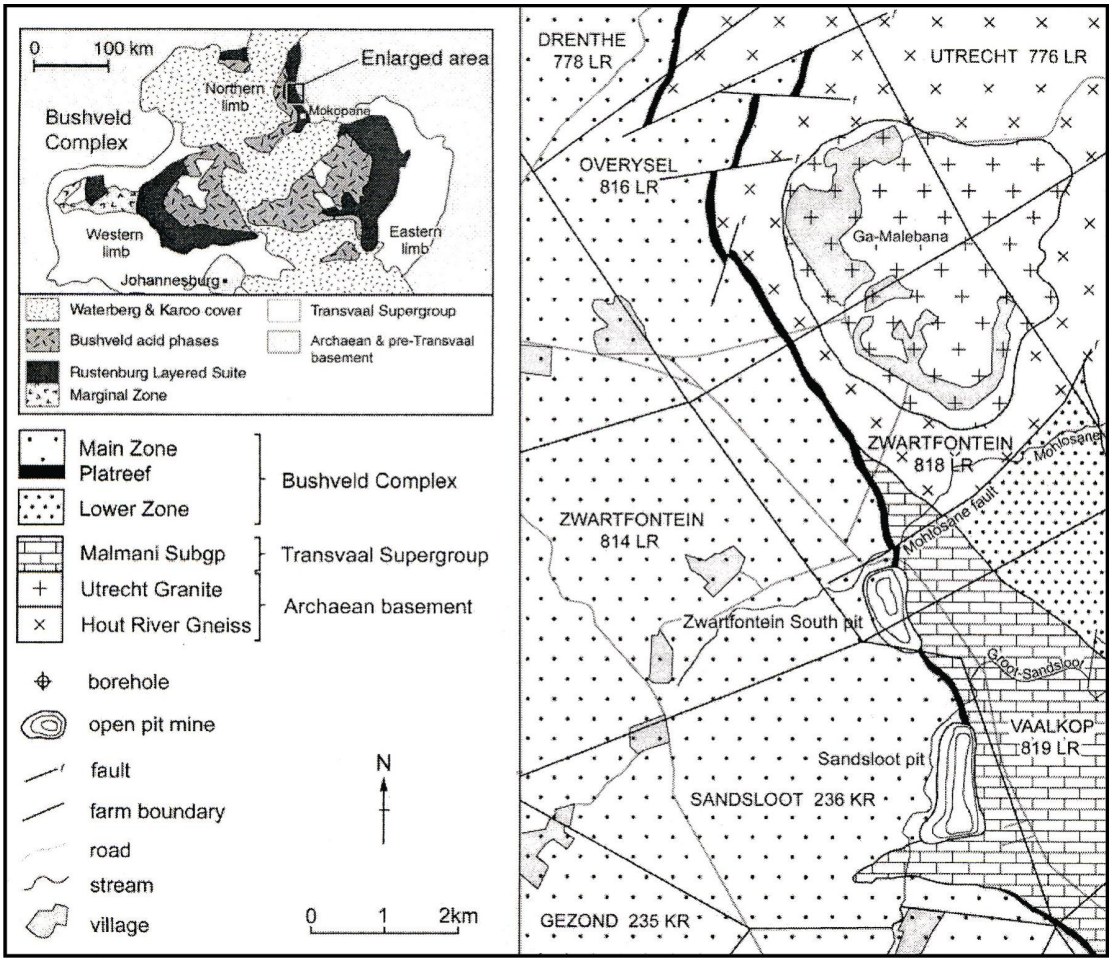

Figure 1.1 Potgietersrust Platinums mining lease area, after Holwell and Jordaan (2006).

The ore grade of the Platreef varies with footwall lithology but the relationship is not clear (Kinnaird *et al*., 2005). At Sandsloot, where the footwall is the Malmani Subgroup dolomite, the average ore grade is greater than 4 g/t. Because of this high ore grade it is possible to use the open pit mining method despite the stripping ratio of 6.2:1. This is a high stripping ratio compared with Phalaborwa copper mine which has a stripping ratio of 1.5:1.

North of Sandsloot open pit a further two open pits are currently being mined by PPRust. Zwartfontein South, on the Zwartfontein 818 LR farm, was opened in 2002 and is at present 1.5 km long, 400 m wide and is 100 m deep. It is on cutback 3 and 4 and has a final depth of 300 m which is estimated to increase down to a depth of 500 m. Blasting and top cover removal began on PPRust North open pit in 2006. This pit straddles farms Zwartfontein 818 LR north and Overysel 816 LR, is currently 15 m deep, 400 m long and 100 m wide. The final pit dimensions are expected to be 5.5 km in length, 800 m in width and 500 m in depth, though these figures

may change as mining progresses. All pit dimensions stated in this research were current in January 2007.

It is intended that the ore from the PPRust North open pit will be processed in the plant developed to process the Sandsloot open pit ore. The possible differences in ore type and their likely impacts on plant throughput therefore necessitate that the Sandsloot ore be well characterised for comparative purposes.

1.4 The Mine-to-Mill Optimisation Concept

Fluctuating commodity prices and competition demand that a mine is run optimally. Keeping ahead requires improvement to operations in more ways than simple cost reduction and cutbacks to staff numbers. Historically the approach to optimisation in a mine has focused on isolated improvement to each operation (Chitombo, 2003). However, research over the last two decades chiefly by the Julius Kruttschnitt Mineral Research Centre (JKMRC) in Queensland, Australia, and its commercial division, JKTech Pty. Ltd (JKTech), has shown that by using the technique of "Mine-to-Mill™ optimisation" greater improvements and higher returns can be achieved.

The concept of mine-to-mill takes a holistic approach to optimisation that encompasses all operational steps between converting solid ore into a 'marketable product'. The first step in mine-to-mill processes for an open pit is the drilling and blasting of the intact rock mass. This is followed by the loading of the fragmented rock into trucks, hauling it out of the pit, crushing the ore and finally milling the ore before it is processed into a concentrate. Mine-to-Mill™ optimisation acknowledges the links between these operations and recognises that optimising some steps can be counterproductive towards optimising others (JKTech, 2008 b). It relies on detailed characterisation of the ore body properties and modelling of the conditions and systems to improve the performance of each step in relation to the others. The result is effective optimisation.

Studies have shown the critical cause and effect relationships which control optimisation are blasting versus crushing and grinding, the feed size for the semi-autogenous mill (SAG) and balanced metallurgical properties of ore feed into the plant (Imrie, 1998). By finding the balance between these relationships unavoidable mining costs can be minimised. Examples of these mining costs include:

- Maintenance and repair costs due to wear and tear or damage to equipment.
- Costs due to down time of the machinery, inefficient or decreased rate of loading, hauling, crushing and milling; in other words the effective productivity of the in pit and plant machinery.
- The energy consumption required to produce the marketable product. This can be in the form of diesel and electrical energy for in-pit equipment and electrical and chemical energy for the processing plant.

Simkus and Dance (1998), Valery *et al.* (2001) and Bye (2003) have shown that along with minimising ore dilution, the fragmentation size of the blasted rock mass is crucial in keeping costs down. Primary fragmentation is controlled by the blast powder factor, which influences the elastic strain generated in the blast, the degree of fragmentation as well as the degree of micro cracking that develops in the fragments. Increasing blast powder factors and therefore blast expenditure will result in an increase in the crushing and milling performance and a decrease in the energy consumption of the plant, resulting in savings (Jankovic and Valery, 2002 and Bye, 2003). However, in order to adjust the blast powder factor for optimised processing performance, a detailed knowledge of the rock properties is required.

The increase in mill throughput due to greater blasting powder factors and therefore smaller fragmentation is illustrated in Table 1.1. Adjusting the drill and blast practices for optimum plant performance and not decreased blast costs results in effective optimisation.

Table 1.1 Increased plant throughput for mines which have increased their Blast Powder Factor (Chitombo, 2003)

Mining Operation	Blast Powder Factor Increase	Increase in SAG Mill Throughput
Porgera Gold Mine (Papua New Guinea)	0.60 kg/m^3 to 1.25 kg/m^3	15 %
Cadia Copper/Gold Mine (Australia)	0.91 kg/m^3 to 1.21 kg/m^3	10 %
KCGM Cold Mine (Australia)	0.55 kg/m^3 to 1.20 kg/m^3	10 %
Potgietersrust Ltd (South Africa)	1.00kg/m^3 to 1.80 kg/m^3	Approx. 11 %

A further example of the mine-to-mill optimisation encompassing multiple steps in the mining process is the optimisation of the mill feed for greater throughput. The mill's performance is a product of the fragment size distribution and the mechanical properties of the material. It is highly sensitive to the crusher feed size it receives (Morrell and Valery, 2001). Ensuring the fragmentation profile received by the mill is constant, through blasting to produce fragments that are optimum size for the crusher and through adjusting the crusher for the material

properties of the ore entering the plant, will facilitate higher mill productivity, performance and lower energy consumption (Valery *et. al.*, 2004). A second measure to ensure that constant feed size is received by the mill is to keep various fragmentation size and grade stockpiles (Bye, 2003). The fragmentation sent to the plant may therefore be adjusted post-blast.

Fragmentation affects two out of three of the key cause and effect relationships which mine-to-mill optimisation focuses on. The third is controlled through prior knowledge of the properties of the ore material. All three are dependent on characterisation of the ore body properties. Therefore successful mine-to-mill optimisation relies on detailed study of the mined material, modelling and a holistic approach.

The objective of this research is to improve the functionality and productivity of Sandsloot open pit mine through detailed study of the orebody rock properties. The geotechnical characterisation of the orebody would facilitate an understanding of blast energy interactions with the rock mass and geological structures. Furthermore, it would improve the prediction of fragmentation size created by drill-and-blast practices. Geochemical and metallurgical characterisation would assist in the prediction of material properties sent to the processing plant. If the ore zone material properties, their variability and the relationships between them can be distinguished the results of this study can be used to predict the conditions of each mining block, depending on the variety and quantity of each orebody rock type present. Consequently mining conditions can be assessed, which would allow forward planning and proactive adjustment of mining practices for optimum results.

Chapter 2

GEOLOGY

2.1 Regional Geology

2.1.1 Geology of the Bushveld Complex

The Bushveld Complex is situated in the north of South Africa and extends over the North West, Limpopo, Mpumulanga and Gauteng Provinces (Figure 2.1). The complex covers an approximate area of 65 000 km^2 and is 500 km from east to west, 100 km north to south with an estimated depth of 13 km (Bye, 2003; Eales and Cawthorn, 1996). The complex is the world's largest layered intrusive body, being 50 – 300 times larger than other petrological equivalent or economically significant layered intrusion, for example Skaergaard; Stillwater and Sudbury (Arndt *et al*., 2005), and it represents the largest reserve of the economically important chrome, vanadium and platinum group elements (PGE) on Earth (Eales and Cawthorn, 1996; Hochreiter *et al*., 1985). Buchanan (1988) estimates the Bushveld Complex holds up to 85% of the total known platinum reserves.

Based on differences in composition and structure, the Bushveld Complex has most recently been described by Kruger (2005) as a magmatic province with five suites; the bimodal Rooiberg Volcanic Suite, the mafic-layered Bushveld Complex or Rustenberg Layered Suite, the marginal pre- and syn-Bushveld sills, intrusions and outer satellite intrusions, the Rashoop Granophyre Suite and the Lebowa Granite Suite.

The floor to the Bushveld Complex is a succession of clastic and chemical sedimentary rocks of the Transvaal Supergroup. The rock types which constitute this supergroup are: a basal unit of quartzite followed by a dolomitic and banded ironstone sequence and an alternating quartzite and shale package with a cap of basaltic and acidic volcanics (Button, 1976). The roof rocks comprise intensely metamorphosed rhyolites and granophyres of the Rooiberg Group (Eales and Cawthorn, 1996). The subvolcanic emplacement of the complex was along and above the

unconformity between the Rooiberg Group and the Transvaal Supergroup (Cheney and Twist, 1991).

Figure 2.1 shows a simplified regional geology of the Bushveld Complex, with a stratigraphic column and age of the units. The age is important in the interpretation of the relationship between the Bushveld Complex and the roof rocks. As suggested by Schweitzer *et al*. (1995) the late Rustenberg Layered Suite or granite emplacement was synchronous with the upper units of the Rooiberg Group.

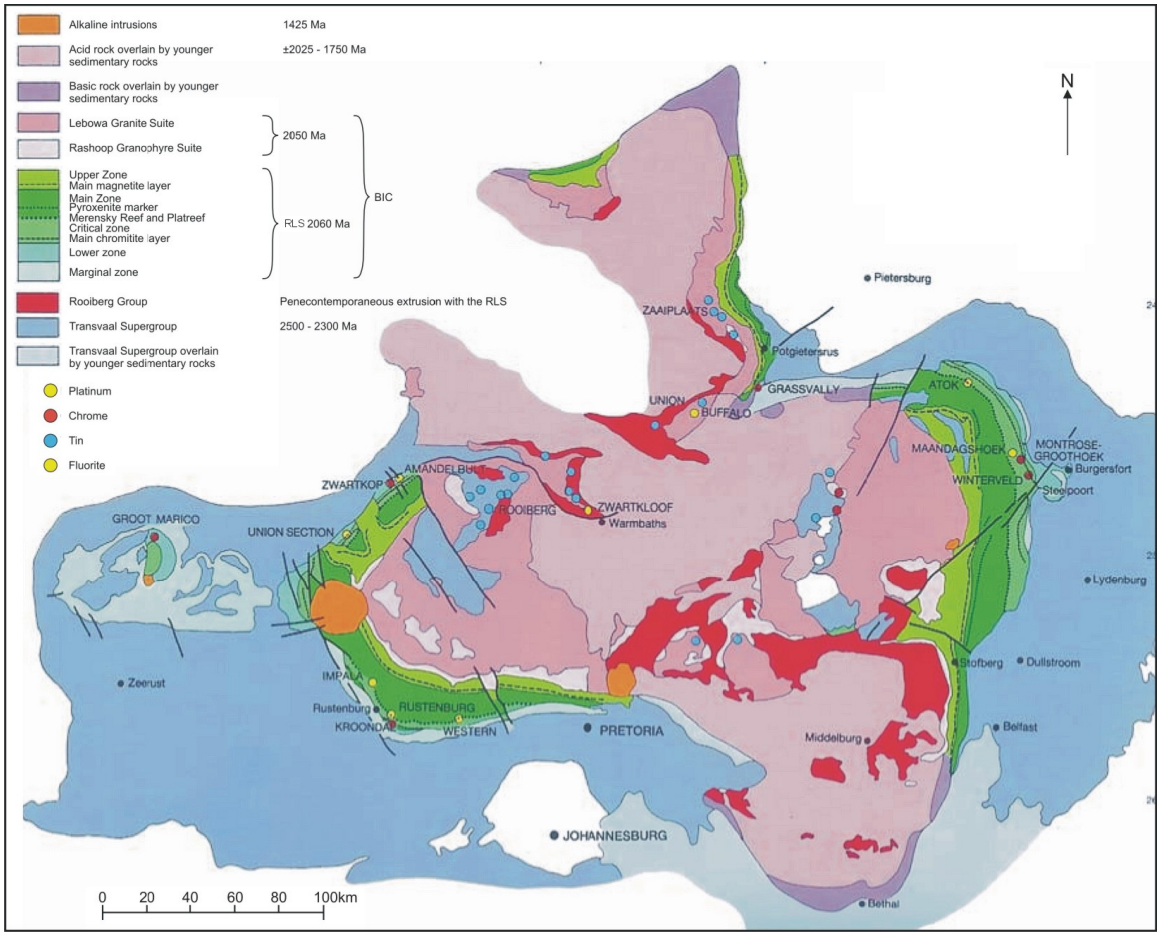

Figure 2.1 Regional Geology of the Bushveld Complex, modified after Friese (2004 b), stratigraphic unit ages taken from Walraven *et al*. (1990).

The Bushveld Complex outcrops in four discrete compartments (Figure 2.1). The compartments or limbs are the Northern or Villa Nora-Potgietersrus Limb, the Eastern Limb, the Western Limb and the Far Western Limb. A fifth limb, the Southeastern or Bethal Limb does not outcrop but has been identified by borehole core information and a high resolution gravity anomaly (Eales and Cawthorn, 1996).

The Rustenburg Layered Suite, in which the platiniferous deposits are located, is broadly divided into five stratigraphic zones: the Marginal, Lower, Critical, Main and Upper Zones. Between the limbs of the Bushveld Complex each of these five zones differ slightly in lithology, degree of unit reoccurrence, layer thickness and mineralogy (Armitage *et al*., 2002; Kinnaird *et al*., 2005; McDonald *et al*., 2005 and van der Merwe, 1976). The difference is most significant in the Northern Limb, the details of which will be discussed under the section of local geology. The predominant dip of the Bushveld Complex layering is centripetal between 10° – 20° for the Eastern and Western limbs, the Northern Limb dips westerly up to 45° (Hochreiter *et al*., 1985; van der Merwe, 1976). Figure 2.2 details the rock types of each of the zones in the Rustenberg Layered Suite and Figure 2.3 depicts the stratigraphic differences between the western Bushveld and the northern Bushveld (Potgietersrus Limb).

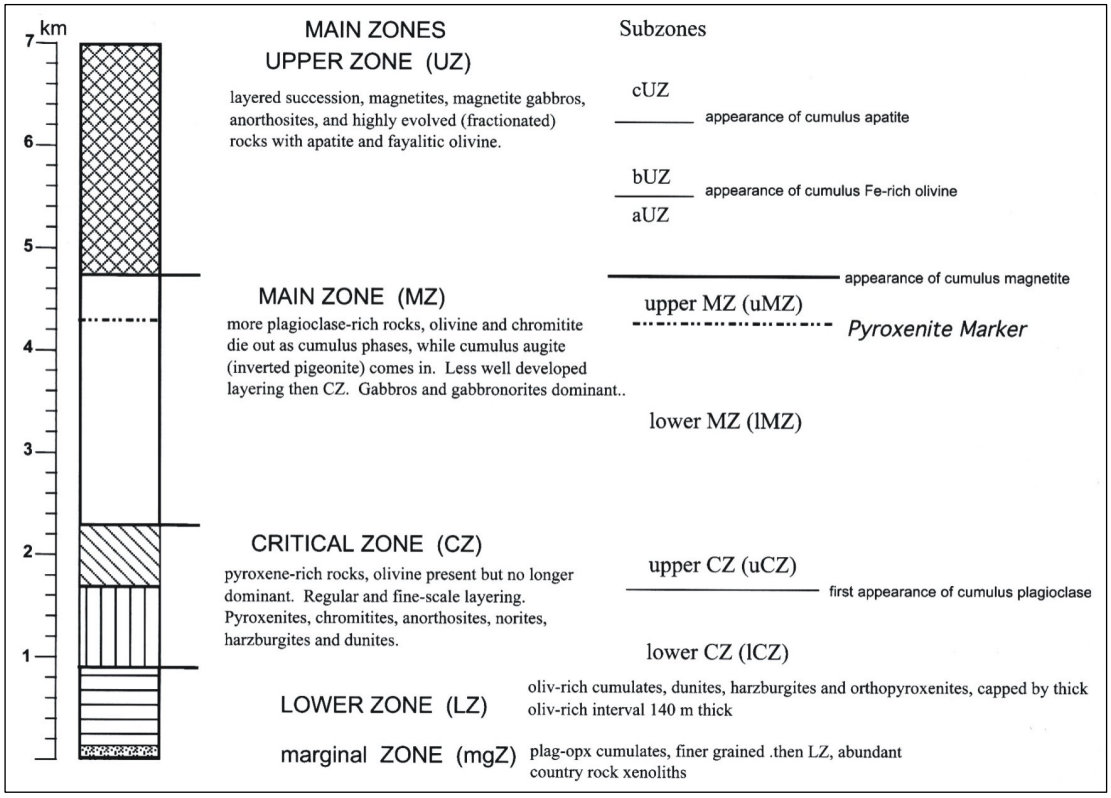

Figure 2.2 Simplified stratigraphy and lithology of the Rustenburg Layered Suite, Bushveld Complex, after Arndt *et al.* (2005).

The platiniferous deposits of the Rustenberg Layered Suite are hosted in the Critical Zone and are associated with the base metal sulphides. In the Western and Eastern Limbs the mineralised zones are concentrated in the Merensky Reef and the UG – 2 chromite layer. In the Northern Limb PGE mineralisation is hosted in the Platreef.

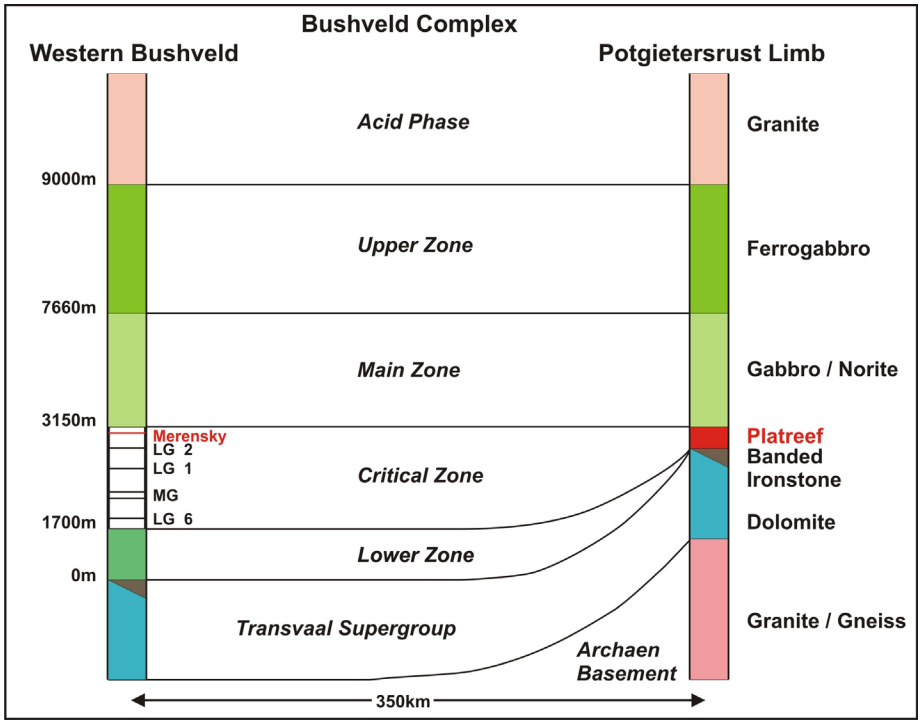

Figure 2.3 Stratigraphic Column comparing the stratigraphy of the western Bushveld to the northern Bushveld, modified after Bye (2003).

2.1.2 Theories of Emplacement Genesis for the Bushveld Complex

Parental magma sources, emplacement mechanisms, ore controls and mineralisation of the Bushveld Complex using petrological, mineralogical and geochemical analysis has been the focus of research surrounding the Bushveld complex for over eighty years; a complete overview of which is given by Eales and Cawthorn (1996). Extensive contributions and many models have been proposed to explain the petrogenesis of the Bushveld and the PGE-enriched sulphide orebodies of the Rustenburg Layered Suite, none of which have been accepted without debate.

The most widely supported model has been the mantle plume model, in which magma rising from the Earth's mantle to the crust created massive magma chambers and was expressed as surface and subsurface volcanic activity (Hatton, 1995). Other less accepted processes describing the mode of formation include meteorite impact processes, subduction zone processes and meteorite impact into active subduction zone evolution processes (Friese, 2004 a and Hamilton, 1970).

Arndt *et al*. (2005) presented evidence that the Bushveld Complex was fed by magma from a deeper magma chamber, which progressively assimilated its crustal wall rocks, giving rise to the suite of rocks present today. Kruger (2005) proposed the Bushveld Complex was a wide and shallow lobate, sill-like sheet during crystallisation and the evolution of the magma chamber occurred in two major stages, resulting in the various stratigraphic zones. In the first stage there were numerous influxes of magma; in the second stage magma layers evolved by fractional crystallisation with no major magma influxes.

Good (1999) proposed the mechanism for Bushveld Complex intrusion utilised the Thabazimbi-Murchinson Lineament, which acted as a conduit allowing magma to ascend along a deep-seated lithospheric shear. He reasons that the massive sill-like intrusion of the Bushveld Complex formed at a critical level in the crust where the lithostatic pressure equalled the magmatic pressure (Figure 2.4).

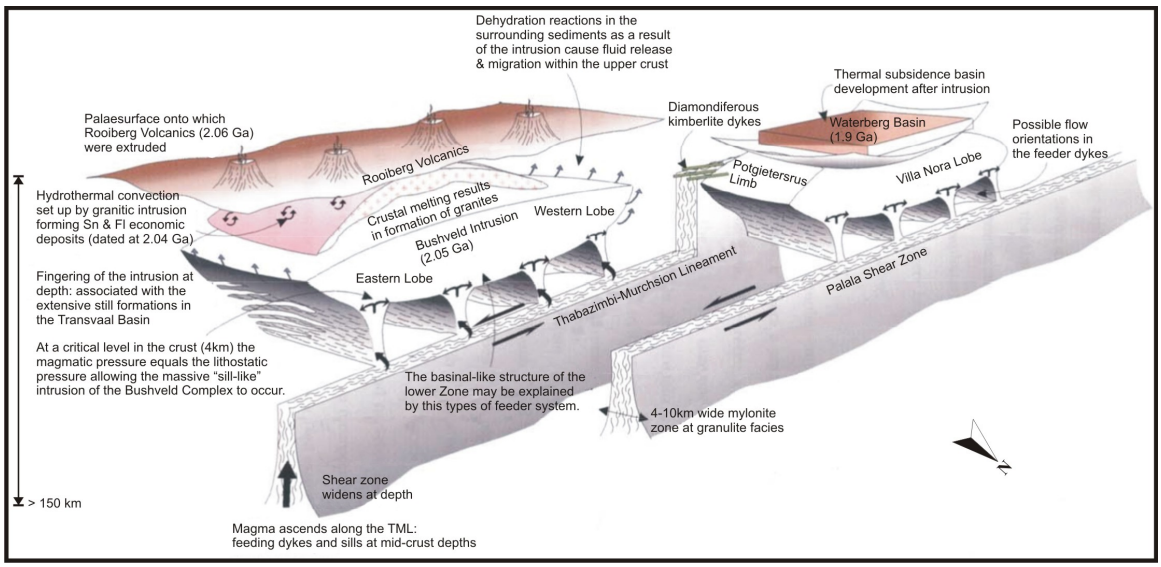

Figure 2.4 Annotated diagram showing intrusion mechanism of the Bushveld Complex proposed by Good (1999), after Good (1999).

Friese (2004 a) focused in detail on the techno-magmatic evolution of the Bushveld Complex using structural geology and deformation history to explain its origin. He put forward a model of non-plume origin, in which continent-continent collision and accretion processes along the north-western margin to the Kaapvaal Craton induced NW-SE compressive field stress in the lithosphere of the northern Kaapvaal Craton (2.06 – 1.8 Ga). The response to the stress was a reactivation of the Archaean translithospheric suture zones and the Neoarchaean Limpopo Orogeny-related shear zones (2.97 – 2.64 Ga) which, in combination with the rejuvenation of

the Pongola Rift Basin, resulted in sublithospheric and upper mantle decompressional melting and formed mafic-ultramafic magma. The magma intruded the continental crust via extensional faults of the Pongola Rift Basin and deep-seated, trans-lithospheric surture zones. In conjunction with the reactivation of the suture zones, the intra-plating of the magmas caused a higher geothermal gradient and thermal softening of the crust which culminated in the emplacement of the Bushveld Complex magmas as a sill like body at critical depth where overburden pressures and magmatic pressures were in equilibrium.

2.2 Local Geology

2.2.1 Geology of the Potgietersrus Limb, Bushveld Complex

Potgietersrust Platinums Limited (PPRust) concession area is located in the Northern (Potgietersrus) limb of the Bushveld Complex (Figure 2.5). The limb is approximately 7275 km^2 in size and outcrops in a slightly sinuous pattern over a length of 110 km, with a maximum width of 15 km (Kinnaird *et al*., 2005; van der Merwe, 1976). The strike of the Rustenberg Layered Suite layering within the limb is north – south but it varies locally along the length of the limb, between northeast and northwest. The dip of the layers within the limb also vary with strike, with a steeper dip (14° - 45°) in the central section of the limb and a shallower dip (14° - 27°) on the northern and southern ends (van der Merwe, 1976).

Although the Northern Limb is a compartment of the Bushveld Complex it differs significantly in lithologies, mineral textures and composition, geochemistry of rare earth elements (REE), platinum group elements (PGEs), layer thicknesses and stratigraphy (Armitage *et al*., 2002; Kinnaird *et al*., 2005; McDonald *et al*., 2005 and van der Merwe, 1976). Unlike the rest of the Bushveld Complex that has cyclical and consistent rock type repetitions, the Northern Limb is highly variable with quasi-continuous rock-strata and mineral deposits over the entire intrusion (Kruger, 2005). It is separated from the Eastern and Western Limbs by the Thabazimbi-Murchison Lineament (TML) and the connection between it and the main Bushveld Complex is not clear (Kinnaird *et al*., 2005).

The mafic intrusion that is the Northern Limb intruded at the level of the Magaliesberg Quartzite Formation in the south. Gravimetric and field observations have placed its feeder just west of Mokopane (van der Merwe, 1976). The intrusion transgresses downwards towards the north; therefore the Northern Limb has many footwall lithologies (Figure 2.6).

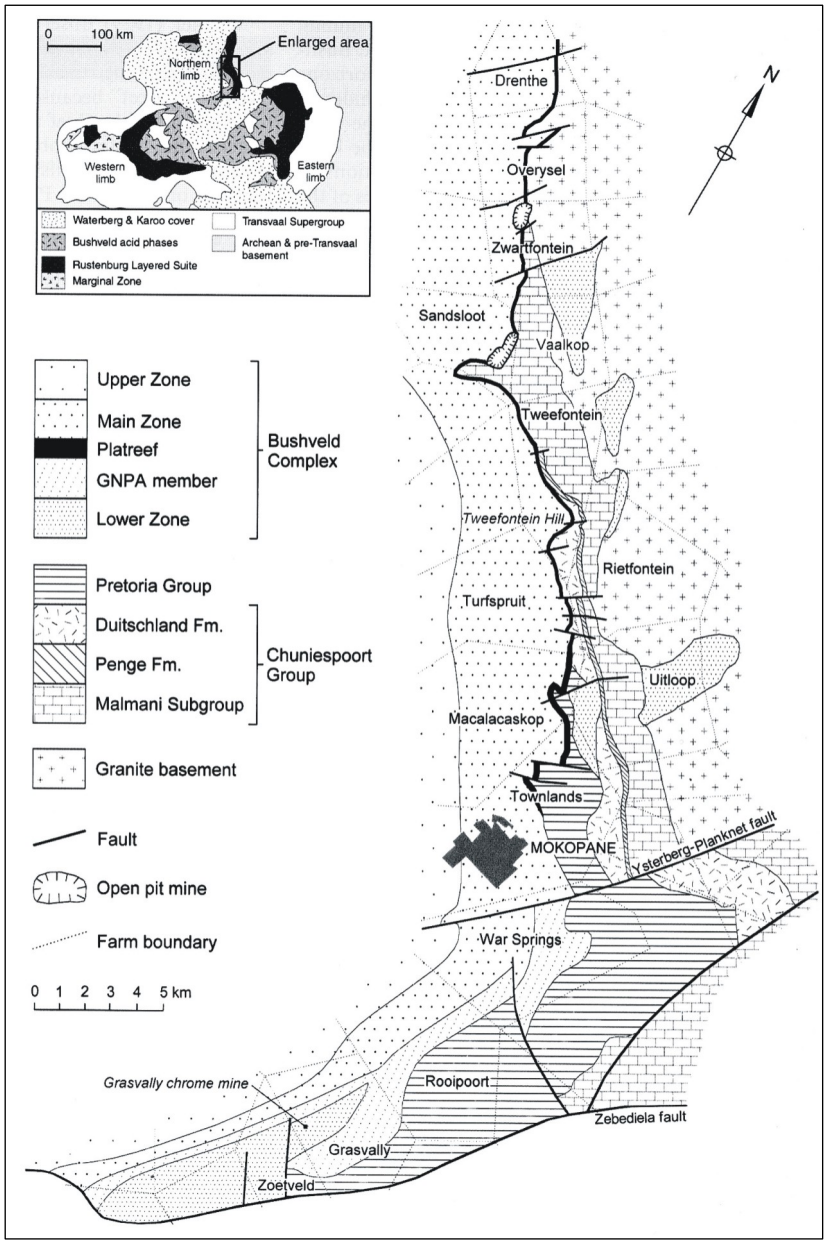

Figure 2.5 (Top map) Simplified regional geology of the Bushveld Complex indicating location of the Northern Limb. (Main map) Geological map of the lower portion of the Northern Limb showing the location of the Sandsloot open pit, after McDonald *et al*. (2005).

These footwall lithologies become progressively older towards the north as the intrusion cuts across the Daspoort Formation quartzites of the Pretoria Group in the south, the Timeball Hill Formation quartzites, shales and dolomite, the Penge Iron Formation, the Malmani Subgroup dolomites and calc-silicates (Figure 2.6), until it rests upon the Archaean basement in the north, which comprises the Hout River gneisses, the Turfloop granites and the Utrecht granites (van der Merwe, 1976; Cawthorn *et al*., 1985). The roof rocks to the mafic intrusion are the Bushveld

granites of the Rashoop and Lebowa Granite Suite and the metasediments of the Waterberg and Soutpansberg Group (Walraven *et al*., 1990).

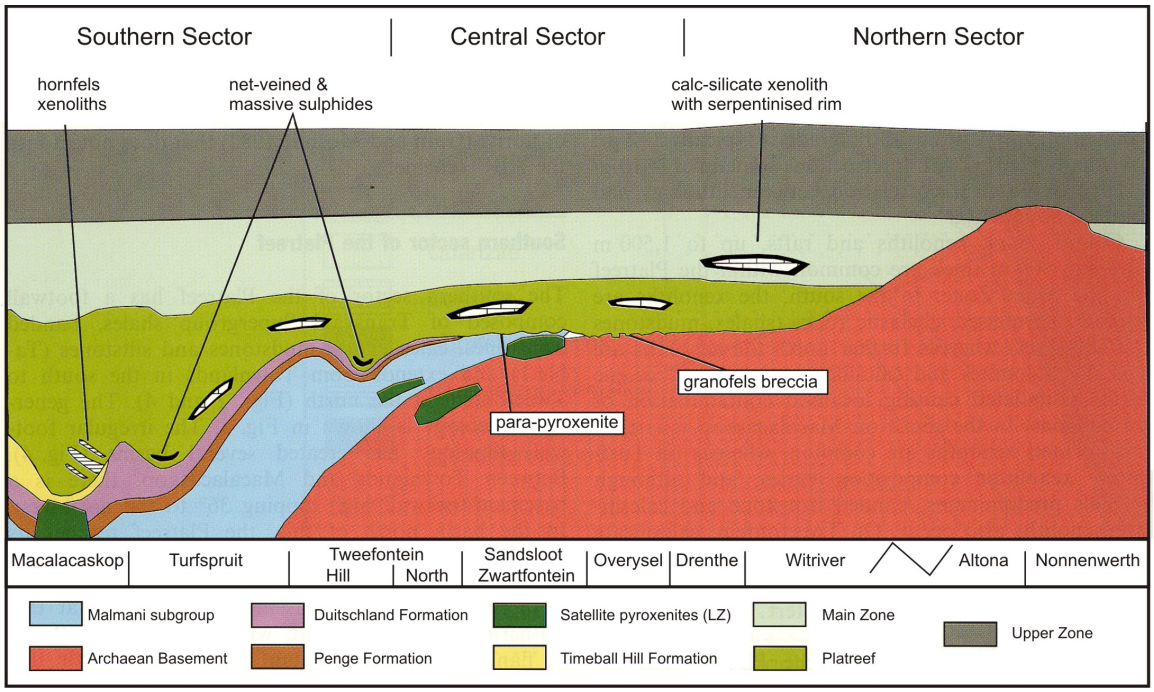

Figure 2.6 Schematic cross-section through the Platreef. The figure is representative of the entire length of the Platreef. Note: a significant strike length has been excluded between Witrivier and Altona, after Kinnaird *et al*. (2005).

As a result of the Rustenberg Layered Suite intrusion and the formation of the orebody, the sedimentary rocks of the footwall have undergone various degrees of assimilation (Harris and Chaumba, 2001). This has resulted in a unique suite of hybrid rock types, with singular and variable geotechnical, geochemical and mining properties. Xenoliths of footwall rocks are common within the intrusion, adding to the diverse properties of the Northern Limb.

The naming of stratigraphic units within the Northern Limb is controversial. The broad stratigraphic subdivisions used for the eastern and western Bushveld are generally accepted for the Northern Limb, as shown by Figure 2.5. However an extra unit, called the Grasvally norite-pyroxenite-anorthosite (GPNA) member, is included above the Lower Zone in the Northern Limb stratigraphy.

The Lower Zone is composed of pyroxenites and hartzburgites and the Marginal Zone is composed of norites. Both these zones occur on a discontinuous basis or as satellite bodies within the Northern Limb (van der Merwe, 1976). The GPNA member contains layered norites,

gabbronorites, anorthosites and a chromitite layer. McDonald *et al*. (2005) refer to the GPNA member as the Critical Zone. The Main Zone consists of gabbronorites and norites with an identifiable layer of troctolite and interlayering of anorthosite. The Upper Zone comprises cyclical units of magnetite layers, magnetite gabbro, gabbro, olivine diorite and anorthosite (Kinnaird *et al*., 2005). The magmatic layering shows an apparent second transgression with respect to the contact lithologies, as rock types within each zone in the south are higher than the equivalent stratigraphic successions in the north (Cawthorn *et al*., 1985; Harris and Chaumba, 2001).

The economically significant body of the Northern Limb is the Platreef. It is a 10 m – 400 m thick package of pyroxenite lithologies that hosts the PGE and base metal sulphide (BMS) mineralisation (Holwell and Jordaan, 2006). Until now work on the Platreef has correlated it with the Critical Zone of the Main Bushveld, calling it a Merensky Reef equivalent in the Northern limb. Von Gruenewaldt *et al.* (1989) and White (1994) place the Platreef within the upper Critical Zone whilst Van der Merwe (1976) places it at the base of the Main Zone. McDonald *et al*. (2005) recently published work that challenges the prevailing interpretation of its stratigraphic position. They present evidence that the Critical Zone of the Northern Limb and the Critical Zone of the rest of the Bushveld Complex are not related and that the Platreef and Merensky Reef are not derived from the same magma type, therefore they should not be correlated. The simplified stratigraphy of the Northern Limb and the Platreef is given in Figure 2.5.

The Platreef is a complex sulphide deposit with many interpretations regarding its origin. Previously it was considered an orthomagmatic sulphide deposit in which mineralisation and PGE concentration developed as the sulphides separated and collected from the main volume of melt (Mostert, 1982 and Barton *et al*., 1986). Armitage *et al*. (2002) suggests that the deposit is more typical of a low – temperature PGE deposit in which mineralisation either ensued syn– to post– magmatic crystallisation or was redistributed by hydrothermal fluids, thus explaining the extensive alteration and high concentration of PGEs and semi-metal (Te, Sb, Se, Bi and Ge) – bearing PGMs within the zones. The PGE, Cu and Ni mineralisation within the Platreef is irregular. The footwall lithology and degree of wall-rock assimilation, which occurred during emplacement, are both important influences on the origin and mineralisation of the reef (Harris and Chaumba, 2001). A second type of mineralisation, termed ‘Platreef – style’ mineralisation, is often observed around the calc-silicate xenoliths within the Main Zone gabbronorites in the north of the limb (Kinnaird *et al*., 2005). Exploration has revealed PGE mineralisation to a

depth of 800 m (Bye, 2003). Figure 2.7 shows an orthophotograph of the dominant structural geology features of the Northern Limb, across the Potgietersrust Platinums Limited (PPRust) concession area.

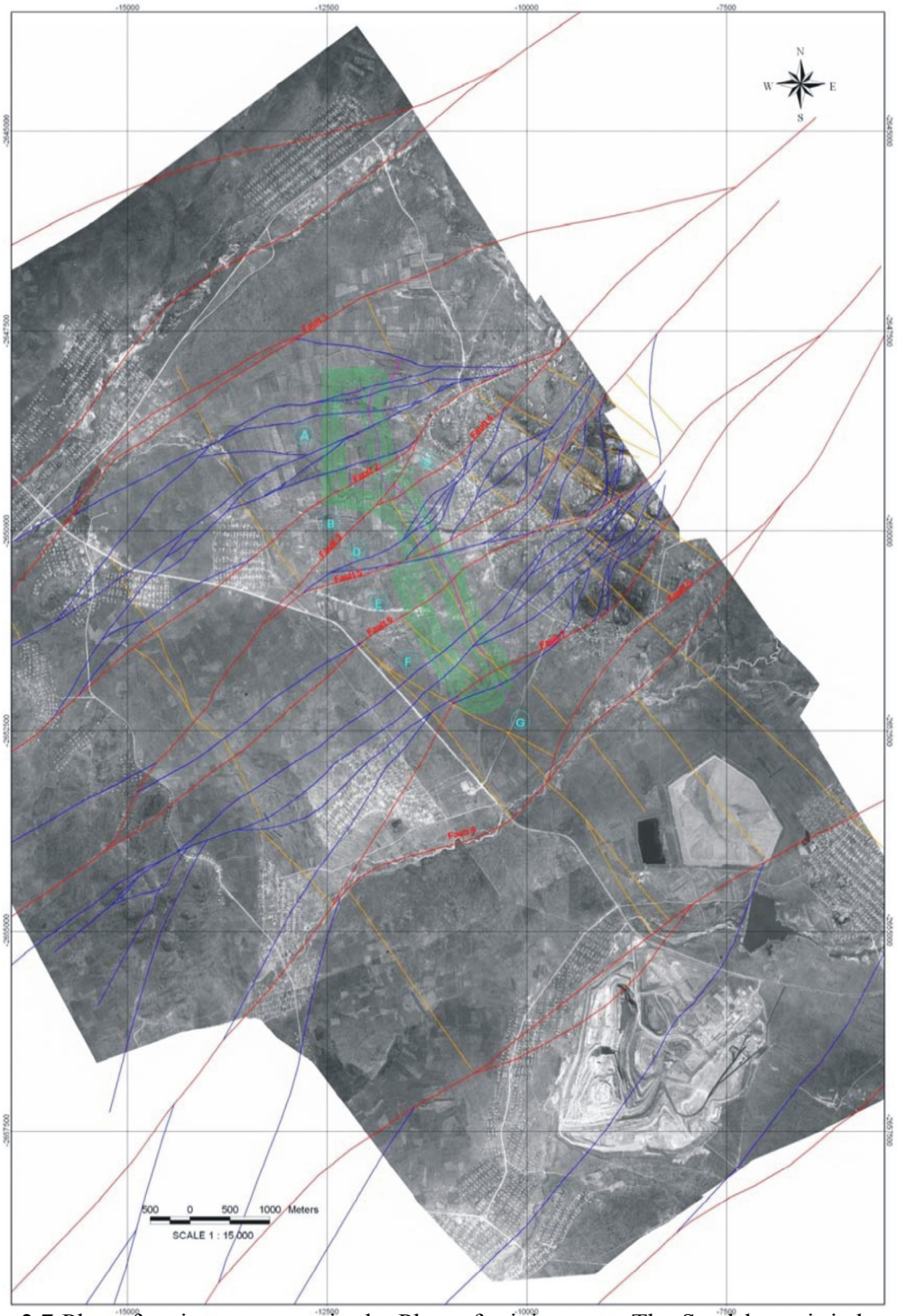

Figure 2.7 Plan of major structures in the Platreef mining area. The Sandsloot pit is located in the bottom right corner. The position of PPRust-North pit is shown by the green wire frame, after Friese (2004 a).

The structural geology in the PPRust concession area is extensively described by Bye (2003) and Friese (2004 a) and is summarized as follows.

Two principal NE trending fault sets dominate the geology. The first set comprises thrust to reverse fault zones that strike NE-SW with a moderate to shallow dip (40˚ – 60˚) to the north-west. The second set comprises reverse to strike-slip shear zones that strike NE-SW and dip steeply (70˚ - 85˚) to the south-east. These two fault sets are shown in the orthophotograph by the red and blue lines respectively. Both fault sets predate the intrusion of the Bushveld Complex and cause large scale folding and changes to unit and facies thicknesses of the Transvaal Group sedimentary rocks. Both have also been active since the Rustenberg Layered Suite intrusion and control the first order fracture pattern in Sandsloot pit and its surrounds (Bye, 2003). A third set of faults (yellow in the orthophotograph) is present in the area. They are a normal to oblique-slip set of fault zones that strike NW-SE with a moderate to shallow dip (40˚ - 60˚) to the south-west. The basal contact between the Bushveld Complex and the underlying Transvaal Supergroup is marked by one of these NNW trending faults (White, 1994).

The mineral assemblages within the metamorphic aureole in the Northern Limb have been used to calculate the temperature and pressure conditions in the country rock during the emplacement of the limb. Nell (1985) proposes a two stage metamorphic event in which the intrusion of the Lower Zone was calculated to have a maximum temperature of 750˚C and pressure of 1.5 kbars. The second stage of intrusion for the Upper Critical, Main and Upper Zones has been calculated to have occurred at 900˚C and 4 – 5 kbars, which is 2 kbars higher than the lithostatic pressure and is believed to have occurred some time after the first event.

2.2.2 Geology of Sandsloot Open Pit

Figure 2.8 depicts the local stratigraphy within Sandsloot open pit. The footwall rock to the Platreef in Sandsloot are the calc-silicates, which were Malmani Dolomites of the Transvaal Supergroup that have undergone metamorphism, metasomatisim and various degrees of assimilation with the Platreef (Harris and Chaumba, 2001). However, mineralisation often extends into the calc-silicate with mineable grades, therefore the footwall is defined by the ore grade and not the lithology. The roof rocks are the PGE-free gabbro norites, equivalent to those of the Rustenberg Layered Suite Main Zone.

The reef within the pit varies in thickness considerably, ranging between 15 m – 100 m. It comprises a suite of PGE mineralised pyroxenites and contaminated pyroxenite layers of parapyroxenite and serpentinised parapyroxenite (Figure 2.8) (Bye, 2003 and Harris and Chaumba, 2001). Serpentinite contaminates the Platreef rock suite to various and irregular degrees.

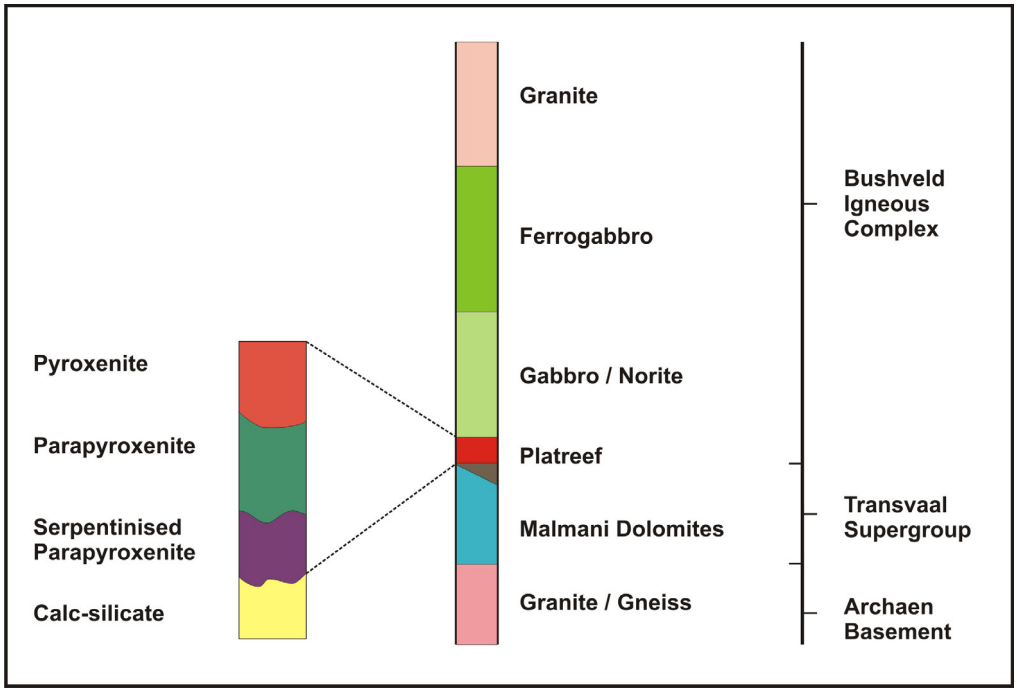

Figure 2.8 Simplified stratigraphic column of the Northern Limb, with dominant rock types which occur in the Sandsloot open pit, modified after Bye (2003).

The term parapyroxenite is used locally by the mine staff in reference to the highly altered rock that is thought to be a mechanical mixture of calc-silicate (footwall dolomite), pyroxenite and minor amounts of serpentinite.

Most of the PGE mineralisation is located within the upper part of the Platreef in Sandsloot pit and accessory phlogopite, base-metal sulphides and oxides are common in the pyroxenite rock suite (Armitage *et al*., 2002). Armitage *et al*. (2002) details a thorough study of the PGE mineralisation in the Platreef and footwall lithologies at Sandsloot open pit.

In the south of the pit the Platreef is interrupted by a tongue of dolomite which is thought to represent a truncated diapir of the footwall material. Locally the pit is disturbed by faulting, veining, shearing and jointing. The following section on the structural geology of Sandsloot open pit summarizes the work and detailed mapping given in Bye *et al*. (1998) and Bye (2003).

Three major northeast trending faults cut through Sandsloot open pit, two of which are normal faults and form a graben structure with a 30 m downthrow in the north of the pit. An oblique-sinstral fault named the “satellite pit fault” displaces the ore-body approximately 400 m to the southeast and has caused extensive deformation and alteration in the surrounding rocks. A late intrusive phase of aplite veining has resulted in the presence of numerous, large veins that cross-cut the pit and strike north-west, parallel to the Murchison lineament. The ore-body and the hanging wall are separated by a highly sheared zone of pyroxenite, with a width of 5m and a dip of 45° (Figure 2.9). The uniaxial compressive strength of this shear zone is approximately 30 MPa and the rock quality designation (RQD) less than 5 %. This zone of shearing is important because it provides a natural drainage path for local groundwater and is used for the dewatering of the pit.

Three major continuous joint sets and one discontinuous set have been identified in the pit. JS1 is the most prominent joint set. It strikes northwest (Figure 2.10), has pronounced slickensides and is associated with the aplite veins. This set dips steeply and laterally, and is vertically continuous over hundreds of metres. Table 2.1 shows the average joint set data from Sandsloot open pit. The minor joints are believed to have formed by randomized contraction jointing as the Bushveld Complex cooled.

Figure 2.9 Sandsloot pit looking north. The difference between the hanging wall and the orebody is clearly visible by the change in colour (below the red line) cause by the drainage of water through the shear zone which separates the two.

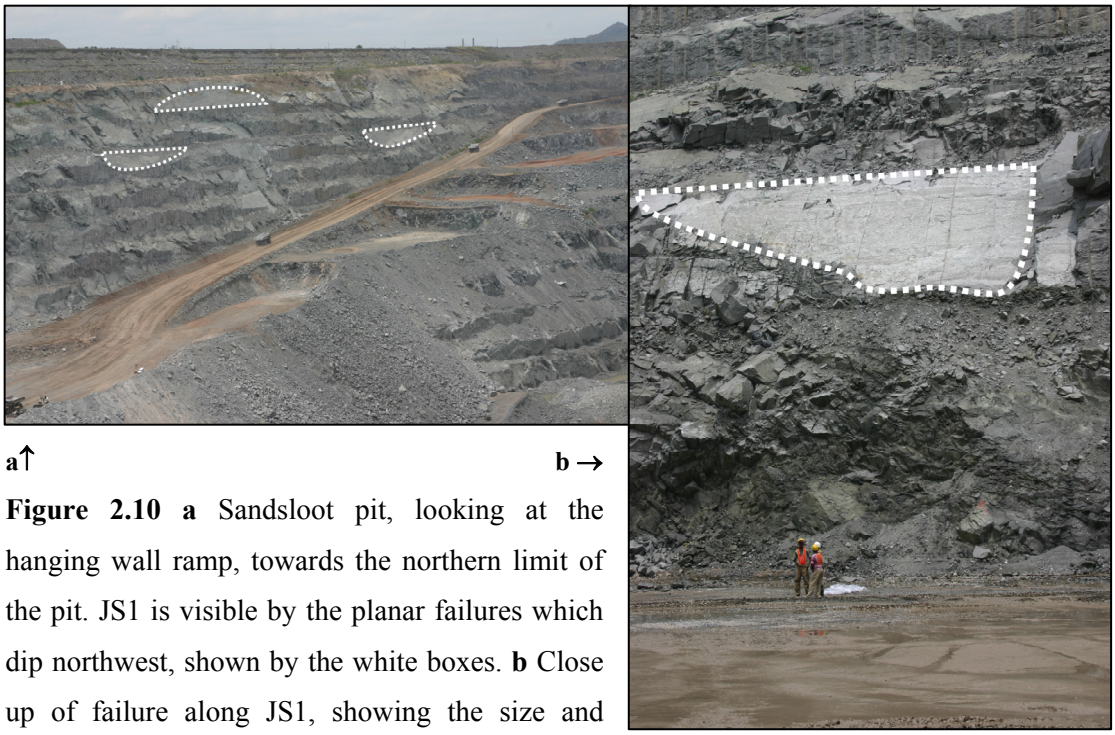

a↑ **b** →

Figure 2.10 a Sandsloot pit, looking at the hanging wall ramp, towards the northern limit of the pit. JS1 is visible by the planar failures which dip northwest, shown by the white boxes. **b** Close up of failure along JS1, showing the size and length of the failure plane.

Table 2.1 Average joint set data from Sandsloot open pit, after Bye (2003).

Joint Set	Dip	Dip Direction	Joint Roughness	Joint Filling	Joint Spacing
JS 1	72	88	(IV) Rough Irregular	Calcite	0.5 m
	73	263	Undulating	Serpentinite	(0.2-2.0m)
JS2	78	357	(II) Smooth Stepped	Calcite	0.4 m
	82	183			(0.2-1.0m)
JS3	70	310	(V) Smooth Undulating	Serpentinite	0.3 m
	62	125			(0.1-5.0m)
JS4	72	237	(VII) Rough/Irregular	Calcite	0.15 m
	63	65	Planar		(0.05-0.40m)

Sandsloot open pit falls within the catchment area of the Mogalakwena River and is situated on the eastern side of the shallow valley of the Groot Sandsloot River (Bye and Bell, 2001). Precipitation in the area occurs mainly in the form of thunderstorms during the summer months, peaking in January. Groundwater enters the pit via the hanging wall and the footwall at roughly 90 $m^3 h^{-1}$ and 22 $m^3 h^{-1}$ respectively, as shown in Figure 2.11a and b. (Bye and Bell, 2001). The phreatic surface within the pit is approximately 40m below the ground level and negatively affects the factor of safety of the slopes, therefore the pit is dewatered by pumping from the sumps when necessary (Bye and Bell, 2001).

←a and b ↑

Figure 2.11 a Substantial flow of ground water entering the pit via an open joint and a slower seepage through the shear zone in the hanging wall, indicated by the darkened colour. **b** Ground water entering the pit through joints in the footwall, indicated by darkened colour.

2.3 Summary

Chapter 2 provides an overview of the regional, local and in-pit geological setting for this research, with references. In summary, the Bushveld Complex intruded between the Transvaal Supergroup clastic sedimentary rocks and the rhyolites and granophyres of the Rooiberg Group approximately 2060 – 2050 Ma. It outcrops in four distinct limbs, with a fifth that lies subsurface and was identified using geophysical techniques. The complex comprises cyclical units of magmatic intrusions that dip centripetally. The main economic reefs are the platinum-rich Merensky Reef and the UG-2.

Sandsloot open pit is situated on the northern limb of the Bushveld Complex. This limb is significantly different to the rest of the Bushveld Complex in lithology, layer thicknesses, stratigraphy, mineral composition, textures and geochemistry. Sandsloot open pit mines the Platreef orebody, which is hosted by a thick package of pyroxenite lithologies. Mineralisation, in the form of PGE, Ni and Cu, is irregular and influenced by the footwall lithologies. The local geology is dominated by northeast trending faults and assimilation, which due to the emplacement of the orebody, has resulted in the formation of several hybrid rock types. The section of the Platreef mined at Sandsloot open pit dips at 45° and strikes N-S. PGE

mineralisation is greatest in the upper pyroxenite unit of the Platreef but is also present at mineable grades in the calc-silicate footwall. Three northeast trending faults crosscut the pit with the greatest displacement, approximately 400 m, occurring in the south of the pit, by the satellite pit fault. Four sets of joints are present in the pit, three of which are major and continuous. Groundwater drains into the pit via the shear zone above the orebody and through joints in the footwall. The pit must be dewatered to minimize the effect of groundwater on the factor of safety for the slopes.

Chapter 3

MINING OPERATIONS ON THE PLATREEF AND AT SANDSLOOT OPEN PIT.

3.1 Introduction

Modern mining has been taking place on the Platreef for over eighty years, since the mid nineteen twenties (Buchanan *et al*., 1981). This chapter reviews the history of mining on the Northern Limb of the Bushveld Complex and the development of the Sandsloot open pit mine, from inception to operation. It also provides details on the open pit and processing plant design and machinery, and a description of the path of the ore from rock mass to concentrate at Sandsloot open pit.

3.2 History of Mining and Development

Mining of the Platreef began with pre-European copper workings on the farm Tweefontein 238 KR (Figure 3.1). In 1924, Dr Hans Merensky identified the pyroxenitic zone at the base of the Rustenburg Layered Suite on the Northern Limb as being similar to the Merensky Reef, causing a "platinum rush", with prospectors quickly entering in this region (Buchanan *et al*., 1981). Over fifty companies were floated on the Johannesburg Stock Exchange to exploit the Potgietersrus deposit by 1925. Potgietersrust Platinums Limited (PPRust), now a subsidiary of Anglo Platinum, was one of the leading South African companies and held extensive mineral prospecting options (White, 1994).

The Platreef was explored and mined systematically. A number of trenches and shafts were sunk, some to a depth of 30m, on the Sandsloot 236 KR, Vaalkop 819 LR and Zwartfontein 814 LR and 819 LR farms (Figure 3.1) and PPRust opened and commenced construction of a treatment plant in 1926 (White, 1994). The Platreef was a hub of platinum extraction and production until the 1929 Great Depression and the subsequent platinum price collapse in 1930. After the price collapse many mining operations were forced to shut down.

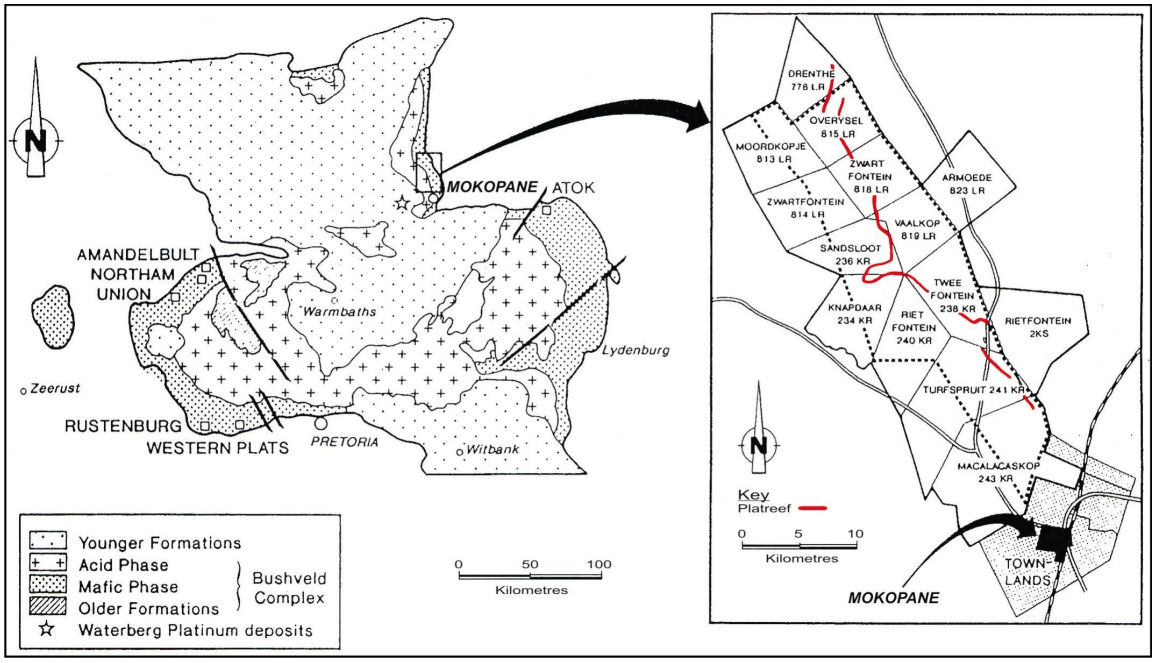

Figure 3.1 Regional geology of the Bushveld complex, the inset shows the surface outcrop pattern of the Platreef and the farm boundaries in the area, modified after White (1994).

It was not until the late nineteen sixties and early nineteen seventies that exploration began again. In 1976, Johannesburg Consolidated Investment Company Limited (JCI), the company that administered PPRust, began a series of exploration programmes that focused on mineralisation and mine feasibility along the strike of the Platreef. By 1987 the Rustenburg Platinum Mines had established an agreement with the Lebowa Government for the rights to exploit the Lebowa section of the Bushveld Complex reserves and in September 1990 the execution of the proposed platinum mine on the Platreef was decided on (White, 1994). An estimated extraction of 200 000 tonnes of ore per month was planned.

In October 1990 the new mine estimates and mining methods were made public. On the 10th January 1992 waste stripping commenced and on the 12th February 1992 the first blast in the Sandsloot open pit area took place (Bye, 2003). Sandsloot open pit was the first of six sequential pits scheduled for mining along the Platreef. Zwartfontein South pit was opened in 2002 and mining of the Zwartfontein North - Overysel (PPRust-North) pit began in 2006 (Figure 3.2).

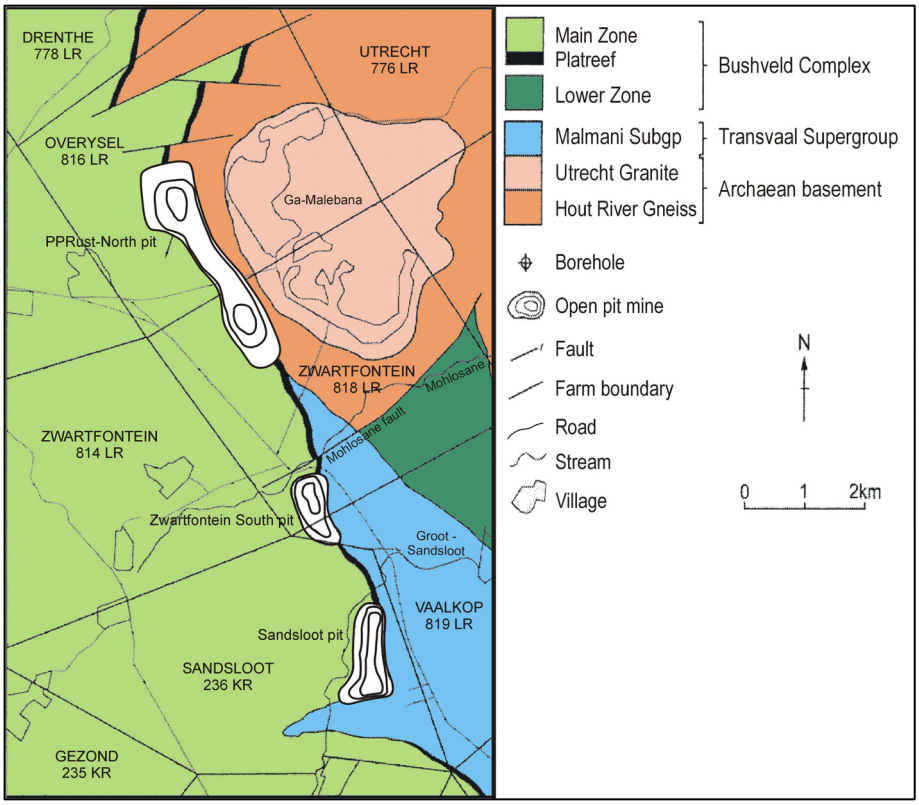

Figure 3.2 Geological map of the central portion of the Platreef showing the locations of Sandsloot pit, Zwartfontein South pit and the PPRust-North pit, modified after Holwell and Jordaan (2006).

3.3 Open Pit Mining

Open pit mining is the most cost effective means of mining expansive and often low grade orebodies because it allows high production volumes and a high degree of mechanisation. The Platreef, although not a low grade or expansive orebody if compared with a porphyry copper deposit, is suitable for open pit mining along much of its strike. This is because of the ore grade, width and the dip of the Platreef that outcrops at ground level. For example, on the Sandsloot 236 KR farm the Platreef average ore grade is greater than 4 grams per tonne (g/t), the width is approximately 50m, it dips at roughly 45 degrees west-southwest and outcrops at ground level. Therefore it is possible to excavate the orebody using open pit mining, without excavating any waste from the footwall, but with a stripping ratio of 6.2:1.

The geological conditions and the resulting mining practices in the northern Bushveld Complex contrast with those in the eastern and western Bushveld Complex. In the east and west the platinum group element (PGE) mineralised zones are concentrated into the Merensky Reef and

Upper Group – 2 chromitite layer (UG-2). These reefs are 30cm – 90cm and 60cm – 100cm in thickness respectively, are 1400m – 1800m deep and dip between 10 degrees and 20 degrees **(**Hochreiter *et al*., 1985). These geological conditions therefore require shallow to intermediate depth underground pillar mining for profitable extraction of the ore.

The high production volume and high degree of mechanisation associated with open pit mining are demonstrated at Sandsloot open pit mine, in which approximately 40 million tonnes of rock is mined annually and due to the high mechanisation in the pit, approximately 37 000 tonnes of rock is mined per employee annually (Bye, 2003).

The length and orientation of the walls of an open pit are controlled by the shape of the ore body. The design of the pit is governed by the ore grade distribution, the production costs and the overall rock mass strength and stability (Sjöberg, 1996). There are two phases to the design of an open pit (Sjöberg, 1996):

1) **Pit Optimisation**, which involves the defining of the final pit outline, total mineable reserves and the setting of the location guidelines for the initial pit and for optimal pit expansion.
2) **Pit Design and Production Planning**, in which the mining sequence, cut off grades, production plans and final layout are determined.

In terms of rock mechanics, pit optimisation is the relationship (balance) between economics and safety. Economics calls for mining of the pit using the steep pit angles, as steeper pit angles means less waste rock that has to be drilled, blasted and hauled out of the pit (Sjöberg, 1996). However, if pit slopes are too steep failure becomes inevitable. Such failures are expensive in terms of time needed for clearing the failure, loss of profit due to reduced production as well as risk to employees. If failures cannot be cleared the pit slopes often have to be mined at shallower, less economical angles and if failure causes the loss of ramps that provide access to the pit, the result can be the closure of the mine.

Essentially, optimal open pit mining requires a good understanding of the rock mechanics that control the rock mass, an accurate ore reserve model and the minimisation of the production costs.

3.4 Mining Operations at Sandsloot

The design of Sandsloot open pit has evolved in a number of steps since operations began in 1992. As a result of gathering more geotechnical data, the observation of slope failure mechanisms that occur in the pit and the application of different slope configurations, the design of the pit has been modified to achieve a greater overall pit wall angle (Figure 3.3). The current overall pit wall angle is 57 degrees, with a bench height of 15m, a stack height of 60m, a stack angle of 71 degrees, a catchment berm of 20.5m and a batter angle of 90 degrees. Two ramps provide access to the pit from the north and the south of the pit. The ramps are 35m in width and have a 10% gradient.

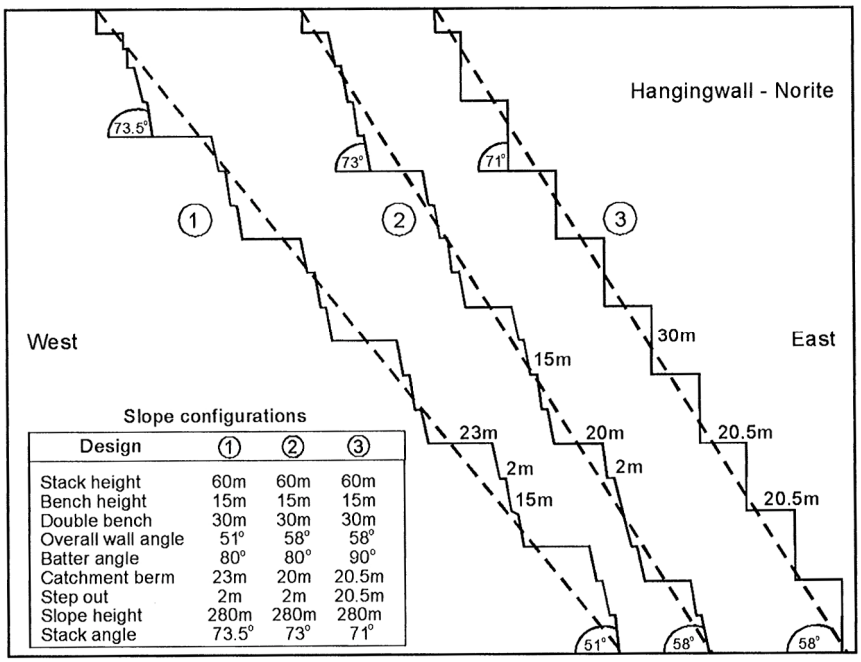

Figure 3.3 Hanging wall slope stack configurations at Sandsloot open pit, after Bye and Bell (2001).

At present the economic limit of the pit is roughly 300m, which will be reached by a series of scheduled cutbacks. The sixth cutback is the final cutback and will take the pit down to the 300m depth, with a length of 1.8km and a width of 600m (Figure 3.4).

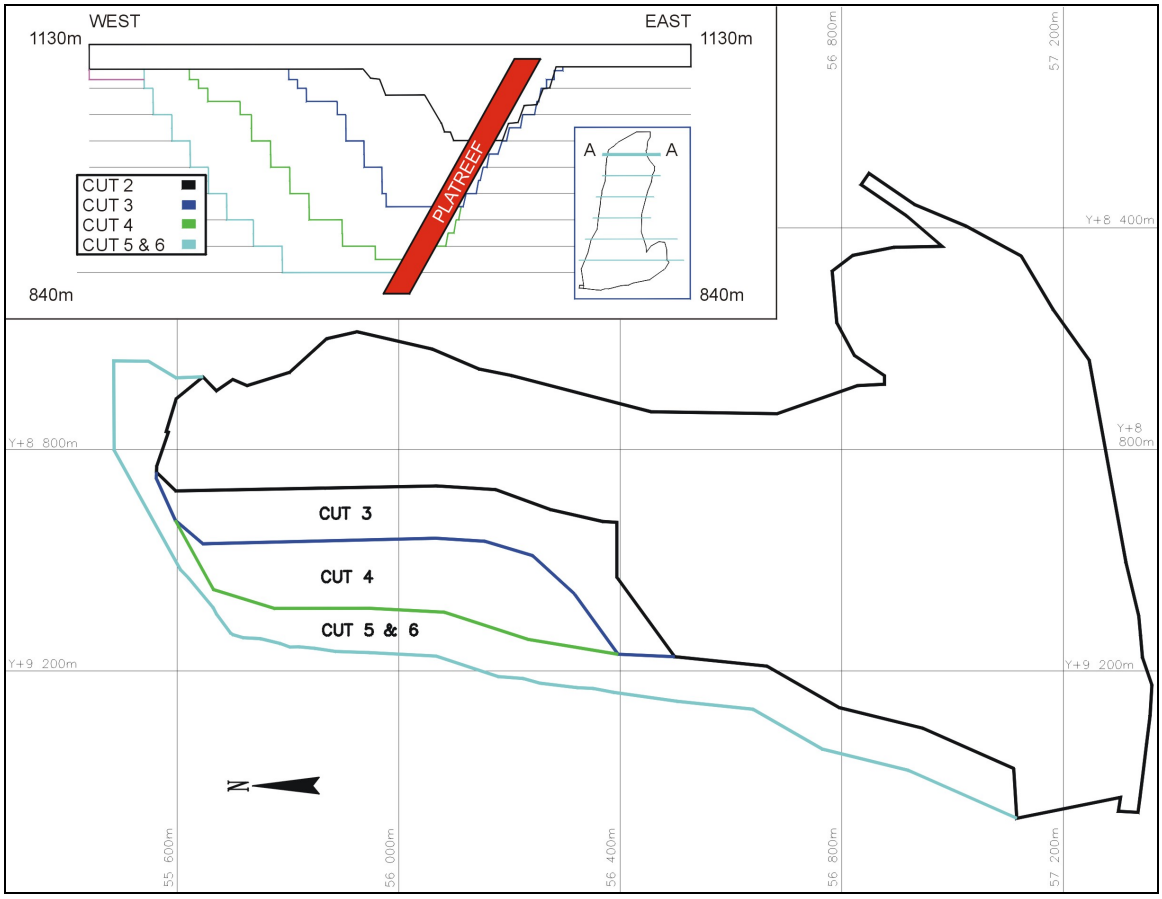

Figure 3.4 Sandsloot open pit cut back phases, modified after Little (2006).

A comprehensive slope monitoring strategy, combining the use of four monitoring systems, has been implemented at Sandsloot. These systems comprise the ISSU™ microseismic monitoring system, a GeoMoS™ automated prism monitoring system, prismless Riegl laser scanners and a GroundProbe™ slope stability radar system. Visual inspections, SiroVision™ digital photogrammetry and groundwater monitoring are also standard practice in the slope stability monitoring plan, which aims to improve safety and the cost-effectiveness of mining.

The general size of a mining block at Sandsloot is 100 m x 50 m x 15 m. Each block is drilled, blasted and thereafter staked out to demarcate the various zones of ore grade. The fragmented material is then loaded using 45 tonne capacity hydraulic face shovels and 130 tonne capacity CAT 785B dump trucks.

Ore that comes out of the Sandsloot open pit has a PGE cutoff grade of 4 grams per tonne (g/t). Material with less than 4 g/t is considered waste and dumped. Depending on the ore grade of a mining block the material is either sent straight to the crushers and processing plant to form the concentrate immediately or it is stockpiled. Ore that is stockpiled is used as necessary to mix

with progressive mining blocks so that the feed size sent to the plant is kept constant and the requirements for optimum processing are maintained.

The mining operations used to convert the unprocessed ore from the pit into the concentrated ore from the PPRust processing plant are shown in Figure 3.5. The plant comprises:

- Two mill-float modules, that share common ore handling, concentrate handling and tailings disposal facilities and use a sequence of primary, secondary and tertiary milling operations to break down the rock for chemical treatment.
- Section-C, built in 1998 to handle oversized pebbles of harder ore rock types, comprising in-circuit crushers and ball mill and flotation modules.

The plant operates at a 425 000 tonne per month throughput and produces 100 g/t concentrate. The concentrate is taken off the mine site for smelting and refining.

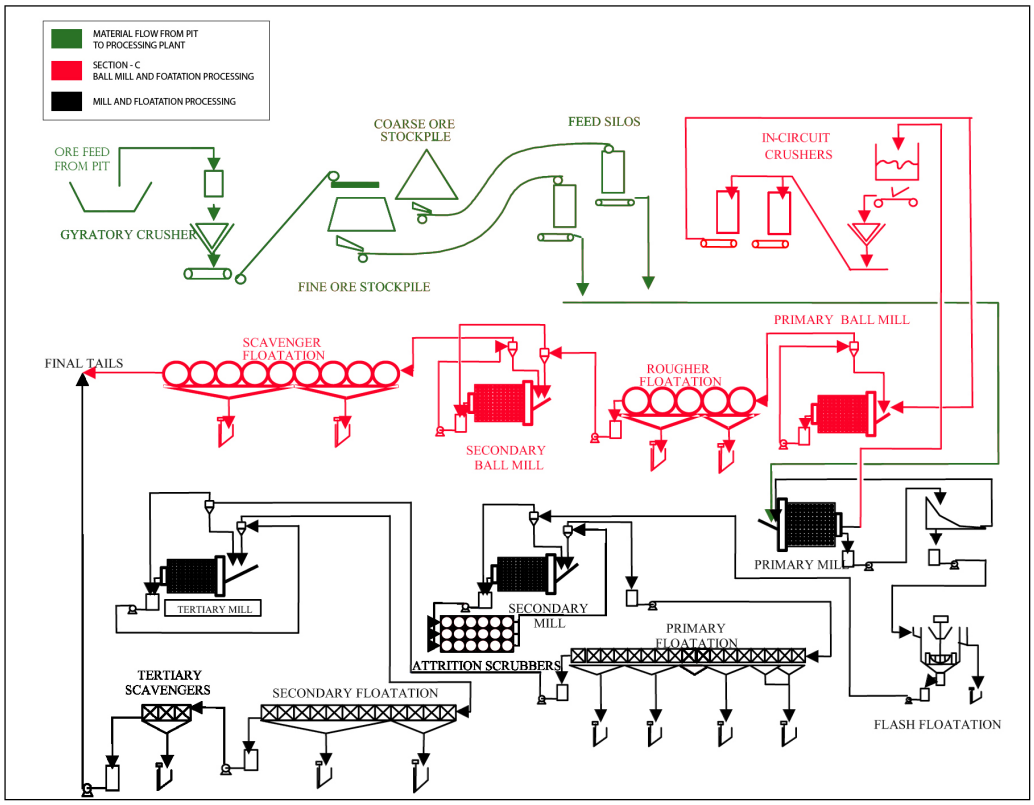

Figure 3.5 Diagram illustrating the mining operations required produce concentrated ore from the pit material at PPRust, modified after Bye (2003).

As part of the mining operations at Sandsloot open pit a number of models have been developed and implemented to assist in informed decision making and planning by mine management. These models are chiefly described by Bye (2003) but are summarised for the purposes of this study to provide the reader with thorough knowledge of the Sandsloot open pit mine workings.

A three-dimensional (3D) geotechnical model, a slope stability model and a fragmentation model were developed specifically for Sandsloot open pit. At the core of the 3D geotechnical model was the division of the pit onto domains of similar geotechnical properties, based on rock type and structure. The domains were determined using line-surveys, in-pit face mapping and drill hole core logging, which recorded parameters required to calculate Bieniawski's (1989) Rock Mass Rating (RMR) classification and Laubscher's (1990) Mining Rock Mass Rating (MRMR) classification. With this model querying of the rock mass conditions before planned mining activity in an area was made possible using the predictions from the geotechnical modelling. The slope stability model made slope evaluation and design per geotechnical domain possible. The model incorporated empirical, kinematic and numerical analysis to determine pit slope and inter-ramp angles, stack heights, safety berm widths, stability at an individual bench level and sensitivity/failure probability of a range of slope configurations per geotechnical domain. The slope stability model was a practical application of the 3D geotechnical model to assist in production, costing and safety improvements. Finally, the fragmentation model, another application of the 3D geotechnical model, was developed to generate area specific geotechnical parameters that could be related to Lilly's blastibiliy index (Lilly, 1986). In turn these parameters per geotechnical zone were related to quantitative data to calculate the explosive volumes required and associated drill and blast costs. The fragmentation model allowed for blasting parameters to be adjusted in advance for the changes in rock mass conditions. The fragmentation profile delivered to the autogenous mills can therefore be adjusted decreasing the impact varying orebody geotechnical properties have on the plant's performance.

Chapter 4

PETROGRAPHY

4.1 Introduction

The geology at Sandsloot open pit comprises gabbro norite in the hanging wall, calc-silicates in the footwall and three main orebody rock types: feldspathic pyroxenite, pyroxenite and parapyroxenite. Serpentinite and calc-silicate are not main orebody rock types however, they are often mined and processed as ore because the former frequently forms lenses or pods of contamination within the main orebody rock types and the latter sometimes contains high enough PGE concentrations to class it as ore grade. It is these five orebody rock types –feldspathic pyroxenite, pyroxenite, parapyroxenite, serpentinite and calc-silicate– that characterisation will focus on for mine-to-mill purposes, therefore in this petrographic analysis, as well as subsequent investigations, the focus will fall on these rock types.

This chapter provides the foundation for distinguishing the primary differences between the orebody rock types. The chapter covers the description and systematic classification of the rock types. It evaluates the mineral composition, texture, fabric and alteration characteristics by means of microscopic examination and X-ray diffraction. Finally, it looks at the similarities and differences between the characteristic properties and assesses the likely effects they may have on the performance of operations that occur in the pit and in the processing plant.

4.2 Methods of Mineral Identification

4.2.1 Transmitted Light Microscopy

Reflected light microscopy was used in this investigation, which enabled examination of the translucent minerals. The aims of microscope analysis were to identify the mineral composition, estimate mineral proportions and to distinguish any textural features, such as grain size, grain shape and nature of grain contacts for the different rock types. Included in the investigation were fabric identification, degree of alteration, presence of micro-fracturing and porosity. These

properties are important due to their influence on the mechanical behaviour of the rock and rock mass.

4.2.2 X-ray Diffraction (XRD)

X-Ray diffraction (XRD) analysis can be used to either identify the minerals present within a whole rock sample or for identifying separated mineral specimens. For this research study XRD was used to determine the minerals within the whole rock sample and therefore compliment the optical microscope study.

The identification of minerals was achieved using a technique in which short wavelength X-rays (of a constant wavelength) are directed onto the pre-packed sample at different angles. As the beams strike the sample the rays are diffracted at an incident angle, θ, which is dependent on the wavelength of the X-ray and the spacing between the planes of the atoms within the mineral. Characteristic diffraction patterns of the minerals present are emitted and recorded as a succession of peaks on a chart. These patterns are compared to a set of known standard patterns and the minerals are identified accordingly (Lapidus *et al*., 2003).

4.3 Sample Selection and Preparation

Potgietersrust Platinums Limited (PPRust) provided diamond drill hole core for testing. The locations of these diamond drill holes are recorded in Table 4.1 and shown in Figure 4.1. Before sampling, the drill hole core was logged for lithology, noting changes in colour, grainsize, texture, weathering and alteration. The drill core photographs and the simplified logs for these drill holes are recorded in Appendix A. The metallurgical drill holes (drill holes SSMET 1, SSMET 2, SSMET 6, SSMET 7 and SSMET 8) were sent to the Anglo Platinum research centre (ARC) for metallurgical testing after being drilled and were therefore not available for logging or photographing. The logs for these drill holes were recorded by PPRust site personnel and are available in Appendix A. Some of the drill holes were logged geotechnically, which is described in detail in Chapter 5.

Table 4.1 Drill hole collar coordinates for the diamond drill holes sampled for petrographic, geotechnical, geochemical and metallurgical testing.

Drill Hole Name	Easting (mE)	Northing (mN)	Relative Level (mRL)	Length (m)	Dip (˚)
SSPIT149	55691	8685	1030	45.00	90
SSPIT150	55506	8763	1031	63.38	90
SSPIT154	55609	8724	1052	56.60	90
SSPIT158	55762	8690	1047	23.00	90
SSPIT159	55713	8685	1050	45.10	90
SSPIT160	55740	8663	1049	45.02	90
SSPIT161	55816	8646	1049	45.02	90
SSMET1	56050	8830	944	60.00	90
SSMET2	56046	8831	945	60.25	90
SSMET3	56075	8831	945	60.15	90
SSMET4	56044	8801	945	30.15	90
SSMET5	56075	8824	945	30.10	90
SSMET6	56032	8870	930	50.46	90
SSMET7	56367	8969	930	50.44	90
SSMET8	57195	9282	1005	51.88	90

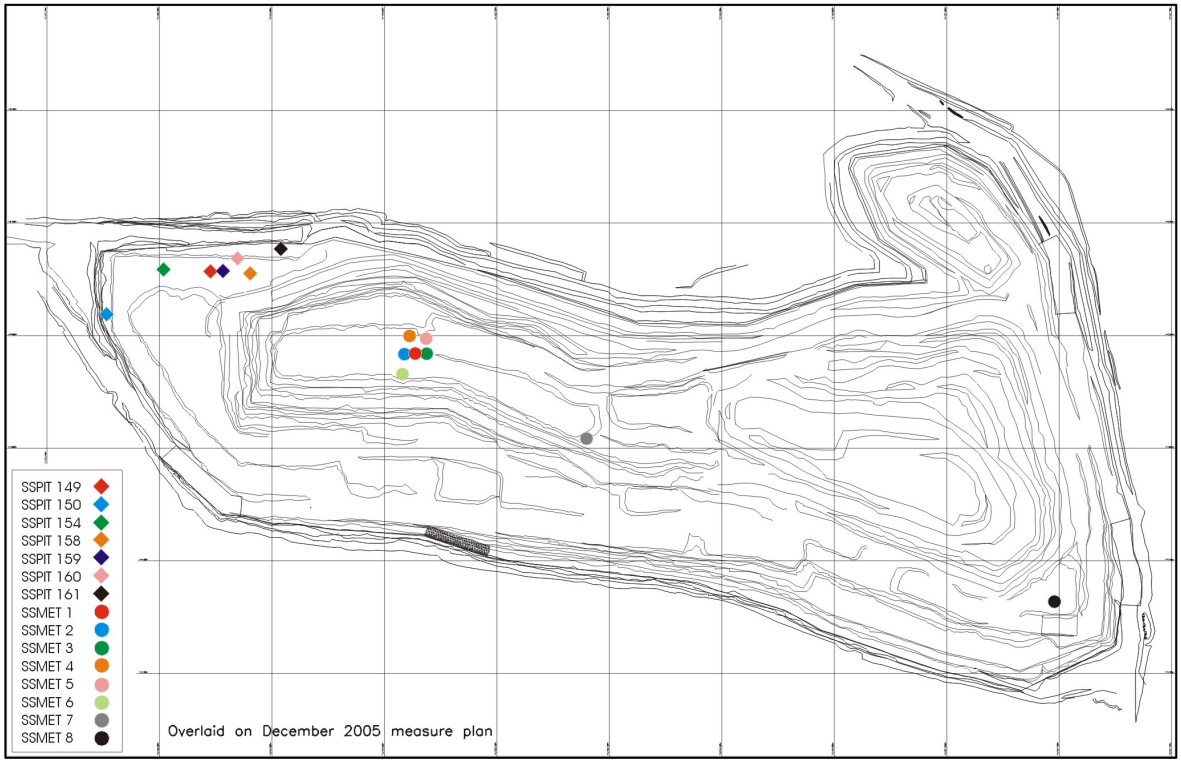

Figure 4.1 Plan view of Sandsloot open pit with locations of the drill holes sampled for petrographic, geotechnical, geochemical and metallurgical testing, modified after Little (2006).

After logging, samples for thin section analysis were taken from positions adjacent to or close to core selected for uniaxial compressive strength (UCS) testing, as shown in the schematic in Figure 4.2. XRD analysis and geochemical testing was performed on UCS samples, which were

measured for density and were adjacent to samples for other strength tests. The close positioning of the samples was important for relating the properties between analyses.

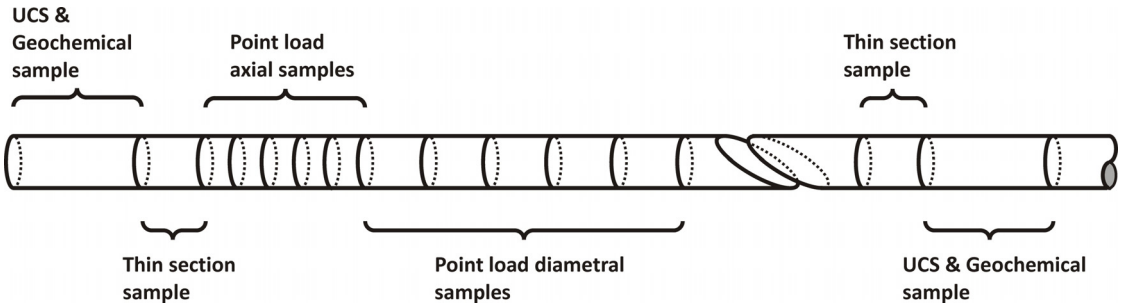

Figure 4.2 Schematic representation of sample positions for petrographic, geotechnical, geochemical testing.

The thin sections were made by the technical staff at the University of the Witwatersrand, Gauteng, South Africa. They were orientated length-wise to the long axis of the core, way up was recorded for each sample and their preparation was according to standard in-house procedures. XRD samples were crushed and milled as described in Appendix B. Fine grade powder was then packed into an aluminum holding container with an imposed near random surface for XRD testing. The preparation of the XRD samples was performed in the laboratories at the School of Geological Sciences, University of KwaZulu-Natal (UKZN).

4.4 Testing Procedures

The thin sections were analysed at the UKZN microscope laboratory using plane polarized light and cross polarized light. Battey (1981) and Deer *et al.* (1992) were used for reference in the identification of mineral properties.

Analysis of the XRD samples was performed in the laboratories at the School of Geological Science, UKZN, using a Philips PW 1710 diffractometer, the specifications for which are described in Appendix B. The raw XRD data files were filtered using *Eva* software, with preset filters to determine the minerals present in the samples. This was undertaken in the Geology department at Potgietersrust Platinums Limited (PPRust) using the *Eva* software and the preset

filters that PPRust uses. A consistent result between XRD results of this research project and XRD results of PPRust was therefore achieved.

4.5 Results

Sixty one thin sections and eighty seven XRD analyses were carried out in order to comprehensively characterise the petrographic properties and identify features of the minerals within the rock types of Sandsloot orebody. Table 4.2 lists the common minerals identified, the individual planar and cross polarized characteristics and describes the crystalline forms of the minerals in the various rock types, as observed in thin section.

Table 4.2 Distinguishing optical properties of the Sandsloot orebody minerals.

Mineral Name	Notes on properties
Amphibole	Present as an alteration product (probably of pyroxene), a reaction product and as individual grains with a euhedral prismatic crystal form and medium to fine grain size. Colourless with a moderate to high relief. Showed a high birefringence and two sets of cleavage 56° apart for the individual crystals. Most likely tremolite.
Biotite	Pleochroic colourless to brown, but colourless phlogopite was present. Minerals showed distinctive mottled extinction. Crystals were mostly subhedral, fine grained and present in accessory abundances.
Calcite	Present as both individual crystals and as a replacement product. Commonly anhedral to subhedral with a high birefringence and often exhibited multiple twins. Individual crystals were fine grained.
Chlorite	Present as an alteration product. Anhedral to subhedral in form, mostly green and sometimes brown in colour, low to isotropic birefringence but also commonly having an anomalous steal-blue birefringence. Very fine grained.
Clinopyroxene	Moderate to high relief, commonly subhedral and light green in colour. High birefringence varying from light blue to green and yellow. Distinct 90° cleavage. Most likely diopside. Less abundant than orthopyroxene. Grain size ranged from fine to coarse, most crystals were coarse grained.
Garnet	High relief and isotropic. Anhedral to subhedral in form, but also interstitial. Colourless but commonly a dusty brown colour indicating the presence of hydrogrossular. Fine grained. It was present where olivine was crystallized, however crystal relationships did not show that olivine was necessarily replaced by garnet but that they perhaps co-crystallized.
Muscovite	Colourless, with a high birefringence. Minerals showed distinctive mottled extinction. Crystals were very fine grained and present only in veins in accessory abundances.

Olivine	Colourless, high relief and fine grained with an anhedral shape. Present as individual rounded grains and as aggregates. Frequently extensively altered along fractures, replaced by serpentine and occasionally amphibole, showing hourglass and mesh alteration textures. Often contains opaque mineral precipitate.
Opaque minerals	Transmitted light analysis was performed therefore identification of opaque mineral types was not possible. Opaque minerals were present as individual crystals of medium grained size and subhedral grain shape. Also present as an alteration product with a fine to very fine grained size and a lath-like or stringer form, controlled by the way in which the host crystal altered.
Orthopyroxene	Moderate to high relief, colourless or occasionally pink with a granular subhedral form. Distinctive double cleavage at 90° to each other, straight extinction. Often more altered than clinopyroxene. Most likely enstatite. Medium to coarse grained.
Plagioclase	Present as interstitial crystal and less commonly as fine grained subhedral crystals. Distinctive albite twinning and a low birefringence were displayed. Generally highly altered, some thin section crystals exhibited an exsolution texture.
Prehnite	Present as a secondary phase mineral, showing a low birefringence. Commonly in the form of an aggregate of randomly orientated fine grained crystals. Found in veins or around altered crystals of plagioclase.
Quartz	Present only as an accessory mineral in some thin sections.
Serpentine	Present as an alteration product. Colourless to light green with a low birefringence. Mesh and hourglass textures were common. Frequently found as serpentine aggregates and in veins with a fibrous lath-like form indicating the mineral was possibly lizardite, a member of the serpentinite group.
Spinel	Present as fine grained subhedral to euhedral grains with an octahedral form. Most commonly with a brilliant green colouring but also transparent. Isotropic with a very high relief. Many of the grains showed alteration.
Talc	Present as an alteration product. Colourless, high birefringence and very fine grained. Gave a dusty appearance to the crystals
Vesuvianite	Present as a secondary phase mineral. Yellow colouring with a very low birefringence, almost isotropic. Fine grained and granular.

A concise transmitted light description for each orebody rock type is presented in Tables 4.3 - 4.7, with photomicrographs which illustrate the general nature of the rock types (Figures 4.3 – 4.7). The five analyses represent the typical characteristics of the 61 thin sections. High detailed thin section analyses were performed on 16 thin sections and are recorded in Appendix B, with the corresponding planar and cross polarized photomicrographs. The remaining 45 thin sections were assessed in a “compare and contrast” style to the 16 high detail analyses to ensure

the descriptions were representative and comprehensive. The descriptions for these analyses and their corresponding planar and cross polarized photomicrographs are given in Appendix B.

Table 4.3 Petrographic description of feldspathic pyroxenite.

Rock Type	Feldspathic pyroxenite
Mineralogy	
Essential	Orthopyroxene (45 – 60%), Clinopyroxene (20 – 40%), Plagioclase (10 – 30%), Calcite and Opaque minerals (< 5%). Amounts are a visual estimate.
Accessory	Biotite, Amphibole, Garnet, Olivine, Opaque and Prehnite minerals. Total count of accessory minerals was less than 40 observed crystals per a thin section.
IUGS Name	Garnet-chromite-bearing gabbronorite
Colour Index	Melanocratic (mafic index 60 – 90%)
Textures	
Grain Shape	Orthopyroxene and clinopyroxene crystals vary from anhedral to subhedral, plagioclase crystals were observed to be interstitial with rare fine grained subhedral individual crystals. The opaque minerals are irregular and blebby in shape.
Grain Size	The average rock grain size is coarse and it ranged from fine to coarse grained. Pyroxene range in size from medium to coarse, plagioclase is medium grained and all other minerals present are fine to very fine grained.
Description	Poikilitic texture with olivine enclosed within pyroxene, plagioclase within the opaque minerals and within pyroxene. The plagioclase shows an exsolution texture and a recrystalisation texture is observed from the irregular grain boundaries of most of the minerals. Veins of a fibrous serpentine are present (possible lizardite). The prehnite often forms zones of randomly orientated crystal aggregate.
Alteration	
Description	Pyroxene is altered to chlorite, amphibole and talc, with a dusty appearance in some minerals where alteration is low. Orthopyroxene shows a higher degree of alteration compared to clinopyroxene. Both types are altered preferentially along cleavages and fractures. Plagioclase is extensively altered to clay minerals and talc. The alteration varies from uniform to spotted, starting in the centre of the minerals. Carbonate and prehnite are present as alteration products, where the carbonate material is present the degree of alteration was higher.
Degree	Low – Moderate (30 – 50%)
Fabric	
Description	The crystals were coarse grained and granular. No preferred orientation or fabric was observed.

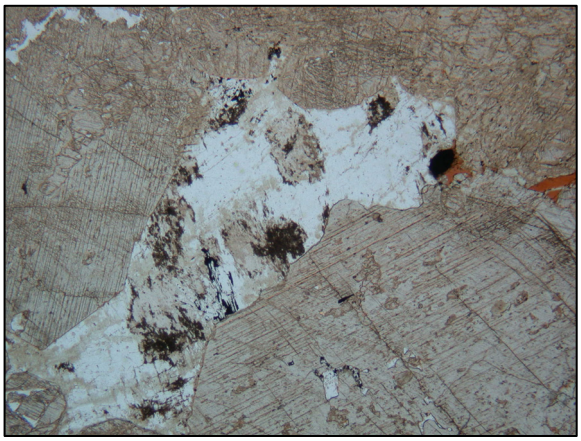

ai Plane polarized light, 7mm crossview

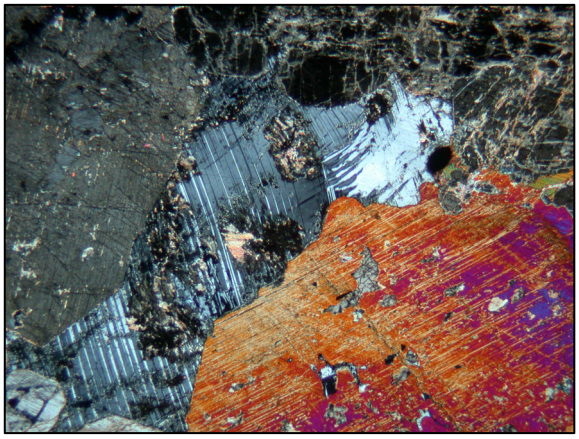

aii Cross polarized light, 7mm crossview

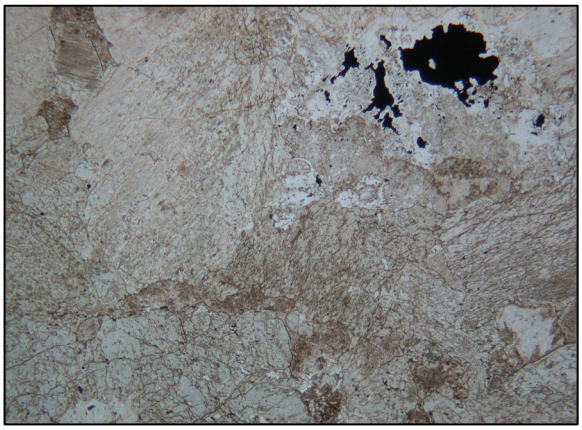

bi Plane polarized light, 7mm crossview

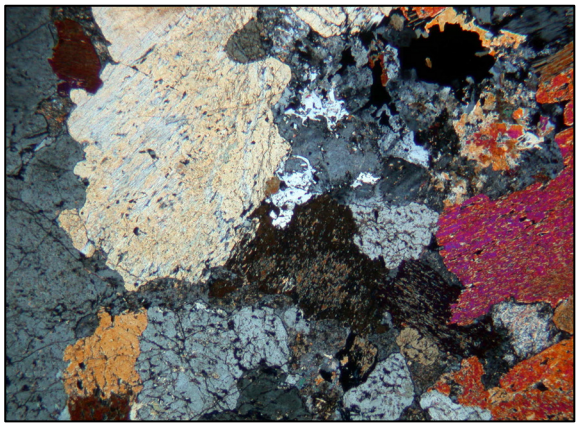

bii Cross polarized light, 7mm crossview

Figure 4.3 Photomicrograph a – b of a feldspathic pyroxenite. **a** Plagioclase crystals are interstitial, show exsolution textures and have spotted alteration. The pyroxene is preferentially altered with orthopyroxene having a higher degree of alteration. **b** A medium to coarse grained feldspathic pyroxenite in which the plagioclase is completely altered. The minerals in this photomicrograph have dusty spotted appearance due to alteration to talc and chlorite.

Table 4.4 Petrographic description of pyroxenite.

Rock Type	Pyroxenite
Mineralogy	
Essential	Orthopyroxene (80 – 88%), Clinopyroxene (5 – 15%), Opaque Minerals (3 – 5%), Calcite (2%) and Prehnite (2%). Amounts are a visual estimate.
Accessory	Biotite, Garnet, Olivine and Muscovite. The total number of accessory minerals counted was less than 26 per thin section.
IUGS Name	Garnet-bearing olivine orthopyroxenite
Colour Index	Ultramafic (mafic index 90 – 100%)
Textures	
Grain Shape	Both orthopyroxene and clinopyroxene are subhedral. The opaque minerals tended to be subhedral to euhedral and all other crystals are anhedral to subhedral.
Grain Size	The average rock grain size is coarse with a range between fine to coarse grained. The pyroxenes are coarse grained and orthopyroxenes are on average greater in size than clinopyroxenes. The opaque minerals are all fine grained.
Description	Poikilitic texture with the opaque minerals enclosed within pyroxene and pyroxene, calcite and opaque minerals ringed by prehnite. A subpoikilitic texture with prehnite partially enclosing calcite is present. Prehnite exhibits a wavy almost radial extinction. Veins of prehnite and calcite are present; occasionally the two are present within the same vein.
Alteration	
Description	Orthopyroxene and clinopyroxene show alteration to chlorite with a dusty speckled appearance however orthopyroxene show a greater alteration. Alteration to amphibole, possible tremolite, and talc is observed in the pyroxene as well. Olivine has a moderate degree of replacement by serpentine. Veins of prehnite are present.
Degree	Low – Moderate (estimated 20 – 50%)
Fabric	
Description	The dominant minerals are pyroxenes which are coarse grained and granular. The opaque minerals show little to no preferred orientation

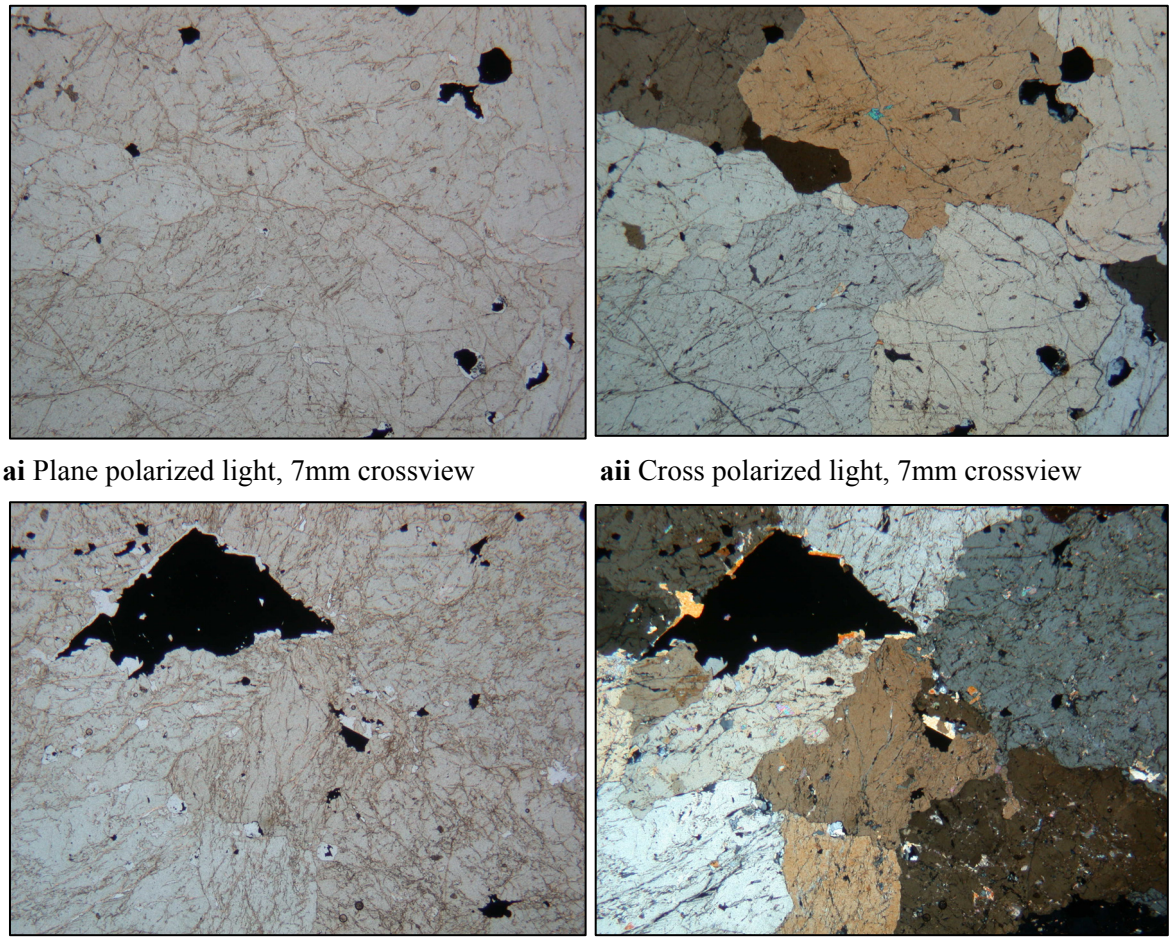

ai Plane polarized light, 7mm crossview

aii Cross polarized light, 7mm crossview

bi Plane polarized light, 7mm crossview

bii Cross polarized light, 7mm crossview

Figure 4.4 Photomicrograph a – b of a pyroxenite. **a** This photomicrograph is dominated by coarse grained orthopyroxene which encloses fine grained opaque minerals and clinopyroxene. **b** A granular coarse grained pyroxenite which exhibits alteration of pyroxene to amphibole and chlorite. In the top left corner there is a medium grained subhedral opaque mineral however the fine grained opaques surrounding it are more common throughout the thin section and for the rock type.

Table 4.5 Petrographic description of parapyroxenite.

Rock Type	Parapyroxenite
Mineralogy	
Essential	Orthopyroxene (20 – 85%), Clinopyroxene (5 – 25%), Olivine (3 – 65%) Calcite (accessory – 4%), Garnet (accessory – 4%), Opaque minerals (2 – 12%), Biotite (accessory – 5%), Chlorite (3%) and Amphibole (accessory – 3%). Amounts are a visual estimate.
Accessory	An unidentified brown mineral and as mentioned above calcite, garnet, biotite and amphibole. The total number of accessory crystals observed is less than 27 per thin section.
IUGS Name	Iherzolite (peridotite type rock)
Colour Index	Ultramafic (mafic index 90 – 100%)
Textures	
Grain Shape	Olivine varies in shape from anhedral to euhedral, orthopyroxene and clinopyroxene are commonly anhedral to subhedral, calcite is present as anhedral and euhedral crystals, garnet is generally subhedral or very irregular, opaque minerals vary from blebby to fine stringers and laths. Biotite, amphibole and chlorite are subhedral with rare euhedral crystals.
Grain Size	The average rock grain size is medium grained with a range from very fine for the opaque minerals and garnet, to medium and coarse grained pyroxene crystals. Olivine is commonly fine to medium grained and rounded.
Description	A poikilitic texture is present with orthopyroxene enclosing olivine, amphibole, clinopyroxene and biotite. Opaque minerals enclose calcite, garnet and olivine in many thin sections. A subpoikilitic texture is present as olivine is partially enclosed by pyroxene. Clinopyroxene is present as interstitial crystals and orthopyroxene often exhibits zoned extinction. Irregular grain boundaries particularly between ortho- and clinopyroxene shows recrystalisation has occurred. Intergrowths of olivine and pyroxene are observed and many grains of pyroxene which enclosed olivine where highly fractured with the fracture radiating out away from the olivine crystals. Olivine is present as individual crystals and as an aggregate; both forms show mesh and hourglass textures resulting from alteration. Opaque mineral are present mainly in the olivine fractures. Veins of carbonate material, fibrous serpentine and opaque minerals are observed in many of the thin sections. Carbonate material is present as whole crystals and as an alteration product. Opaque minerals often linked together forming lacy networks. Biotite is occasionally observed to be kinked.
Alteration	
Description	Olivine crystals are completely altered to serpentine and to a lesser degree to amphibole, carbonate material and talc. Often the serpentinisation appears connected with the

	precipitation of the opaque minerals although there are exceptions. The serpentinisation suggests hydrothermal alteration. Pyroxene crystals often exhibit a dusty speckled appearance resulting from alteration to chlorite, amphibole and talc. Alteration of pyroxene occurs mostly along cleavages and along fractures within the olivine but also along grain boundaries. Orthopyroxene is consistently more altered than clinopyroxene. Pyroxene on the boundary of olivine and carbonate material is more altered at the points of contact between the minerals. Where there is a greater concentration of opaque minerals the alteration is higher. Within a single thin section the alteration across the thin section and between the same minerals varies from extensive to almost unweathered.
Degree	Moderate – High (estimated 50 – 85%). Alteration degree is largely dependent on the amount of olivine and subsequently the amount of serpentinisation the thin section had undergone.
Fabric	
Description	Bands of olivine rich and olivine poor layers are present resulting in bands of high opaque mineral content and zones of high alteration. The fracturing within the olivine and therefore the opaque minerals is often preferentially orientated perpendicular to the length of the borehole core. Veins also commonly exhibited a preferred orientation either perpendicular or parallel to the length of the borehole core.

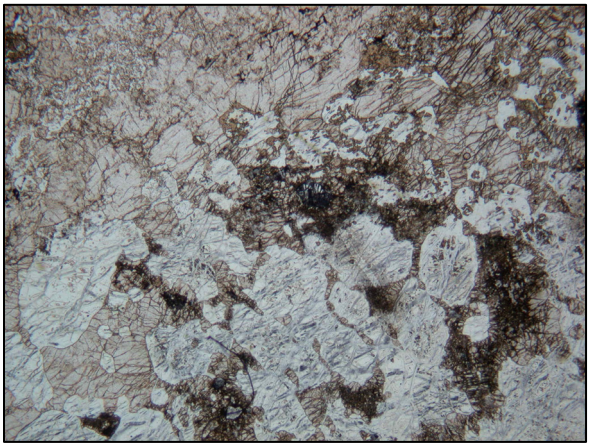

ai Plane polarized light, 7mm crossview

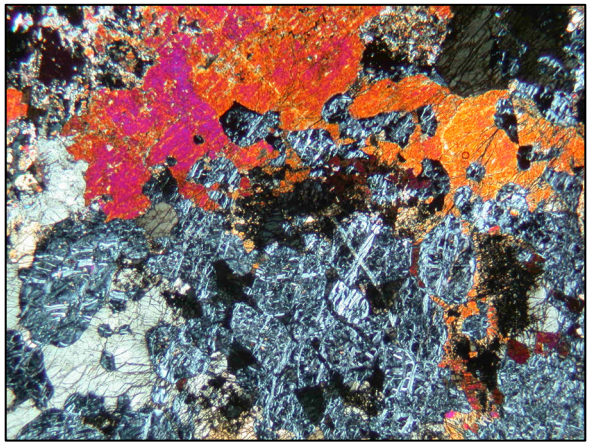

aii Cross polarized light, 7mm crossview

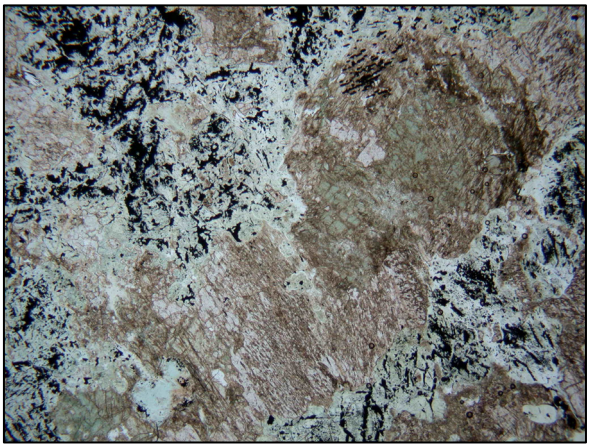

bi Plane polarized light, 7mm crossview

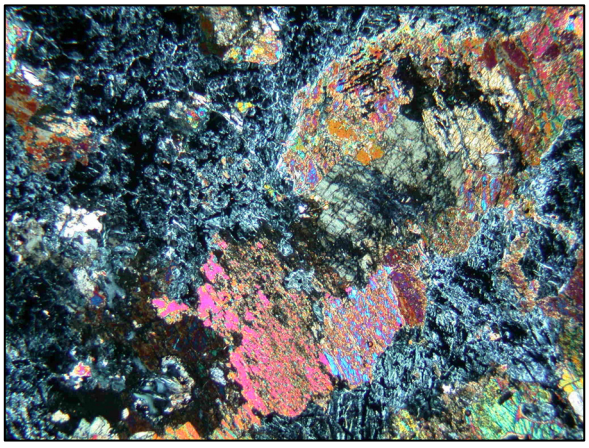

bii Cross polarized light, 7mm crossview

Figure 4.5 Photomicrograph a – b of a parapyroxenite. **a** Fine-grained rounded crystals of completely serpentinised olivine are present, exhibiting distinctive mesh and hourglass textures. Alteration of pyroxene is highest where there is contact between the olivine and pyroxene. **b** A very high degree of alteration in which olivine is entirely serpentinised and there is precipitation of opaque minerals (most probably magnetite) within the olivine. The irregular grain boundaries indicate there has been recrystalisation. Pyroxene exhibits alteration to amphibole, chlorite and talc.

Table 4.6 Petrographic description of serpentinite.

Rock Type	Serpentinite
Mineralogy	
Essential	Opaque minerals (15 – 45%), Pyroxenes (30 – 40%), Olivine (24 – 40%) and Calcite (1%). Amounts are a visual estimate.
Accessory	Amphibole, Rutile and Garnet. Total count of accessory crystals observed was less than 32.
Compositionally defined name	Garnet-bearing serpentinite
Protolith	Metamorphic rock, but principle composition is that of an ultramafic pyroxenite protolith
Textures	
Grain Shape	The crystals of olivine and pyroxene are anhedral to subhedral. Clinopyroxene, when distinguishable, is interstitial. The opaque minerals are either present as a mass interlocking crystals or as fine grained laths.
Grain Size	The average grain size for the rock is fine grained, with a small range from very fine to fine grained. The olivine crystals are very fine grained with the pyroxenes slightly larger

	in size. Calcite, when present, occurs in veins.
Description	A poikilitic texture is observed with olivine enclosing pyroxene. Olivine is present as individual crystals and as an aggregate. All the olivine crystals show mesh and hourglass textures due to alteration. Opaque minerals are present within minerals (mainly olivine) and along grain boundaries. Veinlets of calcite or talc were common, as shown in Figure 4.6 a.
Alteration	
Description	Olivine has been serpentinised extensively which has resulted in the precipitation of magnetite (opaque minerals) following the substitution of Fe^{2+} for Mg, the excess Fe^{2+} was incorporated into the magnetite. The serpentine shows a small degree of alteration to talc. The pyroxenes had been altered to chlorite and exhibit a dusty appearance.
Degree	High (estimated 95%)
Fabric	
Description	Some thin sections showed a preferred orientation of the opaque minerals and veins oblique to roughly perpendicular to the length of the borehole. The opaques were mainly precipitated within the fractures of the olivine, which are aligned and most likely formed in response to a local stress. There is slight banding with opaque-rich and opaque-poor layers.

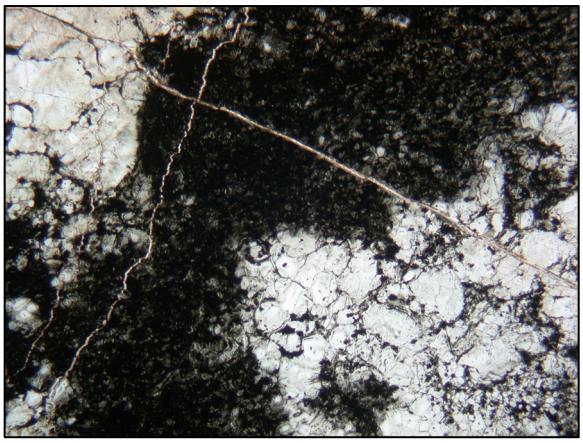

ai Plane polarized light, 7mm crossview

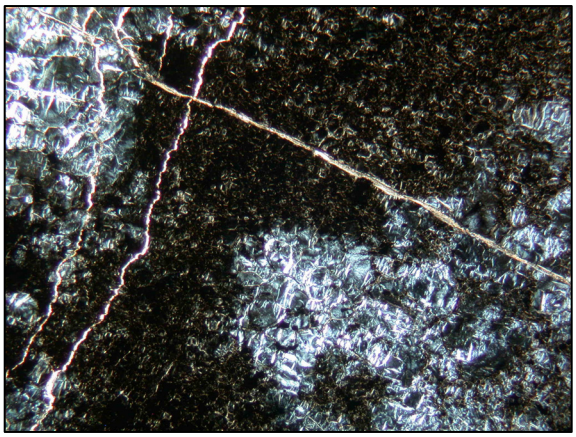

aii Cross polarized light, 7mm crossview

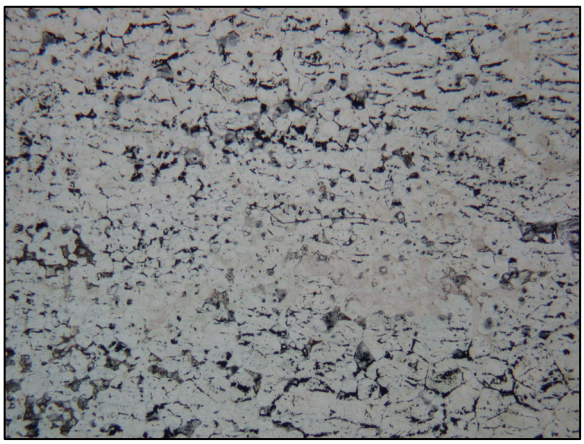

bi Plane polarized light, 7mm crossview

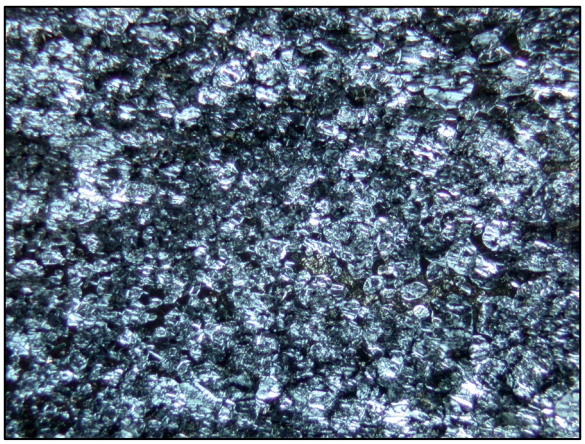

bii Cross polarized light, 7mm crossview

Figure 4.6 Photomicrograph a – b of a serpentinite. **a** This example of a serpentinite is dominated by a massive aggregate of opaque minerals (most likely magnetite). The top left and bottom right corners are of completely serpentinised olivine. Two veins of calcite run perpendicular to each other across the photomicrograph. **b** Very fine grains of olivine and pyroxene. The olivine is extensively serpentinised. Opaque minerals (most likely magnetite) have precipitated within the olivine and along crystal boundaries. The serpentine shows alteration to talc.

Table 4.7 Petrographic description of calc-silicate.

Rock Type	Calc-silicate
Mineralogy	
Essential	Orthopyroxene (15 -25%), Clinopyroxene (5 – 10%), Olivine (10 – 30%), Calcite (10 – 15%), Garnet (2%), Milky white/yellow mineral, possibly hydrogrossular (15 – 38%), Opaque minerals (10%) and Spinel (3%). Amounts are a visual estimate.
Accessory	Biotite. Total count of accessory crystal observed is less than 20 per thin section.
Compositionally defined name	Garnet-spinel-olivine calc-silicate
Protolith	Metamorphic rock, but principle composition is that of a relatively pure carbonate rock of dolomite protolith
Textures	
Grain Shape	The pyroxene crystals are anhedral, with garnet subhedral, spinel euhedral and calcite anhedral to euhedral. Because the milky white/yellow mineral is close to isotropic and is very fine grained its mineral shape could not be determined.
Grain Size	The average rock grain size is fine grained with a range of fine to medium. Olivine, pyroxene and garnet are fine grained. Opaques are fine to medium grained and calcite is medium grained. The milky material is very fine grained forming a matrix type material about the crystals.
Description	All the crystals are heavily fractured, precipitation of the opaque minerals and the milky material occur along fractures and cleavages. Calcite crystals are ringed by serpentine and chlorite. Mesh and hourglass textures in the serpentinised olivine are observed.
Alteration	
Description	Olivine is completely serpentinised and only the remnant shapes of the crystals could be seen. Orthopyroxene and clinopyroxene are altered to chlorite as well as amphibole. Carbonate material is replacing the olivine and there is precipitation of carbonate material and opaque minerals into the fractures of olivine.
Degree	High (estimated 95%)
Fabric	
Description	Bands of orthopyroxene rich and poor layers, with a thickness of approximately 1 cm are observed. The layers poor in orthopyroxene tend to be concentrated with the milky material. The fractures in the olivine show a preferred orientation roughly perpendicular to the long axis of the borehole.

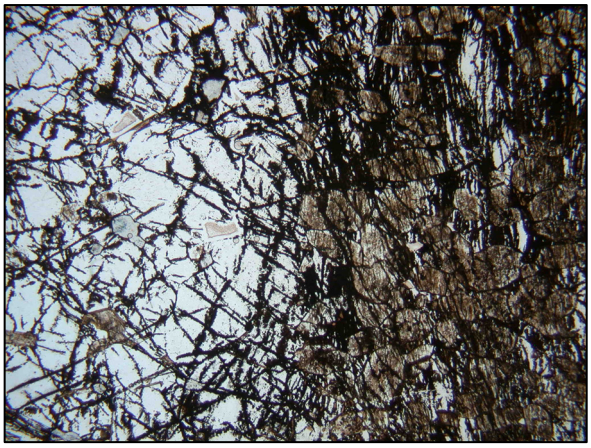

ai Plane polarized light, 7mm crossview

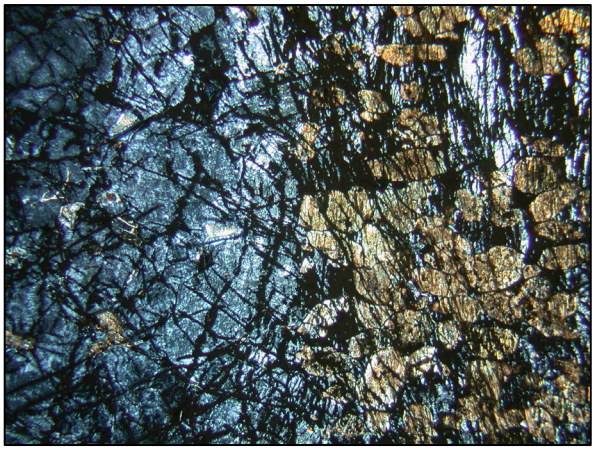

aii Cross polarized light, 7mm crossview

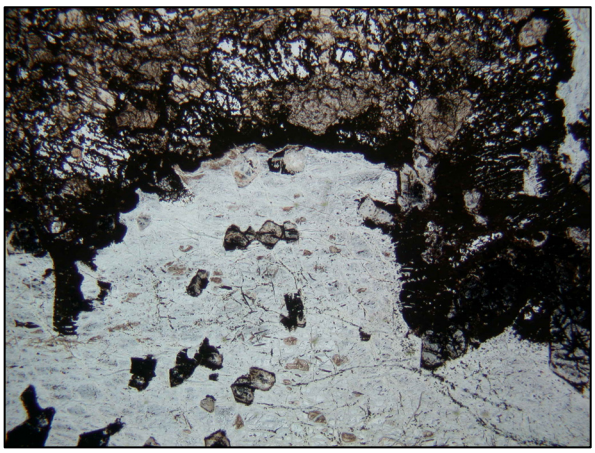

bi Plane polarized light, 7mm crossview

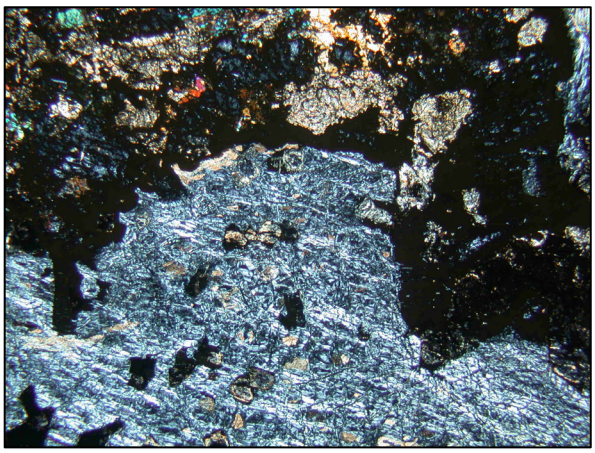

bii Cross polarized light, 7mm crossview

Figure 4.7 Photomicrograph a – b of a calc-silicate rock. **a** Highly fractured calc-silicate in which the precipitation of opaque minerals occurs along fractures and cleavages. The right side of the photomicrographs shows a mass of milky white material (possible hydrogrossular) exhibiting matrix-like properties and appearing almost opaque. **b** Extensively altered olivine and pyroxene. Olivine is present as an aggregate of crystals which is entirely serpentinised and encloses opaque minerals and euhedral grains of spinel. The serpentinisation has occurred along fractures in the olivine and the fractures seem to have a preferred orientation across the aggregate. There is some replacement of olivine with calcite. The pyroxene is extensively altered and the unidentified milky white mass appears almost opaque in plane polarized light.

The results of the XRD testing are given in Table 4.8 – 4.10. These results were used in addition to thin section analysis to aid mineral identification and characterisation of the Sandsloot orebody rock types.

Table 4.8 XRD results for samples SS3/11 – SS4/133 from the orebody at Sandsloot.

Mineral	Composition	Sample Number and Rock Type																																					
		SS3/11 - Fpyx	SS3/69 - Parapyx	SS3/73 - Parapyx	SS3/83 - Parapyx	SS3/100 - Parapyx	SS3/105 - Parapyx	SS3/112 - Parapyx	SS3/151 - Parapyx	SS3/172 - Parapyx	SS3/238 - Parapyx	SS3/270 - Fpyx	SS3/320 - Parapyx	SS3/326 - Parapyx	SS3/347 - Parapyx	SS3/370 - Parapyx	SS3/389 - Parapyx	SS3/413 - Parapyx	SS3/424 - Parapyx	SS3/472 – Calc-sil	SS3/484 - Parapyx	SS3/520 - Parapyx	SS3/525 – Calc-sil	SS3/529 – Calc-sil	SS3/554 - Parapyx	SS3/587 - Parapyx	SS3/607 - Parapyx	SS3/622 - Parapyx	SS3/633 - Parapyx	SS3/664 - Parapyx	SS3/688 - Parapyx	SS4/14 - Parapyx	SS4/36 - Parapyx	SS4/57 - Parapyx	SS4/85 - Parapyx	SS4/93 - Parapyx	SS4/133 - Parapyx
Andradite, syn	$Ca_3Fe_2Si_3O_{12}$	x	x					x	x		x	x	x	x	x	x	x			x	x	x	x	x	x	x	x	x	x	x	x	x			x
Anorthite, sodian, ordered	$(Ca,Na)(Al,Si)_2Si2O_8$	x																	x					x	x	x	x	x	x	x	x						
Calcite, syn	$CaCO_3$																			x		x	x	x	x	x	x	x	x	x	x	x	x		x		
Clinochlore-1MIa, ferroan	$(Mg,Fe,Al)_6(Si,Al)_4O_{10}(OH)_8$						x	x		x		x	x	x	x		x	x			x			x	x	x	x	x	x	x	x		x	x	x	x
Clinochlore-1MIIb, ferrian	$(Mg5Al)(Si,Al)_4O_{10}(OH)_8$	x	x	x	x	x	x	x	x	x	x	x				x		x	x	x		x	x	x	x	x	x	x	x	x	x	x	x	x	x	x	x
Diopside	$CaMgSi_2O_6$	x	x	x	x	x	x	x	x	x	x	x	x	x	x	x	x	x	x	x	x	x	x	x	x	x	x	x	x	x	x	x	x	x	x	x	x
Enstatite, ferroan	$(Mg,Fe)SiO_3$	x	x	x	x	x	x	x	x	x	x	x	x	x	x	x	x	x	x	x	x	x	x	x	x	x	x	x	x	x	x	x	x	x	x	x	x
Felspar	$(Ca,Na)(Al,Si)_2O_8$																																				
Forsterite, ferroan	$(Mg,Fe)_2SiO_4$	x	x	x	x	x	x	x	x	x	x	x	x	x	x	x	x	x	x	x	x	x	x	x	x	x	x	x	x	x	x	x	x	x	x	x	x
Grossular	$Ca_3Al_2Si_3O_{12}$			x	x	x	x	x	x	x	x	x		x	x	x	x	x	x					x	x	x	x	x	x	x	x	x			x		
Lizardite-6T	$Mg_3Si_2O_5(OH)_4$	x	x	x	x	x	x	x	x	x	x	x	x	x	x	x	x	x	x	x	x	x	x	x	x	x	x	x	x	x	x	x	x	x	x	x	x
Mica	$KAl_3Si_3O_{10}(OH)_2$																																				
Monticellite, syn	$CaMgSiO_4$	x	x	x	x	x	x	x	x	x	x	x	x	x	x	x	x	x	x		x	x	x	x	x	x	x	x	x	x	x	x	x	x	x	x	x
Phlogopite-2M1	$KMg_3(Si_3Al)O_{10}(OH)_2$	x	x	x	x	x	x	x	x	x	x	x	x	x	x	x	x	x			x		x	x	x	x	x	x	x	x	x	x	x	x	x	x	x
Phlogopite-3T	$KMg_3(Si_3Al)O_{10}(OH)_2$									x			x	x			x	x	x	x	x	x		x	x	x	x	x	x	x	x		x	x	x	x	x
Prehnite	$Ca_2Al_2Si_3O_{10}(OH)_2$	x		x	x	x	x									x		x	x	x			x	x	x	x	x	x	x	x	x					x		
Talc-2M	$Mg_3Si_4O_{10}(OH)_2$	x	x	x		x	x	x	x	x	x		x		x			x	x	x				x	x	x	x	x	x	x	x	x	x	x		x	x
Tremolite	$Ca_2Mg_5Si_8O_{22}(OH)_2$	x	x	x	x	x	x	x	x	x	x	x	x	x	x	x	x	x	x	x	x	x	x	x	x	x	x	x	x	x	x	x	x	x	x	x	x
Valleriite	$CuFeS_2 1.53((Mg,Al)(OH)_2)$																							x	x	x	x	x	x	x	x						
Vesuvianite, syn	$Ca_{10}Mg_2Al_4(SiO_4)_5(Si_2O_7)_2(OH)_4$	x	x	x	x	x	x	x	x	x	x	x	x	x	x	x	x		x	x	x	x	x	x	x	x	x	x	x	x	x	x	x	x			x
α-Quartz, low	SiO_2											x									x			x	x	x	x	x	x	x	x		x				
Pyrrhotite-3T, syn	Fe_7S_8																							x	x	x	x	x	x	x	x						

Table 4.9 XRD results for samples SS4/166 – SSP154/26 from the orebody at Sandsloot.

Mineral	Composition	Sample Number and Rock Type																																							
		SS4/165 - Parapyx	SS4/187 - Parapyx	SS4/211 - Parapyx	SS4/235 - Fpyx	SS4/247 - Parapyx	SS4/258 - Parapyx	SS4/282 - Parapyx	SS4/292 - Parapyx	SS4/324 - Parapyx	SS5/26 - Parapyx	SS5/44 - Parapyx	SS5/69 - Parapyx	SS5/89 - Parapyx	SS5/108 - Parapyx	SS5/115a - Parapyx	SS5/179 - Parapyx	SS5/199 - Parapyx	SS5/225 - Parapyx	SS5/241 - Parapyx	SS5/290 - Parapyx	SS5/303 - Parapyx	SS5/309 - Parapyx	SS5/314 - Parapyx	SS5/351 - Parapyx	SSP149/5 - Serp	SSP149/12 - Serp	SSP149/15 - Serp	SSP149/16 - Serp	SSP150/1 - Fpyx	SSP150/3 - Fpyx	SSP150/9 - Fpyx	SSP150/17 - Fpyx	SSP150/26 - Fpyx	SSP154/23 - Fpyx	SSP154/24 - Fpyx	SSP154/26 - Fpyx
Andradite, syn	$Ca_3Fe_2Si_3O_{12}$	x		x	x					x		x			x		x	x		x	x	x	x	x											x	x
Anorthite, sodian, ordered	$(Ca,Na)(Al,Si)_2Si2O_8$			x	x		x								x															x	x	x	x	x			
Calcite, syn	$CaCO_3$							x		x			x		x				x	x		x			x					x	x	x		x	x		
Clinochlore-1MIa, ferroan	$(Mg,Fe,Al)_6(Si,Al)_4O_{10}(OH)_8$	x	x	x	x	x	x	x	x	x	x	x	x	x	x	x	x	x	x	x	x	x	x	x	x	x	x	x	x	x	x	x	x		x	x
Clinochlore-1MIIb, ferrian	$(Mg5Al)(Si,Al)_4O_{10}(OH)_8$	x	x	x	x	x	x	x	x	x	x	x	x	x	x	x	x	x	x	x	x	x	x	x	x	x	x	x	x	x	x	x	x	x	x	x
Diopside	$CaMgSi_2O_6$	x	x	x	x	x	x	x	x	x	x	x	x	x	x	x	x	x	x	x	x	x	x	x	x	x	x	x	x	x	x	x	x	x	x	x
Enstatite, ferroan	$(Mg,Fe)SiO_3$	x	x	x	x	x	x	x	x	x	x	x	x	x	x	x	x	x	x	x	x	x	x	x	x	x	x	x	x	x	x	x	x	x	x	x
Felspar	$(Ca,Na)(Al,Si)_2O_8$																																			
Forsterite, ferroan	$(Mg,Fe)_2SiO_4$	x	x	x	x	x	x	x	x	x	x	x	x	x	x	x	x	x	x	x	x	x	x	x	x	x	x	x	x	x	x	x	x	x	x	x
Grossular	$Ca_3Al_2Si_3O_{12}$		x	x	x	x	x		x	x			x	x	x	x	x	x			x		x	x	x	x	x	x	x					x			
Lizardite-6T	$Mg_3Si_2O_5(OH)_4$	x	x	x	x	x	x	x	x	x	x	x	x	x	x	x	x	x	x	x	x	x	x	x	x	x	x	x	x	x	x	x	x	x	x	
Mica	$KAl_3Si_3O_{10}(OH)_2$																																			
Monticellite, syn	$CaMgSiO_4$	x	x	x	x	x	x	x	x	x	x	x	x	x	x	x	x	x	x	x	x	x	x	x	x	x	x	x	x	x	x	x	x	x	x	x
Phlogopite-2M1	$KMg_3(Si_3Al)O_{10}(OH)_2$	x	x	x	x	x	x	x		x	x	x	x	x	x	x	x	x	x	x	x	x	x	x	x	x	x	x	x	x	x	x	x	x	x	x
Phlogopite-3T	$KMg_3(Si_3Al)O_{10}(OH)_2$	x						x	x		x	x	x	x	x	x			x			x			x							x		x	x	x
Prehnite	$Ca_2Al_2Si_3O_{10}(OH)_2$		x	x	x	x	x		x		x			x	x					x						x	x	x	x	x		x	x	x	x	x	x
Talc-2M	$Mg_3Si_4O_{10}(OH)_2$	x	x			x	x	x		x	x	x			x	x	x	x	x		x		x	x		x	x	x	x		x					
Tremolite	$Ca_2Mg_5Si_8O_{22}(OH)_2$	x	x	x	x	x	x	x	x	x	x	x	x	x	x	x	x	x	x	x	x	x	x	x	x	x	x	x	x	x	x	x	x	x	x	x
Valleriite	$CuFeS_21.53((Mg,Al)(OH)_2)$														x																					
Vesuvianite, syn	$Ca_{10}Mg_2Al_4(SiO_4)_5(Si_2O_7)_2(OH)_4$	x	x	x	x	x		x	x	x	x	x	x	x	x	x	x	x	x	x	x	x	x	x	x	x	x	x	x	x	x	x	x	x	x	x
α-Quartz, low	SiO_2														x																				x	x
Pyrrhotite-3T, syn	Fe_7S_8														x																					

Table 4.10 XRD results for samples SSP154/27 – SSP161/24 from the orebody at Sandsloot.

Mineral	Composition	Sample Number and Rock Type														
		SSP154/27 - Pyx	SSP154/29 - Pyx	SSP154/31 - Pyx	SSP154/32 - Pyx	SSP154/34 - Pyx	SSP154/35 - Pyx	SSP154/37 - Pyx	SSP159/27 - Fpyx	SSP159/38 - Fpyx	SSP160/1 - Serp	SSP160/8 - Serp	SSP161/7 - Fpyx	SSP161/15 - Fpyx	SSP161/21 - Fpyx	SSP161/24 - Serp
Andradite, syn	$Ca_3Fe_2Si_3O_{12}$	x	x	x	x	x	x									x
Anorthite, sodian, ordered	$(Ca,Na)(Al,Si)_2Si2O_8$								x	x						x
Calcite, syn	$CaCO_3$							x						x	x	x
Clinochlore-1MIa, ferroan	$(Mg,Fe,Al)_6(Si,Al)_4O_{10}(OH)_8$	x	x	x	x	x	x		x	x	x	x	x	x	x	x
Clinochlore-1MIIb, ferrian	$(Mg5Al)(Si,Al)_4O_{10}(OH)_8$	x	x	x	x	x	x	x	x	x	x	x	x	x	x	x
Diopside	$CaMgSi_2O_6$	x	x	x	x	x	x	x	x	x	x	x	x	x	x	x
Enstatite, ferroan	$(Mg,Fe)SiO_3$	x	x	x	x	x	x	x	x	x	x	x	x	x	x	x
Felspar	$(Ca,Na)(Al,Si)_2O_8$															
Forsterite, ferroan	$(Mg,Fe)_2SiO_4$	x	x	x	x	x	x	x	x	x	x	x	x	x	x	x
Grossular	$Ca_3Al_2Si_3O_{12}$							x	x	x	x	x	x			x
Lizardite-6T	$Mg_3Si_2O_5(OH)_4$		x					x	x	x	x	x	x	x	x	x
Mica	$KAl_3Si_3O_{10}(OH)_2$															
Monticellite, syn	$CaMgSiO_4$	x	x	x	x	x	x	x	x	x	x	x	x	x	x	x
Phlogopite-2M1	$KMg_3(Si_3Al)O_{10}(OH)_2$	x	x	x	x	x	x	x	x	x	x	x	x	x	x	x
Phlogopite-3T	$KMg_3(Si_3Al)O_{10}(OH)_2$	x	x	x	x	x	x	x								x
Prehnite	$Ca_2Al_2Si_3O_{10}(OH)_2$	x	x	x	x	x	x	x	x	x		x	x	x	x	x
Talc-2M	$Mg_3Si_4O_{10}(OH)_2$					x			x	x	x	x	x	x	x	x
Tremolite	$Ca_2Mg_5Si_8O_{22}(OH)_2$	x	x	x	x	x	x	x	x	x	x	x	x	x	x	x
Valleriite	$CuFeS_21.53((Mg,Al)(OH)_2)$															x
Vesuvianite, syn	$Ca_{10}Mg_2Al_4(SiO_4)_5(Si_2O_7)_2(OH)_4$	x	x	x	x	x	x	x	x	x	x	x	x	x	x	x
α-Quartz, low	SiO_2	x		x	x		x									x
Pyrrhotite-3T, syn	Fe_7S_8							x			x					x

4.6 Discussion

Interpretation of the thin section and XRD analyses of the various rock types revealed that the names currently used to describe the rocks of the Sandsloot orebody are general and in some cases inaccurate. Using the standards recommended by the International Union of Geological Sciences Subcommission on the Systmatics of Igneous Rocks (IUGS) (Le Maitre, 1989), which classify igneous rock types according to mineral composition and abundance, it was determined that feldspathic pyroxenite and pyroxenite rock types are more appropriately named gabbronorite and orthopyroxenite respectively, with the qualifiers garnet- and chromite-bearing for the gabbronorites and garnet-bearing olivine for the orthopyroxenites, to indicate the presence of these distinguishing minerals. Parapyroxenite is more accurately named Iherzolite, or olivine websterite, because of the high abundance of olivine and the presence of two pyroxenes. Serpentinite and calc-silicate are both metamorphic rocks and therefore their nomenclature is classified by protolith and distinguishing minerals. The distinguishing minerals are added as a prefix to the name and indicate the metamorphic grade of the rock. Serpentinite and calc-silicate are more exactly named garnet-bearing serpentinite and garnet-spinel-olivine calc-silicate. The term calc-silicate used on its own is in fact misleading because despite the dolomite protolith and remnant bedding structures the estimated proportion of olivine identified was 10 – 30%, which is much higher than that expected in a calc-silicate. Therefore the prefix ‘olivine’ in the name denotes this important variation in composition.

These nomenclature differences are meaningful in the interpretation and understanding of the geological processes which have given rise to the rock types that constitute the orebody. They also highlight the complex geological origins of the orebody material and possible implications for geotechnical and metallurgical strengths. For example garnet, which is present at accessory levels in four of the five orebody rock types, and diopside, a type of clinopyroxene, present in all the orebody rock types, will both increase the difficultly of milling and negatively affect the mill throughput because of their abrasiveness. The difference in naming is important, however, for ease of compatibility the mining terms of feldspathic pyroxenite, pyroxenite, parapyroxenite, serpentinite and calc-silicate will continue to be used in this thesis.

As expected, for rock types which comprise a layered igneous intrusion, the feldspathic pyroxenite, pyroxenite and parapyroxenite are all medium to coarse grained and are dominated by orthopyroxene, clinopyroxene and olivine. Thin section analysis reveals these rock types to have similar accessory minerals but that parapyroxenite has a distinctively more

varied composition compared to the feldspathic pyroxenite and pyroxenite. This could be because the more mafic rock types crystallized out of the magma earlier and/or because of the varying degree of parapyroxenite contamination due to serpentinisation. Serpentinite and calc-silicate are both fine grained, with the serpentinite composition dominated by opaque minerals and olivine; and the calc-silicates composition dominated by an unidentified milky-white almost isotropic mineral (possibly hydrogrossular), pyroxene and on occasion olivine. The differences in grain size may be predicted to impact the intact geotechnical and metallurgical strengths, with finer grained rock types typically having stronger intact strengths. The intact strength will influence the fragmentation of the rock mass, which will affect the processing plant feed size profiles, crusher performance and in particular the mill performance. The relatively homogenous compositions of the feldspathic pyroxenite, pyroxenite and parapyroxenite suggest that the geotechnical and metallurgical performances rock types will resemble one another, whereas serpentinite and calc-silicate rock types may be expected to differ from these three, as well as from one another. It is hoped that these behaviours may be qualified and/or quantified in the investigations of the geotechnical, geochemical and metallurgical properties.

The textures between the five rock types are comparable. Poikilitic and subpoikilitic textures between olivine, orthopyroxene and clinopyroxene, in accordance with Bowens' continuous reaction series, are present in most of the thin sections. Irregular grain boundaries, which indicate recrystallisation, are commonly observed. Recrystallisation commonly results in increased grain size, which may lower the intact strength, although the irregular grain boundaries may add to the strength between crystals and therefore to the overall strength (Brace, 1961). Irregular grain boundaries will also affect the propagation of fractures, which may occur through the crystal or along the boundary between crystals (Hoek, 1965). The ease at which fractures propagate depends on the composition of the mineral, the bonds between the crystal cell units, the bonds between adjacent crystals and the blast energy. Blast energy will determine the primary fragmentation but the degree of micro-fracturing, which will affect the intact strength and the performance in the processing plant will be influenced by the bonds and the grain boundaries. It may be valuable to prepare thin sections from samples that have been strength tested. These thin sections could be used to gauge the effect of recrystalisation on the propagation of fractures, but this is beyond the level of detail for this research. Mesh and hourglass textures of the serpentinised olivine are a distinguishing characteristic of the olivine especially in the parapyroxenite, serpentinite and calc-silicate rock types. Olivine is also frequently observed as individual crystals and as aggregates of crystals. Opaque minerals have been precipitated preferentially along fractures, cleavages and grain boundaries. Veins tend to be infilled with serpentine, carbonate material and prehnite.

The degree of alteration is highly variable from uniform and extensive, to spotted or unaltered. This variation ranges between thin sections of the same rock type, across a single thin section and for the same mineral within a thin section. In general, alteration is highest in the parapyroxenite, serpentinite and calc-silicate and is low to moderate in the feldspathic pyroxenite and pyroxenite. In the context of the orebody stratigraphy, the feldspathic pyroxenites overlie the pyroxenites which in turn overlie the parapyroxenite, serpentinised rock types and the calc-silicates. The latter constitutes the footwall lithology. Therefore the alteration of the orebody rock types appears to increases with proximity to the footwall. Olivine is extensively altered to serpentine in all thin sections, consequently with an increased abundance of olivine there is an increase in the alteration. Serpentinisation suggests hydrothermal alteration, which has resulted in precipitation of opaque minerals, most likely magnetite. This finding corresponds with recently published work by Armitage *et al*. (2002), Harris and Chaumba (2001) and McDonald *et al*. (2005). Alteration products for the rock types are similar with pyroxene altering to chlorite, amphibole and talc, olivine to serpentine and serpentine to talc. Orthopyroxene is consistently more altered than clinopyroxene. The physical properties of serpentine with its fibrous structure and splintery fracture are expected to result in differences in geotechnical and metallurgical properties compared to minerals types with, for example, columnar structure and conchoidal fracture. Therefore with increased serpentinisation of any particular rock type a change in the compressive and tensile strength, the failure type, the grinding properties and the milling properties could be expected.

Neither the feldspathic pyroxenite nor the pyroxenite rock types show any preferred fabric. They are consistently granular and therefore may be expected to behave uniformly in metallurgical and geotechnical conditions and applications. Parapyroxenite regularly displays banding with olivine-rich and olivine-poor layers. These bands correspond with high and low serpentinised layers respectively and therefore corresponded with opaque-rich and poor layers. The olivine is highly fractured which is typical of this mineral. The fractures show a preferred orientation between 45˚ - 90˚ to the long axis of the drill hole core. This fabric coupled with the presence of the fibrous serpentine represents a degree of anisotropy within the rock, which is likely to have an appreciable affect on the rocks' strength and other physical properties. Both serpentinite and calc-silicate exhibit the same preferred orientation of serpentine minerals and fractures in the olivine, therefore their strengths could similarly be affected.

The XRD results reflect the observed mineralogy for all the rock types well, with one exception. The results did not pick up the presence of the green spinel which is common in many of the parapyroxenite thin sections and in some of the calc-silicate thin sections. Overall

the XRD results were an effective gauge of the mineral composition of the rock types. However, by using this method of investigation on its own it is not possible to distinguish any textural and fabric features or the degree of alteration of a rock type. Therefore the potential influence of these properties on the performance of rock cannot be assessed.

4.7 Summary and Conclusions

In this chapter the characteristics of the orebody rock types were assessed using thin section and XRD analysis. The study of the minerals revealed the rock names used to describe the orebody are simplified and do not lend themselves to either the accurate interpretation of the complex geological processes which gave rise to the rock types or the assessment of the rock properties. The petrographic classification for feldspathic pyroxenite is garnet – chromite – bearing gabbronorite. Pyroxenite is classified garnet – bearing olivine orthopyroxenite. Parapyroxenite is classified Iherzolite or olivine websterite. Serpentine is classified garnet – bearing serpentine and calc-silicate is classified garnet – spinel – olivine calc-silicate. The difference in naming highlights possible negative implications for geotechnical and metallurgical strengths, milling and plant throughput. For instance both garnet and diopside indicate a potential negative impact on the effectiveness of processing. Though these naming differences are important it is reiterated that the mining terms of feldspathic pyroxenite, pyroxenite, parapyroxenite, serpentinite and calc-silicate will be used in this thesis, for ease of compatibility.

Composition and microscopic analysis of properties such as grain size, textures, alteration and fabric reveal characteristics upon which the orebody rock types can be differentiated. Composition clearly distinguishes each rock type however, similarities between mineral type and abundance indicate that feldspathic pyroxenite, pyroxenite and parapyroxenite are more similar to one another than they are to either serpentinite or calc-silicate. Composition also distinguishes the variability of parapyroxenite. Grain size likewise separates feldspathic pyroxenite, pyroxenite and parapyroxenite from serpentinite and calc-silicate. The degree of alteration and presence of a weak fabric distinguish feldspathic pyroxenite and pyroxenite from serpentinite and calc-silicate. Once more parapyroxenite is distinguished from the other rock types due to its variability in alteration and irregular presence of fabric. Texture is the only property studied that does not identify any particular rock type. These differences between orebody rock types are anticipated to influence the geotechnical, geochemical and metallurgical strengths and properties, which will in turn influence the mining and milling qualities. It is therefore expected that the basic similarities and relationships identified in this investigation will be reflected in the results of the following investigations.

Because the XRD analysis on the whole was an effective gauge of the minerals within the rocks, this analysis may be judged as sufficient for general purposes of prediction of rock mass mineral properties. However, it is recommended that thin section analysis also be performed before new mining areas are put into production. Thin section work will provide a check on the accuracy of the XRD results and will provide relevant data regarding rock properties, such at alteration, textures and fabrics, which influence the mining strengths and processing properties of the orebody.

Chapter 5

GEOTECHNICAL INVESTIGATION

5.1 Introduction

Knowledge of an orebodies' geotechnical properties can be used for more than the design and design optimisation of an open pit or underground mine. Inherent properties of strength, ultrasonic velocity and density will influence the Blastability Index (Lilly, 1986) of a rock mass and will impact on the drill and blast practices and resultant fragmentation. In turn, fragmentation will influence the loading, crushing and milling rates and ultimately the processing plant throughput. Furthermore, geotechnical data may be used in combination with the geochemical and metallurgical properties to characterise the orebody and predict mining properties.

This chapter investigates the geotechnical properties of density, ultrasonic velocity and strength of the Sandsloot orebody rock types. It focuses on the variability of the properties, the relationships between the properties and their use in the prediction of mining conditions. The strengths that will be considered include the uniaxial compressive strength, the Brazilian disc tensile strength and point load diametral and axial index strengths. The point load index strengths will also be compared to those being used on the mine. This chapter will characterise the rock mass from which the test specimens were sampled, based on lithological, geotechnical and structural logging of diamond drill core. In addition, this chapter will introduce the statistical methods that are used to assess the geotechnical data, as well as the data in subsequent chapters.

5.2 Methods of Investigation

5.2.1 Drill Hole Logging

Before sample preparation and testing began ten diamond drill hole cores were logged according to:

- Lithological boundaries, using crystal size, visible changes in the mineral composition and textures to mark divisions.
- Geotechnical intervals which characterised each rock type, by dividing the core into groups of similar weathering, alteration, hardness, joint spacing, joint conditions and structural features. Lithological boundaries were adhered to in the determination of the geotechnical intervals and intervals less than one metre were incorporated into the surrounding intervals as it is believed that the influence of such small changes is unlikely to be significant to the geotechnical assessment of the rock mass.

Parameters needed to calculate Bieniawski's (1989) RMR were also recorded.

The standards set out by the Core Logging Committee of the South Africa Section of the Association of Engineering Geologists (1979) were used in the logging and discontinuity descriptions. Roughness and joint spacing were determined using the guidelines by Bieniawski (1989). A Corstor - 168 colour chart was used for the colour descriptions. Fracture frequency (FF/m) and rock quality designation (RQD) were determined against the drillers log, at three metre intervals and against the geotechnical intervals for lithological and geotechnical logging, respectively.

Only BQ (36mm) core was available from Potgietersrust Platinums (PPRust) for testing. In accordance with Nickson *et al.* (1996) a threshold value of 75mm for RQD was used in place of the standard 100 mm threshold value. The 100mm standard is derived from the original concept of RQD, based on NQ (47.6mm) size core, with a threshold of roughly twice the core diameter. The adjusted threshold allows sensitivity for drilling and handling conditions, especially in the case of smaller diameter core.

5.2.2 Laboratory Testing

5.2.2.1 Moisture Content and Porosity

The presence of free water within a sample tends to decrease the strength of the rock, provided re-cementation of the sample composition does not occur. When reporting the results of any geotechnical test it is important to report the water content and degree of saturation of the samples at the time of testing, for accurate analysis and interpretation of results later. Knowledge of the porosity of a sample is equally important as it has a significant effect on the mechanical performance of a sample and correlates to the density of the sample (ISRM, 1981).

A sample with a high porosity will have a lower strength and a higher deformability versus a sample with a low porosity. Moisture content was calculated using equation 5.2.1 and porosity was calculated using equations 5.2.2 and 5.2.3.

$$\textbf{Moisture content (M\%)} = (M_w / M_s) * 100$$

Eqn 5.2.1

Where M_w = mass of water (kg)

M_s = mass of sample (kg)

$$\textbf{Porosity (n \%)} = (100V_v) / V$$

Eqn 5.2.2

Where V = bulk sample volume (m^3)

and

$$\textbf{Volume of voids } (V_v) = (M_{sat} - M_s) / \rho_w$$

Eqn 5.2.3

where M_{sat} = saturated mass of the sample (kg)

M_s = dry mass of the sample (kg)

ρ_w = 1000 kg / m^3

5.2.2.2 Density

Density is defined as a material's mass per unit volume at a specific temperature and can be used as a means to determine composition change within the core and therefore detect subtle changes in rock type. Density is a function of both mineral composition as well as volume void space (Bell, 1992). For this research project it has been studied as an indicator of mineral changes down the drill hole core and as a material constant to characterise different rock types. It was determined by dividing the dry weight of a sample by the difference between its mass in air and its mass in water using equation 5.2.4, using the standard in-house buoyancy method as referred to in Bell (1993).

$$\textbf{Density} = \textbf{(weight in air (g))/ (weight in air (g) – weight in water (g))}$$

Eqn 5.2.4

5.2.2.3 Ultrasonic Velocity

Ultrasonic velocity tests are used to determine the velocity with which elastic stress waves are transmitted through rock. The velocity depends on the density and the elastic properties of the material and hence by calculating the velocity theoretically the degree of fissuring within rock specimens can be determined (Goodman, 1989). A Portable Ultrasonic Non-destructive Digital Indicating Tester (PUNDIT) machine, using a 54 kHz ultrasonic pulse was used to determine the ultrasonic velocity values down the drill hole core, with mineral changes (Figure 5.1). Due to limitations on the apparatus shear wave properties could not be determined. The velocity of the wave moving through the core was calculated using equation 5.2.5.

$$\textbf{Velocity (m/s)} = \textbf{l / t}$$

Eqn 5.2.5

where l = length of sample (m)

t = amount of time it took for the wave to pass through the sample (sec)

Figure 5.1 PUNDIT apparatus used for ultrasonic velocity determinations.

5.2.2.4 Point Load Testing

This test was developed as a rapid field test of a rock specimen's Strength Index and Strength Anisotropy Index. These two properties correlate to the uniaxial compressive and tensile strength of a rock specimen and can be used to determine and classify the strength of rock material (ISRM, 1981). Specimens were loaded diametrally and axially, using the apparatus in Figure 5.2. However, random orientation testing could not be undertaken due to the shape and size of the drill hole core. The maximum load (P) at failure was recorded and samples studied to determine the mode of failure and to record any relevant observations. Using equations 5.2.6

– 5.2.10 the point load axial and diametral index strengths were determined according to the ISRM (1981) standard procedures.

$$\mathbf{T_p\ (MPa) = P / D^2}$$

Eqn 5.2.6

Where T_p = the tensile strength (MPa) = I_s (the uncorrected point load strength)

P = load at failure (kN)

D = diameter of the specimen (m)

and where

$$\mathbf{D^2 = D_c^2}\ \text{for the diametral test}$$

D_c^2 = test dependent method for determining the sample diameter

and

$$\mathbf{D_c^2 = 4\ A/\ \pi}\ \text{for the axial test}$$

Eqn 5.2.7

where

$$\mathbf{Area\ (A) = W*D}$$

Eqn 5.2.8

and W = smallest specimen width

$$\mathbf{Is_{(50)}\ (MPa) = F*I_s}$$

Eqn 5.2.9

where $Is_{(50)}$ = point load strength at 50 mm diameter (MPa)

F = the size correction factor

$$\mathbf{F = (D_c / 50)^{0.45}}$$

Eqn 5.2.10

In addition the point load strength anisotropy index was calculated and the equivalent uniaxial compressive strength results were determined using the correlation table in Bell (1993).

Figure 5.2 Point load apparatus.

5.2.2.5 Brazilian Disc Test

The Brazilian Disc Test measures the tensile strength of a rock specimen indirectly by creating a biaxial stress field in which one principal stress is tensile and the other is compressive, with a magnitude less than three times that of the tensile principal stress (ISRM, 1981). The load is applied perpendicular to the diameter of the sample and the maximum load at failure (P) is recorded (Figure 5.3). After each test was completed the failed specimens were studied to determine the mode of failure and to record any relevant observations. The tensile strength was calculated using the equation 5.2.11.

$$\mathbf{T_b\,(MPa) = (2P) / (\pi)(D*L)}$$

Eqn 5.2.11

Where P = load at failure (kN)

D = diameter of the test specimen (m)

L = the length of the test specimen (m)

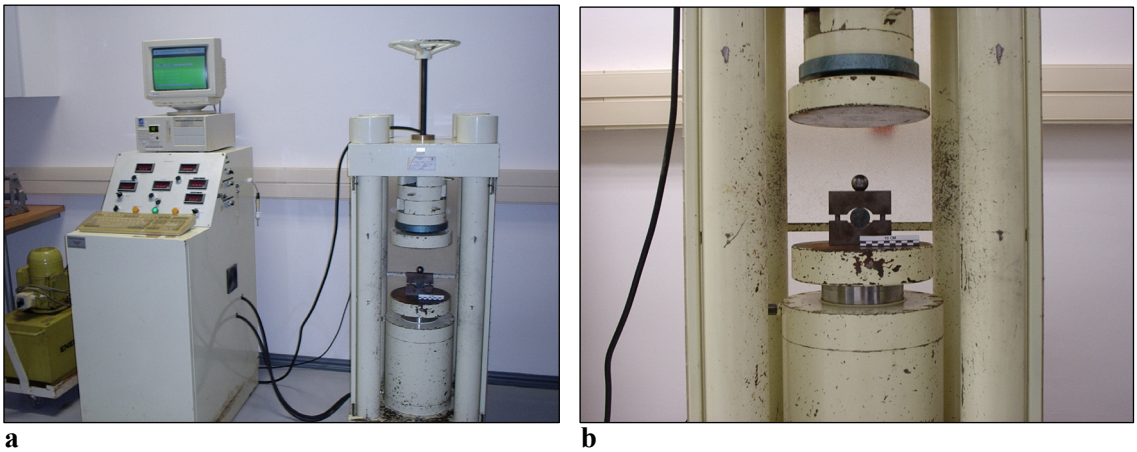

a **b**

Figure 5.3 a The Relsma Universal Compression - Tension soft testing machine with Brazilian disc sample, before testing. **b** Close up of apparatus, Brazilian disc jaws and test sample.

A tensile strength to compressive strength ratio of 1:8 is suggested by ISRM (1981) and between 1:15 and 1:25 is suggested by Bell (1993). This relationship will not be investigated in this study because it is a comparison between uniaxial tensile strength and uniaxial compressive strength, and the Brazilian disc tensile strength is an indirect measure of tensile strength.

5.2.2.6 Unconfined Compressive Strength (UCS) Testing

Uniaxial compressive strength (UCS) is a measure of the maximum load or unidirectional stress a rock specimen can withstand before it fails. The test is used for the classification and characterisation of intact rock strength when subjected to a confining force in one direction (ISRM, 1981). For the test, specimens were subjected to an applied load perpendicular to the long axis of the sample and the maximum load (P) at failure was recorded, according to the standard ISRM (1981) procedures (Figure 5.4). After failure the rock specimens were studied to determine the mode of failure and to record any relevant observations. Equation 5.2.12 was used to calculate the uniaxial compressive strength.

$$\textbf{UCS (MPa) = max load (kN) / original cross-sectional area of specimen (m}^2\textbf{)}$$

Eqn 5.2.12

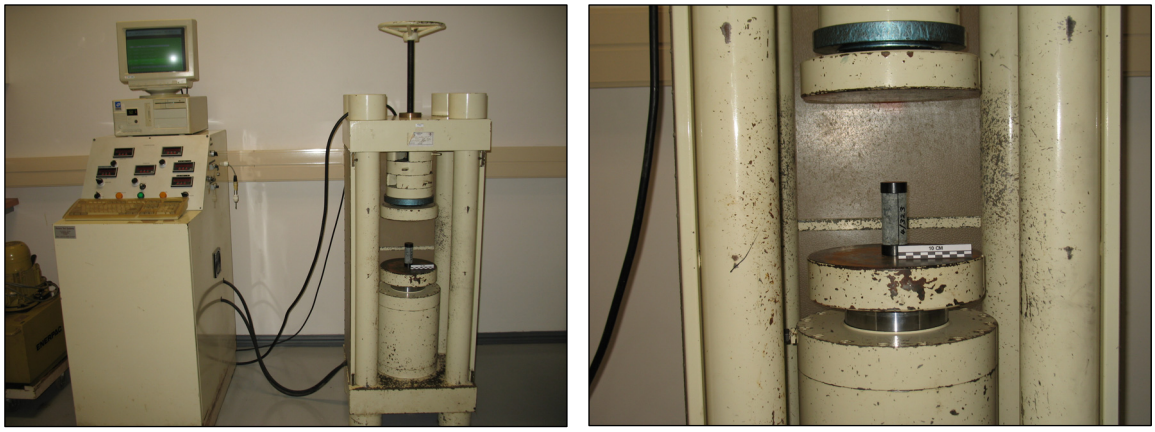

a **b**

Figure 5.4 a The Relsma Universal Compression - Tension soft testing machine, with UCS sample before testing. **b** Close up of UCS sample with test platons.

The compressive strength to the tensile strength ratio has been determined in previous studies, with approximate ratios of 1:8 (ISRM, 1981) and between 1:15 and 1:25 (Bell, 1993). For this research, however, the ratio will not be considered because the method of Brazilian disc tensile strength determination is an indirect tensile strength determination.

5.3 Sample Selection and Preparation

Representative samples of the five orebody rock types were selected for testing from the diamond drill hole core provided by PPRust. Samples for the different geotechnical tests were selected from positions close to or adjacent to one another, as shown in Chapter 4, Figure 4.2. Therefore the results between tests could be related. Samples with visible discontinuities were not tested, to minimize the chance of attaining invalid test results. The samples were cut and prepared according to the suggested methods laid out by the ISRM (1981) standard procedures. All samples were cut perpendicular to the length of the core. Freshly cut surfaces were smooth and were without uneven ridges or chips. The angle of the surface did not depart more than 0.05° from the perpendicular. The samples used for ultrasonic velocity and uniaxial compressive strength testing were then ground flat to 0.002 mm, (ISRM, 1981). The dimensions to which the cores were cut were:

- 1.5:1 (L/D) ratio for all moisture content and porosity samples
- 1:1 (L/D) ratio for all the point load diametrical samples
- 0.5:1 (L/D) ratio for all the point load axial and Brazilian disc samples

- 2:1 length to diameter (L/D) ratio for all the UCS samples

5.4 Testing Procedures

Procedures and apparatus specifications for each test conformed to the standards required by ISRM (1981). The in-house test procedures are detailed in Appendix C. The Relsma Universal Compression - Tension soft testing machine and the point load apparatus were both calibrated before testing began.

5.5 Results and Analysis

Localities of the diamond drill holes sampled for laboratory testing are shown in Figure 4.1, Chapter 4. These drill holes were logged lithologically and for basic geotechnical properties of recovery, rock quality designation (RQD), fracture frequency per metre (FF/m), estimated hardness and weathering. The logs for these drill holes are recorded in Appendix A and a summary is presented by rock type in Table 5.1. Detailed discontinuity logs were recorded for three of the drill holes. The logs detail joint dip, relative dip direction, joint spacing and joint surface conditions such as infill type, infill thickness, surface roughness and planarity for each of the drill holes and are included in Appendix A. Requirements for assay sampling by PPRust site personnel and time constraints on site meant the remaining drill holes could not be logged at this level of detail.

Table 5.1 Summarised geotechnical properties for the rock mass represented by the drill core logged and laboratory tested.

Rock Type		No core	Fpyx	Pyx	Parapyx	Serp	Calc-sil	Qzfs	Norite
No. of Intervals		10	17	12	72	8	4	2	2
Intervals Length (m) summed		28.00	34.00	65.24	249.39	6.07	8.00	1.04	51.88
Recovery (%)	Avg.	-	98	97	96	96	99	63	100
	Range	-	70 - 100	70 - 100	79 - 100	83 - 100	96 - 100	26 - 100	100 - 100
RQD (%)	Avg.	-	85	92	86	91	85	60	98
	Range	-	42 - 98	59 - 97	0 - 100	82 - 94	52 - 100	20 - 100	96 - 98
FF/m	Avg.	-	2.3	2.4	4.3	4.2	2.6	0	0.9
	Range	-	0 - 4	1- 4	0 - 20	2 - 5	0 - 4	0 - 0	0 - 1
Estimated Hardness*	Avg.	-	R5	R5	R5	R5	R5	R5	R5
	Range	-	R5 - R5	R5 - R5	R5 - R5	R4 - R5	R4 - R5	R4 - R5	R5 - R5
Weathering	Avg.	-	F †	F	F	F	F	MW †	F
	Range	-	F - F	F - F	F – SW †	F - F	F - 2	F - MW	F - F

* using the ISRM R0 – R6 standards, †F: fresh, SW: slightly weathered, MW: medium weathered

Joints were typically slightly rough (Bieniawski 1989), with an infilling of either calcite or serpentine and an infilling thickness of less than 2 mm. The typical dip of the joints ranged between 60 and 80 degrees, and although the relative dip directions were plotted onto a stereonet using the RocScience DIPS™ program, no joint sets were distinguishable. Bieniawski (1989) RMR classification of the rock mass, using the assumption that the rock mass would be free draining due to the mining and an average joint spacing based on work by Bye (2003), catagorised the rock mass as typically "Good Rock" (RMR: 61 – 80).

The results of the laboratory testing were assembled into a database, grouping together sample density and ultrasonic velocity results with the corresponding point load, Brazilian disc or uniaxial compressive strength results. The database further grouped the data according to the drill hole from which the sample came from, the sample depth and the rock type. Using the database, analysis and interpretation of the results were carried out with the *Statgraphics Centurion XV* statistical program. The database in conjunction with *Statgraphics* proved to be a powerful tool with which multi-level queries could be defined and interrogated for relationships and correlations.

Results Layout

The results are presented in two forms. Firstly, in a table of summary statistics, which characterises the parameters of the sample population and defines the essential descriptives. These values predict the geotechnical properties that may be expected per rock type. The second is as a box and whisker plot which is graphical display of these population characteristics. This format for presenting the laboratory results is followed throughout this chapter as well as in the geochemical and metallurgical investigation chapters.

The box and whisker plot, first described by Turkey in nineteen seventy-seven, (Swan and Sandilands, 1995) has been chosen as it is an uncomplicated yet highly informative graph. It is especially good in the comparison of two or more samples when establishing similarities or differences. The primary statistical values of a sample population/ data set are represented by:

- a *box* which defines the main body of the data, where fifty percent of the data values fall (Figure 5.5)
- *lines* 'whiskers' from the box which indicate the tails of the distribution
- *point* symbols which represent the outside or anomalous values in the population (Swan and Sandilands, 1995).

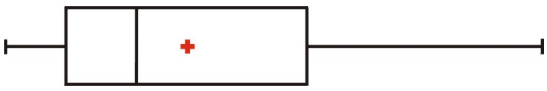

Figure 5.5 Asymmetrical box and whisker plot.

A further six population variables are illustrated by the box and whisker plot.

- the 'hinges' which define the upper and lower quartile statistics of the population.
- the median (middle value), which is the line inside the box
- the sample mean (average), identified by the plus sign in the box
- the maximum and minimum, indicated by ends of the whiskers
- an approximate of the population distribution
- the dispersion of a population

If outside points, which are anomalous values that fall more than 1.5 times the interquartile range (the box width) outside the box, exist within the data set then the ends of the whiskers extend to the maximum and minimum values that are not outside points. Far outside points or outliers are values that fall more than 3 times the interquartile range outside the box and are displayed as points beyond the ends of the whiskers with plus signs in them. In the purest statistical analyses such outliers are removed from the database and the procedures re-run. However, due to the inherent variability of geological data and the lack of an adequate body of general theory about the nature of geological populations, sticking strictly to pure statistical procedures may produce a biased database with a false precision (Davis, 1986). Therefore where there was no apparent cause for the outlier, evidence of human error or incorrect testing procedure, the outliers have been kept in the database to show the true variability of the property being studied.

In addition to displaying the population descriptives the box and whisker plot shows an approximation of the population distribution. If the data is normally distributed the mean, median and mode roughly coincide and the box and whisker plots show the mean and median close together (Figure 5.6 a). If the data is skewed (non-normal) either positively or negatively the median will fall to the far left or right of the mean respectively (Figure 5.6 b). If outside points are present in the data set they may weigh the box and whisker plot, causing the distribution to appear non-normal. A statistical analysis for normality must be performed as a box and whisker plot must not be relied upon as an accurate method for determining normality.

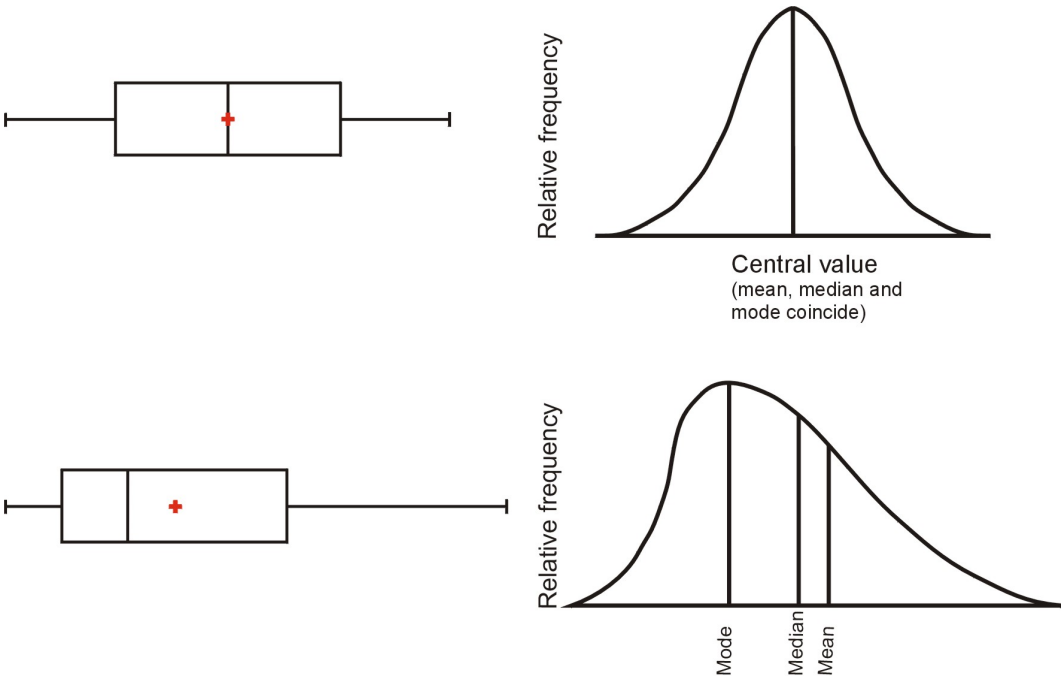

Figure 5.6 a Box and whisker plot for a normally distributed population and corresponding distribution curve. **b** Box and whisker plot for a population with a non-normal distribution (positive skew) and corresponding distribution curve, modified after Davis (1986).

The dispersion of the sample population may also be assessed from this plot as a narrow box indicates a narrow sample dispersion about the mean and a likewise a wide box indicates a wide population dispersion.

Analysis Layout

The analysis of the laboratory results was performed using a number of statistical tests. These tests are described below and like the presentation of the results, the layout and types of analyses used in this chapter are used in the geochemical and the metallurgical investigation chapters. Where a statistical procedure is used uniquely in an investigation it will be discussed where first mentioned.

- The Chi-squared (χ^2) test for normality (Davis, 1986). The χ^2 test is used as a measure of 'goodness of fit' to determine if the data set in question fits a normal distribution. This test is imperative in the initial analysis of the data as the choice of subsequent statistical testing procedures, parametric or non-parametric, is based on the property of population distribution.

- The One way analysis of variance (ANOVA) (Davis, 1986). This test is a parametric analysis, applied to determine how groups of observations compare and used to establish the significance of the similarities or differences between the groups. The groups in this study are rock types or drill holes.
- Duncan's multiple range test (Statpoint, 2005) compares the means between different sets, and sorts them into homogenous groups in which there are no significant differences. The results of the Duncan's Multiple Range analysis are presented in a table that visually groups together the rock types or drill holes per test type that are expected to have statistically similar geotechnical properties.

All statistical analyses in this chapter, as well as those on the geochemical and metallurgical investigations chapters, were performed at a confidence level of 95% (C.I. 95%).

On a note regarding the statistical analysis of data sets; it is important to establish the type of distribution a data set possesses as it is this characteristic that determines whether parametric or non-parametric statistical procedures must be applied during analysis. The difference between using parametric or non-parametric statistics is the use of the sample mean (average) or median (middle value), respectively, as a basis of comparison within and between populations/ data sets (Davis, 1986). By using the mean it is assumed that the mean, median and mode approximately coincide, producing a normal distribution. Therefore a fundamental assumption for all parametric statistical procedures is that the data to which the tests are being applied is normally distributed. Non-parametric statistical procedures on the other hand do not assume normality. These tests instead do not specify any conditions about the population distribution and rank the data, using the median for comparison. Therefore these statistical procedures are less sensitive to outside points, which are likely the cause of skewed/non-normal distribution, but are less rigorous and therefore are not the preferred choice for analysis. If parametric statistics are applied to non-normally distributed data the underlying assumptions of the test are violated and the results are not a true reflection of the population properties. Therefore when subjecting any data set to further analysis, regardless of whether the analysis includes interrogation of similarities and differences or model building through correlations and regressions the choice of statistical procedures will influence the results.

The following results section will cover the basic summary statistics for each of the tests performed, together with a brief analysis and classification of the results. In addition the sample population distributions are discussed, establishing whether the use of parametric or non-

parametric statistical procedures are most appropriate and thereafter the variance and homogeneity within and between data sets are examined.

5.5.1 Moisture Content and Porosity

All specimens tested for moisture content (M %) and porosity (n %) were crystalline unweathered samples of the five rock types: feldspathic pyroxenite, pyroxenite, parapyroxenite, serpentinite and calc-silicate.

Table 5.2 Results of moisture content and porosity determination.

Rock Type	Moisture Content (%)				Porosity (%)			
	Avg.	Min	Max	Standard dev.	Avg.	Min	Max	Standard dev.
Fpyx	**0.04**	0.00	0.14	0.05	**0.53**	0.43	0.62	0.08
Pyx	**0.05**	0.00	0.11	0.05	**0.39**	0.13	0.68	0.24
Parapyx	**0.15**	0.00	0.56	0.18	**0.59**	0.34	0.71	0.17
Serp	**0.14**	0.07	0.30	0.08	**0.77**	0.71	0.82	0.05
Calc-sil	**0.15**	0.10	0.14	0.06	**0.88**	0.63	1.14	0.22

Table 5.3 Porosity classifications, modified after Anon., 1970.

Class	Porosity (%)	Description
1	Over 30	Very High
2	30 - 15	High
3	15 - 5	Medium
4	5 – 1	Low
5	Less than 1	Very low

Moisture content (M %) tests showed the specimens of each rock type had very little free water within the rock, with an average M % of less than 0.2 % and a range between 0.00 % and 0.56 % (Table 5.2). Results from the porosity (n %) tests indicated the average n % for all the rock types is less than 1% which is classified as “very low” (Anon., 1970) (Table 5.3).

Due to the “very low” porosity, the low moisture content and the high crystallinity of each sample the moisture content of the material was considered in equilibrium with the environment in which it was tested. Therefore oven drying each sample before geotechnical testing was not regarded as necessary. Furthermore saturated samples were not used in any geotechnical testing because the porosity tests revealed that saturation was unlikely to have a significant effect on both the compressive and tensile strength.

Further statistical analyses on the results of moisture content and porosity test results were not performed as the effect of drying or saturating the samples was negligible.

5.5.2 Density

The results for the density testing are tabled in Table 5.4. Included amongst the density tests for the orebody rock types are the results for six quartz-feldspathic samples. These samples came from a large vein in drill hole SSMet 3. All the samples tested were included in the data set.

Table 5.4 Results of density (g/cm^3) testing.

Rock Type	Count	Avg.	Median	Standard dev.	Min	Max	Range	Interquartile range
Fpyx	181	**3.13**	3.13	0.07	2.81	3.28	0.47	0.11
Pyx	82	**3.30**	3.32	0.06	3.10	3.37	0.27	0.05
Parapyx	1359	**3.08**	3.08	0.13	2.69	3.37	0.68	0.22
Serp	64	**2.78**	2.73	0.16	2.56	3.24	0.67	0.10
Calc-sil	87	**3.00**	2.93	0.20	2.65	3.32	0.66	0.42
Qzfd	6	**3.15**	3.19	0.08	3.03	3.25	0.21	0.15
Total	1779	**3.08**	3.09	0.15	2.56	3.37	0.80	0.23

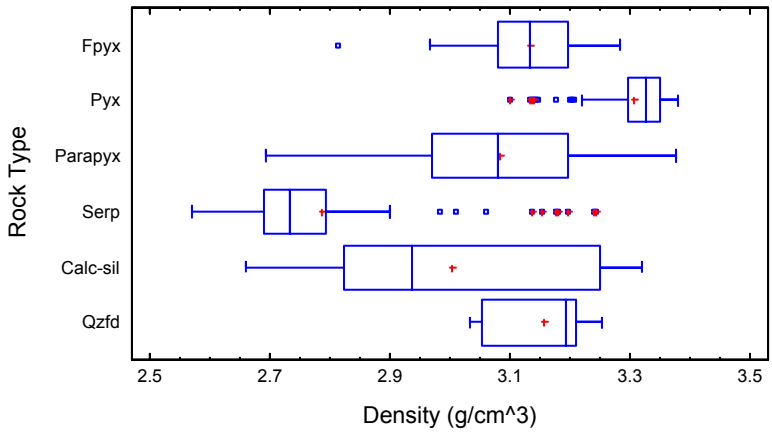

Figure 5.7 Box and whisker plot for density for each rock type.

The density results in Table 5.4 show pyroxenite has the highest average density at 3.30 g/cm^3. Pyroxenite is followed by feldspathic pyroxenite, parapyroxenite and calc-silicate which have decreasing densities of 3.13 g/cm^3, 3.08 g/cm^3, 3.00 g/cm^3 respectively. Serpentinite has a distinctively lower average density of 2.8 g/cm^3, which is below the 3.0 g/cm^3 boundary the other rock types are above. The density of the quartz-feldspathic material was similar to that of feldspathic pyroxenite, at an average of 3.15 g/cm^3. The spread of the data was large for both calc-silicate and parapyroxenite (Figure 5.7). These rock types will therefore vary the greatest in density. Pyroxenite, on the other hand, has the most uniform dispersion of results and therefore

will vary in density the least. None the less all the density results are relatively regular with very low (> 0.4 g/cm^3) interquartile ranges. The density for the quartz-feldspathic vein material is not only similar to feldspathic pyroxenite in value but also in standard deviation and interquartile range.

The box and whisker plots showed a combination of seemingly normal and non-normal population distributions for the different rock types (Figure 5.7). To confirm these visual estimations the Chi-squared (χ^2) test for normality (C.I. 95%) was applied to the data sets. Results revealed that the distributions of for feldspathic pyroxenite and parapyroxenite densities were normal but that the distributions for the pyroxenite, serpentinite and calc-silicate data were not normal. Based on this non-parametric statistical analyses would be considered appropriate during further analysis of the density properties. However, it was decided that the density data for all the rock types in the Sandsloot orebody would be treated as normally distributed and parametric statistics would be applied during analyses. This was decided because of the similar geological origins of all the orebody rock types, which meant that the density testing covered in this research looked only at a narrow subset/ range (2.8 – 3.3 g/cm^3) of rock densities versus the larger population. Within this context the Central Limits Theorem (Davis, 1986), which states that the distribution of a subset will tend towards normal as the number of samples tested increases, was used to justify the treatment of the data as normally distributed and the subsequent application of parametric statistical analyses. Some examples of the varied densities of geological material, depending on its origin, are given in Table 5.5.

Table 5.5 Range of densities for different geological materials.

Material	Density
pumice	0.6 – 1.1 g/cm^3
coal	1.1 – 1.4 g/cm^3
hematite	4.5 – 5.3 g/cm^3
gold	19.3 g/cm^3
stoney meteorite	3500 kg/m^3

In assessing the variance of density between rock types the parametric one way analysis of variance (ANOVA) test (C.I. 95%) was employed. The tests showed that the densities between the rock types varied significantly. Duncan's multiple range test (C.I. 95%) was applied to determine which rock types were different. Results showed serpentinite, calc-silicate and pyroxenite were significantly different to the other rock types and to each other. They fell into groups of their own, indicated by the 'crosses' in Table 5.6. Parapyroxenite, feldspathic

pyroxenite and the quartz-feldspar samples were similar in character as the 'crosses' indicated their properties fell into a vertical group (Table 5.6). These three rock types therefore do not have significant differences in their densities were classed as a homogenous group.

Table 5.6 Duncan's multiple range test results for density (g/cm^3).

Rock Type	Count	Mean	HG
Serp	64	2.78	X
Calc-sil	87	3.00	X
Parapyx	1359	3.08	X
Fpyx	181	3.13	X
Qzfd	6	3.15	X
Pyx	82	3.30	X

HG, homogenous group

The one way ANOVA was run on the database a second time to analyse the variance of the density results for the rock types between drill holes. The outcome of the analysis is shown in Duncan's multiple range test table (Table 5.7). Each rock type except calc-silicate showed significant differences in density between drill holes. Feldspathic pyroxenite, pyroxenite, parapyroxenite, serpentinite and the quartz feldspathic vein material may therefore be expected to vary spatially. The lack of significant difference in the calc-silicate density results does not point exclusively to its spatial consistency but rather indicates that the limited drill holes, from which specimens could be sampled, has influenced the results.

Table 5.7 Duncan's multiple range tests for density between drill holes for each rock type.

Fpyx		Pyx		Parapyx		Serp		Calc-sil	
BH	HG	BH	HG	BH	HG	BH	HG	BH	HG
159	X	159	X	3	X	160	X	3	X
150	X	154	X	5	X	149	X	4	X
3	X			4	X	161	X	5	X
149	XX					158	X		
4	XX					3	X		
161	X					5	X		

BH, drill hole; HG, homogenous group

5.5.3 Ultrasonic Velocity

The database of 777 valid ultrasonic velocity test results were compiled, the results of which are given in Table 5.8. For every UCS sample that was tested an ultrasonic velocity test was performed on the same sample. This was used for the direct correlation between the two in section 5.6 Discussion and Correlations. Also included under Section 5.6 is the relationship between density and ultrasonic velocity.

Table 5.8 Results of the ultrasonic velocity (m/s) testing.

Rock Type	Count	Avg.	Median	Standard dev.	Min	Max	Range	Interquartile range
Fpyx	139	**6018.8**	6069.0	460.2	4675.7	7229.3	2553.6	686.3
Pyx	80	**6156.2**	6300.4	601.2	4202.4	7352.0	3149.7	588.1
Parapyx	474	**6048.5**	6126.1	594.0	4266.7	7597.9	3331.3	713.0
Serp	55	**5439.3**	5429.7	349.8	4705.1	6145.2	1440.0	471.0
Calc-sil	29	**5645.1**	5647.1	696.6	4232.6	6699.1	2466.5	864.7
Total	777	**5996.1**	6083.3	588.7	4202.4	7597.9	3395.6	787.9

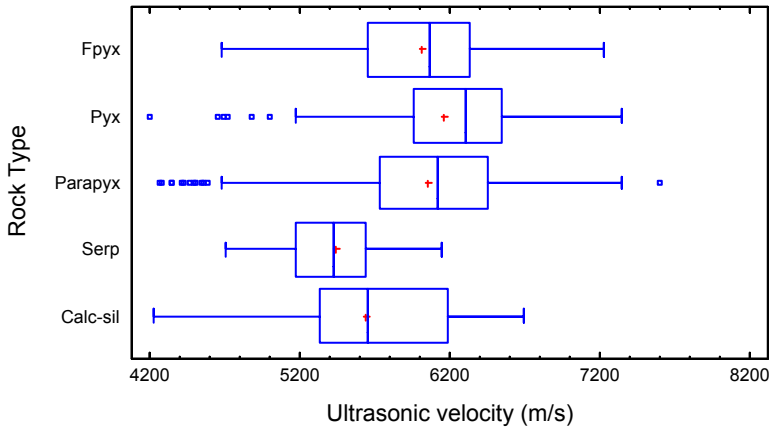

Figure 5.8 Box and whisker plot for ultrasonic velocity for each rock type.

Pyroxenite has the highest ultrasonic velocity followed by parapyroxenite and feldspathic pyroxenite. The average values for each of these rock types were 6156.2 m/s, 6048.5 m/s and 6018.8 m/s respectively (Table 5.8). Calc-silicate and serpentinite have ultrasonic velocity averages below the 6000.0 m/s level, at 5645.1 m/s and 5439.3 m/s respectively. The spread of the data, based on both the interquartile range and standard deviation, is similar and relatively large for each rock though it is the lowest for serpentinite (Table 5.8). The variability may be expected to be similar to that of the degree of dispersion.

Using the χ^2 test (C.I. 95%) the populations for all the rock types were determined to be normal despite pyroxenite and parapyroxenite appearing to have slightly negative skewed populations (Figure 5.8). The negative skew is probably due to a few of the lower ultrasonic velocity results causing the population to become weighted. These points were not far outside points (> 3 time the interquartile range) therefore they have not been excluded from the data analysis. It is likely the lower values were a result of undetectable discontinuities within the samples.

Normality having been determined, the parametric one way ANOVA test (C.I. 95%) was used to determine whether the ultrasonic velocities, between the rock types, were significantly different. Results revealed that there were statistical significant differences between the rock

types. Duncan's multiple range test (C.I. 95%) showed that there were three distinct groups of ultrasonic velocity properties (Table 5.9). The three groups comprised feldspathic pyroxenite, parapyroxenite and pyroxenite, which fell into one group, and calc-silicate which fell into a second group and serpentinite which fell into a third. The behaviour of these five rock types is anticipated to be most similar or contrasting, according to which homogenous group they fall into.

Table 5.9 Duncan's multiple range test results for ultrasonic velocity (m/s).

Rock Type	Count	Mean	HG
Serp	55	5439.3	X
Calc-sil	29	5645.1	X
Fpyx	139	6018.8	X
Parapyx	474	6048.5	X
Pyx	80	6156.2	X

HG, homogenous group

One way ANOVA tests were run between samples of the same rock type to test for differences between drill holes. Results showed that there were statistical significant differences in the ultrasonic velocity results of the feldspathic pyroxenite, pyroxenite and parapyroxenite rock types depending on which drill holes the samples came from. The test showed that the serpentinite and calc-silicate ultrasonic velocities were similar across drill holes. Table 5.10 shows the drill holes in which the ultrasonic velocities were homogenous according to Duncan's multiple range test (C.I. 95%).

Table 5.10 Duncan's multiple range tests for ultrasonic velocity between drill holes for each rock type.

Fpyx		Pyx		Parapyx		Serp		Calc-sil	
BH	HG	BH	HG	BH	HG	BH	HG	BH	HG
161	X	159	X	4	X	161	X	4	X
159	X	154	X	5	XX	160	X	3	X
150	X			3	X	158	X		
149	X					3	X		
3	X					149	X		
4	X					5	X		

BH, drill hole; HG, homogenous group

5.5.4 Point Load Index (PLI)

Point load testing was carried out to determine the strength of the five rock types using a means that could be replicated in the field with restricted resources and time. Both point load axial and point load diametral tests were performed and it was intended to use the data gathered to:

- Quantify the Is_{50} strength of the orebody rock types and thereafter to classify the strength of the intact rock (Table 5.11).
- Determine the degree of strength anisotropy by comparing the Is_{50} axial and Is_{50} diametral strengths.
- Correlate the Is_{50} strength to the uniaxial compressive strength for each rock type.
- Compare the correlations between the Is_{50} strengths and uniaxial compressive strengths with those used on the mine site.

Table 5.11 Point-load strength classification, after Bell (1993) and ISRM (1981).

Point-load strength index (MPa)	Description (ISRM, 1981)	Equivalent UCS (MPa) (Bell, 1993)
Less than 0.03	Extremely low strength	Less than 0.5
0.03 – 0.1	Very low strength	0.5 – 1.6
0.1 – 0.3	Low strength	1.6 – 5
0.3 – 1	Medium strength	5 – 16
1 – 3	High strength	16 – 50
3 – 10	Very high strength	50 – 160
Over 10	Extremely high strength	Over 160

All samples tested had valid failures as shown in Figures 5.9 a and b, however upon analyzing the results it was recognized that they were unreliable.

a **b**

Figure 5.9 a Samples of valid failure for axial PLI test. **b** Samples of valid failure for diametral PLI test.

Some of the indicators which pointed to the unreliability of the data included:

- An unusual distribution of the parapyroxenite Is_{50} vs. parapyroxenite UCS results.

The scatter formed a highly distinctive but peculiar narrow vertical column with a very large range of UCS results for a very small range of Is_{50} results.

- A sizable difference between the research Is_{50} results and the Sandsloot mine Is_{50} results for each rock type.
- Poor correlation values between the Is_{50} strengths and the UCS results for each rock type.
- Unconventional pyroxenite and serpentinite strength anisotropy results.

The calculations, corrections and apparatus were rechecked and it was found that despite being calibrated before the testing programme commenced, the point load machinery was inaccurate. Testing of the gauges found the large gauge, designed for hard rock and measuring strengths between 0 – 50 kN, was not sensitive enough to accurately record lower value strengths between 0 – 15 kN and the smaller gauge (0 – 10 kN), designed for soft sedimentary rocks and weaker rock, did not read values high enough for the rocks being tested in this research study. At the time a digital gauge covering the entire range was not available.

Although the point load results could not be used and restrictions due to lack of sample availability meant that testing could not be re-done, the point load data base from the mine has been assessed and will be used in the correlation with the research UCS results.

The database provided by PPRust comprised 252 point load test results from Sandsloot open pit diamond drill core for the feldspathic pyroxenite, pyroxenite, parapyroxenite, serpentinite and calc-silicate rock types. The tests were performed on site by PPRust personnel on diamond drill core with the diameters of 32mm, 35mm and 37mm, which were corrected to the Is_{50} standard by the Author. All the test results were diametral point load strengths. The database of these test results is in Appendix C. Table 5.12 defines the population descriptives for each rock type and thereafter the results and analyses follow the standard layout used in previous results and analysis sections.

Table 5.12 Results of the PLI Is_{50} diametral (MPa) tests by PPRust Sandsloot.

Rock Type	Count	Avg.	Median	Standard dev.	Min	Max	Range	Interquartile range
Fpyx	34	**7.6**	7.5	3.1	1.3	16.3	15.0	3.6
Pyx	47	**10.5**	9.7	5.5	1.7	34.1	32.4	4.7
Parapyx	93	**6.7**	6.3	4.8	1.3	36.9	35.6	5.7
Serp	14	**4.7**	4.6	1.4	1.8	7.3	5.5	1.6
Calc-sil	64	**5.5**	4.3	3.7	0.3	17.4	17.0	5.1
Total	252	**7.1**	6.5	4.7	0.3	36.9	36.6	5.3

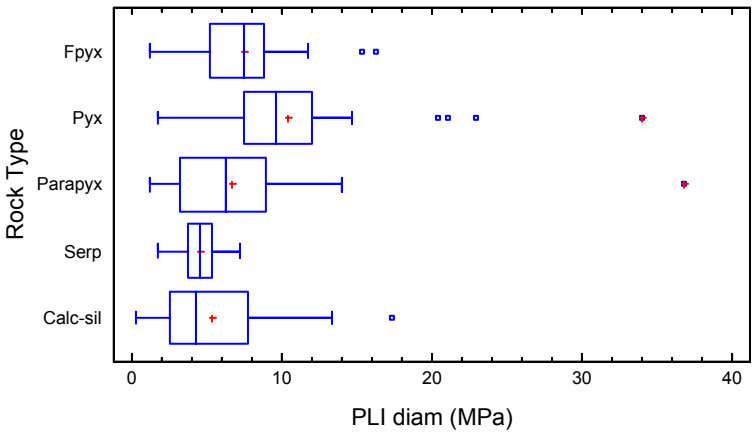

Figure 5.10 Box and whisker plot for PLI diametral for each rock type.

The point load diametral tests showed pyroxenite had the highest Is_{50} strength at 10.5 MPa (Table 5.12) followed by feldspathic pyroxenite, at 7.6 MPa and parapyroxenite at 6.7 MPa. Calc-silicate and serpentinite had the two weakest PLI Is_{50} diametral strengths at 5.5 MPa and 4.7 MPa respectively. The dispersion was greatest for parapyroxenite, followed closely by calc-silicate and parapyroxenite, therefore they have the most variability in terms of strength index. Serpentinite was the least variable and therefore likely to have the greatest strength index predictability (Figure 5.10).

When classified according to the ISRM (1981) scheme pyroxenite was described as extremely high in strength (Table 5.11) whilst the other four rock types were described as very high in strength. If a correlation factor of 16 was used to estimate the uniaxial compressive strength (UCS), as recommended by Bell (1993), the equivalent UCS values were >160 MPa for the pyroxenite and between 50 MPa and 160 MPa for the feldspathic pyroxenite, parapyroxenite, serpentinite and calc-silicate rock types. The more common conversion factor of 24, suggested by Bieniawski (1975), estimates the UCS values to be >160 MPa for feldspathic pyroxenite, pyroxenite and parapyroxenite, and between 50 MPa and 160 MPa for serpentinite and calc-silicate.

The χ^2 tests (C.I. 95%) confirmed the normality of the sample population distributions for all the rock types and the parametric one way ANOVA (C.I. 95%) showed that a significant difference existed between point load diametral strengths for each rock type. Duncan's multiple range test identified the pyroxenite diametral strength as unique, with a significantly higher strength when compared to the other rock types (Table 5.13). Feldspathic pyroxenite and serpentinite were significantly different to one another but both share similar population

characteristics to parapyroxenite and calc-silicate. To determine the differences between feldspathic pyroxenite, parapyroxenite, calc-silicate and serpentinite more testing would be required.

Table 5.13 Duncan's multiple range test results for PLI diametral strength (MPa).

Rock Type	Count	Mean	HG
Serp	14	4.7	X
Calc-sil	64	5.5	XX
Parapyx	93	6.7	XX
Fpyx	34	7.6	X
Pyx	47	10.4	X

HG, homogenous group

The one way ANOVA (C.I. 95%) was run on the database a second time to determine if significant differences in the PLI diametral strengths existed between drill holes of the same rock, therefore showing spatial variability of significance. Table 5.14 shows the results for the one way ANOVA tests. Each rock type varied in diametral strength spatially.

Table 5.14 Duncan's multiple range tests for PLI diametral strength between drill holes for each rock type.

Fpyx		Pyx		Parapyx		Serp		Calc-sil	
BH	HG	BH	HG	BH	HG	BH	HG	BH	HG
258	X	258	X	4	X	SS303	X	2	X
303	XX	303	X	3	X	SS257	XX	303	XX
2	XX	257	X	5	X	SS242	X	3	XX
256	X	256	X	2	XX			247	XXX
		259	X	303	XX			242	XXX
		242	X	257	XX			258	XX
				256	XX			259	X
				258	XX			256	X
				259	X			257	X
				242	X				

BH, drill hole; HG, homogenous group

Strength Anisotropy, which is the ratio between the greatest and the least point load strength (ISRM, 1981) is calculated using the average results for the axial and diametral tests for each rock type. A ratio close to 1.0 indicates a quasi-isotropic rock and higher ratio values indicate anisotropy. The strength anisotropy for the orebody rock types at Sandsloot could not be calculated in this study because the Sandsloot database results are all diametral point load index strengths.

5.5.5 Brazilian Disc Tensile Strength

A data set of 130 valid failure results for indirect tensile strength testing was compiled. The common mode of failure for the feldspathic pyroxenite, pyroxenite, serpentinite and calc-silicate

samples was a single split failure. Parapyroxenite tended to fail with single or double splits. Figure 5.11 a and b show the modes of failures. The results of the testing are detailed in Table 5.15.

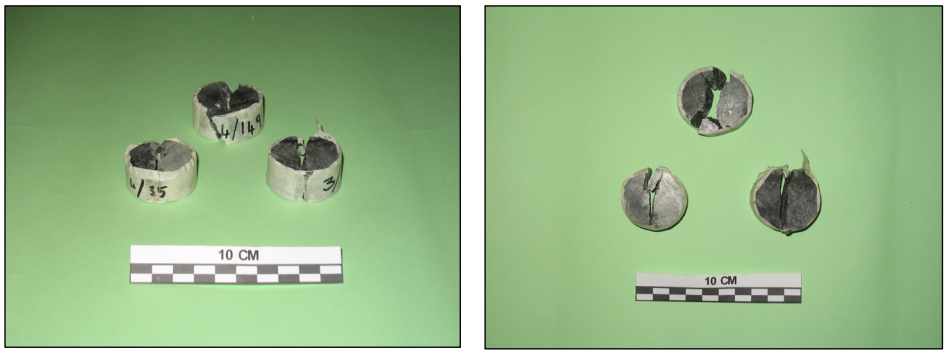

a **b**

Figure 5.11 a and b. Modes of valid failure for Brazilian disc tensile strength test samples.

Table 5.15 Results of the Brazilian disc tensile strength (MPa) testing.

Rock Type	Count	Avg.	Median	Standard dev.	Min	Max	Range	Interquartile range
Fpyx	32	**24.9**	25.5	4.0	16.1	33.9	17.8	6.5
Pyx	20	**23.2**	23.1	2.9	17.8	28.9	11.2	4.9
Parapyx	60	**26.7**	25.5	5.9	16.5	40.1	23.6	8.9
Serp	14	**21.8**	21.3	5.5	12.7	31.1	18.4	9.3
Calc-sil	4	**24.4**	24.5	6.6	18.2	30.4	12.2	11.4
Total	130	**25.1**	24.6	5.3	12.7	40.1	27.4	7.7

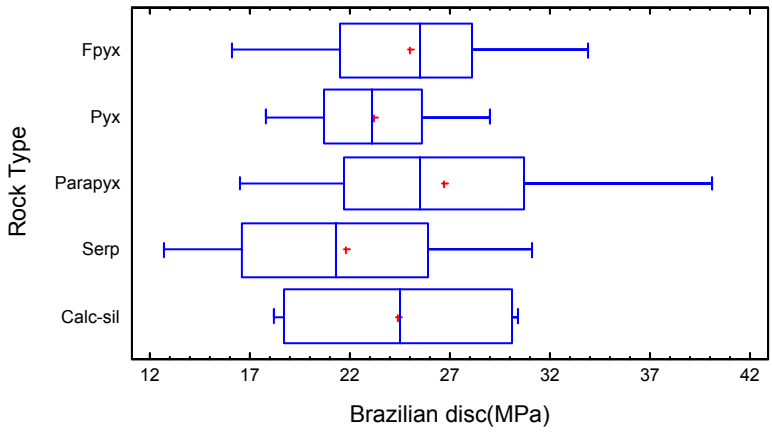

Figure 5.12 Box and whisker plot for Brazilian disc tensile strength for rock type.

Parapyroxenite has the highest tensile strength, followed by feldspathic pyroxenite and calc-silicate, the latter two being very similar in strength to each other. Pyroxenite has the second lowest or weakest tensile strength while serpentinite has the weakest tensile strength out of the orebody rock types. Despite these differences the actual range between all the rock types sits

between the mid to low twenties, varying by approximately 5 MPa (Table 5.15). These differences are small therefore the tensile strength for each rock type is similar. Parapyroxenite has the highest visual spread out of all the orebody rock types but it is calc-silicate that has the greatest dispersion of data (Figure 5.12). Pyroxenite has the smallest variability and is therefore the most predictable in terms of tensile strength.

The χ^2 normality test (C.I. 95%) proved the normality for the tensile strength data of each rock type and parametric one way ANOVA test (C.I. 95%) distinguished a statistically significant difference between the results from the different rock types. Groups of homogenous rock types expected to behave similarly when under tensile stress are displayed in Table 5.16.

Table 5.16 Duncan's multiple range test results Brazilian disc tensile strength (MPa).

Rock Type	Count	Mean	HG
Serp	14	21.8	X
Pyx	20	23.8	XX
Calc-sil	4	24.4	XX
Fpyx	32	25.0	XX
Parapyx	60	26.7	X

HG, homogenous group

Duncan's multiple range test table (Table 5.16) suggests parapyroxenite and serpentinite will behave differently to each other; however each on their own will behave similarly to pyroxenite, calc-silicate and feldspathic pyroxenite.

Variations between the drill holes of the same rock type were assessed with the one way ANOVA (C.I. 95%) test. Results revealed significant differences for the feldspathic pyroxenite, parapyroxenite and serpentinite rock types. These results are presented in Table 5.17. Calc-silicate samples for tensile strength testing were only available from drill hole SSMet 3 therefore the strength differences between drill holes could not be assessed.

Table 5.17 Duncan's multiple range tests for Brazilian disc tensile strength between drill holes for each rock type.

Fpyx		Pyx		Parapyx		Serp		Calc-sil *	
BH	HG	BH	HG	BH	HG	BH	HG	BH	HG
161	X	154	X	5	X	149	X	n/a	n/a
3	X	159	X	3	X	161	XX		
159	X			4	X	5	XX		
150	X					158	X		
149	X					3	X		

BH, drill hole; HG, homogenous group
*All the calc-silicate TS samples came from one drill hole

5.5.6 Uniaxial Compressive Strength

A total of 166 valid UCS tests were performed and included into the statistical geotechnical database. The most common mode of failure for the feldspathic pyroxenite and calc-silicate samples was a single shear failure with angles of 75° – 85° and 70° – 75° respectively (Figure 5.13 a). The pyroxenites most frequently failed with a double cone shear with top angles between 70° – 75° and bottom angles between 70° – 85° (Figure 5.13 b). The parapyroxenites shattered due to total brittle failure with no evidence of shearing at all (Figure 5.13 c) and the serpentinites repeatedly splintered into fine, sharp, elongate rock fragments upon failure (Figure 5.13 d). Furthermore, serpentinite failed with invalid results more frequently than the other rock types, due to the presence of discontinuities not visible to the naked eye.

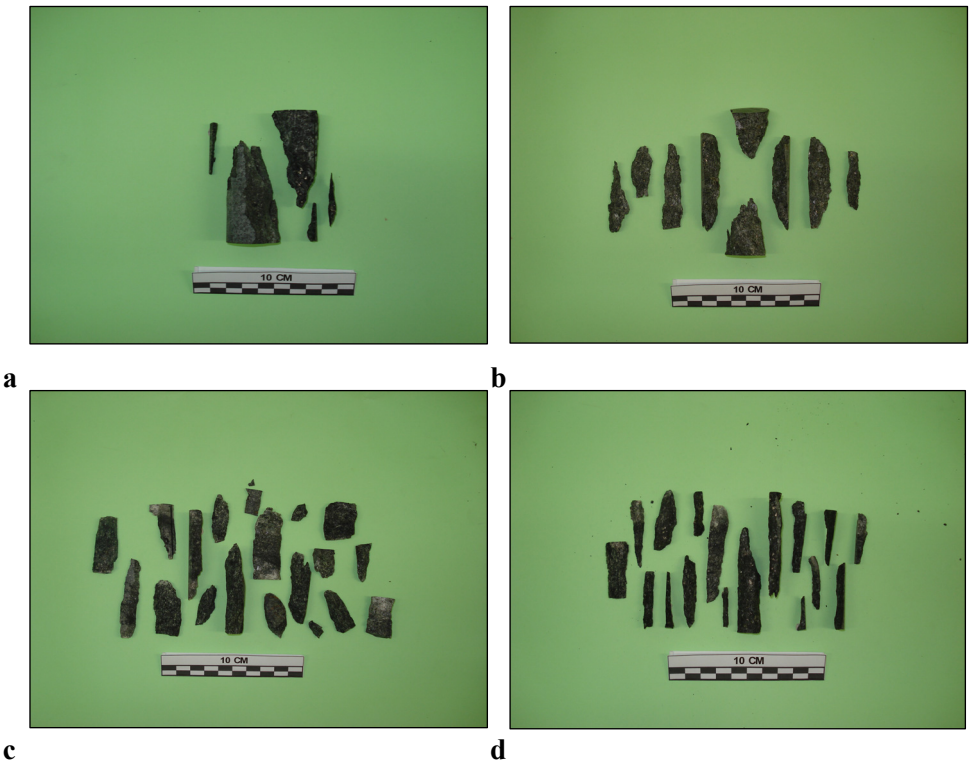

Figure 5.13 Modes of valid failure for UCS test samples. **a** Single cone shear. **b** Double cone shear. **c** Total brittle failure. **d** Total brittle failure of serpentinite specimen, showing splintered appearance of rock fragments.

The results of the UCS testing are presented in Table 5.18 and Figure 5.14.

Table 5.18 Results of the uniaxial compressive strength (MPa) testing.

Rock Type	Count	Avg.	Median	Standard dev.	Min	Max	Range	Interquartile range
Fpyx	33	**135.6**	132.2	35.7	73.2	232.8	159.7	53.8
Pyx	17	**110.5**	114.0	20.9	71.0	141.0	70.0	28.5
Parapyx	107	**132.0**	123.3	49.9	58.3	271.7	213.4	78.6
Serp	4	**62.9**	61.7	7.7	55.0	73.2	18.2	10.6
Calc-sil	5	**89.6**	81.4	37.4	45.2	144.3	99.1	33.4
Total	166	**127.6**	117.4	46.1	45.2	271.7	226.5	68.5

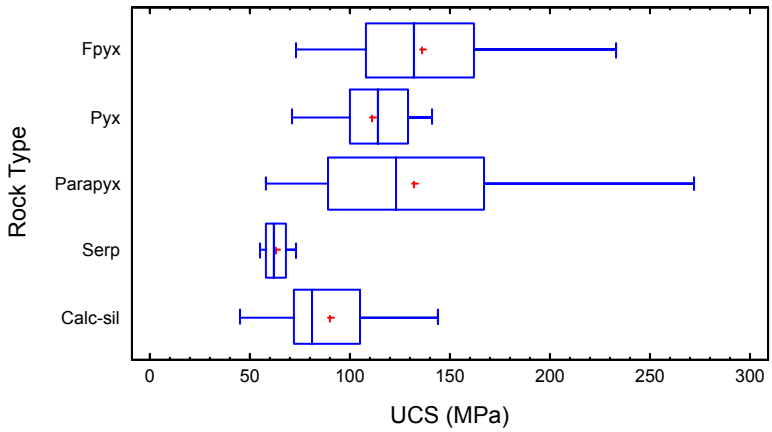

Figure 5.14 Box and whisker plot for uniaxial compressive strength for each rock type.

Testing showed feldspathic pyroxenite had the highest average UCS followed closely by parapyroxenite and thereafter pyroxenite, 135.6 MPa, 132.0 MPa and 110.5 MPa respectively (Table 5.18). Calc-silicate and serpentinite are the two weakest rock types with both UCS averages sitting below 100 MPa, at 89.6 MPa and 62.9 MPa respectively. The difference in strength between the three main constituents of the orebody, feldspathic pyroxenite, pyroxenite and parapyroxenite is approximately 25 MPa and the difference between all the rocks which are mineralised, i.e. each rock type in this study, is approximately 72 MPa. Parapyroxenite results had the greatest spread and data dispersion, therefore this rock type has the most variable strength. Feldspathic pyroxenite also showed a high data dispersion but serpentinite and pyroxenite showed the least spread and corresponding variability.

Using the Geological Society (Anon., 1970) and IAEG (Anon., 1979) classifications (Table 5.19) for intact rock strength the five orebody rock types fall into two categories. These are ‘strong rock’ for the serpentinite and calc-silicate rock types and ‘very strong rock’ for the feldspathic pyroxenites and parapyroxenites. Depending on which classification scheme is used pyroxenite is classified as either ‘strong rock’ or ‘very strong rock’ for the Geological Society

(Anon., 1970) and IAEG (Anon., 1979) respectively. The ISRM classification (Table 5.19) does not distinguish between any of the rock types, describing them all as 'high' in strength. Therefore this classification scheme is not detailed enough to distinguish the differences in strength in the rock types of this study.

Table 5.19 Uniaxial compressive strength classification, modified after Bell, 1993.

Geological Society (Anon., 1970)		IAEG (Anon., 1979)		ISRM (1981)	
Strength (MPa)	Description	Strength (MPa)	Description	Strength (MPa)	Description
Less than 1.25	Very weak	1.5 – 15	Weak	Under 6	Very low
1.25 – 5.00	Weak	15 – 50	Moderately strong	6 – 20	Low
5.00 – 12.50	Moderately weak	50 – 120	Strong	20 – 60	Moderate
12.50 – 50	Moderately strong	120 – 230	Very strong	60 – 200	High
50 – 100	Strong	Over 230	Extremely strong	Over 200	Very high
100 – 200	Very strong				
Over 200	Extremely strong				

IAEG, International Association of Engineering Geology

Normal distributions were established for the data sets of each rock type using the χ^2 test (C.I. 95 %). Thereafter the parametric one way ANOVA (C.I. 95%) test was applied to determine if a significant difference in UCS existed between the rock types. Results concluded uniaxial compressive strengths were significantly different for each rock type. Duncan's multiple range test predicts that feldspathic pyroxenite, parapyroxenite and pyroxenite are most likely to behave similarly but the parapyroxenite and pyroxenite will share strength characteristics with calc-silicate (Table 5.20). More testing would be required to substantiate this association with calc-silicate as the low number of calc-silicate test samples may be distorting the results. The serpentinite is predicted to show dissimilar strength characteristics to all the rock types except calc-silicate.

Table 5.20 Duncan's multiple range test results for uniaxial compressive strength (MPa).

Rock Type	Count	Mean	HG
Serp	4	62.9	X
Calc-sil	5	89.6	XX
Pyx	17	110.5	XX
Parapyx	107	132.0	XX
Fpyx	33	135.6	X

HG, homogenous group

Using the one way ANOVA (C.I. 95%) it was proven that significant differences exist between the UCS results per drill hole for each rock type except for serpentinite. The results of Duncan's multiple range test which distinguished which drill holes are similar are given in Table 5.21.

Table 5.21 Duncan's multiple range tests for uniaxial compressive strength between drill holes per rock type.

Fpyx		Pyx		Parapyx		Serp		Calc-sil *	
BH	**HG**	**BH**	**HG**	**BH**	**HG**	**BH**	**HG**	**BH**	**HG**
161	X	159	X	5	X	161	X	n/a	n/a
150	X	154	X	3	X	149	X		
159	XX			4	X	160	X		
3	XX								
149	XX								
4	X								

BH, drill hole; HG, homogenous group
*All calc-silicate UCS samples came from one drill hole

UCS test results for the same rock type between drill holes are different at a significant level for feldspathic pyroxenite, pyroxenite and parapyroxenite samples. These rock types may therefore be expected to show variability in strength at a statistical level, spatially. The calc-silicate samples only came from drill hole (SSMet 3) and therefore differences between drill hole strength could not be assessed.

5.6 Discussion and Correlations

In the previous section the geotechnical properties were considered individually, examining the possible causes for each set of the test results. For mining purposes however, it is also necessary to know which rock types will standout geotechnically, how the geotechnical properties relate and how the data may be interpreted for the benefit of mining.

The results for the geotechnical testing are summarised in Figures 5.15 a – e, defining the highest and lowest value for each geotechnical property and ranking the remaining rock types using the averages. The maximum and minimum points in these graphs are defined by one standard deviation above and below the average. This is where 68 % of new observations are predicted to fall.

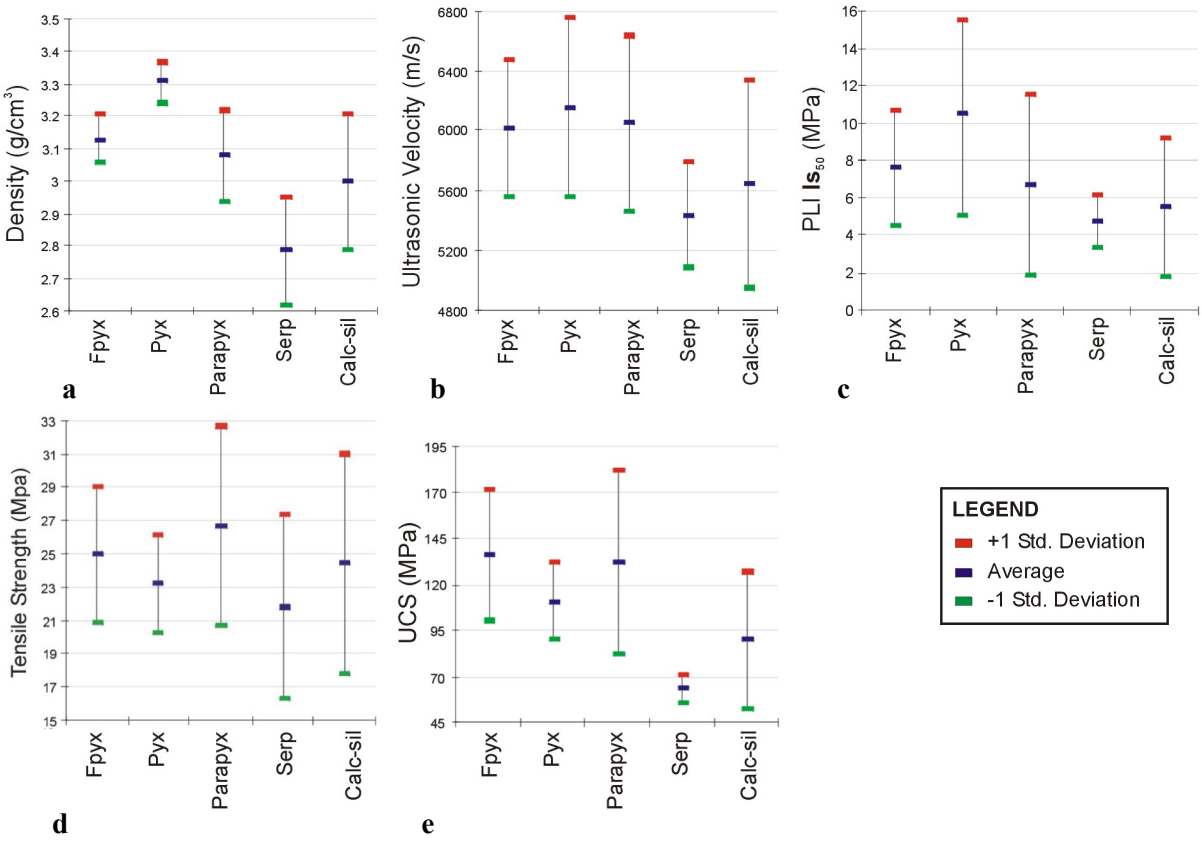

Figure 5.15 a - e. Average results for each geotechnical test, plus and minus one standard deviation.

There are four general trends which may be deduced from the testing results to characterise the orebody rock types. These are:

- For each geotechnical property studied, except tensile strength, feldspathic pyroxenite, pyroxenite and parapyroxenite stand out as having the three highest results.
- For density, ultrasonic velocity and point load index strength pyroxenite had the highest results.
- For each geotechnical property studied, barring tensile strength again, calc-silicate had the second lowest results.
- For each geotechnical property studied serpentinite had the lowest results.

Statistical analysis of the data confirmed the differences between the rock types for each property studied were significant. However, not all the differences were distinguishing at a 95% confidence level for each rock type. For each test type the rock types which are expected to show such differences are grouped individually in Table 5.22.

Table 5.22 Summary of the Duncan's multiple range test per test type.

	Density	Ultrasonic Velocity	Point Load Index	Tensile Strength	Uniaxial Compressive Strength
Highest	Pyroxenite	Pyroxenite	Pyroxenite	Parapyroxenite	Feldspathic pyroxenite
	Feldspathic pyroxenite	Parapyroxenite	Feldspathic pyroxenite	Feldspathic pyroxenite	Parapyroxenite
	Parapyroxenite	Feldspathic pyroxenite	Parapyroxenite	Calc-silicate	Pyroxenite
	Calc-silicate	Calc-silicate	Calc-silicate	Pyroxenite	Calc-silicate
Lowest	Serpentinite	Serpentinite	Serpentinite	Serpentinite	Serpentinite

Some general trends which may be deduced from this data are:

- The orebody rock types are separated into more distinct groups using density and ultrasonic velocity compared with the strength type tests of PLI Is_{50}, tensile strength and UCS.
- There is no difference between feldspathic pyroxenite and parapyroxenite for each of the properties studied. Therefore they are most similar to one another.
- Where pyroxenite has the highest values for a property, the difference is typically significant.
- Feldspathic pyroxenite, pyroxenite and parapyroxenite frequently have similar values to one another for each of the properties studied and are frequently significantly different to the results of serpentinite and calc-silicate. This was similarly observed in the petrographic assessment.
- Serpentinite will typically behave differently to feldspathic pyroxenite, pyroxenite and parapyroxenite.
- Parapyroxenite shows the least distinguishing properties.
- Serpentinite and calc-silicate will often show similarities to one another.

Considering the statistical significance of the variability between drill holes for each of the properties studied showed:

- The density for all ore body rock types except calc-silicate will vary spatially.
- Ultrasonic velocity and compressive strength will vary spatially for feldspathic pyroxenite, pyroxenite and parapyroxenite. Serpentinite and calc-silicate are predicted not to vary significantly, therefore based on the data in this study these properties will be more consistent and predictable compared to the other rock types.

- The point load index strength of all the ore body rock types will vary spatially.
- Tensile strength will vary spatially for parapyroxenite, feldspathic pyroxenite and serpentinite but not for pyroxenite and calc-silicate.

This suggests feldspathic pyroxenite and parapyroxenite will be the most variable in terms of the properties studied, followed by pyroxenite, then serpentinite and finally calc-silicate. The variations in properties for rock types between drill holes may arise from the typical heterogeneous nature of any rock unit due to spatial variability in mineralogy, crystal packing, porosity, alteration and weathering.

To study the geotechnical properties of the orebody further it is necessary to build relationships between properties. These can be used to define the exhibited behavior and accurately predict expected properties. The relationships need to consider both within rock type properties and between rock types properties, using not only lithology as a basis for analysis but possibly also combinations of the various geotechnical properties which have been characterised for each rock type

Initially, the properties were related to one another using linear regression. The results of which are given as a correlation coefficient and an R-squared (R^2) value. The former is a measure of the strength of the linear relationship between the two variables (+1 representing a perfect positive relationship and -1 representing a perfect negative relationship), the latter represents the variability which is explained by the fitted regression. If R^2 is multiplied by 100 it gives the percentage of variability explained by the fitted regression (Statpoint, 2005).

For each ultrasonic velocity and UCS result there were unique density results for the same sample. Linear regressions were therefore drawn from directly related/paired data points. For relationships between properties such as UCS and tensile strength, where the same sample could not be tested twice, the “missing values” were derived by taking values for adjacent test samples of the same rock type (Figure 4.2, Chapter 4). The data was therefore indirectly related.

Correlation results for the rock types as a whole and per rock type showed weak to moderate relationships. Correlation coefficients and R^2 values varied respectively between 0.12 and 0.57 and between 0.01 and 0.33, for the rock types as a whole. The correlation coefficients and R^2 values, per rock type, varied respectively between 0.1 and 0.62 and between 0.01 and 0.39. Figures 5.16 a and b are typical examples of the dispersion of correlation points. The data shows

partial to complete overlap of the rock types, with dispersion that varies between moderately linear to uniformly scattered, with a "shot-gun" appearance.

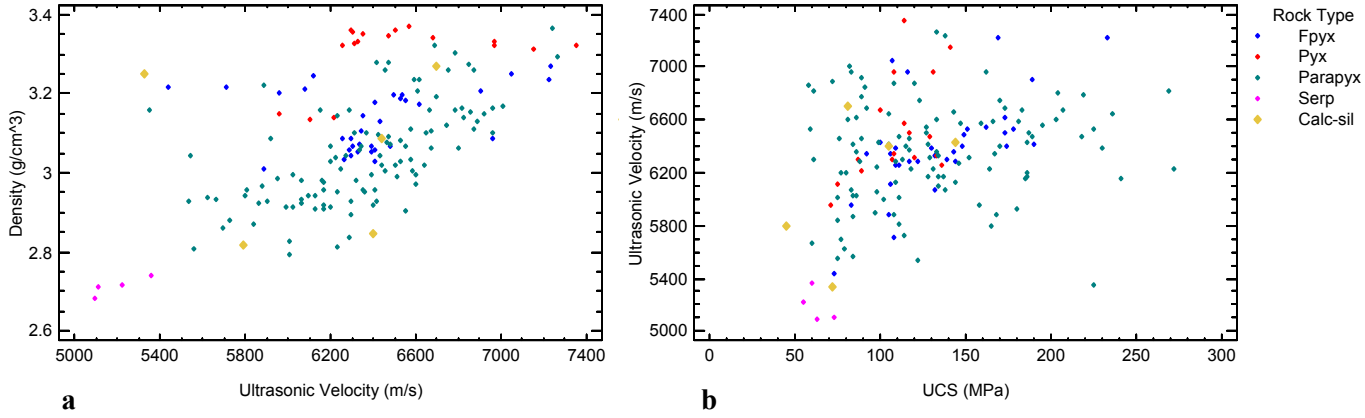

Figure 5.16 a and b Typical examples of the data dispersion in the comparison of geotechnical properties. Figure 5.16 a shows distinction between rock types, with some overlap of the populations and a moderate positive linear trend. Figure 5.16 b shows poor distinction between rock types, complete overlap and a "shot-gun" uniform scatter of data.

The overlaps of properties between rock types are similar to those identified in the Duncan's multiple range tests. They represent similarities that stem from the geological origin of the rock, with the igneous rock types showing similar properties to one another, differences to the metamorphic rock types and with overlaps between the rock types that have been altered. The scatter demonstrates the inherent variability of these properties for each rock type. Both the overlaps and the scatter of the data indicate that complicate relationships exist between the different orebody rock types. This has resulted in statistical population overlaps, which cloud the trends between properties. Therefore the averages have been plotted against one another to clarify the trends and relationships.

The studied geotechnical properties have been plotted, distinguishing rock type and fitting linear regressions to the data (Figures 5.17 a – j.). The results of the correlations and the equations for the linear regressions are detailed in Table 5.23. It was decided that the regression line fitted between UCS and PLI Is_{50} would be plotted to pass through the x:y origin, which is not the "best-fit" line for the data (Figure 5.17 i.). This is because the PLI Is_{50} was developed to replicate the UCS of a sample. Therefore a sample should not have a uniaxial compressive strength if it does not have a point load index strength, or vice versa. However, the regression lines between the other properties were plotted to give the "best-fit" for the data. This is because

the remaining properties may have controlling factors that are not related to the properties that are being compared. They therefore may be disproportionally related. An example is between density and tensile strength. Some rock types may show a great degree of proportionality between these properties but samples of the UG – 2 chromitite seams in Western and Eastern Bushveld break apart easily because the bonds between the chromite grains are very weak. It therefore has a very low tensile strength but the density of the samples are disproportionally high (chromite density is between 4.1 – 5.1 g/cm^3). It is the bonds between the grains which are the controlling factor of the strength and not the density.

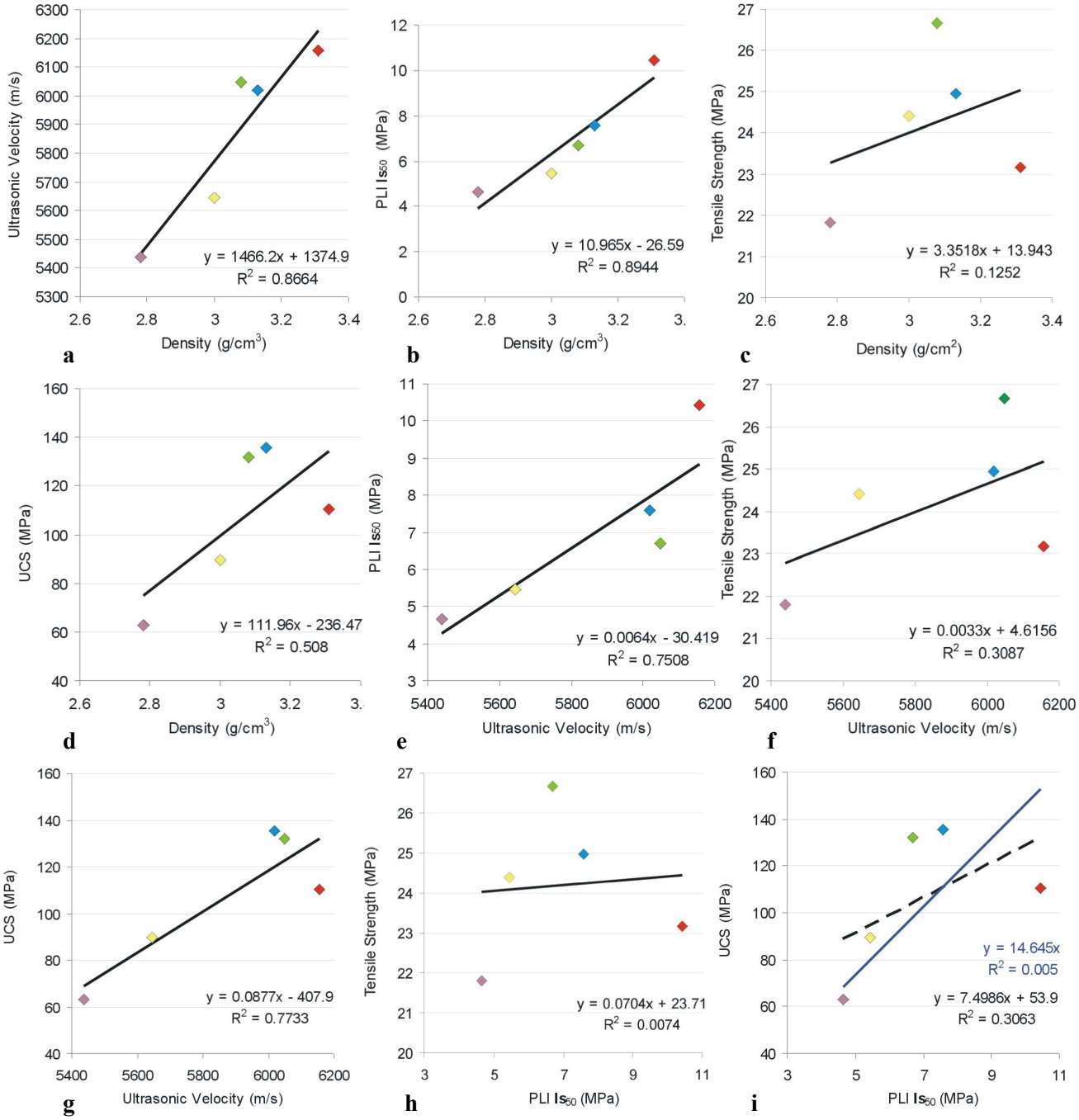

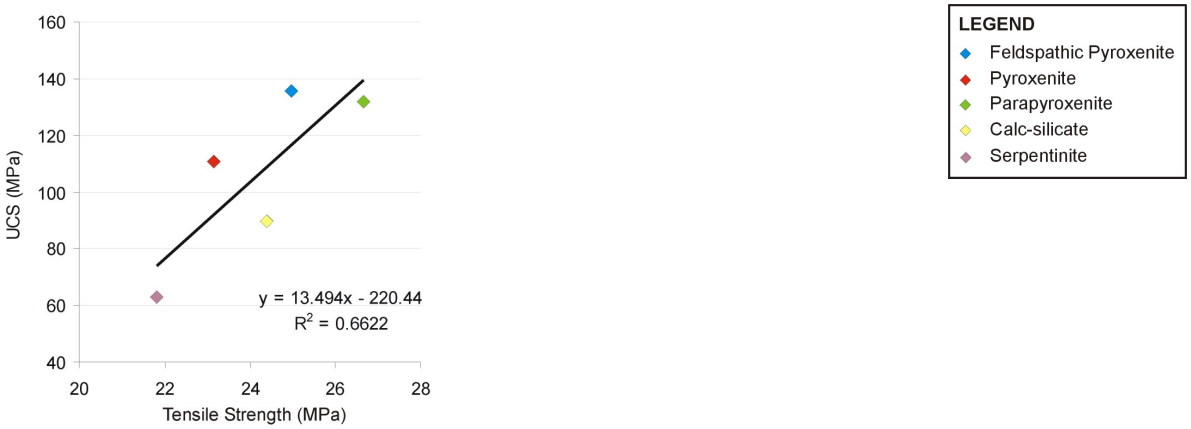

j

Figure 5.17 a – j. Linear regressions between geotechnical properties. Note in Figure 5.17 i. two regression lines have been fitted. The black dashed line shows the regression which best fits the data. The blue line shows the regression which passes through the x:y, 0:0 intercept.

Table 5.23 Linear regression models fitting the properties studied between the orebody rock types.

y	*x*	Correlation coefficient	R^2	Linear regression
UCS	Density	0.71	0.51	y = 111.96 * *x* - 236.47
	Ultrasonic Velocity	0.88	0.77	y = 0.088 * *x* - 407.90
	PLI Is_{50}	0.55	0.005	y = 14.65 * *x*
	Tensile strength	0.81	0.66	y = 13.50 * *x* - 220.44
PLI Is_{50}	Density	0.95	0.89	y = 10.97 * *x* - 26.59
	Ultrasonic Velocity	0.87	0.75	y = 0.0064 * *x* - 30.42
	Tensile strength	0.09	0.01	y = 0.11* *x* + 4.41
Tensile strength	Density	0.35	0.13	y = 3.35* *x* +13.94
	Ultrasonic Velocity	0.56	0.31	y = 0.0033* *x* + 4.62
Ultrasonic Velocity	Density	0.93	0.87	y = 1466.24* *x* + 1374.88

The relationships between the geotechnical properties are typically strong. Density, ultrasonic velocity and tensile strength relate well to UCS. The relationships are positive and moderate to strong. Therefore an increase in any of these properties will correspond with an increase in the UCS of the rock types which comprise the orebody at Sandsloot. Looking at the correlation between UCS and PLI Is_{50} it may be expected that with an increase in the UCS there would be an increase in PLI Is_{50} but as shown in Figure 5.17 i and Table 5.23 the correlation is weak. Serpentinite, calc-silicate, parapyroxenite and feldspathic pyroxenite fit the expected theory well. The odd rock type appears to be pyroxenite and it is clear that it stands out because of its disproportionately high PLI Is_{50} (Figure 5.17 i). This suggests there are factors, which control the differences between these properties that are not accounted for in the tests. Differences may

stem from the different ways force is applied to a sample between the various tests or from the surface size of the sample that is tested. The strong, positive relationship between compressive strength and tensile strength is not expected. The strength of a sample in compression does not influence the strength of a sample in tension but for the Sandsloot orebody rock types these properties seem to reflect each other well. This is possible because the rock types are not dominated by a strong anisotropy such as schistose fabric or bedding planes. Therefore the strengths of the Sandsloot rocks are controlled by the interlocking of the crystals, though this may not be the only factor controlling intact strength.

The correlations between PLI Is_{50} and the other geotechnical properties are expected to be similar to those between UCS and the geotechnical properties. Like UCS, PLI Is_{50} correlates well with ultrasonic velocity, showing an increase in the PLI Is_{50} of a rock with an increase in the ultrasonic velocity. However, PLI Is_{50} has a better correlation with density (Table 5.23). The relationship is strong and may indicate that the composition plays a bigger factor in the PLI Is_{50} result than it does for UCS. It is also possible that the size of the sample is influencing the correlation of the two, and though point load index strength is meant to replicate the failure of a sample in uniaxial compressive strength testing, this strong relationship may indicate there is a difference in the way the tests assess strength. PLI Is_{50} does not relate as well with tensile strength as UCS does. It appears pyroxenite stands out, with an disproportionally high PLI Is_{50} (Figure 5.17 h).

Tensile strength is weakly related to density and ultrasonic velocity. They do not reflect the tensile strength well but for the Sandsloot orebody rock types the relationships do show that an increase in the density or ultrasonic velocity will correspond with an increase in the tensile strength. It appears that it is the pyroxenite rock type which stands out again, with a disproportionately low tensile strength (Figure 5.17 c and f).

Ultrasonic velocity and density correlate well, with a strong positive relationship. The ultrasonic velocity of a rock type may therefore be predicted satisfactorily using the density.

Despite the weak correlation between PLI Is_{50} and UCS it is necessary to look at the ratios between these strengths for each rock type in greater detail. This is because these ratios are regularly used as conversion factors to determine the intact strength of the rock mass on a mine. This in turn is used to calculate the blasting requirements for the fragmentation and the intact strengths of the material entering the processing plant. Table 5.24 summarises the PLI Is_{50}:UCS

ratios for the orebody rock types at Sandsloot, plus and minus one standard deviation. For comparative purposes Table 5.25 details the PLI Is_{50}:UCS ratios calculated using the mine strength database for the orebody rock types at Sandsloot open pit and for the average of all the open pits at PPRust. This data was standardized to 50 mm diameter core by the Author.

Table 5.24 PLI Is_{50}:UCS ratios for the orebody rock types at Sandsloot open pit mine.

Rock Type	PLI Is_{50} (MPa)		UCS (MPa)		PLI Is_{50} : UCS Ratio		
	Avg.	Standard dev.	Avg.	Standard dev.	Avg.	- 1 standard dev.	+ 1 standard dev.
Feldspathic pyroxenite	**7.6**	3.1	**135.6**	35.7	**17.8**	22.2	16.0
Pyroxenite	**10.5**	5.5	**110.5**	20.9	**10.5**	17.9	8.2
Parapyroxenite	**6.7**	4.8	**132**	49.9	**19.7**	43.2	15.8
Serpentinite	**4.7**	1.4	**62.9**	7.7	**13.4**	16.7	11.6
Calc-silicate	**5.5**	3.7	**89.6**	37.4	**16.3**	29.0	13.8

Table 5.25 PLI Is_{50}:UCS ratios for the orebody rock types at Sandsloot open pit mine and across all the PPRust open pits, based on the mine strength database.

Rock Type	Sandsloot Open Pit			All PPRust Open Pits		
	PLI Is_{50} (MPa) Avg.	UCS (MPa) Avg.	PLI Is_{50} : UCS Ratio Avg.	PLI Is_{50} (MPa) Avg.	UCS (MPa) Avg.	PLI Is_{50} : UCS Ratio Avg.
Feldspathic pyroxenite	7.6	192.8	**25.4**	12.4	164.8	**13.3**
Pyroxenite	10.5	142.5	**13.6**	7.5	149.1	**19.9**
Parapyroxenite	6.7	163.5	**24.4**	10.1	176.5	**17.5**
Serpentinite	4.7	180.5	**38.4**	8.1	126.3	**15.6**
Calc-silicate	5.5	127.7	**23.2**	8.3	132.1	**15.9**

ISRM (1981) suggest the conversion factor between Is_{50} and UCS ranges from 20 to 25, independent of rock type. However, these conversion factors have been found to be highly variable and can range between 8 and 45, though commonly they range between 16 and 24 (Bell, 1992). It is well recognized that site specific conversion factors are required and should be used in place of these very broad values. For the Sandsloot orebody rock types the conversion factors vary between 10.5 and 19.7 (Table 5.24). For each rock type the factor is less than that predicted using the mine database for the rocks in Sandsloot open pit, but is similar to those predicted when an average of the PPRust open pit data is used (Table 5.25). The difference arises from the UCS values predicted for each of the rock types. The Sandsloot database predicts higher uniaxial compressive strengths than those predicted in this study. However, in each case the number of samples tested in the Sandsloot database is lower than that tested in this study (Appendix C - Sandsloot open pit Rock Testing Database). Therefore it is possible that Sandsloot database is less accurate. Another source of error could be the calculations and the size correction factors applied to the Sandsloot UCS database results.

Because the raw database was not available, it was not possible to check the calculations and correction factors, therefore it has not been possible to determine if this is a source of error.

Multiple regression analysis was undertaken on the geotechnical data to determine if significant relationships could be built on more than two sets of properties. A good relationship between UCS, density and ultrasonic velocity was determined. The regression model which fits this data is given by equation 5.6.1.

$$\textbf{UCS (MPa) = 0.054886 * ultrasonic velocity(m/s) – 52.1215 * density (g/cm}^3\textbf{)}$$

Eqn: 5.6.1

R^2 for this regression was 0.96. They modelled UCS results with a 96% accuracy (95% C.I.) and therefore may be used to predict intact strengths with confidence where tests cannot be performed. The other geotechnical properties cannot be linked and therefore need to be studied individually.

5.7 Summary and Conclusions

The geotechnical properties of the Sandsloot orebody rock types were assessed for predictability in mining by looking at the density, the ultrasonic velocity, the point load index strength and the tensile and compressive strengths of intact samples. The drill hole core, from which the samples were selected, was characterised by logging the lithology, geotechnical properties and structural features. Thereafter the rock mass was classified according to Bieniawski's (1989) RMR, which rated the rock mass as good rock. Samples were tested in accordance with in-house procedures and procedures laid out by the ISRM (1981). The results were assembled into a database for interrogation and modelling using *Statgraphics Centurion XV*.

For each of the orebody rock types the characteristic values and variability of the properties studied were identified. Feldspathic pyroxenite, pyroxenite and parapyroxenite typically had the highest density, ultrasonic velocity and strengths, with pyroxenite commonly having the highest value for each property. Calc-silicate frequently had the second lowest and serpentinite had the lowest values for these geotechnical properties. Analysis of the statistical similarities between rock types for each property frequently distinguished feldspathic pyroxenite, pyroxenite and parapyroxenite as similar to each other, different to serpentinite and calc-silicate and distinguished differences between serpentinite and calc-silicate. The analyses identified density

and ultrasonic velocity as the properties which clearly distinguished the differences between the rock types as a 95% C.I. Furthermore, the analyses identified feldspathic pyroxenite and parapyroxenite as statistically indistinct from each other, as the most variable with respect to the properties studied and finally established parapyroxenite as the least distinguishable of the orebody rock types. The values and the relationships determined in this study can be used to predict the conditions of each mining block depending on the variety and quantity of each orebody rock type present. This knowledge will assist in the design of drill and blast plans and the prediction of the fragmentation size. Consequently loading, haulage, crushing and milling rates can be forecast and this data can be used for optimising the mine-to-mill processes.

The geotechnical properties were further assessed by comparing the properties between the orebody rock types as a whole and per rock type. The objective of the comparison was to determine if any of the properties were related and if so, how could this be used to facilitate appropriate and cost effective mining and processing practices. Results for the directly paired and indirectly related samples exhibited overlaps between rock type populations, similar to those identified with the Duncan's multiple range test, and scatter that clouded the trends and relationships. A study using the averages revealed the properties were commonly characterised by moderate to strong positive relationships. Density and ultrasonic velocity were identified as effective gauges of UCS and PLI Is_{50}. Ultrasonic velocity was also a good gauge of density. Tensile strength, on the other hand, cannot be estimated with these properties. The comparisons distinguished pyroxenite as frequently causing weakened correlations, with its disproportionately high PLI Is_{50} and low tensile strength. The only properties that were identified as valuable in combination with each other as reasonable estimates of another property were density and ultrasonic velocity. They modelled UCS results with a 96% accuracy (95% C.I.). The relationship between UCS and PLI Is_{50} was determined to be weak, indicating PLI Is_{50} did not model the UCS results well. However, a comparison between the two was undertaken and for each of the orebody rock types the ratio used to estimate UCS was less than that used currently for Sandsloot open pit and similar to those used for PPRust operations as a whole.

Knowledge of these relationships and their effectiveness in determining particular properties could be used to predict mining conditions where some or most of the data is either missing or is difficult to assess. In addition, these relationships may be used in comparison with properties that are studied in subsequent chapters, which will add to the characterisation of the orebody rock types.

Chapter 6

GEOCHEMICAL INVESTIGATION

6.1 Introduction

The objective of the geochemical analysis within this research study was to look at the multi-element data as being representative of specific rock types in the ore zone of Sandsloot open pit and to use it to assist in the prediction of the mining properties. This investigation is not intended to be a petrogenetic interpretation of the rock types in the pit. The aim is to examine the characteristics of the element data and describe the relationships, determining whether any elements, on their own or in combination, can be used to distinguish rock types for the prediction of geochemical properties. This data may be used in combination with the geotechnical properties and metallurgical properties to further charaterise the orebody rock types and predict mining properties.

This chapter gives a brief description of the methods of investigation which include X-ray Flourescence Spectroscopy (XRF) and Inductively Coupled Plasma Mass Spectroscopy. It reports the sample selection, preparation and testing procedures and lists the results of the analysis. Thereafter the results are discussed and statically interpreted, focusing on the distinguishing characteristics for each of the orebody rock types.

6.2 Methods of Investigation

6.2.1 X-ray Fluorescence Spectroscopy (XRF)

This analytical technique is used to quantitatively determine whole-rock major and trace elements present at concentration levels from 1 percent to 1 part per million (ppm). The XRF equipment is shown in Figure 6.1. Fine grade (< 20 μ particle size) milled powder of each sample was fused into a disc or pressed into a pellet for major and trace element analysis, respectively. The fusion discs or pellets were exposed to high-energy X-rays which cause excited electrons in the sample to move to higher orbital shells, specific for each element. The essential aspect of this method is that when the electrons return to their stable ground state they

emit a secondary radiation, which is characteristic for each element. This fingerprint transition radiation is used to identify the elements by comparing it to standards of known composition (Lapidus *et al*., 2003). In-house procedures were used to correct for matrix effects.

Figure 6.1 X-ray Fluorescence Spectroscopy Equipment, University of KwaZulu-Natal.

6.2.2 Inductively Coupled Plasma Mass Spectrometer (ICP-MS)

The ICP-MS technique is used to measure the concentrations of whole-rock trace elements to sub-parts per million levels and platinum group element (PGE) concentration to parts per billion. Figure 6.2 shows the machinery used to ICP-MS analyse the geochemical samples. The prepared sample, which is in solution form, is injected into an ionized medium of plasma. The plasma is created by introducing an electron into a field of support gas, in this case the support gas was Argon (Ar), which is charged by an alternating current of between at 1100 Watts. The addition of the electron causes a series of chain reactions and the ionized plasma medium is created. As the sample is injected into the plasma it too becomes ionized and the ions are filtered through the quadropole mass spectrometer. Depending on the mass of the ion it is allowed to pass through the quadropole filter, which is set at a particular voltage corresponding to the mass for each element. The filter is changed sequentially through all the masses until a statistically accurate measurement is found. The abundance of each element is compared to the intensity of specific standards and the concentration of the elements in the sample is calculated.

Figure 6.2 Inductively Coupled Plasma Mass Spectrometer, University of KwaZulu-Natal.

6.3 Sample Selection and Preparation

Specimens of each rock type were randomly selected from the core samples that had been uniaxial compressive strength (UCS) tested in the geotechnical investigation. The concentrations of elements and geochemical properties of each specimen could therefore be directly correlated to its geotechnical strengths. A total of eighty seven samples, from drill holes SSMet 3, SSMet 4, SSMet 5, SSPit 149, SSPit 150, SSPit 154, SSPit 159, SSPit 160 and SSPit 161 (Figure 4.1, chapter 4),were geochemically analysed using XRF and ICP-MS techniques.

After the core specimens were UCS tested the broken rock fragments were collected and bagged. All apparatus was thoroughly cleaned between tests to avoid contamination between samples. The bagged specimens were crushed and milled to three powder grades, that of coarse, normal and fine grade for the different analytical operations.

Fine grade powder was fused into Norrish fusion discs for XRF major element analysis and pressed into pellets for XRF trace element analysis using Mowiol as a binder. ICP-MS solution samples were prepared from fine grade powder which was digested by HF and HNO_3, evaporated and then added to HNO_3 of varying concentrations. PGE samples were prepared from normal grade powder. The powder was sent to Genalysis Laboratories in Perth, Australia where it was fused into a small Ni-sulphide bead or prill and returned to the laboratories at the School of Geological Science, University of KwaZulu-Natal. The prill was dissolved in HCl and

HNO_3, filtered, evaporated and added to pure HCl and deionized water for ICP-MS analysis. A more detailed description of the procedures and machinery used for geochemical sample preparation is given in Appendix D.

6.4 Testing Procedures

XRF and ICP-MS analysis were performed in the laboratories at the School of Geological Science, University of KwaZulu-Natal. The testing procedures followed those of the in-house practices. XRF analysis was performed using a Philips PW 1404 spectrometer. The spectrometer was calibrated using international standards and internal synthetic standards and blanks, detailed in Appendix D. ICP-MS analysis was performed using the Perkin-Elmer 6100 and the Perkin-Elmer DRC-e ICP-MS instruments. Three standards were used, BIR 1, BCR 1 and BHVO 1. A total procedural blank (TPB) of 100 µl of pure nitric acid dissolved in 5% concentrate nitric acid was used. For PGE analysis a composite standard solution of PE 1602, containing PGEs at 10 ppm was diluted to create calibration standards at 10, 20, 50 and 100 ppb levels. An in-house control sample and the international PGE standard SARM-7 were run to confirm reproducibility.

6.5 Results and Analysis

The results of the geochemical analyses were assembled into a second database, separate to the geotechnical results database, with each one of the eighty seven samples grouped on the basis of its major and trace element concentration and with corresponding geotechnical properties of density, ultrasonic velocity and uniaxial compressive strength. The database further classified the samples using drill hole location, sample depth down drill hole and lithology. As with the geotechnical database the analysis and interpretation of the results were carried out using the *Statgraphics Centurion XV* statistical program which again proved to be a powerful tool allowing drill hole, lithology and composition specific data to be queried. The statistical program provided a significant aid in the building and examination of relationships between the numerous variables in the database and which then could be used in a predictive way.

As described in the results of the geotechnical investigation (section 5.5, Chapter 5) the study of the data distribution is an important first step when statistical analysis is undertaken. Distribution analysis was performed on all 41 elements for each rock type, using the χ^2 test at a 95 % confidence interval (C.I. 95 %). The results showed that the distributions for 90 % of the

elements for each rock type were normal. The remaining 10 % were found to be a combination of apparent normal distributions with a few outside points (6 %) and log normal distributions (4 %). Figure 6.3 a and b show an example of each of these distributions, respectively. Both distributions are positively skewed, indicating a high frequency of low values, with a truncation of the left tail and an extended tail on the right, which indicates a low frequency of very high values. Figure 6.3 a. also shows two outside points which are causing the distribution to skew therefore not fitting a normal distribution.

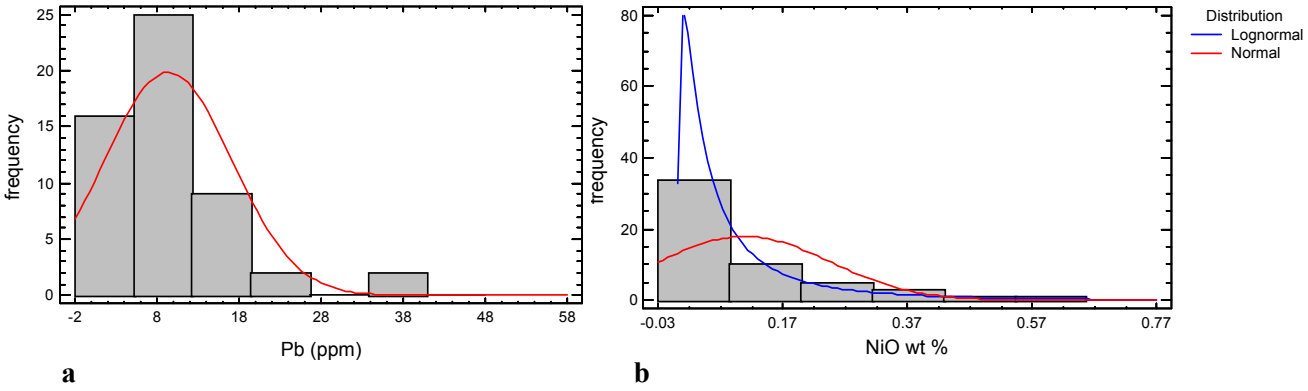

Figure 6.3 Non-normal distribution examples from the geochemistry data.

Causes of the non-normality relate to three unavoidable factors that are problematic when dealing with geochemical data. These are the spatial dependence of the data, the potential error involved in sampling, sample preparation and analysis, and the detection limit of the apparatus used (Reimann and Filzmoser, 2000; Rollinson, 1995). The outside points, which are the unusual high concentrations separate from the main population (Figure 6.3 a) originate from more than one geological process affecting the sample (Rollinson, 1995). The truncation of the left tail (Figure 6.3 b) is caused by the measuring equipment having a low concentration detection limit therefore some elements with concentrations below the detection limit can not be analysed, causing an apparent lognormal distribution (Figure 6.3 b).

The standard step, subsequent to identifying the anomalous points is to remove these points (like those in Figure 6.3 a) from the statistical treatment of the data. This would generally result in a normalized distribution, however, because these points are not far outside points and therefore not outliers (> 3 time the interquartile range) they have not been removed.

To deal with the lognormal distributed data it is standard practice to perform a transformation on the data thereby making the data more normal (Swan and Sandilands, 1995). A log-

transformation (log_{10} or ln), which was chosen because it applies to positively skewed data, was performed and the results studied to determine whether the transformed data approached log-normal distribution. The transformations were unsuccessful with many of the distributions showing little or no change towards log-normality.

Because the amount of data showing these different distributions was small (10 %) and for the reasons stated regarding the probable causes of non-normality, the values could be regarded as a subset of the larger range of geochemistry compositions, which are assumed to have arisen from a normally distributed population. The Central Limits Theorem (Davis, 1986) was therefore used to justify the use of parametric statistics on this small subset. Consequently the data sets for each of the rock types have been treated as normally distributed.

The results section arranges the analyses of major (XRF), trace (XRF and ICP-MS) and PGE element concentrations into groups of similar atomic properties according to the periodic table. The following sections divide the 41 elements analysed into groups of major element oxides, base metals, PGEs, alkali elements, rare earth elements (REE) and incompatible elements. These groups do not classify the elements based on predicted element behavior, therefore associations between the elements, within the groups and their characteristics are not expected. Where the same element has been analysed using both the XRF and the ICP-MS technique the results of the ICP-MS analyses are studied due to the superior precision and accuracy compared with the XRF results. Finally, all statistical procedures that have been used on the geochemical data are described in the Results and Analysis section for the geotechnical data (section 5.5, Chapter 5) unless they are used for the first time in this section. In which case they are described under the appropriate subsection where their use is first mentioned.

6.5.1 Major Element Oxides

Major element analysis was performed on eighty seven samples, all of which were included in the data analysis. The elements analysed, which are expresses as oxides, were SiO_2, Al_2O_3, FeO, MgO, CaO, Na_2O, K_2O, TiO_2, P_2O_5, Cr_2O_3 and NiO. The loss of ignition (L.O.I.) was also recorded for each sample. Table 6.1 shows the average abundance of each element analysed per rock type and their standard deviation. Other summary statistics such as median, maximum, minimum, range and interquartile range have not been included in the tables below because of the large number of data points. These descriptives for the major element oxides, and the other

groups of elements, are tabulated in Appendix D. Note the number of decimal places (precision) quoted is dependent on the element and conforms to geochemical standards.

Table 6.1 Summary statistics for major elements for each rock type.

Rock Type		Fpyx	Pyx	Parapyx	Serp	Calc-sil
Count		13	10	54	7	3
SiO_2 (wt %)	Avg.	**48.60**	**46.41**	**44.68**	**37.99**	**46.61**
	Std. dev^n	3.42	0.36	2.94	3.06	7.60
Al_2O_3 (wt %)	Avg.	**7.04**	**5.84**	**7.84**	**6.34**	**4.92**
	Std. dev^n	1.66	0.16	3.44	3.58	5.76
FeO (wt %)	Avg.	**8.00**	**7.18**	**7.57**	**12.84**	**4.34**
	Std. dev^n	2.42	0.31	1.63	1.87	2.90
MnO (wt %)	Avg.	**0.31**	**0.28**	**0.44**	**0.27**	**0.51**
	Std. dev^n	0.13	0.01	0.12	0.09	0.09
MgO (wt %)	Avg.	**15.53**	**13.03**	**23.16**	**39.32**	**23.16**
	Std. dev^n	3.94	0.14	5.00	2.48	6.49
CaO (wt %)	Avg.	**17.31**	**24.35**	**14.65**	**0.48**	**19.80**
	Std. dev^n	4.96	0.10	5.09	0.44	6.96
Na_2O (wt %)	Avg.	**0.89**	**0.10**	**0.18**	**0.03**	**0.02**
	Std. dev^n	0.79	0.04	0.12	0.04	0.04
K_2O (wt %)	Avg.	**0.15**	**0.01**	**0.13**	**0.01**	**0.01**
	Std. dev^n	0.15	0.00	0.16	0.01	0.00
TiO_2 (wt %)	Avg.	**0.25**	**0.36**	**0.29**	**0.17**	**0.18**
	Std. dev^n	0.07	0.00	0.12	0.10	0.21
P_2O_5 (wt %)	Avg.	**0.02**	**0.01**	**0.01**	**0.00**	**0.00**
	Std. dev^n	0.01	0.00	0.01	0.00	0.00
Cr_2O_3 (wt %)	Avg.	**0.14**	**0.02**	**0.01**	**0.02**	**0.01**
	Std. dev^n	0.13	0.00	0.04	0.02	0.01
NiO (wt %)	Avg.	**0.24**	**0.37**	**0.10**	**0.23**	**0.07**
	Std. dev^n	0.12	0.04	0.13	0.30	0.06
L.O.I. (wt %)	Avg.	**2.80**	**0.92**	**6.04**	**12.48**	**5.97**
	Std. dev^n	1.59	0.16	2.25	0.62	5.05

The chief elements which make up these five rock types are SiO_2, Al_2O_3, FeO, MgO, and CaO. The most abundant element is SiO_2. It forms roughly 38 – 49 % of the total weight of each rock type, comprising just under half of feldspathic pyroxenite (Table 6.1). Serpentine has the lowest amount of SiO_2 but still comprises almost 38 % by weight. MgO and CaO are the second and third most abundant elements respectively. Roughly 13 – 39 % of each of the five rock types is made up of MgO and 0.3 – 24 % is CaO. CaO has the widest range of abundance between rock types, out of all the major elements analysed. Note that whilst feldspathic pyroxenite has the highest SiO_2 and lowest MgO contents, serpentine in contrast has the lowest SiO_2 and highest MgO. These two elements behave in an opposite fashion. Al_2O_3 and FeO each form less than

13 % of the composition of each rock type. Al_2O_3 ranges between roughly 5 – 8 % and FeO ranges roughly 4 – 13 %. MnO, Na_2O_3, K_2O, TiO, P_2O_5, Cr_2O_3 and NiO individually account for less than 1 % of the weight of each rock type and therefore are only a small constituent of the rocks. The percentage of rock weight which was lost on ignition (L.O.I.) was highest for serpentinite. This was expected due to the hydrous chemical composition of serpentine, $Mg_3Si_2O_5(OH)_4$, which is four parts water. Parapyroxenite had the second highest L.O.I., which results from the breakdown of serpentine. Calc-silicate L.O.I. follows closely behind that of parapyroxenite, whilst feldspathic pyroxenite and pyroxenite have much lower L.O.I.

In Table 6.1 some of the standard deviation results are close in value to that of the mean and in later analyses the standard deviation results are greater than that of the mean, such is the case for the base metals, PGE, alkali and incompatible elements. Examination of these results revealed that this was most likely to occur for elements in calc-silicate and parapyroxenite, with the occasional element in feldspathic pyroxenite exhibiting a similar trend. The large standard deviation values indicate a wide spread of the data and are probably caused by the influence of the previously discussed outside points or apparent non-normality, as well as low numbers of sample tests for calc-silicate. As in the geotechnical investigation no evidence for error was detected, therefore the outside points were kept in the analysis to show the true variability of the data. In such cases the interquartile range and the box and whisker plot may be more appropriate means of measuring the data spread.

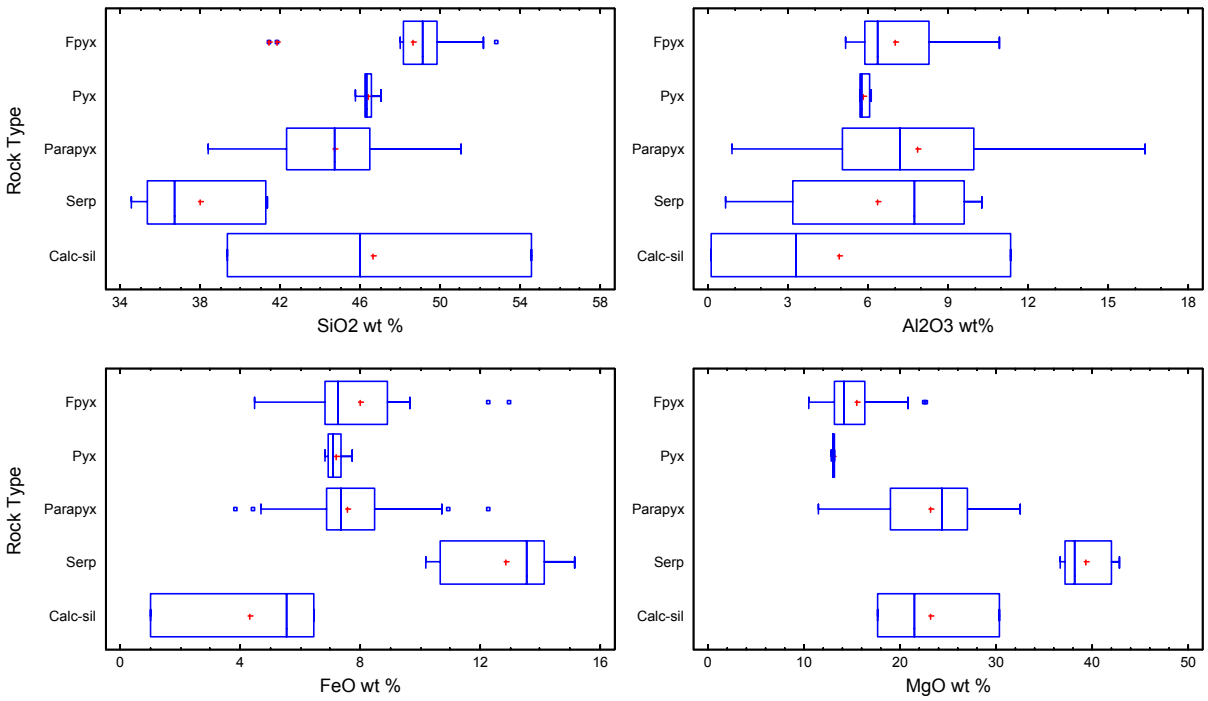

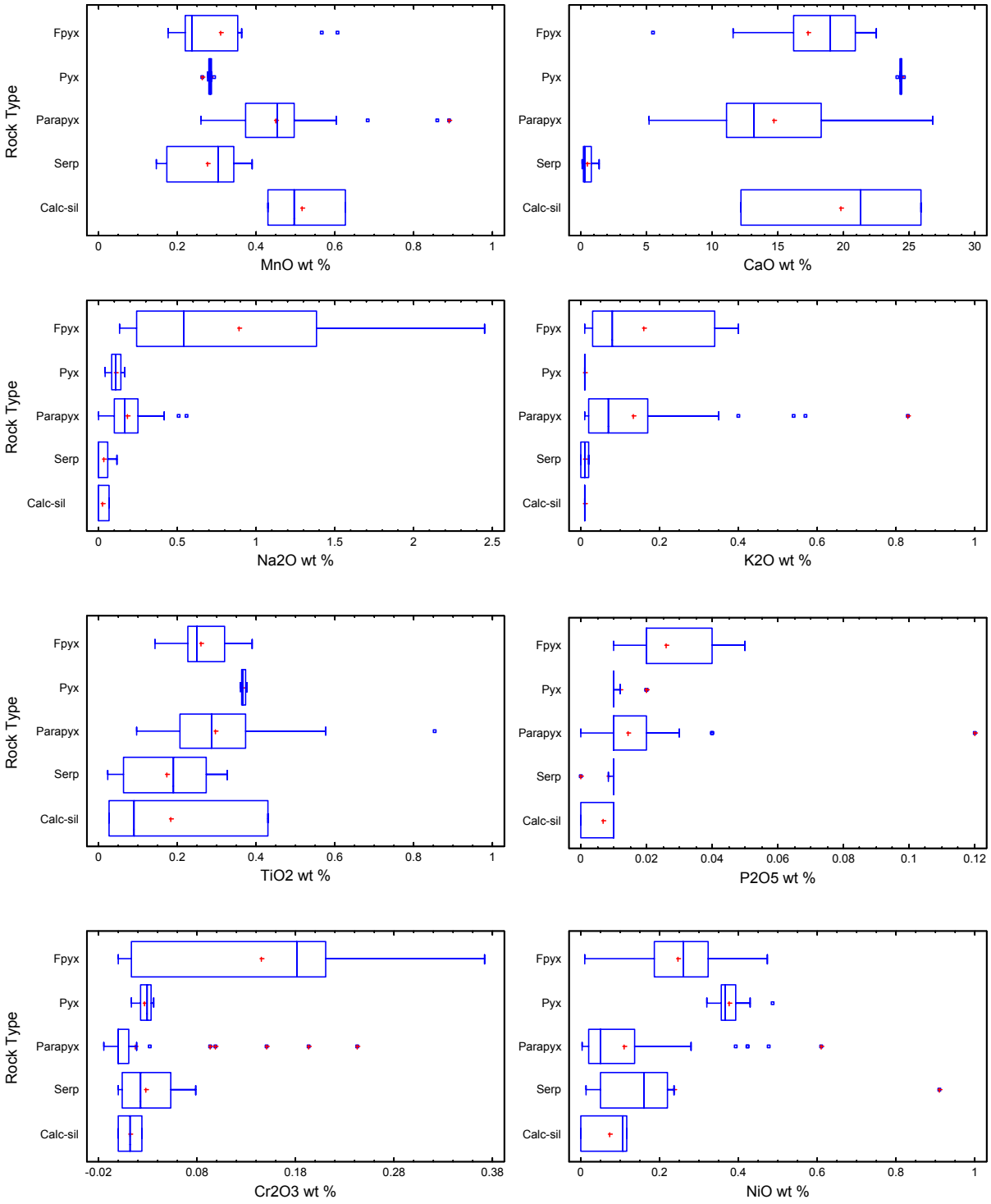

Figure 6.4 Box and whisker plot for major elements for each rock type (refer to figure notations used in box and whisker plots, as first described under section 5.5 Results and Analysis, Chapter 5, for the geotechnical data).

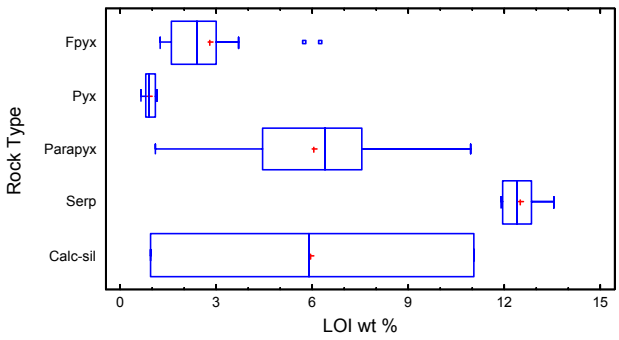

Figure 6.4 Box and whisker plot for loss on ignition for each rock type (refer to figure notations used in box and whisker plots, as first described under section 5.5 Results and Analysis, Chapter 5, for the geotechnical data).

The box and whisker figures above show graphically the characteristic sample population descriptives which can be used as a measure of the expected geochemical properties. These diagrams also give a good visual estimation of the similarities and differences between various rock types for the same element and the behaviour of the different elements for the same rock type. A brief examination of the figures reveals that pyroxenite shows the narrowest population dispersion for every element, indicating that this rock type does not vary in composition greatly. Parapyroxenite has the widest dispersion for SiO_2, Al_2O_3, MnO, MgO, CaO, K_2O, TiO_2 and LOI, whereas feldspathic pyroxenite has the widest dispersion for Na_2O_3, P_2O_5, Cr_2O_3 and NiO. Therefore, these two rock types will show the most variability in terms of composition. FeO is as variable in feldspathic pyroxenite as it is in parapyroxenite. The box and whisker plots for the calc-silicates show no 'tails' and appear to have the widest dispersion of the central 50 % of the data (area shown by the box), which is confirmed by this rock type frequently having the highest standard deviation. However, because this rock type is only a minor constituent of the orebody little of it was drilled and consequently the amount of material available for testing was limited. Therefore, only three samples of this rock type were geochemically tested causing the box and whisker plots and dispersions to be distorted.

The one way analysis of variance (ANOVA) (Davis, 1986) was used to examine the differences between the means of different groups (in this case different rock types) and to determine the significance of these differences. For major element analysis the one way ANOVA (C.I. 95 %) test revealed there was a significant difference in major element abundance between rock types for each element analysed, except for Al_2O_3 and K_2O.

Although box and whisker plots (Figure 6.4) are good visual displays of comparison for the same element between different rock types, these plots do not discern the differences or similarities at any level of significance. Hence the Duncan's multiple range test (Statpoint, 2005) was used to determine which elements had similar abundances for different rock types. Table 6.2 shows the results of the Duncan's multiple range test (C.I. 95 %). The 'crosses' represent the rock types which show similar compositions of a specific element. When these 'crosses' fall into vertical groups across rock types the abundance of that element is similar at a 95 % confidence interval for those rock types. They may therefore be regarded as a statistically homogenous group. The test confirms the results of the one way ANOVA for Al_2O_3 and K_2O. It shows Na_2O and Cr_2O_3 can be used to distinguish feldspathic pyroxenite from the other rock types. SiO_2 and CaO can be used to differentiate serpentinite. MnO, MgO and L.O.I can be used to separate calc-silicate and parapyroxenite and FeO may be used to distinguish between calc-silicate, serpentinite and the feldspathic pyroxenite, parapyroxenite and pyroxenite rock types. Individually no single major element can be used to differentiate between the various rock types.

Table 6.2 Duncan's multiple range tests for major elements between rock types.

SiO_2 wt %		Al_2O_3 wt %		FeO wt %		MnO wt %		MgO wt %		CaO wt %		Na_2O wt %	
RT	**HG**	**RT**	**HG**	**RT**	**HG**	**RT**	**HG**	**RT**	**HG**	**RT**	**HG**	**RT**	**HG**
Serp	X	Calc-sil	X	Calc-sil	X	Serp	X	Pyx	X	Serp	X	Calc-sil	X
Parapyx	X	Pyx	X	Pyx	X	Pyx	X	Fpyx	X	Parapyx	X	Serp	X
Pyx	XX	Serp	X	Parapyx	X	Fpyx	X	Calc-sil	X	Fpyx	XX	Pyx	X
Calc-sil	XX	Fpyx	X	Fpyx	X	Parapyx	X	Parapyx	X	Calc-sil	XX	Parapyx	X
Fpyx	X	Parapyx	X	Serp	X	Calc-sil	X	Serp	X	Pyx	X	Fpyx	X

RT, rock type; HG, homogenous group

K_2O wt %		TiO_2 wt %		P_2O_5 wt %		Cr_2O_3 wt %		NiO wt %		L.O.I. wt %	
RT	**HG**	**RT**	**HG**	**RT**	**HG**	**RT**	**HG**	**RT**	**HG**	**RT**	**HG**
Pyx	X	Serp	X	Calc-sil	X	Calc-sil	X	Calc-sil	X	Pyx	X
Calc-sil	X	Calc-sil	X	Serp	X	Parapyx	X	Parapyx	XX	Fpyx	X
Serp	X	Fpyx	XX	Pyx	XX	Pyx	X	Serp	XX	Calc-sil	X
Parapyx	X	Parapyx	XX	Parapyx	XX	Serp	X	Fpyx	XX	Parapyx	X
Fpyx	X	Pyx	X	Fpyx	X	Fpyx	X	Pyx	X	Serp	X

RT, rock type; HG, homogenous group

The one way ANOVA (C.I. 95 %) test was run a second time to determine if significant differences existed for the same element within the same rock type but from different drill holes. Results revealed that for feldspathic pyroxenite, parapyroxenite and serpentinite the abundances of the same element varied between different drill holes. The elements which showed a variance were SiO_2, FeO, MnO, MgO, CaO, Na_2O_3, TiO_2, Cr_2O_3, NiO and L.O.I. This indicates that for

the majority of the major elements which constitute the orebody rock types, the abundance varies spatially.

Due to the limited amount of pyroxenite and calc-silicate sample available for testing, specimens tested for these rock types each came from a single drill hole. Differences in major element concentration between drill holes could therefore not be examined. Testing for differences in base metal, platinum group element, alkali earth, rare earth and incompatible elements, between drill holes, will likewise not be examined for these two rock types.

6.5.2 Base Metal Elements

Elements commonly associated with base metals are Ni, Cu, S, Co, V, As, Sc, Pb, Cr and Zn. These elements were considered as a single ground and shall be referred to as the base metal group. The base metal elements were analysed and the results are summarised in Table 6.3, which gives the concentration for each rock type using the average and standard deviation for each element. In total 87 samples of the five rock types were tested and all the results were included into the data analysis.

Table 6.3 Summary statistics for base metal group of elements per rock type.

Rock Type		Fpyx	Pyx	Parapyx	Serp	Calc-sil
Count		13	10	54	7	3
Ni (ppm)	Avg.	**1821**	**2852**	**779**	**1577**	**551**
	Std. dev^{n}	904	308	1023	2143	470
Cu (ppm)	Avg.	**1085**	**1853**	**392**	**893**	**307**
	Std. dev^{n}	695	194	591	985	418
S (ppm)	Avg.	**5751**	**22770**	**4748**	**16514**	**1679**
	Std. dev^{n}	4509	2887	8292	9402	1652
Co (ppm)	Avg.	**76.1**	**83.7**	**40.8**	**94.2**	**26.5**
	Std. dev^{n}	28.4	7.6	23.9	73.0	25.2
V (ppm)	Avg.	**135.7**	**262.7**	**78.5**	**25.1**	**35.3**
	Std. dev^{n}	62.2	34.4	47.4	12.8	43.6
As (ppm)	Avg.	**0.958**	**0.710**	**0.458**	**0.633**	**1.448**
	Std. dev^{n}	1.332	0.091	0.418	0.359	1.940
Sc (ppm)	Avg.	**26.8**	**32.0**	**15.6**	**7.1**	**6.7**
	Std. dev^{n}	9.6	4.2	9.3	5.2	7.6
Pb (ppm)	Avg.	**39.282**	**5.211**	**9.368**	**9.691**	**111.272**
	Std. dev^{n}	83.023	1.992	7.759	10.220	180.706
Cr (ppm)	Avg.	**848**	**140**	**148**	**143**	**84**
	Std. dev^{n}	774	35	319	162	72
Zn (ppm)	Avg.	**78**	**31**	**43**	**51**	**72**
	Std. dev^{n}	70	5	20	33	87

The Platreef is a PGE deposit with associated Cu and Ni mineralisation. The rock types which have been tested are those which comprise the orebody at Sandsloot therefore the high concentrations of Cu and Ni, especially in the pyroxenite and feldspathic pyroxenite rock types, as observed in Table 6.3, were expected. The concentration of S is also high, notably in the pyroxenite and serpentinite. The concentration of Cr is extremely high (848 ppm) in the feldspathic pyroxenite relative to the other rock types (84 – 148 ppm), V is much higher in the pyroxenite (262.7 ppm) compared with 25.1 – 135.7 ppm for other rock types and Pb is higher in calc-silicate (111.272 ppm) compared to the other rock types (9.368 – 39.282 ppm). The remaining base metal elements are present in the rocks at levels below 79 ppm and therefore have very low concentrations.

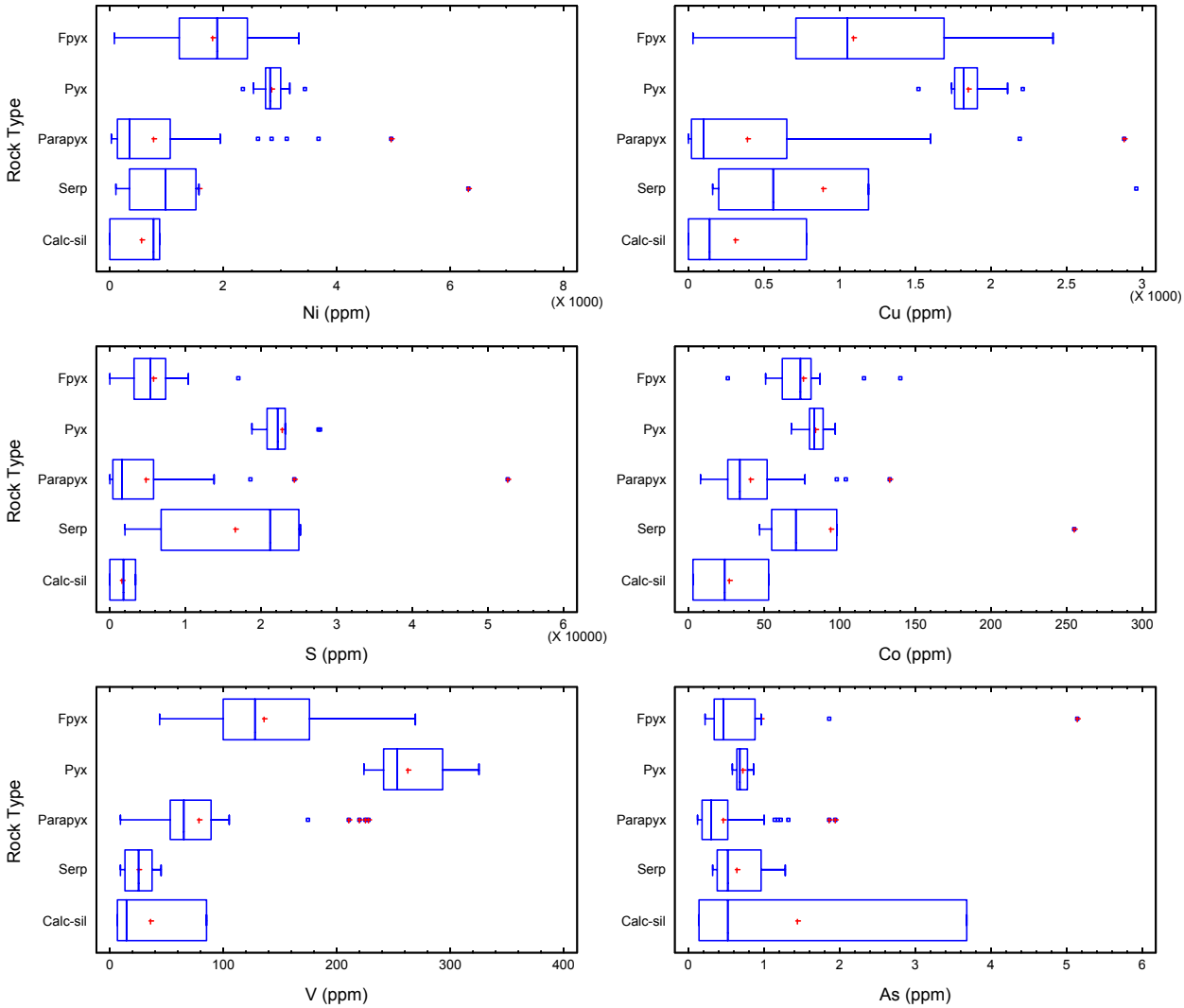

Figure 6.5 Box and whisker plot for base metal group of elements for each rock type.

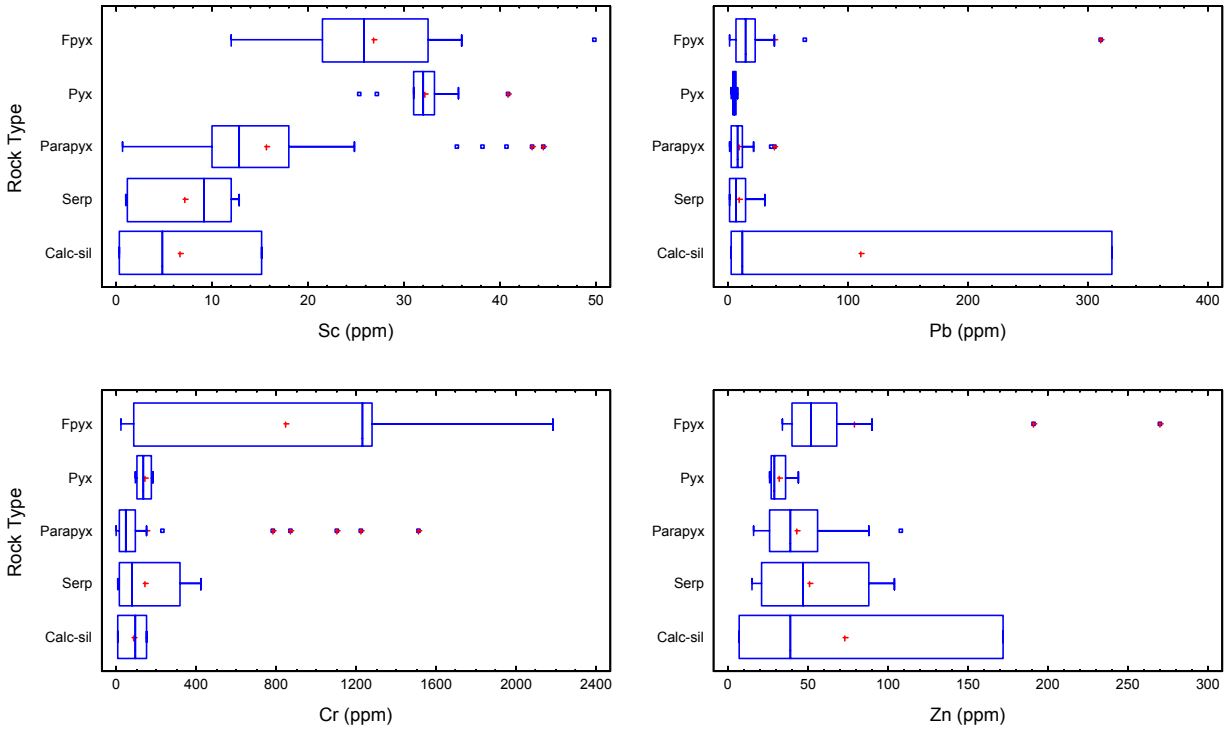

Figure 6.5 Box and whisker plot for base metal elements for each rock type.

As with the major element analysis for calc-silicate the wide dispersion of data and the distorted box and whisker plots may be attributed to the low number of samples analysed (Figure 6.5). Pyroxenite shows the narrowest dispersion for all the base metal group of elements except V and therefore its base metal concentrations are the most predictable out of all the rock types. Parapyroxenite shows the widest dispersions for S, Co, As and Zn whilst feldspathic pyroxenite shows the widest population dispersions for Ni, Cu, V and Cr. These two rock types are expected to be the most variable in terms of the concentrations of the base metal group. A noteworthy observation is that the Cu, Ni and S, which are secondary mining products, will vary in feldspathic pyroxenite and particularly in parapyroxenite the most. Cr has a similar concentration in all the rock types except feldspathic pyroxenite for which it is much higher. Pb has a very narrow dispersion for all the rock types except for calc-silicate, for the reason stated above. Pb concentration is highly predictable although not distinguishing for any rock type.

Applying the one way ANOVA (C.I. 95 %) revealed all the elements of the base metal group, except Pb, have significant differences in concentrations between different rock types. Table 6.4 shows the results of Duncan's multiple range test (C.I. 95 %). This table confirms the ANOVA results for Pb, indicating that its concentration is very predictable but the same for each rock type. The table also shows that the concentration of Cu can be used to discern pyroxenite from

the other rock types, Cr distinguishes feldspathic pyroxenite and S distinguishes pyroxenite and serpentinite. Co distinguishes calc-silicate and parapyroxenite and Sc distinguishes pyroxenite and feldspathic pyroxenite. It is clear no element on its own is a satisfactory indicator for a particular rock type, however, V can be used to satisfactorily discern between feldspathic pyroxenite and pyroxenite.

Table 6.4 Duncan's multiple range tests for base metal elements between rock types

Ni (ppm)		Cu (ppm)		S (ppm)		Co (ppm)		V (ppm)		As (ppm)	
RT	HG	RT	HG	RT	HG	RT	HG	RT	HG	RT	HG
Calc-sil	X	Calc-sil	X	Calc-sil	X	Calc-sil	X	Serp	X	Parapyx	X
Parapyx	XX	Parapyx	X	Parapyx	X	Parapyx	X	Calc-sil	XX	Serp	X
Serp	XX	Serp	XX	Fpyx	X	Fpyx	X	Parapyx	X	Pyx	XX
Fpyx	XX	Fpyx	X	Serp	X	Pyx	X	Fpyx	X	Fpyx	XX
Pyx	X	Pyx	X	Pyx	X	Serp	X	Pyx	X	Calc-sil	X

RT, rock type; HG, homogenous group

Sc (ppm)		Pb (ppm)		Cr (ppm)		Zn (ppm)	
RT	HG	RT	HG	RT	HG	RT	HG
Calc-sil	X	Pyx	X	Calc-sil	X	Pyx	X
Serp	X	Parapyx	X	Pyx	X	Parapyx	XX
Parapyx	X	Serp	X	Serp	X	Serp	XX
Fpyx	X	Fpyx	X	Parapyx	X	Calc-sil	X
Pyx	X	Calc-sil	X	Fpyx	X	Fpyx	X

RT, rock type; HG, homogenous group

The difference in the concentration of base metal elements, for the same rock type between different drill holes was determined using the one way ANOVA (C.I. 95 %). Parapyroxenite varied the most between drill holes with 80 % of the elements (Ni, Cu, S, Co, V, As, Sc and Cr) differing in concentration. Feldspathic pyroxenite varied for 60 % of the elements (Ni, S, Co, V, Sc and Zn) whilst serpentine varied only in Sc, between drill holes. Differences for pyroxenite and calc-silicate could not be determined for reasons stated previously in the sections on major elements analysis.

6.5.3 Platinum Group Elements

Analysis of the platinum group elements (PGEs) Ir, Os, Pd, Pt, Rh and Ru was performed on each of the eighty seven samples tested geochemically. Included in this analysis was the Au concentration, as Au commonly occurs as the alloy electrum with the PGEs observed at Sandsloot open pit. All the results were added to the data set and a summary of the PGE concentrations per rock type are given in Table 6.5.

Table 6.5 Summary statistics for platinum group elements per rock type.

Rock Type		Fpyx	Pyx	Parapyx	Serp	Calc-sil
Count		13	10	35	7	3
Au (ppb)	Avg.	**168**	**156**	**227**	**91**	**132**
	Std. dev^{n}	92	25	271	104	178
Ir (ppb)	Avg.	**23**	**26**	**26**	**7**	**35**
	Std. dev^{n}	16	6	50	9	48
Os (ppb)	Avg.	**12**	**15**	**13**	**3**	**18**
	Std. dev^{n}	8	4	25	4	25
Pd (ppb)	Avg.	**1308**	**1332**	**1477**	**546**	**1883**
	Std. dev^{n}	783	179	2860	704	2639
Pt (ppb)	Avg.	**1035**	**1234**	**1258**	**324**	**2209**
	Std. dev^{n}	611	149	2223	323	2170
Rh (ppb)	Avg.	**106**	**100**	**111**	**33**	**154**
	Std. dev^{n}	68	22	210	40	211
Ru (ppb)	Avg.	**94**	**108**	**97**	**25**	**143**
	Std. dev^{n}	67	35	186	31	196

The rock types tested in this study come from the orebody therefore high PGE concentrations are expected. Calc-silicate has the highest PGE concentrations (Table 6.5) despite being considered the footwall to the igneous deposit. This is not unusual as in the Sandsloot pit the footwall is often mineralised and has grade sufficiently high enough for it to be mined. The concentration of PGEs between feldspathic pyroxenite, pyroxenite, parapyroxenite and calc-silicate are similar whereas serpentinite concentrations are consistently the lowest. Feldspathic pyroxenite shows the lowest concentrations of the PGEs out of the three main orebody rock types. The concentration of Au decreases from parapyroxenite to feldspathic pyroxenite, pyroxenite, calc-silicate and then to serpentinite.

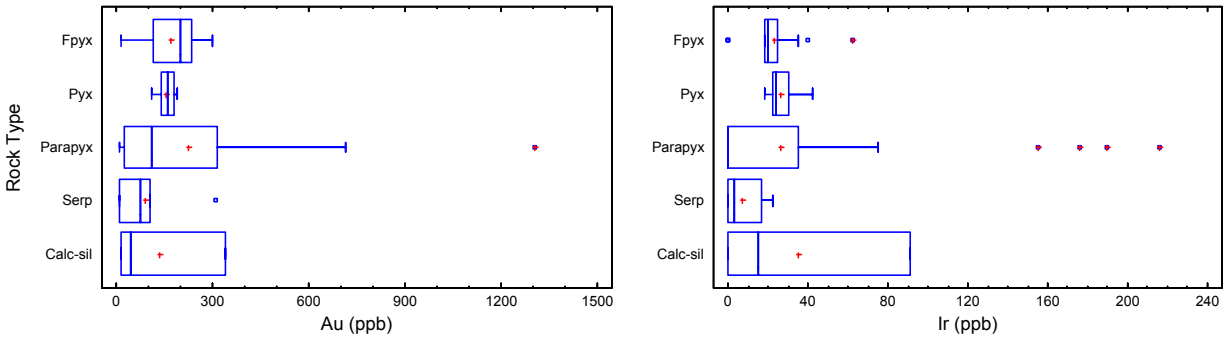

Figure 6.6 Box and whisker plot for gold and platinum group elements for each rock type.

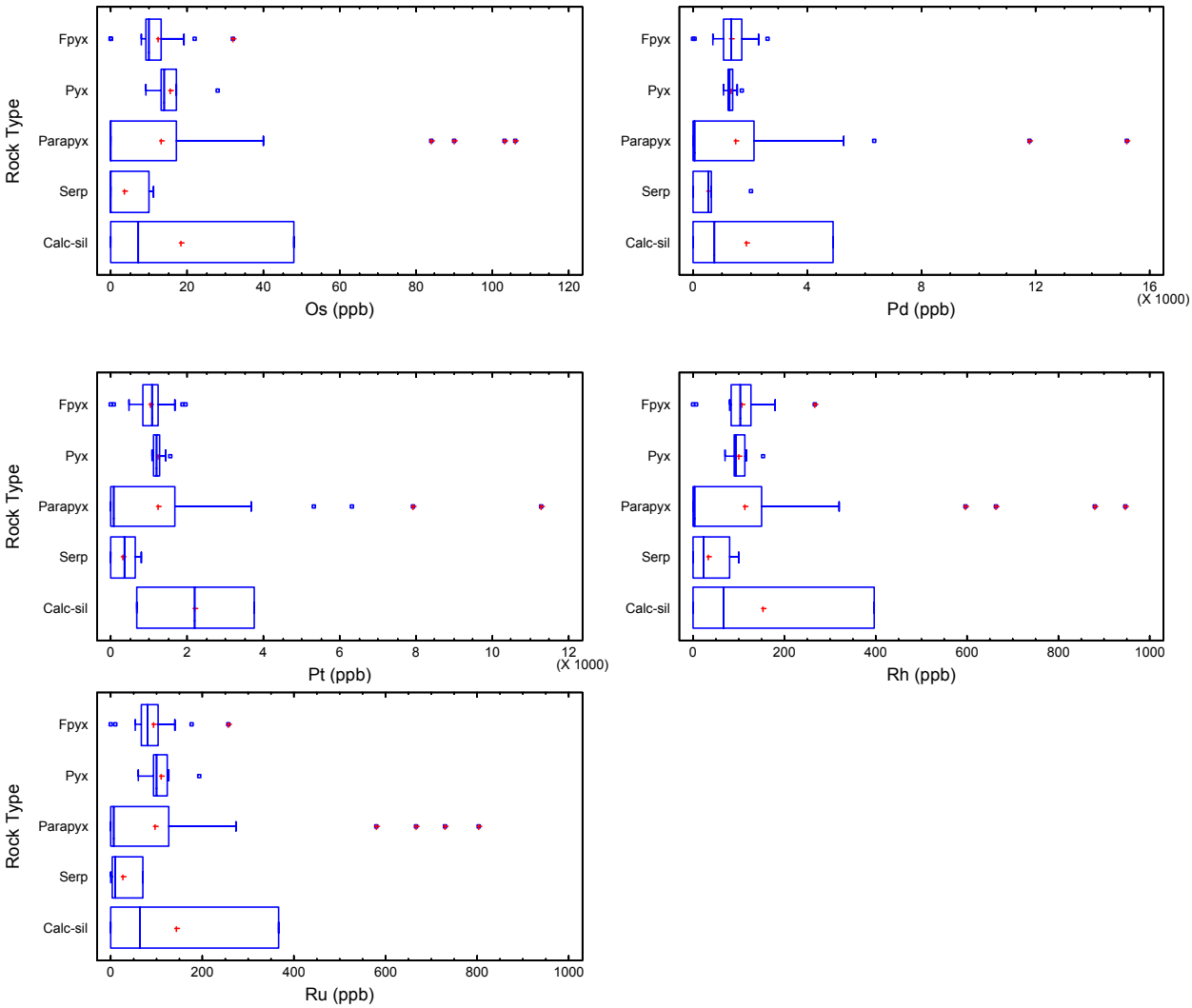

Figure 6.6 Box and whisker plot for gold and platinum group elements for each rock type.

The overall dispersion of the PGEs and Au is narrow for all the rock types (Figure 6.6) although the dispersion for PGEs within the parapyroxenite is very high, which indicates parapyroxenite can be expected to have the most variable concentrations. Calc-silicate results are distorted by the low number of samples tested and therefore have an exaggerated variability.

No statistically significant differences exist between the rock types for the concentrations of PGEs and Au. This was determined using the one way ANOVA (C.I. 95 %). The same results are displayed for Duncan's multiple range test (C.I. 95 %) in Table 6.6.

Table 6.6 Duncan's multiple range tests for platinum group elements between rock types.

Au (ppb)		Ir (ppb)		Os (ppb)		Pd (ppb)		Pt (ppb)		Rh (ppb)		Ru (ppb)	
RT	HG	RT	HG	RT	HG	RT	HG	RT	HG	RT	HG	RT	HG
Serp	X	Serp	X	Serp	X	Serp	X	Serp	X	Serp	X	Serp	X
Calc-sil	X	Fpyx	X	Fpyx	X	Fpyx	X	Fpyx	X	Pyx	X	Fpyx	X
Pyx	X	Pyx	X	Parapyx	X	Pyx	X	Pyx	X	Fpyx	X	Parapyx	X
Fpyx	X	Parapyx	X	Pyx	X	Parapyx	X	Parapyx	X	Parapyx	X	Pyx	X
Parapyx	X	Calc-sil	X	Calc-sil	X	Calc-sil	X	Calc-sil	X	Calc-sil	X	Calc-sil	X

RT, rock type; HG, homogenous group

Despite not showing any difference in concentration between rock types, the amount of PGEs do vary significantly between drill holes for the same rock type. Using the one way ANOVA (C.I. 95 %) PGE concentrations were determined to vary for all the PGEs for both feldspathic pyroxenite and parapyroxenite. Serpentinite PGE concentrations were not significantly different between drill holes. Au concentration was only variable between drill holes for feldspathic pyroxenite.

6.5.4 Alkali and Alkali Earth Elements

The concentrations of alkali elements and alkali earth elements are given in Table 6.7. Na_2O and K_2O are quoted as percentage weight of the whole rock sample, where as Sr and Rb are given in parts per million. Analysis for alkali and alkali earth element concentration was performed on eighty seven samples and all the results were included into the database.

Table 6.7 Summary statistics for alkali and alkali earth elements for each rock type.

Rock Type		Fpyx	Pyx	Parapyx	Serp	Calc-sil
Count		13	10	54	7	3
Na_2O (wt %)	Avg.	**0.89**	**0.10**	**0.18**	**0.03**	**0.02**
	Std. dev^n	0.79	0.04	0.12	0.04	0.04
K_2O (wt %)	Avg.	**0.15**	**0.01**	**0.13**	**0.01**	**0.01**
	Std. dev^n	0.15	0.00	0.16	0.00	0.00
Sr (ppm)	Avg.	**58**	**32**	**27**	**1**	**10**
	Std. dev^n	50	3	32	0	2
Rb (ppm)	Avg.	**5.806**	**0.157**	**5.543**	**0.578**	**0.170**
	Std. dev^n	6.489	0.033	7.962	0.465	0.094

Feldspathic pyroxenite shows the highest concentrations for all of the alkali and alkali earth elements (Table 6.7). This result was expected as it is rich in alkali feldspar and plagioclase ($NaAlSi_3O_8$ - $CaAl_2SiO_8$) containing sodium and small amounts of potassium. Parapyroxenite

and pyroxenite alternate in having the second highest concentrations of these elements followed by serpentinite and calc-silicate.

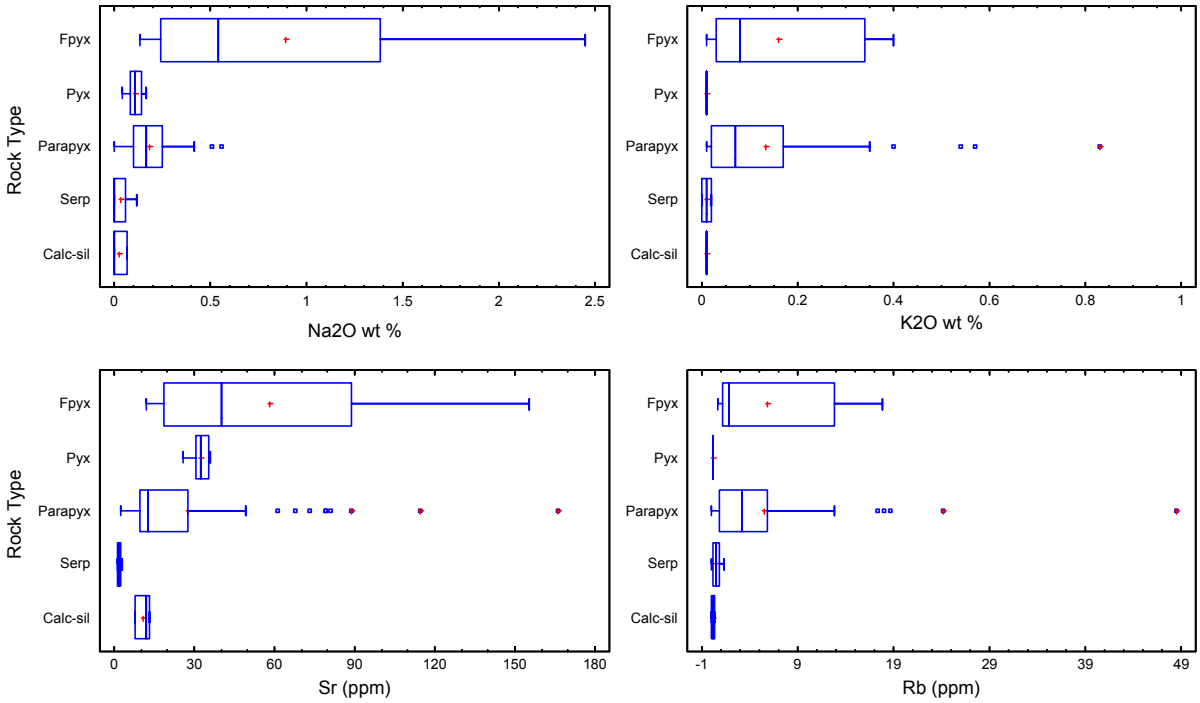

Figure 6.7 Box and whisker plot for alkali and alkali earth elements for each rock type.

Variability, which has been assessed by observing the box and whisker plots (Figure 6.7) and the values for standard deviation (Table 6.7) is low for all the elements, especially for K_2O and Rb, within the pyroxenite, serpentinite and calc-silicate rock types. Feldspathic pyroxenite shows the widest dispersions of data about the mean and therefore the greatest variability for each element. Parapyroxenite shows the second highest variability.

Using the one way ANOVA (C.I. 95 %) significant differences in concentrations for Na_2O, and Sr were found between the different rock types (Table 6.8). The concentration of K_2O and Rb is uniform for all rock types. These two elements are not good indicators of rock type at a 95 % confidence interval. Concentration of Na_2O predicts feldspathic pyroxenite and Sr distinguishes serpentine and calc-silicate from feldspathic pyroxenite.

Table 6.8 Duncan's multiple range tests for alkali and alkali earth elements between rock types

Na_2O (wt %)		K_2O (wt %)		Sr (ppm)		Rb (ppm)	
RT	**HG**	**RT**	**HG**	**RT**	**HG**	**RT**	**HG**
Calc-sil	X	Pyx	X	Serp	X	Pyx	X
Serp	X	Calc-sil	X	Calc-sil	X	Calc-sil	X
Pyx	X	Serp	X	Parapyx	XX	Serp	X
Parapyx	X	Parapyx	X	Pyx	XX	Parapyx	X
Fpyx	X	Fpyx	X	Fpyx	X	Fpyx	X

RT, rock type; HG, homogenous group

The one way ANOVA (C.I. 95 %) test for elements within the same rock type, from different drill holes indicated Na_2O varied for feldspathic pyroxenite and parapyroxenite. K_2O also varied for parapyroxenite and Sr varied for serpentinite. The other alkali and alkali earth elements did not vary for any of the rock types between drill holes. It is important to note that the alkali elements tend to be mobile and subject to disturbances with even minor degrees of alteration.

6.5.5 Rare Earth Elements

Fifteen rare earth elements (REE) were analysed. These were La, Ce, Pr, Nd, Sm, Eu, Gd, Tb, Dy, Ho, Er, Tm, Yb, Lu and Y. Rare earth elements are metallic elements with similar chemical properties and which behave similarly to incompatible elements in a melt. The sum of the rare earth elements is assessed in this section rather than each element individually because these elements behave in a similar manner (Rollinson, 1995) therefore, for the purposes of this study they have been regarded as a single group. Table 6.9 shows the average and standard deviation for the total count of rare earth elements for each rock type. Only the total counts of the REE were included into the data analysis.

Table 6.9 Summary statistics for rare earth elements for each rock type.

Rock Type		**Fpyx**	**Pyx**	**Parapyx**	**Serp**	**Calc-sil**
Count		**13**	**10**	**54**	**7**	**3**
Total REE	Avg.	**43.3**	**34.7**	**27.5**	**10.5**	**43.5**
	Std. dev^n	17.9	3.1	11.2	5.3	60.0

Analysis of eighty seven samples revealed that the calc-silicates had the highest REE count followed by feldspathic pyroxenite the pyroxenite and parapyroxenite. Serpentinite has a much lower count of REE (Table 6.9).

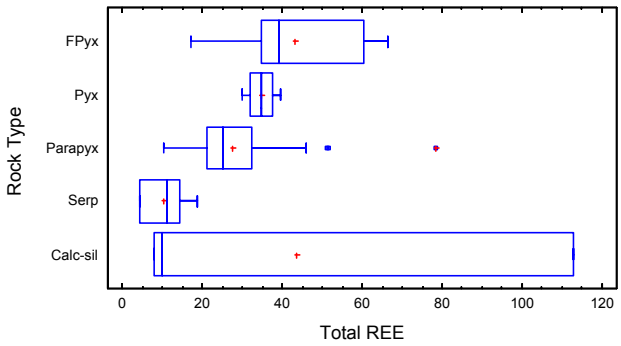

Figure 6.8 Box and whisker plot for total count of rare earth elements for each rock type.

Calc-silicate shows the greatest spread of data and highest standard deviation (Figure 6.8 and Table 6.9 respectively) but these results are misleading as the low number of samples has exaggerated the variability. Pyroxenite has the lowest spread of data and therefore is the most predictable in terms of REE concentration. Feldspathic pyroxenite is the most wildly dispersed population of REE followed by parapyroxenite.

Analysis of the data by applying the one way ANOVA test (C.I. 95 %) revealed that there is a significant difference in REE concentration between rock types. The results of Duncan's multiple range test (C.I. 95 %) (Table 6.10) shows that parapyroxenite, pyroxenite, feldspathic pyroxenite and calc-silicate are similar in REE concentration and that serpentinite can be discerned from these rock types on the basis of REE concentration.

Table 6.10 Duncan's multiple range tests for total rare earth elements between rock types.

Rock Type	HG
Serp	X
Parapyx	X
Pyx	X
Fpyx	X
Calc-sil	X

RT, rock type; HG, homogenous group

Applying the one way ANOVA (C.I. 95 %) a second time on the data to determine if any significant differences exist between drill holes for the same rock type, revealed that only feldspathic pyroxenite REE abundance levels varied significantly between drill holes.

6.5.6 Incompatible Elements

Incompatible elements are defined as those elements which have the greatest affinity for the liquid phase in a crystallizing magma, with their degree of compatibility being dependent on the physical and chemical environment during crystallization or melting (Lapidus *et al*., 2003). These elements are effectively and variably rejected by the early formed silicate minerals and therefore tend to increase in concentration in the liquid. Eighty seven samples were analysed and all the results were included into the database. The results are given in Table 6.11.

Table 6.11 Summary statistics for incompatible elements for each rock type.

Rock Type		Fpyx	Pyx	Parapyx	Serp	Calc-sil
Count		13	10	54	7	3
Ba (ppm)	Avg.	**40.3**	**2.7**	**20.9**	**2.9**	**1.3**
	Std. dev^{n}	63.9	1.4	40.5	1.9	1.6
Th (ppm)	Avg.	**0.931**	**0.513**	**0.804**	**0.247**	**1.424**
	Std. dev^{n}	0.726	0.083	2.590	0.293	1.214
U (ppm)	Avg.	**0.336**	**0.227**	**0.202**	**0.145**	**0.482**
	Std. dev^{n}	0.239	0.015	0.371	0.146	0.664
Ta (ppm)	Avg.	**0.077**	**0.055**	**0.056**	**0.046**	**0.050**
	Std. dev^{n}	0.056	0.004	0.064	0.030	0.081
Zr (ppm)	Avg.	**28.2**	**42.9**	**32.6**	**21.5**	**22.2**
	Std. dev^{n}	11.8	5.0	18.5	18.8	34.7
Nb (ppm)	Avg.	**1.181**	**0.876**	**0.674**	**0.354**	**0.607**
	Std. dev^{n}	0.998	0.092	0.762	0.241	0.712
P (ppm)	Avg.	**97**	**28**	**59**	**20**	**30**
	Std. dev^{n}	60	16	74	11	15
Hf (ppm)	Avg.	**0.942**	**1.583**	**1.299**	**0.833**	**0.671**
	Std. dev^{n}	0.364	0.172	0.733	0.547	1.077

Ba, Zr and P have the highest relative concentrations of all the incompatible elements in these rocks. The remaining incompatible elements have very low concentrations, all < 2 ppm. Table 6.11 shows feldspathic pyroxenite has the highest concentration of Ba and P (40.3 and 97 ppm respectively) and pyroxenite has the highest Zr concentration (42.9 ppm). Calc-silicate has the highest concentrations of Th and U at 1.424 ppm and 0.482 ppm respectively.

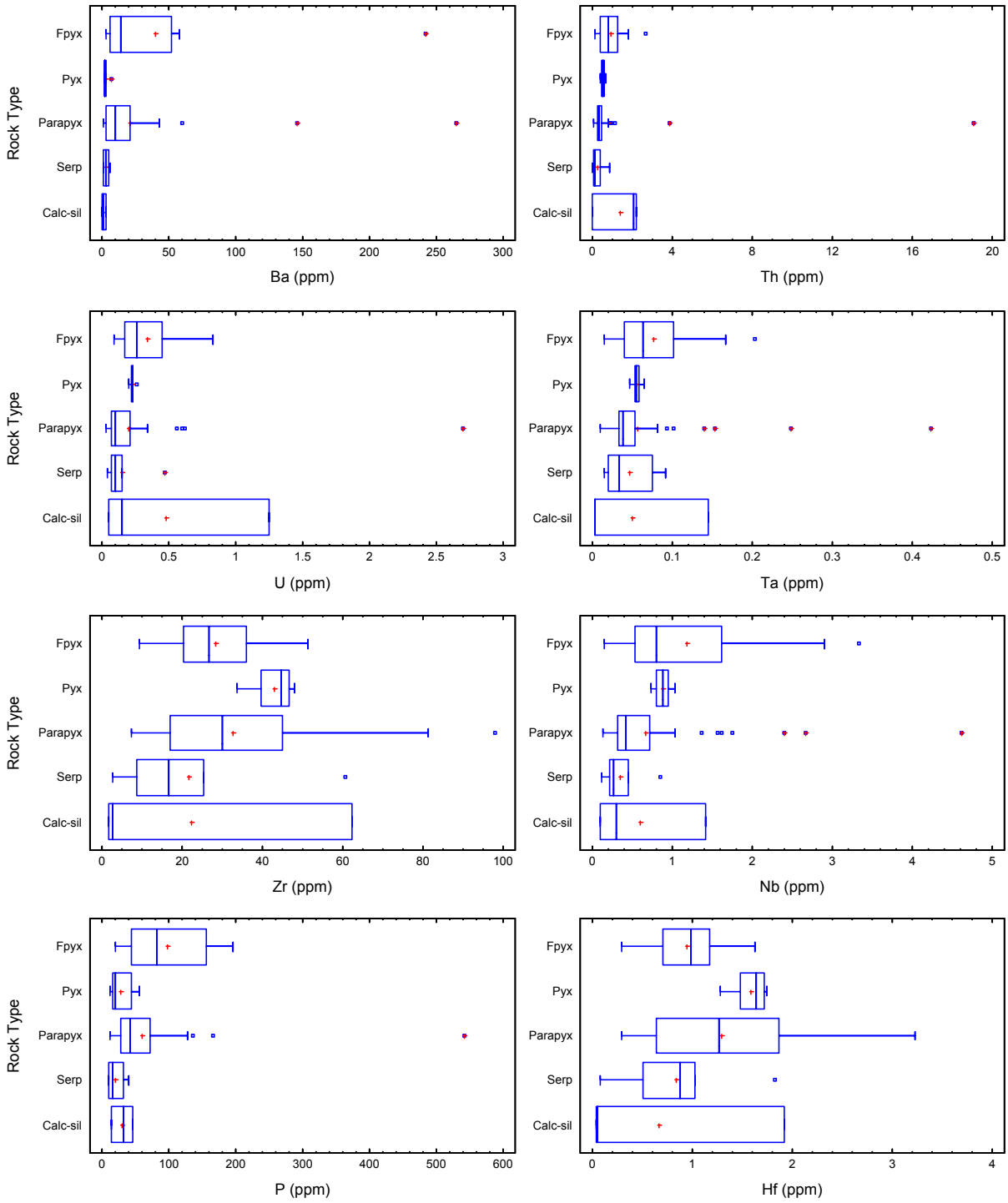

Figure 6.9 Box and whisker plot for incompatible elements for each rock type.

Using Figure 6.9 the dispersion of the data for each element per rock type can be assessed. All the elements for each rock type have a very narrow spread, except for Zr, P and Ba. Therefore, the predicted variance in concentration for these elements is small. Zr and P are predicted to be

the most variable. The concentration values of Ta, Hf, U, Nb and Th are extremely low at < 2 ppm.

The difference in concentration of each incompatible element was assessed by applying the one way ANOVA (C.I. 95 %). Results showed that only Zr, P and Hf differed in concentration significantly between rock types. Table 6.12 below shows which rock types have differences in these element concentrations by applying Duncan's multiple range test (C.I. 95 %). It is clear that no single incompatible element can be used to determine one rock type from another. However, Zr and Hf may be used to discern pyroxenite from serpentinite and calc-silicate because they are slightly less incompatible in pyroxene and therefore can reflect pyroxene content. P concentration may be used to differentiate feldspathic pyroxenite from the serpentinite.

Table 6.12 Duncan's multiple range tests for incompatible elements between rock types

Ba (ppm)		Th (ppm)		U (ppm)		Ta (ppm)		Zr (ppm)		Nb (ppm)	
RT	HG	RT	HG	RT	HG	RT	HG	RT	HG	RT	HG
Calc-sil	X	Serp	X	Serp	X	Serp	X	Serp	X	Serp	X
Pyx	X	Pyx	X	Parapyx	X	Calc-sil	X	Calc-sil	X	Calc-sil	X
Serp	X	Parapyx	X	Pyx	X	Pyx	X	Fpyx	XX	Parapyx	X
Parapyx	X	Fpyx	X	Fpyx	X	Parapyx	X	Parapyx	XX	Pyx	X
Fpyx	X	Calc-sil	X	Calc-sil	X	Fpyx	X	Pyx	X	Fpyx	X

RT, rock type; HG, homogenous group

P (ppm)		Hf (ppm)	
RT	HG	RT	HG
Serp	X	Calc-sil	X
Pyx	XX	Serp	X
Calc-sil	XX	Fpyx	XX
Parapyx	XX	Parapyx	XX
Fpyx	X	Pyx	X

RT, rock type; HG, homogenous group

Using the one way ANOVA (C.I. 95 %) it was determined that serpentinite did not vary in incompatible element concentrations between drill holes, where as feldspathic pyroxenite showed variability in Ba, Th, U, Ta, Nb and P (75 % of the incompatible elements) and parapyroxenite showed variability for Zr, P and Hf (38 %) between drill holes.

6.6 Discussion and Correlations

XRF major element analyses and ICP-MS trace element and PGE analyses have revealed the compositions, element concentrations and the differences between these for each of the five rock types in the orebody. The initial investigation differentiated concentration differences, at a 95 % confidence interval, for major, base metal group, alkali, alkali earth and incompatible elements for each rock type, except for the oxides and elements Al_2O_3, K_2O, Pb, Rb, Ba, Th, U, Ta and Nb. These elements are therefore not helpful in the classification of the orebody rock types. PGE concentrations are statistically the same for all the rock types therefore these elements also cannot be used in the differentiation of the orebody rock types. REE counts are statistically the same for all the rock types except for serpentinite. REE count therefore characterises this rock type. The results suggest that few elements on their own may be used to distinguish between the rock types to a high degree of significance. However, using a combination of the elements, their abundances and their dispersions, the different rock types can be categorized as follows.

Feldspathic pyroxenite has a wide range of element concentration for all majors, for Cr, V, Ni, Cu and Sc of the base metals and for REE. The range is narrow for incompatible elements, barring Zr and Hf and for alkali elements, despite having the highest range out of all the rock types for the alkali elements. Au concentration varies widely as do the concentrations of Pt, Pd, Rb and Ru. Elements with distinct differences at a 95 % confidence interval and which therefore distinguish feldspathic pyroxenite from pyroxenite, parapyroxenite, serpentinite and calc-silicate are Na_2O from the major elements, Cr_2O_3 or Cr from the major or base metals respectively, and the base metal V.

Pyroxenite has very narrow ranges for the major, base metal group, PGEs, alkali and alkali earth elements, REE and incompatible elements. Therefore the concentrations of these elements are highly predictable. This rock type is significantly different from the four other orebody rock types at a 95 % confidence interval. However, only Cu and V on their own will distinguish pyroxenite.

Parapyroxenite has a wide range of element concentrations for the major oxides of SiO_2, Al_2O_3, FeO, MgO and CaO, for the base metal group elements of Ni, Cu, S, Co, Cr and Zn and for the PGEs of Ir, Pd, Pt, Rb, Ru and Au. REE count, alkali and alkali earth elements and incompatible elements exhibit narrow ranges, except for Zr and P. PGE concentrations for this rock type vary

the most of out all the orebody rock types, especially for Au, Ir, Pd, Pt, Rb and Ru. No element on its own can be used to distinguish parapyroxenite from the other orebody rock types.

Ranges of serpentinite major element oxide concentrations show little variation for the major elements except for SiO_2 and Al_2O_3. Like parapyroxenite the base metal group elements Ni, Cu, S, Co, Cr and Zn vary widely in concentration. PGEs show a distinct range of variation for Pd, Pt, Rb, Ru and Au. Alkali and alkali earth elements, REE count and incompatible elements show little range in concentration. The composition of serpentinite is therefore highly predictable. It is significantly different to the other rock types of the orebody at a 95 % confidence interval. The elements which can be used on their own to distinguish this rock type are SiO_2, CaO, FeO and L.O.I. from the major element oxides.

Although the box and whisker plots for calc-silicate were misleading it was still possible to assess the range of concentration values for the elements in comparison to the other rock types. Ranges are wide for the major element oxides of SiO_2, Al_2O_3, MgO, CaO and L.O.I. They are wide for all the base metal group elements, barring Sc and As, are wide for the PGEs of Ir, Pd, Pt, Rb, Ru and Au and are wide for the REE count. Narrow ranges are exhibited for the alkali and the alkali earth elements and the incompatible elements except Zr. Only FeO has a distinct difference, at a 95 % confidence interval, for calc-silicate and therefore this element in its major oxide concentration can be used to distinguish this rock type from the other orebody rock types. It is recommended additional testing be performed on calc-silicate samples to define its precise geochemical characteristics.

The difference in element concentration was examined for each rock type, between drill holes. The data was used to assess the variability of the rock types with distance and identify the rock type with the most variable and therefore least predictable composition. The elements which varied with distance are tabulated (Table 6.13). The analysis was restricted to the rock types: feldspathic pyroxenite, parapyroxenite and serpentinite due to the limited material available for testing.

Table 6.13 Oxides and elements which varied between drill holes, per rock type.

Element Group	Rock Type	Variable Elements
Major Element Oxides	Feldspathic pyroxenite	SiO_2, FeO, MnO, MgO, Na_2O, NiO, TiO_2, Cr_2O_3, LOI
	Parapyroxenite	FeO, MgO, Na_2O, K_2O, NiO, TiO_2, Cr_2O_3, P_2O_5, LOI
	Serpentinite	SiO_2, FeO, MgO and Al_2O_3
Base Metal Group Elements	Feldspathic pyroxenite	Ni, S, Co, V, Sc, Cr
	Parapyroxenite	Ni, Cu, S, Co, V, As, Sc, Cr
	Serpentinite	Sc
Platinum Group Elements + Gold	Feldspathic pyroxenite	Ir, Os, Pd, Pt, Rh, Ru
	Parapyroxenite	Ir, Os, Pd, Pt, Rh, Ru
	Serpentinite	None
Alkali and Alkali Earth Elements	Feldspathic pyroxenite	Na_2O
	Parapyroxenite	Na_2O, K_2O
	Serpentinite	Sr
Rare Earth Element Count	Feldspathic pyroxenite	Total count varied
	Parapyroxenite	Total count did not vary
	Serpentinite	Total count did not vary
Incompatible Elements	Feldspathic pyroxenite	Ba, Th, U, Ta, Nb, P
	Parapyroxenite	Zr, P, Hf
	Serpentinite	None

Of the five chief major element oxides, Al_2O_3, SiO_2, FeO, MgO and CaO, that make up the chemical character of each rock type, all but CaO varied at a significant level between drill holes and therefore with distance. This is significant because it indicates that the variability within the composition of each rock type can be an expected to change across the pit. Five general trends may be expected from this data:

- Up to 30 % of the composition of serpentinite will vary spatially. Between 25% – 85 % and 40 % - 85 % of the feldspathic pyroxenite and parapyroxenite composition, respectively, will vary.
- Serpentinite shows the least variability in composition between drill holes. As with the "within rock type" variability, the composition of this rock type across the pit will be the most constant and therefore most predictable.
- Parapyroxenite and feldspathic pyroxenite show the greatest variability, therefore their composition may be expected to be less predictable.
- Although the range of variability for feldspathic pyroxenite is greater than that of parapyroxenite, parapyroxenite will typically have a higher degree of variability when it does vary. The composition of parapyroxenite is therefore less predictable than feldspathic pyroxenite
- The element groups which are predicted to be the most variable, spatially, are the PGEs, followed by the major elements and base metals group elements.

It is recommended that samples of pyroxenite and calc-silicate be similarly analysed for variability between drill holes, across the pit, to complete this assessment of the spatial variability of the rock types in the orebody.

To gauge the nature of the relationships between rock type and geochemistry the results of the whole rock major element oxide analyses were plotted against one another. Major element oxides were used because they are representative of the rock type mineralogy. The resulting comparisons were used to determine which elements were related and if so, whether the data plotted in regions or envelopes according to origin/ rock type.

The plots showed data fell into narrow, discrete or wide/diffuse zones (Figure 6.10). Three types of trends were noted and are described below.

- **Random:** In which no relationship was observed between the elements. Rock types were not sorted or were poorly differentiated according to origin and the data had either a scattered ‘shot gun’ distribution or a vertical/ horizontal distribution.

Every element that was plotted against Na_2O, K_2O, TiO_2, P_2O_5, Cr_2O_3, NiO, Al_2O_3 and FeO showed random plots.

- **Positive relationship with differentiation between rock types:** In which the increase of one element corresponded with an increase in another and element concentrations could be subdivided into groups according to origin.

The elements which plotted with this type of relationship included SiO_2 vs. CaO (diffuse), MgO vs. L.O.I. (discrete) and MgO vs. MnO (diffuse).

- **Negative relationship with differentiation between rock types:** In which the increase in one element corresponded with a decrease of another and element concentrations fell into groups according to origin.

The elements which plotted with this relationship included SiO_2 vs. MgO (diffuse), SiO_2 vs. L.O.I. (diffuse) and SiO_2 vs. MnO (discrete), MgO vs. L.O.I. (discrete), CaO vs. MgO (discrete), CaO vs. L.O.I. (discrete) and CaO vs. MnO (diffuse).

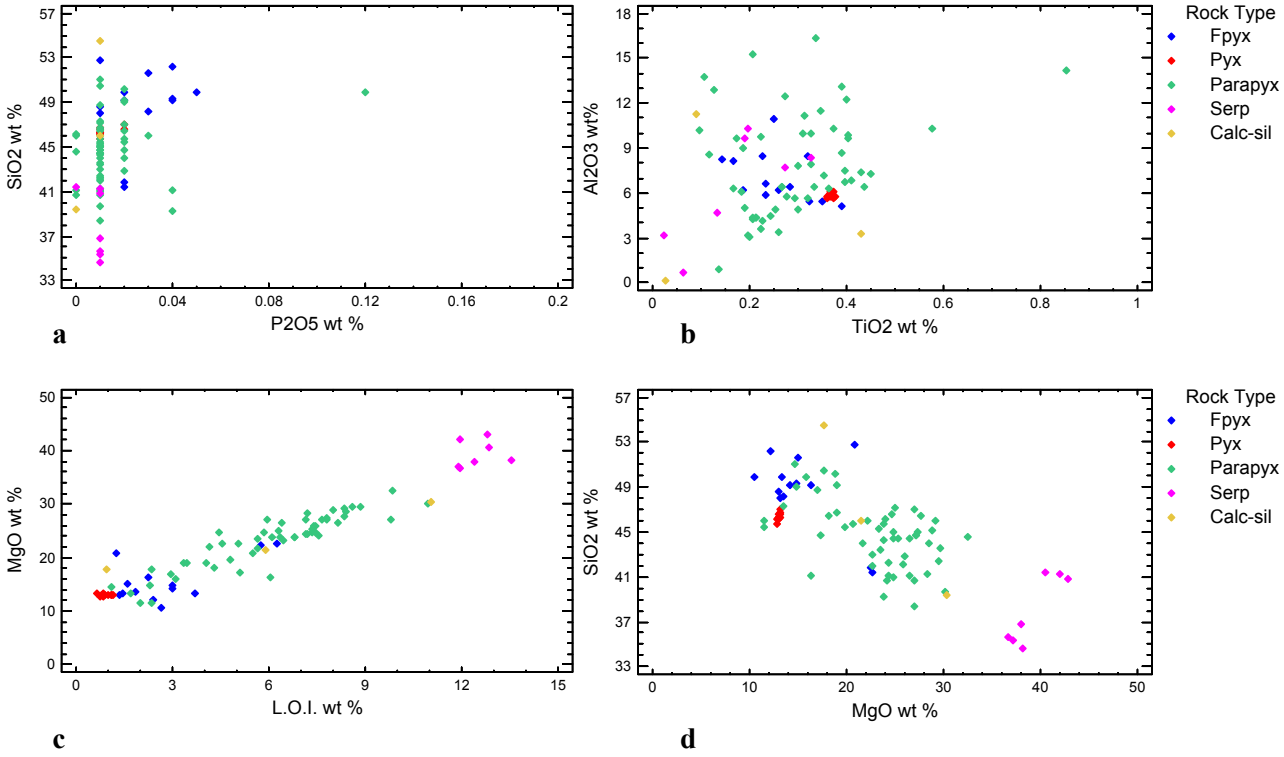

Figure 6.10 Examples of the relationships observed when major elements were plotted against one another. **a** and **b** Random plots: no relationship between the elements is present. **c** Discrete positive relationship between MgO and L.O.I. showing the different rock types plotting within different envelopes and therefore giving a good differentiation between rock types of different origin. **d** Diffuse negative relationship between SiO_2 and MgO, showing the rock types falling into different envelopes and therefore a good differentiation between rock types of different origin.

6.6.1 Discriminant Analysis

Discriminant analysis is a multivariate procedure which is regularly applied to large sets of data, allowing the influence of a number of variables to be collectively assessed in the determination of different populations (Davis, 1986). Data is plotted to find linear combinations of the variables which separate the data into differing populations. The results of the analysis are categorized and given by two discriminant functions, representing the vertical and horizontal components of the discriminant analysis. Categorization or discrimination of the data is different to classification. Categorization requires prior knowledge of the relations, with each observation having been predefined as belonging to a specific group. Classification requires no prior knowledge, instead it allows an observation to enter any group to which it is most similar (Davis, 1986).

In this study discriminant analysis has been applied to the major elements. Using a combination of these geochemical variables the data was categorized and the rock types (different populations) identified. *Statgraphics Centurion XV* statistical program was used to manipulate and plot the data. The discriminant analysis takes the measured geochemical variables as well as the rock type which they belong to and transforms them into a single discriminant score. This score represents the position of a sample along the line defined by a linear discriminant function of the geochemical components. The analysis finds the function of these variables which produce the maximum significant difference between the different rock types, The objective is to define the function which most succinctly defines the complex relationships between the variables (Statpoint, 2005).

Figure 6.11 is the plot of the linear discriminant functions that define the rock types of Sandsloot orebody, using all the major elements. Eighty seven observations were used to fit the model. Function 1. defines the vertical coordinate and Function 2. defines the horizontal coordinate.

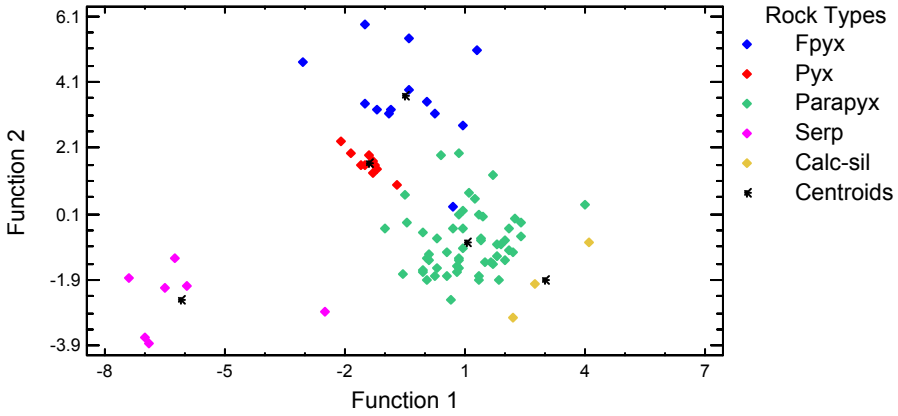

Figure 6.11 Plot of the discriminant functions defining the rock types of the orebody for all the major elements.

The standardized discriminant functions with coefficients used to discriminate amongst the different rock types for Figure 6.11 are given by equation 6.6.1 and 6.6.2.

Function 1.

$-0.0753693*Cr_2O_3 + 0.394422*NiO + 5.28029*SiO_2 + 0.462588*TiO_2 + 4.19398*Al_2O_3 + 2.57205*FeO + 1.45427*MnO + 5.28751*MgO + 6.89253*CaO + 0.542959*Na_2O + 0.895294*K_2O - 0.85071*P_2O_5 + 1.12702*L.O.I.$

Eqn: 6.6.1

Function 2.

$0.579782*Cr_2O_3 - 0.442677*NiO - 4.48869*SiO_2 - 0.0330901*TiO_2 - 4.81005*Al_2O_3 - 3.3111*FeO - 0.157031*MnO - 8.36213*MgO - 8.49333*CaO - 0.240632*Na_2O - 0.457049*K_2O + 0.0420981*P_2O_5 + 0.0119106L.O.I.$

Eqn: 6.6.2

The plot of function 1 vs. function 2 provides a good visual separation of the rock types (Figure 6.11). Five discrete envelopes, one for each rock type of the ore body, are present. There is a slight overlap of the feldspathic pyroxenite with the parapyroxenite and the closeness of the envelopes for feldspathic pyroxenite; pyroxenite and parapyroxenite indicate the similarity of their origins. Serpentinite plots at a distance to the other rock types, clearly indicating its unique origin.

From the relative magnitude of the coefficients in equations 6.6.1 and 6.6.2 the independence of the variables, used to discriminate amongst the rock types, may be assessed. SiO_2, Al_2O_3, FeO, MgO and CaO are the most independent elements oxides and significantly influence the rock type discrimination.

Using the discriminant functions, classification coefficients can be calculated for each rock type per geochemical component, thereafter classification functions per rock type can be calculated. These classification functions, together with probability that a sample will fall into a particular rock type and the relative distance of a samples position to the group centroid are used to determine a new score which classifies both the observed samples as well as classifies new samples (Statpoint, 2005). This classification when compared to the actual rock type for the sample, known prior to the analysis, using a simple percentage calculation of the number of correctly classified samples, is a gauge of the accuracy of the discriminant functions.

For discriminant functions eqn: 6.6.1 and 6.6.2 the model fits 94.25 % of the observed data correctly.

Using all the major element oxides, to define the geochemical variable of each rock types, results in a complex relationship. To simplify the analysis and resultant discriminant functions the analysis was re-run using only the five element oxides identified in the previous discriminant analysis as being highly significant. The plot of the new analysis is given in Figure 6.12 and the functions which define the plot are given by equations 6.6.3 and 6.6.4.

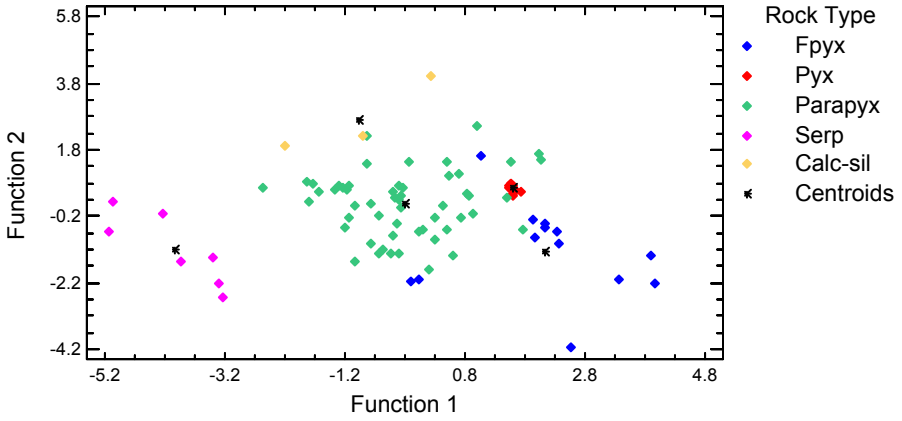

Figure 6.12 Plot of the discriminant functions defining the rock types of the orebody for SiO_2, Al_2O_3, FeO, MgO and CaO. The centroids are the mean values of each group.

Function 1.

$$-1.11598*Al_2O_3 - 2.60642*CaO - 0.872757*FeO - 3.10838*MgO - 0.901059*SiO_2$$

Eqn: 6.6.3

Function 2.

$$4.03218*Al_2O_3 + 5.90348*CaO + 1.89315*FeO + 5.35885*MgO + 3.62721*SiO_2$$

Eqn: 6.6.4

Figure 6.12 displays the different rock types according to origin. As with the discriminant analysis, which used all the major element oxides, the plot for these discriminant functions shows the different rock types are recognized and displayed by the clustering of the data for each rock type. There is more overlapping of the envelopes and a lesser spread between envelopes compared to Figure 6.11. This indicates a reduced difference between the functions which define the various rock types.

The model fitted by discriminant functions 6.6.3 and 6.6.4 correctly classifies 89.66 % of the data samples. This is approximately 5 % lower that the initial model (eqn. 6.6.1 and 6.6.2) therefore quantifying the observed reduced spread of data and increased overlapping of the envelopes noted in Figure 6.12. In this study the lower the number of element oxides used in the model the lower the accuracy of the model obtained.

The model described by the discriminant functions 6.6.1 and 6.6.2 was tested using randomly selected data from other geochemical analyses of the orebody rock types in Sandsloot open pit. Data was taken from two papers, Harris and Chaumba (2001) and McDonald *et al.* (2005). The

geochemical variables were scored according to the classification functions defined by discriminant functions 6.6.1 and 6.6.2 and classified per rock type. The results of the classifications were compared to the known rock types given by Harris and Chaumba (2001) and McDonald *et al.* (2005) and are tabulated in Table 6.14. Seven out of ten geochemical observations were correctly classified using the discriminant functions which model their data against the data set collected and analysed in this research study.

Table 6.14 Classification of geochemical data from Harris and Chaumba (2001) and McDonald *et al.* (2005)* using the model described by discriminant functions 6.6.1 and 6.6.2.

Data source	Sample number	Given rock type	Results of Function 1.	Results of Function 2.	New classification of rock type
McDonald *et al.* (2005)	E205	Parapyroxenite	71221.03	71205.2	Parapyroxenite
McDonald *et al.* (2005)	N1-6a	Parapyroxenite	68286.89	68843.34	Feldspathic pyroxenite
McDonald *et al.* (2005)	N1-6b	Serpentinite - vein	62149.45	62170.82	Serpentinite
McDonald *et al.* (2005)	N1-14	Feldspathic pyroxenite	74762.62	75070.3	Feldspathic pyroxenite
McDonald *et al.* (2005)	N1-22	Feldspathic pyroxenite	73895.44	74194.98	Feldspathic pyroxenite
Harris and Chaumba (2001)	PP 11	Pyroxenite	74468.3	74880.03	Feldspathic pyroxenite
Harris and Chaumba (2001)	PP 14	Parapyroxenite	67640.01	67673.6	Parapyroxenite
Harris and Chaumba (2001)	PP15	Parapyroxenite	70068.28	70149.65	Parapyroxenite
Harris and Chaumba (2001)	PP 22	Calc-silicate	62686.26	62724.94	Parapyroxenite
Harris and Chaumba (2001)	PP 53	Pyroxenite	68609.72	69066.83	Pyroxenite

* The geochemical data from these two papers did not include the values of Cr_2O_3 wt % and NiO wt %. A substitution of Cr (ppm) and Ni (ppm) was made, with no effect on the original models 94.25 % accuracy in classification.

Discriminant functions 6.6.1 and 6.6.2 describe the relationships between the geochemical compounds for the data set collected and used in this research study of the Sandsloot orebody rock types. The disadvantage of using discriminant analysis is that it cannot be used for initial classification purposes. This is because when the discriminant analysis is derived the rock type, to which the geochemical variables belong, must be entered into the analysis along with the variables describing the rock types. For use in predicting rock type mining properties, and ultimately for use in mine-to-mill optimisation, the database used in this study must be expanded and must include data from pits north and south of Sandsloot. A different classification system would be required to tentatively allocate new samples of unknown origin

to a rock type. Thereafter, the new sample can be plotted using the discrimination analysis and its position among other samples be assessed. This type of analysis may also be used as a measure of the accuracy of other identification systems.

6.7 Summary and Conclusions

The geochemical analysis of the orebody rock types at Sandsloot open pit was used in the prediction of mining properties. Using XRF, to determine whole-rock major and trace element abundance, and ICP-MS analysis, to measure whole-rock trace element concentrations and PGE concentrations, eighty seven samples from nine drill holes were examined to define characteristics and relationships for each of the five orebody rock types. The study used UKZN in-house testing procedures, international and blank standards and internal synthetic standards to determine element concentrations. Thereafter the multi-element data was combined into a database for modelling using *Statgraphics Centurion XV*.

Handling the data statistically required assembling the elements into groups of similar chemical properties for primary comparison. It required the identification and understanding of the unique factors that influenced the population distributions. Each element was analysed by studying its individual descriptive properties of average, standard deviation and population distribution and then compared between rock types and between drill holes.

It was found that some oxides and elements were present in the orebody rock types at statistically the same concentrations for each rock type. These oxides and elements are K_2O, Al_2O_3, Pb, Rb, Ba, Th, U, Ta, Nb, PGEs. They are therefore not useful in distinguishing the rock types and may not be helpful in the prediction of mining properties. REE count was the same for all rock types, except for serpentinite, therefore these elements are not useful for distinguishing the main ore rock types, but are useful for distinguishing serpentinite.

A select few oxides and elements are useful in distinguishing the rock types of the orebody. It was found Na_2O, Cr_2O_3 or Cr and V distinguished feldspathic pyroxenite, Cu and V distinguish pyroxenite, SiO_2, CaO, FeO and L.O.I. are useful in distinguishing serpentinite and FeO is distinguishes calc-silicate. Only four of the five orebody rock types can be separated looking at the significant differences in geochemistry. Parapyroxenite cannot be distinguished using any of the oxides or elements.

Looking at the range in concentration of each oxide and element for each rock type showed pyroxenite followed by serpentinite typically had the narrowest ranges. Geochemically, they are the least variable rock types in the orebody respectively and their concentrations are therefore expected to be the most predictable. Parapyroxenite and feldspathic pyroxenite have the widest ranges for most of the oxide and element concentrations, and although difficult to visually assess, calc-silicate also had typically wide ranges. The concentrations in these rock types are expected to be least predictable. However, typically parapyroxenite will be the most variable. More samples should be analysed define the calc-silicate geochemistry more precisely.

Variability analysis of the oxides and elements for each rock type between drill holes showed serpentinite to be the least variable in composition, followed by parapyroxenite, then feldspathic pyroxenite. Predictably is expected to follow this order. However, it is expected that parapyroxenite would have a higher degree of variability compared to the other rock types, when it does vary. The concentration of PGEs, followed by major element oxides and base metal group elements would be expected to vary spatially more than any other groups of elements.

Comparing the major element oxides against one another revealed that the majority of the oxides did not relate to one another for each rock type. The data distributions were scattered randomly and the rock types were poorly differentiated. However, for the combination of the elements SiO_2, CaO, MgO, MnO and L.O.I. both positive and negative relationships were identified, with good distinction between the rock types. The data plotted in narrow, discrete or diffuse zones and was clearly separated into groups of major element oxides according to origin/ rock type.

Discriminant analysis was performed on the major element oxides to determine if the data could be represented by a horizontal and vertical linear function that distinguished the rock types. A model which fitted approximately 95 % of the data and correctly categorized each of the rock types, showing good visual separation, was identified. The analysis allowed the influence of the oxide variables to be collectively assessed in the determination of different populations/ rock types. Removing the oxides with the smallest coefficients (lowest influence on the categorization) to simplify the functions decreased the accuracy of the model by approximately 5 %. The functions were applied to geochemical data from published studies of rock types from the Sandsloot open pit. The results showed good agreement between predicted versus actual observed rock type classification. These functions are therefore robust models of the Sandsloot

data set. Expansion of the database, upon which these functions are derived, may be used to classify rock types from other PPRust open pits, and therefore possibly predict their geochemical characteristics. Discriminant analysis is shown to be a useful tool, which may also be used as a measure of the accuracy of other identification systems.

Chapter 7

METALLURGICAL INVESTIGATION

7.1 Introduction

Metallurgy, in the context of mining operations, is the process of extracting the metal from the ore. Broadly the process begins with fragmentation in the pit, but to liberate the metal, the rock fragments must be reduced to a fine powder for chemical treatment. Reduction of the ore particle size to that of a powder requires comminution using a series of crushers and mills in the processing plant, with the choice of crusher, mill type and the circuit design based on knowledge of the metallurgical strength of the ore.

Research by Bye (2003), Pease *et al*, (1998), and Simkus and Dance (1998) show significant cost benefits through increased mill throughput, lowered energy consumption in the plant and decreased power costs. This processing plant optimisation is achieved by the correct selection and calibration of the processing machinery for the site-specific ore types and by improving the mill feed grade through decreasing variability and increasing predictability (Simkus and Dance, 1998).

This chapter reports on the metallurgical properties of the orebody rock types at Sandsloot open pit mine. It aims to characterise the properties and identify distinguishing trends which may be used for processing predictability and control over the variability of the ore sent to the plant. The selection, preparation and testing procedures used in the metallurgical investigation are described. The resistance of the orebody rock types to breakage through abrasion and impact and the resistance to milling are assessed, providing a statistically sound database and set of results for use in the geotechnical model per rock type. This may then be used for blast design, real time calibration of the plant crushers and mills and in the comparison of Sandsloot ore to PPRust North ore.

7.2 Methods of Investigation

7.2.1 Drop Weight Testing

Drop Weight testing comprises two tests, which measure the breakage parameters of ore. These parameters are used to predict the performance of an autogenous mill (AG) or semi autogenous mill (SAG) when used to break up the ore. The two tests are the Tumbling test and the Julius Kruttschnitt (JK) Drop Weight test. Both were developed at the Julius Kruttschnitt Mineral Research Centre (JKMRC) in Queensland, Australia and are standard in industry.

7.2.1.1 Tumbling Test

The Tumbling test is a low energy experiment that measures the resistance of the ore to abrasion. The abrasion parameter (ta) is calculated by tumbling ore particles of a selected size in a laboratory mill with lifter bars to simulate the abrasion mechanism within the mill (Figure 7.1). After a predetermined amount of time at 70% critical speed, the percentage of broken ore that is smaller than one tenth of the original particle size is measured and recorded as t_{10}. Using equation 7.2.1 the abrasion parameter ta is calculated (JKTech Pty, 2008 a).

$$\mathbf{ta = t_{10}/10} \qquad \text{Eqn: 7.2.1}$$

Where ta = the resistance of the ore to abrasion

t_{10}= percentage broken ore smaller than 1/10 original particle size

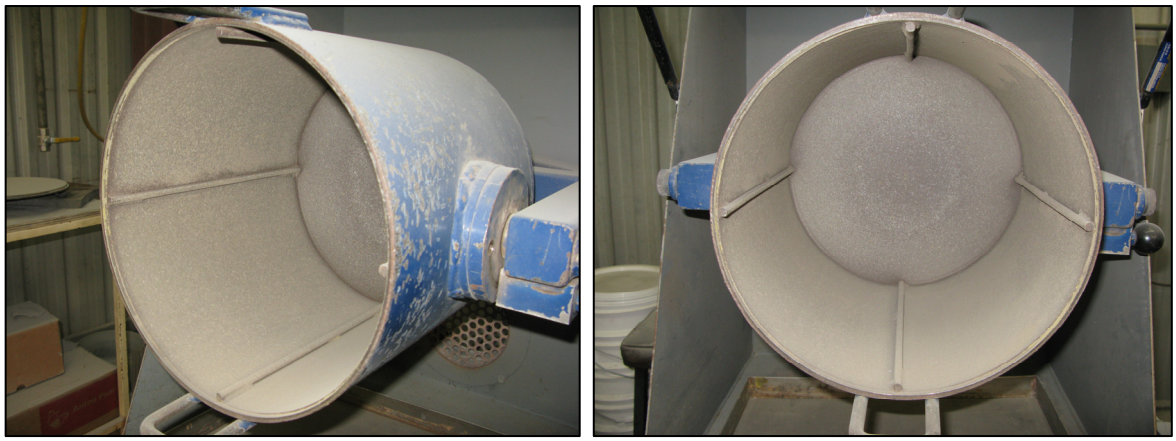

Figure 7.1 Abrasion mill, 12” x 12” with rounded corners and four 8 mm lifter bars, after JKTech Pty (2008 c).

7.2.1.2 Julius Kruttschnitt (JK) Drop Weight Test

The JK Drop Weight test is a high energy test that measures the impact breakage parameters *A* and *b* of the ore, to determine its resistance to impact breakage. The test uses a weight to break the test specimen particles of a particular size fraction by dropping the weight from a selected height (Figure 7.2). Five particle-size fractions are tested with three energy levels for breakage (three heights from which the weight is dropped), resulting in fifteen size/energy combinations that characterise the ore.

Figure 7.2 JK Drop Weight apparatus, after JKTech Pty (2008 a).

The broken fragments are collected, sized and t_{10}, as described under the tumbling test, is determined from the normalized size distribution. The t_{10} value, which is calculated for each sample is plotted against the specific energy [Ecs (kWh/t)] for that test (Figure 7.3). Factors A and b are derived empirically from the t_{10} vs. Ecs graph, where A is the maximum t_{10} value achieved and b is a factor required to achieve the graph shape. Equation 7.2.2 relates the amount of breakage, t_{10}, to the specific energy, Ecs (kWh/t).

$$\mathbf{t_{10}=A\,(1-E^{-bECS})}$$

Eqn: 7.2.2

Where A = the maximum t_{10} value achieved

b = on its own does not describe any particular aspect but is required in conjunction with the A to describe the shape of the curve (Figure 7.3).

E_{CS} = the specific energy of comminution

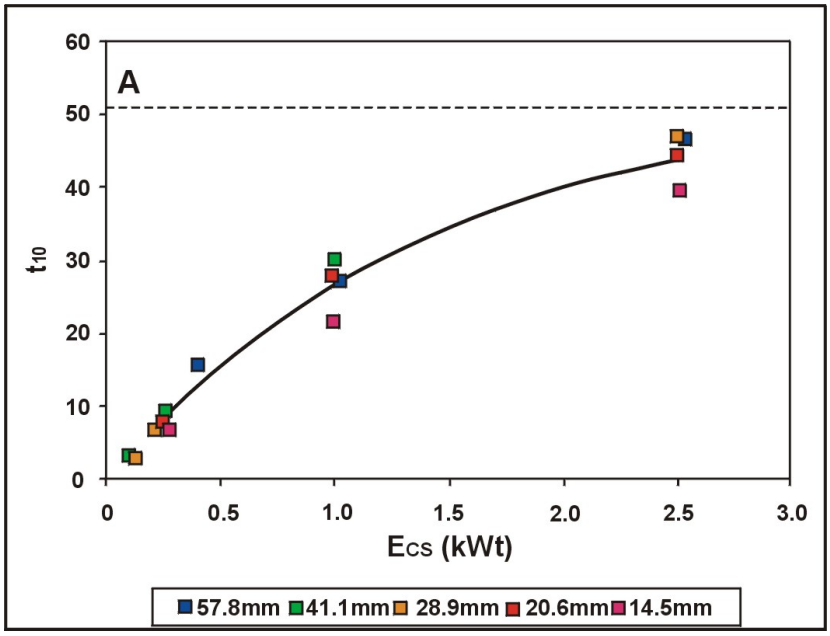

Figure 7.3 Typical curve of t_{10} vs. E_{CS}. It shows the results of a JK Drop Weight test, with five particle size fractions (57.8 mm, 41.1 mm, 28.9 mm, 20.6 mm and 14.5 mm) tested at three energy levels, modified after JKTech Pty (2008 a).

The product of A and b (Eqn: 7.2.3) is the slope of the t_{10} vs. E_{CS} curve where, E_{CS} is 0 kWh/t.

$$\mathbf{DWT = A*b}$$

Eqn: 7.2.3

where DWT = resistance to impact breakage

DWT is used as a direct measure of comparison between the resistance to impact breakage for ore samples (JKTech Pty, 2008 a).

7.2.2 Bond Ball Mill Work Index

A Bond ball mill Work Index (BWI) measures the resistance of a material to crushing and grinding. The index is used to determine the grinding power/energy required to reduce one tonne of rock to the desired fragmentation size in a comminution circuit.

In the test, the sample material is ground in a series of consecutive batches using a standard Bond mill for 100 revolutions (Figure 7.4). Between each grind-batch the contents of the mill are sieved to remove 80% of the product, at a size fraction equal to that of 80% (P80) which is expected from the mill circuit in the mine processing plant. Fresh material of equal weight to that removed is added, in batches, until the undersized sample removed reaches equilibrium. The ball mill grindability (Gbp) in grams per revolution is calculated by averaging the net mass per revolution of the last three cycles of milling. BWI is calculated using the Bond Equation (Bond, 1961), (JKTech Pty, 2008 a).

$$\mathbf{BWI = 44.5 / (P_1)^{0.23} * (Gbp)^{0.80} * ((10 / \sqrt{P}) - (10 / \sqrt{F}))}$$

Eqn. 7.2.4

where P_1 = the opening of the sieve size tested, in microns

Gbp = the ball mill grindability, net grams per revolution

P = 80 % of the last cycle sieve undersize product which passes, in microns

F = the size which 80 % of the new ball mill feed passes, in microns

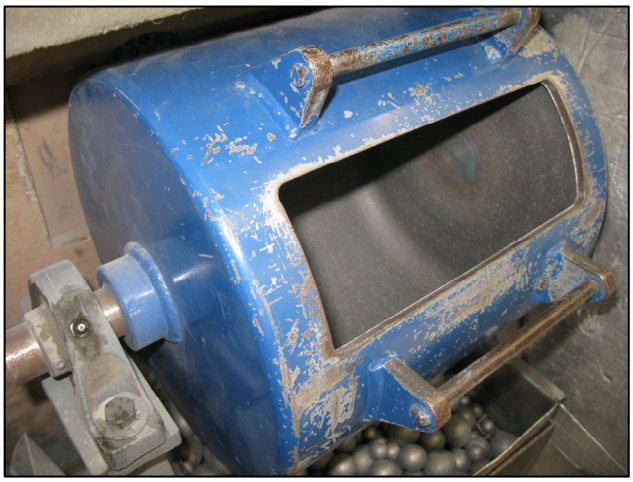

Figure 7.4 Bond ball mill, 12” x 12” with rounded corners, with balls below, after JKTech Pty (2008 c).

7.3 Sample Selection and Preparation

Samples were selected from five drill holes. Two drill holes were located within the blast block 138 – 055, which stands for the 55th blast on bench 38 in Sandsloot open pit, (SSMet 1 and SSMet 2) and three located in the across the length of the pit (SSMet 6, SSMet 7 and SSMet 8). The positions of these drill holes are shown in Figure 4.1, Chapter 4. Samples were also randomly chosen from post-blast material of blast block 138 – 055, collected either within the pit (SSGrab P, 138055, 138055Grab and 138055HPGR) or in the processing plant (SSGrab M and SSGrab T). Samples of each orebody rock type were selected and composite samples, comprising a combination of the various Sandsloot orebody rock types were selected. By selecting samples from within a blast block the data could be compared to plant performance results for the same block and optimisation could follow. However, not all the orebody rock types were present in blast block 138 – 055 and in some instances the number of test results for each rock type within the block was low, which lessened the reliability of the statistical analysis. Hence, samples from outside the blast block were included.

Approximately 60 – 100 kg of material, broken into fragments 75 – 87 mm in size was prepared for each of the Drop Weight tests. For the BWI test approximately 10 kg of sample was crushed into fragments less than 10 mm in size. The tests require samples of untested rock fragments, however, for two tests there was insufficient mass of a specific rock type. Therefore a small portion of rock fragments from the UCS testing was used. It is believed that this portion of tested rock fragments will not influence the results significantly.

7.4 Testing Procedures

The testing was carried out at the Anglo Platinum Research Centre (ARC), Germiston, South Africa and the test procedures followed those of the in-house practices developed by the Julius Kruttschnitt Mineral Research Centre Laboratories (JKMRC). The results for the testing were supplied in the form of unpublished internal Anglo Research reports and MS Access data sheets from the Sandsloot mine database.

7.5 Results and Analysis

A third database was constructed for this study using the metallurgical data. Included in this database were the results for drop weight testing, the Bond ball mill Work Index, sample lithology, collection method and corresponding geotechnical data for density and uniaxial compressive strength testing. As with the geotechnical and geochemical results, the metallurgical database was analysed and interpreted using the *Statgraphics Centurion XV* statistical program. This software with the database allowed for the interrogation of the results and relationships within metallurgical tests as well as between metallurgical and geotechnical tests (Chapter 8) by defining multi-level queries using test type, collection method, lithology and corresponding geotechnical results.

The presentation of the results and analysis layout for the metallurgical testing are given in the same format as that in the geotechnical and geochemical investigations. The statistical procedures used in the analyses have been described in the Results and Analysis section in the geotechnical investigation (section 5.5, Chapter 5). All the one way analyses of variance (ANOVA) and multiple range tests were performed at 95% confidence intervals (C. I. 95 %).

7.5.1 Drop Weight Testing

7.5.1.1 Drop Weight Tumbling Test

A total of 24 abrasion drop weight tests were performed for the various orebody rock types from Sandsloot open pit. The calculated results of *ta* (the resistance to abrasion) for each ore type is given in Table 7.1. All the results were valid and therefore included into the data analysis.

Table 7.1 Results of abrasion parameter, *ta*, testing.

Rock type	Count	Avg.	Median	Standard dev.	Min	Max	Range	Interquartile range
Fpyx	6	**0.28**	0.30	0.05	0.19	0.34	0.15	0.04
Pyx	4	**0.41**	0.36	0.13	0.32	0.60	0.28	0.15
Parapyx	7	**0.27**	0.26	0.05	0.22	0.36	0.14	0.03
Serp	2	**0.28**	0.28	0.01	0.27	0.28	0.01	0.01
Calc-sil	1	**0.22**	0.22	n/a	0.22	0.22	n/a	n/a
Comp	4	**0.25**	0.26	0.06	0.19	0.31	0.12	0.10
Total	24	**0.28**	0.28	0.06	0.24	0.35	0.14	0.06

All the rock types, including the composite, have similar characteristics of abrasion resistance, except pyroxenite (Table 7.1). The range of average values is narrow, varying between

0.22 - 0.28. Pyroxenite on the other hand has an abrasion parameter that is significantly higher with an average value of 0.41.

Table 7.2 shows the classification of the relative hardness of a material/ rock type according to its properties of *ta* or DWT (JKTech, 2008 a). The lower the value of *ta* the more resistant the material is to abrasion and therefore the more difficult it is to mill. Calc-silicate is classified as very hard and appears will be the most difficult to mill. However, because only one sample was tested more testing is required to confirm the result. The composite material, parapyroxenite, serpentinite and feldspathic pyroxenite are classed as hard and pyroxenite is classed as moderately hard. Pyroxenite would therefore be the easiest material to mill in the SAG mill where as the former four rock types would be slightly harder and require longer milling times.

Table 7.2 Classification for drop weight results, after JKTech Pty (2008 a).

Property	Very Hard	Hard	Mod. Hard	Medium	Mod. Soft	Soft	Very Soft
ta	<0.24	0.24-0.35	0.35-0.41	0.41-0.54	0.54-0.65	0.65-1.38	>1.38
DWT(A*b)	<30	30 - 38	38 - 43	43 - 56	56 - 67	67 - 127	>127

Normal distributions were established for the data sets of each rock type using the χ^2 test (C.I. 95 %). Box and whisker plots indicate pyroxenite has the widest range of expected values and the highest standard deviation, therefore this rock type would be the most variable in terms of predicting its behavior (Figure 7.5). Its minimum value is also higher than the average value for the other rock types. Therefore it appears there would be little overlap in the properties compared with other orebody rock types. Calc-silicate and serpentinite have very narrow ranges but this is likely a result of the low number of tests for each rock type. The composite sample average is lower than the average value for all the rock types combined and is similar to the calc-silicate average. This may indicate the composite “uni-rock” is less susceptible to abrasion or that there may have been over representation of calc-silicate.

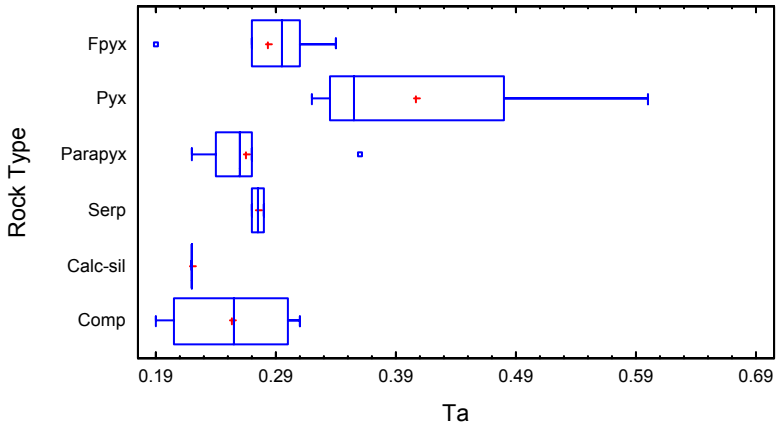

Figure 7.5 Box and whisker plot for the abrasion parameter, *ta*, per rock type (refer to figure notations used in box and whisker plots, first described under section 5.5 Results and Analysis, Chapter 5).

Normality was established using the one way analysis of variance (ANOVA). It was determined that significant differences exist between abrasion resistance behaviour per rock type (C.I. 95 %). Duncan's multiple range tests (Table 7.3) indicates parapyroxenite, calc-silicate and composite sample material will perform with significant similarity (C.I. 95 %) in the SAG mill. Pyroxenite will perform significantly differently to these three material types and more testing is required to determine which group/s of material feldspathic pyroxenite and serpentinite are most likely to be similar to.

Table 7.3 Duncan's multiple range test results for abrasion parameter *ta*.

Rock type	Count	Mean	HG
Calc-sil	1	0.22	X
Comp	4	0.25	X
Parapyx	7	0.26	X
Serp	2	0.27	XX
Fpyx	6	0.28	XX
Pyx	4	0.40	X

HG, homogenous group

The one way ANOVA (C.I. 95 %) was run a second time on the data to determine if the collection method for sampling had an influence on the test result. Only parapyroxenite varied depending on the collection method/ test sample location. Not enough results were available for this analysis for the serpentinite and calc-silicate rock types. Table 7.4 shows samples randomly chosen from the pit (SSGRAB) for parapyroxenite can have a significantly different value for abrasion resistance (C.I. 95 %). For feldspathic pyroxenite, pyroxenite and the composite material the results may be considered the same regardless of sampling method.

Table 7.4 Duncan's multiple range test results for abrasion parameter *ta* by rock type per sample method/ location.

Fpyx		Pyx		Parapyx		Comp	
Sample method	**HG**	**Sample method**	**HG**	**Sample method**	**HG**	**Sample method**	**HG**
SSMET1	X	SSGRABP	X	SSMET1	X	138055GRAB	X
138055GRAB	X	138055GRAB	X	138055GRAB	X	SSGRABM	X
		SSMET1	X	SSGRABP	X		

HG, homogenous group

7.5.1.2 Julius Kruttschnitt (JK) Drop Weight Test

The JK drop weight test was performed on a number of samples for each of the dominant rock types in the Sandsloot pit as well as for a composite of material. The results for the ore impact breakage parameters A and b are given as their product (A*b) in the form of drop weight test (DWT) parameter (Table 7.5). The actual values of A and b, for each rock type and their summary statistics may be found in Appendix E. All the test results were valid and therefore included into the database.

Table 7.5 Results of JK drop weight testing, DWT (A*b).

Rock Type	Count	Avg.	Median	Standard dev.	Min	Max	Range	Interquartile range
Fpyx	11	**35.12**	35.20	7.91	21.60	49.92	28.32	12.61
Pyx	4	**40.54**	38.60	9.94	31.20	53.75	22.55	14.98
Parapyx	11	**31.29**	28.60	6.34	23.80	46.98	23.18	8.11
Serp	2	**29.65**	29.65	0.49	29.30	30.00	0.70	0.70
Calc-sil	5	**35.64**	34.98	5.25	28.60	43.02	14.42	3.35
Comp	4	**34.05**	33.55	2.16	32.00	37.08	5.08	2.79
Total	37	**34.38**	33.43	5.35	27.75	43.46	15.71	7.09

As with the tumbling test the lower the value the more difficult the material is to mill. The highest result for the DWT was for the pyroxenite with an average of 40.54 (Table 7.5). Average values for parapyroxenite, the composite material, calc-silicate and feldspathic pyroxenite fall between the low to mid thirties, whilst the average DWT for serpentinite falls below 30. Using Table 7.2 serpentinite is classed as very hard and will be the most resistant to impact brakeage out of all of the orebody rock types, because it has the lowest value for DWT. Parapyroxenite, the composite material, calc-silicate and feldspathic pyroxenite are classified as hard rock therefore will be more susceptible to breakage through impact compared to serpentinite. Pyroxenite is classified as moderately hard and will accordingly be the most susceptible to impact breakage out of the Sandsloot orebody rock types. For this drop weight test the composite average is similar to the average DWT for all the rock types combined, which is expected.

The χ^2 (C.I. 95 %) test confirmed the normal distribution of DWT data for each rock type, which is shown by the box and whisker plots in Figure 7.6. The widest population distributions and therefore the most variable properties are expected for feldspathic pyroxenite and pyroxenite. This observation is supported by the large standard deviation values calculated for these two rock types. Serpentinite has a narrow range, and appears will have a very predictable resistance to impact breakage. However, the low number of tests performed on this rock type could be distorting the results. Therefore the results for this rock type should be regarded with caution until more testing is performed.

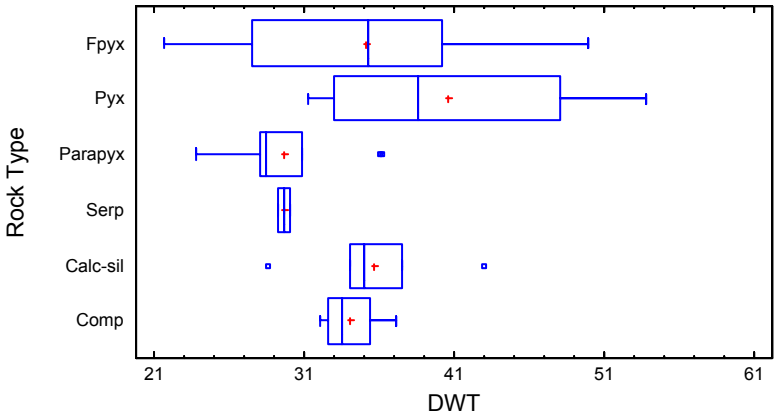

Figure 7.6 Box and whisker plot for the JK drop weight test (DWT) per rock type.

One way ANOVA (C.I. 95 %) for differences between the values of DWT per rock type reveal there is a significant difference in the performance of the various rock types when subjected to milling through impact. Duncan's multiple range test (C.I. 95 %) shows serpentinite and parapyroxenite will behave similarly to one another, whereas pyroxenite will behave significantly differently under the mill under the same conditions (Table 7.6). Calc-silicate, feldspathic pyroxenite and the composite material will be similar in performance but more testing is required to determine if they are likely to behave more like parapyroxenite and serpentinite or like pyroxenite.

Table 7.6 Duncan's multiple range test results for JK drop weight test (DWT).

Rock type	Count	Mean	HG
Serp	2	29.65	X
Parapyx	10	29.72	X
Comp	4	34.04	XX
Fpyx	11	35.11	XX
Calc-sil	5	35.63	XX
Pyx	4	40.53	X

HG, homogenous group

Again the differences in sample collection method and results for DWT were analysed using the one way ANOVA (C.I. 95 %). Table 7.7 shows pyroxenite, serpentinite and the composite material DWT values are the same regardless of sampling method or location. Feldspathic pyroxenite is significantly different for values from drill holes SSMet 1 and 7, with more testing required to differentiate between SSMet 2, 138055Grab and SSMet 6 results. There are two distinct groups of DWT results for the parapyroxenite rock type, with SSMet 1, SSMet 8 and 138055Grab behaving similarly and SSMet 6 and SSGrabP behaving similarly. More testing is required to determine which group SSMet 2 is more likely to behave like. Not enough tests were performed on the calc-silicate rock type for this analysis to be run on the data.

Table 7.7 Duncan's multiple range test results for impact breakage parameter DWT (A*b) by rock type per sampling method/ location.

Fpyx		Pyx		Parapyx		Serp		Comp	
Sample method	**HG**	**Sample method**	**HG**	**Sample method**	**HG**	**Sample method**	**HG**	**Sample method**	**HG**
SSMET1	X	138055GRAB	X	SSMET1	X	138055GRAB	X	138055GRAB	X
SSMET2	XX	SSMET1	X	138055GRAB	X	SSMET6	X	SSGRABM	X
138055GRAB	XX	SSGRABP	X	SSMET 8	X	SSMET 8	X		
SSMET6	XX			SSMET2	XX	SSMET 7	X		
SSMET 7	X			SSMET6	X				
				SSGRABP	X				

HG, homogenous group

7.5.2 Bond Ball Mill Work Index

Thirty six Bond ball mill Work Index (BWI) tests were performed on the orebody rock types from Sandsloot open pit. No tests were performed on the calc-silicate rock type. Table 7.8 gives the energy requirements to mill one tonne of material in kilowatts hours per tonne (kWh/t) for each rock type. From these values the expected performance of the material in a ball mill can be assessed. All the test results were valid and therefore were included into the data analysis.

Table 7.8 Results of Bond ball mill Work Index (BWI) testing (kWh/t).

Rock Type	Count	Avg.	Median	Standard dev.	Min	Max	Range	Interquartile range
Fpyx	5	**25.07**	25.20	2.51	21.33	28.10	6.77	1.90
Pyx	7	**22.09**	22.35	2.07	17.75	24.26	6.51	1.47
Parapyx	13	**23.95**	23.73	1.62	21.72	27.20	5.48	1.73
Serp	1	**29.50**	29.50	n/a	29.50	29.50	n/a	n/a
Comp	10	**24.05**	23.84	1.07	22.80	26.20	3.40	1.40
Total	36	**24.93**	24.92	1.81	22.62	27.05	5.54	1.63

Of all the rock types tested serpentinite has the highest average BWI at 29.50 kWh/t but this result may be distorted as it is based on only one test (Table 7.8). Results for feldspathic

pyroxenite, pyroxenite, parapyroxenite and composite material are comparable, with all the results falling in the low to mid twenties. Pyroxenite has the lowest BWI at 22.09 kWh/t avg. The composite BWI is similar to the average of the combined BWI for all rock types, which is expected.

Using the BWI classification table (Table 7.9) all the rock types tested are categorized as very hard. With BWI the higher the value the more difficult the material is to mill, therefore all the rock types in the Sandsloot pit will prove difficult to grind and will require a high energy input for processing.

Table 7.9 Bond ball mill Work Index classifications (kWh/t), after JKTech Pty (2008 a).

Property	Soft	Medium	Hard	Very Hard
BWI (kWh/t)	7.0 - 9.0	9.0 - 14.0	14.0 -20.0	> 20.0

The χ^2 test (C.I. 95 %) revealed the data for each rock type came from a normally distributed population, as is shown by Figure 7.7. The population dispersion assessed from the box and whisker plots as well as from the standard deviations in Table 7.8, indicates the range of values to be expected for BWI for each rock type, is narrow. Parapyroxenite is predicted to be the most variable in terms of input energy requirements for milling.

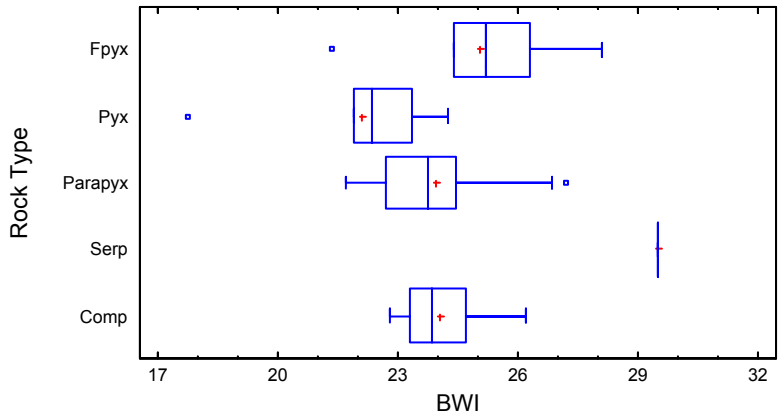

Figure 7.7 Box and whisker plot for the Bond ball mill Work Index (BWI) per rock type.

A statistical assessment of the significance for the energy requirement differences per rock type was performed using the one way ANOVA. At a 95% confidence interval the differences between rock types was found to be significant. Duncan's multiple range test (C.I. 95 %) which determine the rock types that are different was run and the results are given in Table 7.10. The

test results show that pyroxenite, parapyroxenite, the composite material and feldspathic pyroxenite are grouped as one and are predicted to behave similarly. The test also reveals that serpentinite will behave significantly different to all the rock types.

Table 7.10 Duncan's multiple range test results for the Bond ball mill Work Index (BWI).

Rock type	Count	Mean	HG
Pyx	7	22.08	X
Parapyx	13	23.95	X
Comp	10	24.04	X
Fpyx	5	25.06	X
Serp	1	29.50	X

HG, homogenous group

The one way ANOVA (C.I. 95 %) was run a second time on the BWI data to determine if any differences in sampling method of location resulted in BWI differences. Table 7.11 shows pyroxenite and parapyroxenite BMI values differ depending on the manner in which the sample is collected.

Table 7.11 Duncan's multiple range test results for Bond ball mill Work Index by rock type per sampling method/ location.

Fpyx		Pyx		Parapyx		Comp	
Sample method	**HG**	**Sample method**	**HG**	**Sample method**	**HG**	**Sample method**	**HG**
138055GRAB	X	SSGRAB	X	SSGRABP	X	138055 HPGR	X
SSMET1	X	138055GRAB	X	138055	X	SSGRABM	X
		SSMET1	X	SSMET1	XX	SSGRABT	X
		SSGRABP	XX	138055GRAB	X		
		138055	X				

HG, homogenous group

7.6 Discussion and Correlations

The results for each test are displayed in Figure 7.8. These graphs define the expected range of values for metallurgical properties, predicted from the results in the previous section. The maximum and the minimum points on these graphs are defined by one standard deviation above and below the average, and represent where 68% of any new observations are predicted to fall.

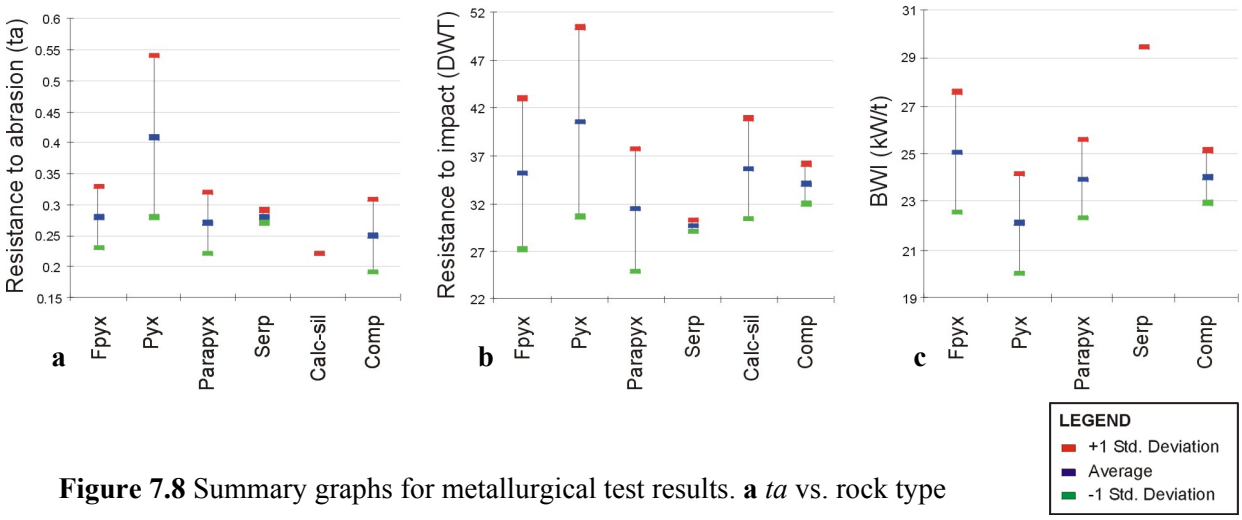

Figure 7.8 Summary graphs for metallurgical test results. **a** *ta* vs. rock type **b** DWT (A*b) vs. rock type. **c** BWI vs. rock type.

The semi autogenous (SAG) mills used in the Sandsloot plant require material with good properties of abrasion and impact breakage for successful milling. The results for the tumbling test and JK drop weight test were comparable, identifying pyroxenite as most susceptible to abrasion and impact breakage, *ta* = 0.41 and DWT = 40.54. BWI results indicate pyroxenite will be the most susceptible to crushing and grinding, therefore this rock types will be the easiest to mill and will require the least energy input into the plant circuit for its breakage. Serpentinite was identified as the least affected by crushing and grinding breakage, BWI = 29.50, requiring the highest inputs of circuit energy to break it down. It was also identified as having the most resistance to impact breakage, DWT = 29.65, but contrastingly had the second least resistance to abrasion breakage. Serpentinite typically appears to be the most difficult rock type out of the Sandsloot orebody to mill under SAG conditions, but is one of the more susceptible rock types to abrasion breakage.

The metallurgical strengths of the remaining Sandsloot orebody rock types fall between these two. Feldspathic pyroxenite typically shows higher-end strengths, with more resistance to abrasion and impact breakage and requiring greater energy to break it down using crushing and grinding. Parapyroxenite and the composite typically show middle of the range type strengths, the latter is commonly expected because it is a “uni-rock” comprising all the orebody rock types. Calc-silicate has the highest resistance to abrasion breakage but the second least resistance to impact breakage. The results of the abrasion resistance are based on a single test and there was no BWI testing for this rock type, therefore further testing is recommended to clarify the metallurgical strengths.

Duncan's multiple range test was used to determine which of the differences between metallurgical properties for each rock type were significant. The results are summarized in Table 7.12.

Table 7.12 Summary of the Duncan's multiple range test per test type.

Resistance to abrasion and impact breakage	*ta*	DWT	BWI	Energy required to mill
Highest	Calc-silicate	Serpentinite	Serpentinite	Highest
	Composite	Parapyroxenite	Feldspathic pyroxenite	
	Parapyroxenite	Composite	Composite	
	Feldspathic pyroxenite	Feldspathic pyroxenite	Parapyroxenite	
	Serpentinite	Calc-silicate	Pyroxenite	
lowest	Pyroxenite	Pyroxenite	-	lowest

These results indicated the lower pyroxenite strengths are significant and are likely to cause the pyroxenite to behave differently compared to most other orebody rock types when under milling conditions. Therefore this rock type may be expected to break down faster when a composite load of rock types is milled at once. Serpentine was identified as having significantly different properties to the other rock types when tested in the bond ball mill. Further testing is recommended to confirm this result as only one sample was tested. Extra testing will also clearly define the variability of the results for this rock type. Otherwise, there was not a great distinction between the rock types at a significant level. Only pyroxenite was distinguished as significantly different to parapyroxenite, calc-silicate and the composite for abrasion resistance and significantly different to serpentinite and parapyroxenite for resistance to tumbling resistance. The remaining rock types showed overlapping properties and therefore will share similar characteristics when milled.

The range of values for each test is narrow and the low significant difference confirms the classifications that all the rock types are typically hard, and fall into the categories moderately hard, hard or very hard rock. Therefore feldspathic pyroxenite, parapyroxenite, calc-silicate, the composite material as well as pyroxenite and serpentinite are all predicted to be difficult to mill, requiring a relatively high energy for breakdown.

Variation, identified by running Duncan's multiple range test per collection method, shows different properties may be expected for the same rock type between the drill holes and from different sampling sites of the same blast. Parapyroxenite was identified to vary in resistance to impact breakage and resistance to crushing and grinding. Pyroxenite was distinguished as variable in resistance to impact breakage and crushing and grinding. Feldspathic pyroxenite varied in its resistance to impact breakage. This variability could be due to differences in composition, grain size and alteration between rocks of the same type across the orebody. However, these possible petrographic influences will be discussed under Chapter 8. Serpentinite and calc-silicate variability could not be statistically assessed due to lack of samples. It is recommended that sample of these rock types be tested from different locations in the pit and using different sample collections methods.

The variation in metallurgical strengths per collection method may also indicate that blasting has an impact the metallurgical strengths of a rock type. Blasting is recognized as influencing the micro fracturing and stress within the rock, therefore rocks which have been selected from drill hole core versus post-blast grab samples may differ in strengths. More testing would be required, comparing the results of the samples from drill hole collection versus post-blast grab samples collection, to quantitatively assess the influence. Testing for these properties for serpentine and calc-silicate is recommended

7.7 Summary and Conclusions

The resistance of the orebody rock types to abrasion breakage, impact breakage, crushing and grinding were examined using the drop weight tumbling test, the JK drop weight test and the Bond ball mill Work Index. Samples were collected from drill holes within blast block 138 – 055, outside the block, as well as randomly from the post-blast material either in the pit or in the plant. Testing was performed by the staff at the Anglo Research centre and the results were arranged into a database which was used, with the *Statgraphics Centurion XV* software to interrogate the data.

Statistical analysis using the one way ANOVA and Duncan's multiple range test revealed significant differences between the performance of each of the rock type for each of the metallurgical tests. Analysis also revealed significant differences between the results of the same rock type from different drill holes and sampling sites of the same blast. These differences were determined at a 95% confidence interval.

The range in rock strengths, gauged by the metallurgical testing, is narrow with all the orebody rock types falling into the categories of moderately hard rock, hard rock or very hard rock. Therefore all the orebody rock types are expected to be relatively difficult to crush, grind and mill and will require high energy input for breakdown.

Results from the two types of drop weight tests and the Bond ball mill Work Index are comparable. They indicate pyroxenite has the lowest metallurgical strengths, performing the best under semi autogenous milling conditions. Serpentinite will typically have higher strengths, performing more poorly than the other orebody rock types. Feldspathic pyroxenite, parapyroxenite and the composite material will have strengths which range between pyroxenite and serpentinite.

Only serpentinite was distinctly differentiated from the other rock types for a metallurgical property. It has a significantly higher resistance to crushing and grinding, indicated by BWI. Therefore serpentinite will require significantly higher inputs of energy, into the plant circuit, to break down the rock fragments. Pyroxenite was the other rock type identified as showing differences to parapyroxenite, calc-silicate and the composite for abrasion resistance and significantly different to serpentinite and parapyroxenite for resistance to tumbling resistance. The remaining rock types will share similar characteristics when milled.

Variability in milling properties between rock types and between different sample locations indicate that petrographic properties influence the milling performance of the rock type. Parapyroxenite, feldspathic pyroxenite and pyroxenite are predicted to vary depending on the location in the pit and sample collection methods. The impact of blasting is also recognized as important, influencing the micro fracturing and stress within the rock. To quantitatively assess the influence of blasting on the milling process more testing which compares the results of the samples from drill hole collection versus post-blast grab sample collection, would be required.

Due to the limited data for serpentinite and calc-silicate it is recommended that more testing be undertaken for these two rock types. This will expand the database, improve the prediction limits, clear up the distortions caused by low test sample numbers and will verify the previous conclusions.

Chapter 8

DISCUSSION

This chapter draws comparisons and contrasts between the findings and conclusions of the previous chapters. It looks at defining relationships and general trends between the petrography, geotechnical, geochemical and metallurgical properties that are interdisciplinary. Where possible the properties are linked with statistical associations or correlations.

A literature search for journal articles relating the geotechnical, geochemical and metallurgical properties to one another generated few references. The relevant references are reviewed in the appropriate section and the research in this chapter therefore represents a new contribution to these fields. Though relating these properties has not been common, the objective of these comparisons for this study was to determine if the properties from the orebody rock types at Sandsloot could be identified using few, relatively simple tests. These tests having been based on the characterisation of all aspects of the physical and chemical properties of commonly occurring rock types in the orebody.

8.1 Comparisons between Petrography and Geotechnical, Geochemical and Metallurgical Properties

It was anticipated that the basic petrographic similarities, differences and relationships identified between the various rock types in this study would be reflected in the investigations of the geotechnical, geochemical and metallurgical properties. This proved to be the case between the petrographic and geotechnical investigations, which tended to distinguish the rock types into similar groups. For example, similarities in composition, grain size, textures and degree of alteration grouped feldspathic pyroxenite, pyroxenite and parapyroxenite as being similar, distinguishing them from serpentinite and calc-silicate and distinguishing serpentinite from calc-silicate. Feldspathic pyroxenite, pyroxenite and parapyroxenite were distinguished as having similar properties of ultrasonic velocity, UCS and indirect tensile strength, whilst feldspathic pyroxenite and parapyroxenite were typically similar for properties of density and PLI Is_{50}, as well. These properties were distinguished as being higher and significantly different to those of serpentinite and calc-silicate. Serpentinite and calc-silicate were distinguished as similar in

strength but different to each other for density and ultrasonic velocity. These relationships reflect the rock types distinguished by petrography. The variability in petrographic properties exhibited by parapyroxenite was reflected in the geotechnical properties. Parapyroxenite was distinguished as displaying the least unique properties, showing similarities to many of the other orebody rock types. The presence of a fabric and the degree of alteration, which distinguished serpentinite and calc-silicate were reflected in similar properties of UCS, tensile and PLI Is_{50} strength for these rock types. With the presence of these petrographic properties there was an observed decrease in the values of strength.

Differences in composition were reflected well with changes in density. For example the composition change in pyroxenite to include feldspar –SG of ~ 2.5 to 2.6– or contamination of pyroxenite with calc-silicate and serpentinite –SG of 3.0 and 2.8, respectively– to form parapyroxenite, resulted in lowered densities for these hybrid rock types. The presence of a fabric in serpentinite was reflected in its ultrasonic velocity value. Convention accepts that ultrasonic velocity is dependent on density and elastic properties and is influenced by grain size, with rock types of finer grain size having faster ultrasonic velocity values (Goodman, 1989). Serpentine has the lowest ultrasonic velocity despite having the finest grain size. It is likely that the fabric and preferred orientation of the fractures in the olivine, orientated obliquely to the long axis of the core, observed in the petrography study, act to impede the ultrasonic waves. Pyroxenite, parapyroxenite and feldspathic pyroxenite have average ultrasonic velocities above 6000 m/s, where as calc-silicate and serpentinite have ultrasonic velocities below this value. It is possible that any rock contaminated by these two rock types will result in lower ultrasonic velocities, as shown by the ultrasonic values of parapyroxenite versus pyroxenite. The failure of serpentinite UCS samples reflected the fibrous habit of the serpentine, its fabric and preferred orientation. Fragments from the valid tests were observed to be elongate and splinter-like, dissimilar to the failure modes of all the other orebody rock types. The presence of calcite or talc infilled veinlets was also reflected in the frequent failure of the serpentinite UCS samples along discontinuities not visible to the naked eye. These veinlets resulted in more invalid UCS test results than observed for the other rock types. The veinlets would have compounded the impediment of the ultrasonic waves as well.

The strength anisotropy, calculated by comparing PLI Is_{50} axial and diametral results could not be calculated because the Sandsloot database results are all diametral point load index strengths. However, it can be assumed that the serpentinite, with its slight preferred orientation of minerals and calc-silicate with its partial zoning of mineralogy and high variability, would show a degree

of anisotropy when the strength is tested in different directions. Pyroxenite, feldspathic pyroxenite and parapyroxenite on the other hand would probably not show any anisotropy in strength because of the granular fabric. Serpentinite may be predicted to have the lowest diametral strength because the loading direction would be almost sub-parallel with the slight preferred orientation of the minerals.

In the comparison between petrographic and geochemical observations, properties such as grain size, textures and fabric are not expected to be reflected in the geochemical properties. Composition or mineralogy, which would include the degree of alteration, however, may be expected to be reflected by the whole rock major element oxide composition.

The grouping of the rock types by composition, previously described in the comparison between petrographic and geotechnical properties, was compared to the grouping of the rock types distinguished by statistically significant similarities and differences between the concentrations of major element oxides (see Chapter 6, section 6.5.1 and Table 6.2 which details the results of the Duncan's multiple range test applied to the major element oxides). Though some of the oxides did distinguish feldspathic pyroxenite, pyroxenite and parapyroxenite as similar to each other, different to serpentinite and calc-silicate and distinguished differences between serpentinite and calc-silicate, the trend was not reflected strongly. The groupings showed overlapping similarities between most of the rock types and examples where the general trend did not fit.

A detailed investigation revealed that feldspathic pyroxenite and pyroxenite were strongly similar, with the concentration of 10 out of 12 of the major element oxides and the percentage weight lost on ignition (L.O.I.) displaying no significant differences. Pyroxenite and parapyroxenite were moderately similar, with 8 out of 12 major element oxides displaying no statistical difference in concentration. Feldspathic pyroxenite and parapyroxenite, however, were distinguished as only weak to moderately similar, with 6 out of 12 major elements displaying similarities and no similarity in the percentage weight L.O.I. The difference between serpentine and calc-silicate to the other rock types was moderate, as was the difference between serpentinite and calc-silicate. The investigation did distinguish a strong similarity in concentrations of major element oxides for parapyroxenite and calc-silicate, which was not displayed by the petrographic investigation. Of the major element oxides, 10 out of 12 displayed no significant differences and neither did the percentage weight lost on ignition (L.O.I.). From this comparison between trends shown by petrographic and geochemical investigations it

appears the geochemical similarities based on major element oxides revealed the subtle differences and similarities between the rock types, especially those distinguished by element oxides that are not major components.

In the comparison between metallurgical strengths and petrographic properties de Vaux and Schouwstra (2006) identified changes in grain size (fine to pegmatiodal), serpentinisation and feldspar-content affected the milling performance of the rock types. Similar deductions can be made from the results of this study. For example, the larger grain size of pyroxenite parallels with the high parameters of *ta* and DWT, and the BWI results confirmed the good milling properties of pyroxenite. Serpentinite, which is very fine-grained, was commonly the most difficult to mill. The high resistance to impact breakage identified for serpentinite was also identified for parapyroxenite. It is therefore likely that the alteration caused by serpentinisation has influenced the breakage properties of parapyroxenite, especially the impact breakage. Parapyroxenite is also predicted to have the most variable properties when milled, which is most likely a function of the varying degree of serpentinisation, grain size and composition, as identified in the petrography study. Finally, feldspathic pyroxenite was identified as having higher metallurgical strengths in the range of the Sandsloot orebody rock types. Therefore feldspar appears to increase the resistance of a rock type to abrasion, impact breakage and crushing and grinding. Textures such as recrystalised grain boundaries may affect the metallurgical properties as well. However, in this study recrystalised grain boundaries were identified for each of the orebody rock types, therefore this property cannot be assessed. It is recommended that testing of samples with greater and lesser degrees of recrystalised grain boundaries be tested to qualify the affect.

8.2 Geotechnical and Geochemical Relationships

A comparison of geotechnical uniaxial compressive strength (UCS), density and ultrasonic velocity to the geochemistry was undertaken. For this study directly related pairs of data were compared because it was possible to geochemically test samples that had been tested for density, ultrasonic velocity and uniaxial compressive strength. Using *Statgraphics Centurion XV* these properties were assessed to determine if, on the basis of selected chemical analysis, mining conditions as derived from geotechnical properties could be predicted with some degree of certainty.

A search for literature and journal publications relating the UCS and geochemistry yielded few results. Many papers looked at the strength of clays and their major element oxide composition but only one paper focused on the comparison between UCS and the whole rock and trace element geochemical analysis for unweathered igneous rocks. The paper, by Wilson *et al*. (2005), compared the two for the norite rocks that are stratigraphically above the Merensky and Bastard Reefs in the Bushveld Complex. Zr and normative quartz (volume %) were determined to relate moderately to UCS. It was postulated that the two reflect the development of late-stage minerals that act as cementing medium to cumulates during formation of the rock. The cementing medium affects the fracture propagation when the rock is placed under stress and ultimately influences the rock strength. The study identified an increase in Zr and normative quartz (volume %) resulted in an increased UCS strength.

Results of correlations between UCS, ultrasonic velocity and density with geochemistry are given in Table 8.1. Less than half the 41 elements studied related to density with any degree of statistical significance, just over half the elements related to ultrasonic velocity with statistical significance and less than one fifth of the elements related to UCS with statistical significance. Of the elements that were relatable, the majority were element oxides and most showed weak relationships, with correlation coefficients varying between 0.21 and 0.49 and R^2 values varying between 0.01 and 0.24. The relationships between Zr and strength, identified by Wilson *et al.* (2005), were not found in this study of the Sandsloot orebody rock types.

Table 8.1 Results of comparisons between geochemistry and density, ultrasonic velocity and UCS.

Elements related to density				Elements related to ultrasonic velocity				Elements related to UCS			
	Corr. Coeff.*	R^2	Descrip		Corr. Coeff.	R^2	Descrip		Corr. Coeff.	R^2	Descrip
SiO_2	0.65	0.42	M*	SiO_2	0.25	0.06	W	Al_2O_3	0.24	0.06	W
Al_2O_3	-0.24	0.05	W*	FeO	-0.14	0.16	W	MnO	0.31	0.10	W
FeO	-0.54	0.29	M	MgO	-0.51	0.26	M	K_2O	0.44	0.20	W
MgO	-0.91	0.83	S*	CaO	0.46	0.22	W	Ba	0.37	0.14	W
CaO	0.91	0.84	S	TiO_2	0.46	0.17	W	P	0.23	0.06	W
TiO_2	0.38	0.14	W	P_2O_5	0.27	0.08	W	Sr	0.49	0.24	W
Cr_2O_3	0.21	0.05	W	L.O.I.	-0.47	0.22	W	Rb	0.33	0.11	W
NiO	0.31	0.09	W	Au	0.08	0.01	W				
L.O.I.	-0.95	0.91	S	Os	0.08	0.01	W				
REE	0.45	0.21	W	Pd	007	0.01	W				
Nb	0.31	0.10	W	Pt	0.11	0.01	W				
U	0.21	0.05	W	Ru	0.08	0.01	W				
Zr	0.27	0.07	W	REE	0.41	0.17	W				
Cu	0.36	0.13	W	Nb	0.31	0.09	W				
V	0.70	0.50	M	Ba	0.21	0.05	W				
Sc	0.58	0.34	M	Ta	0.25	0.06	W				
Cr	0.23	0.06	W	P	0.28	0.08	W				
Ni	0.34	0.12	W	Hf	0.29	0.09	W				
				Zr	0.31	0.09	W				
				Sr	0.26	0.07	W				
				V	0.35	0.12	W				
				Sc	0.31	0.10	W				

*Corr. Coeff: correlation coefficient, W: weak, M: moderate, S: strong

The elements SiO_2, FeO, V and Sc showed moderate relationships to density, with correlation coefficients varying between 0.54 and 0.70, and with R^2 values between 0.29 and 0.5. Only MgO showed a moderate relationship with ultrasonic velocity, with a correlation coefficient of 0.51 and R^2 value of 0.26.

MgO, CaO and L.O.I. showed strong relationships with density. The correlation coefficients are 0.91, -0.91 and -0.95 for CaO, MgO and L.O.I. respectively and the R^2 values are 0.84, 0.83 and 0.91, respectively. Figure 8.1 shows these major oxides plotted against density. The various orebody rock types are distinguishable, with separate populations clearly visible for pyroxenite and serpentinite. There is overlap between the populations of feldspathic pyroxenite and parapyroxenite, with parapyroxenite overprinting the feldspathic population due to its variable concentration of these elements. There are not enough samples of calc-silicate to define its population but the spread of the three samples is large.

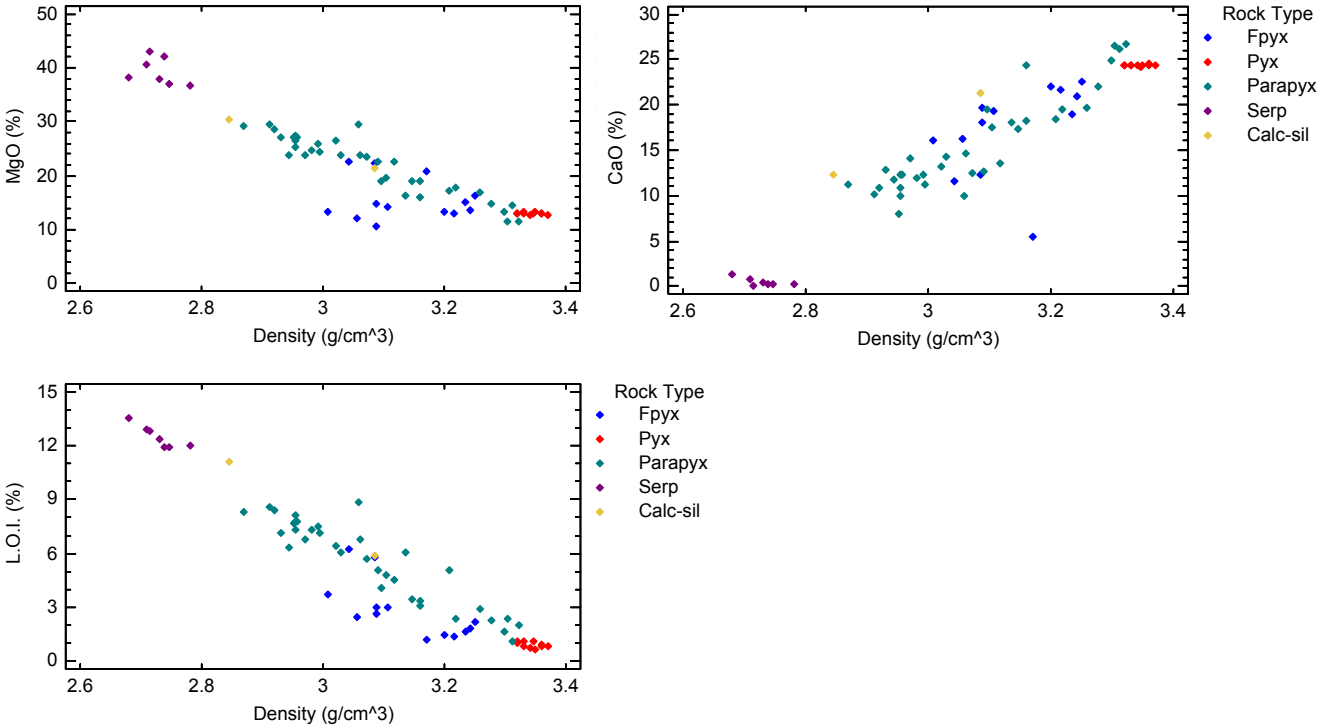

Figure 8.1 Comparison of density versus MgO (wt %), CaO (wt %) and Loss of ignition (L.O.I.) (wt %).

None of the elements geochemically analysed showed either moderate or strong relationships with uniaxial compressive strength. Therefore on the basis of chemical analysis, mining conditions as derived from UCS cannot be predicted with any certainty, by correlation with geochemistry.

8.3 Geotechnical and Metallurgical Relationships

Relating geotechnical properties to metallurgical properties is useful if they indicated similar strengths and strong relationships, thus making it possible to predict one using the other. Geotechnical strength tests, especially point load index testing, as well as density and ultrasonic velocity tests are easier to perform and require less sample that metallurgical tests. If these properties relate well to metallurgical strengths this could provide the mine with the benefits of knowing the metallurgical properties without the associated cost of developing a large metallurgical database. The relationships could also be used to assist in the prediction of the ore crushability, grindability and future mining and milling rates.

Previous research has found that UCS is related to drop weight test results (Bye and Hansmann, 2004). The two were shown to complement each other. They indicate the same strength indices and good correlations. Likewise point load index strength (PLI Is_{50}) and drop weight tests (DWT) may be expected to be related. Relationships and correlations between UCS and bond work index (BWI) are inconsistent. Studies between these properties indicating some mines have rock types that show significant correlations whilst others do not (Bye and Hansmann, 2004, Doll *et al*., 2001). Therefore forecasting of the grinding circuit throughput and future mine production is not always possible using UCS measurements, but may be applicable in specific instances.

Results from comparisons of the UCS and metallurgical testing for this research found the UCS results are comparable to DWT results. Both tests indicate similar strength indices, with rock types defined as geotechnically strong also described as hard metallurgically. But the correlation was poor, with a correlation coefficient of 0.29 and $R^2 = 0.08$ (Figure 8.2). Point load index strengths compliment the DWT results, with PLI Is_{50} results indicating the same strength indices (Figure 8.3) and a moderate correlation to DWT, where the correlation coefficient = 0.83 and $R^2 = 0.69$.

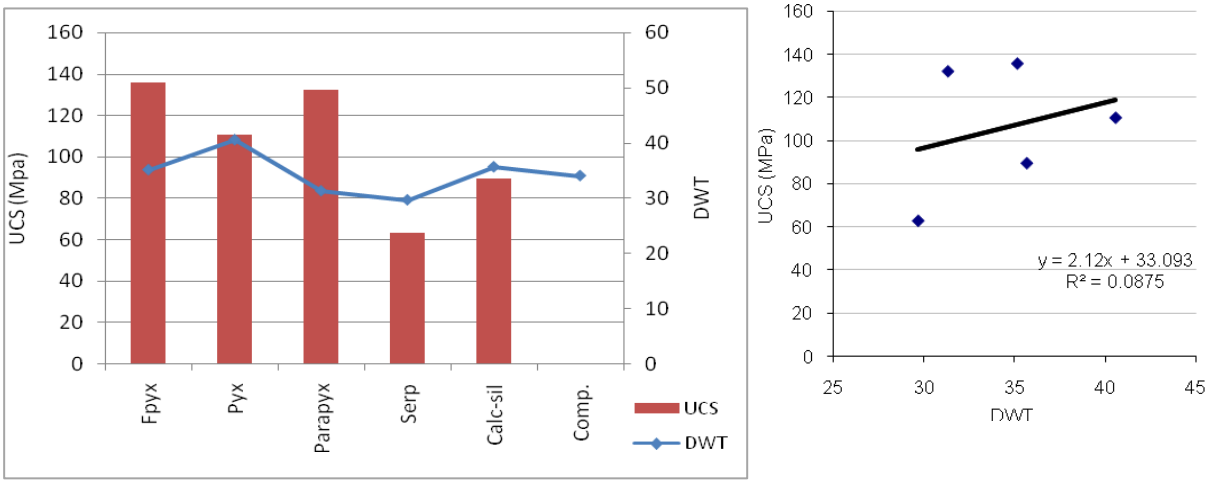

Figure 8.2 Comparison of UCS against DWT, bar graph and scatter plot showing the line of fitted linear regression.

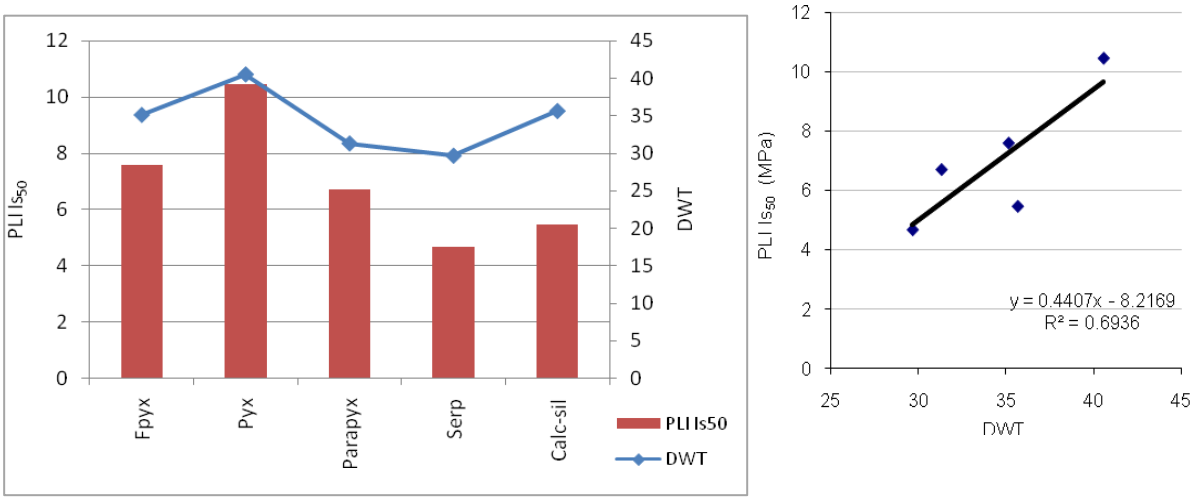

Figure 8.3 Comparison of PLI Is_{50} against DWT, bar graph and scatter plot showing the line of fitted linear regression.

Results for comparisons between UCS and PLI Is_{50} with *ta* are comparable to those with DWT, indicating similar strengths. However the correlation coefficients and R^2 values for UCS are 0.18 and 0.03 respectively, which is marginally worse (Figure 8.4) and correlation coefficients and R^2 values for PLI Is_{50}, 0.88 and 0.77 respectively, which is slightly better (Figure 8.5).

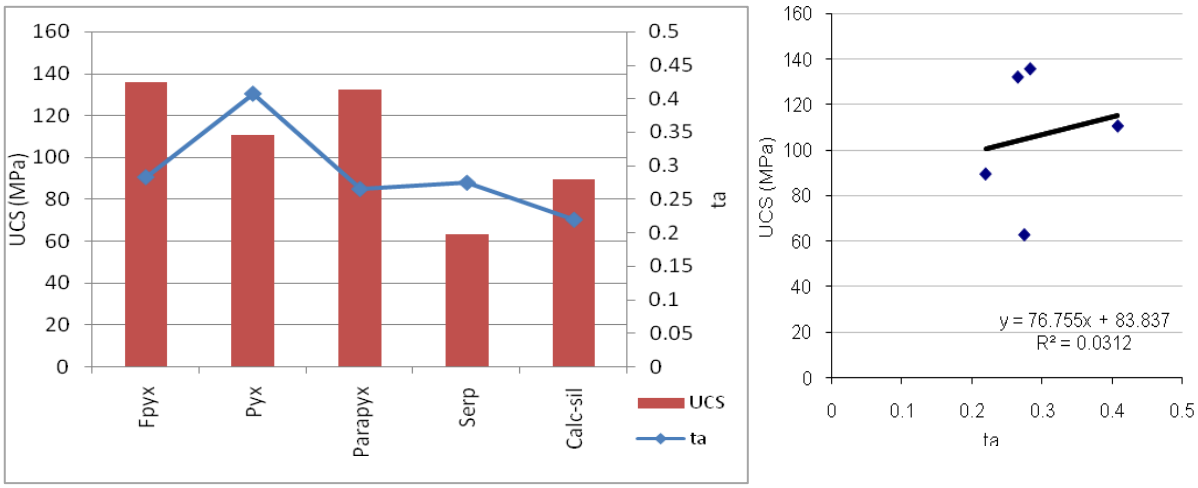

Figure 8.4 Comparison of UCS against *ta*, bar graph and scatter plot showing the line of fitted linear regression.

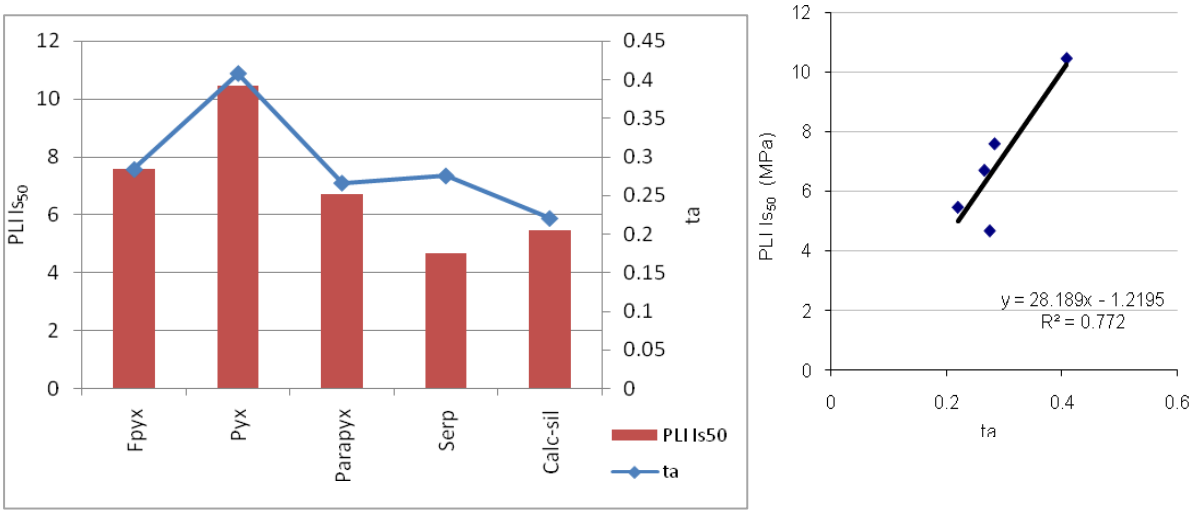

Figure 8.5 Comparison of PLI Is_{50} against *ta*, bar graph and scatter plot showing the line of fitted linear regression.

One of the difficulties in comparing geotechnical strength to metallurgical strength is that UCS, for example, is a measure of a rocks initial strength to first failure of rock. Metallurgical strengths on the other hand are a measure of the strength or resistance of a rock to break down to a final fragment size, defined by requirements for further processing. This could explain the poor correlations but similar strength indices.

A correlation coefficient of -0.74 and a R^2 value of 0.55 was calculated for UCS versus BWI (Figure 8.6). Although the correlation appears moderate the negative correlation coefficient does not seem sensible. It is intuitive that a rock with high UCS should not have a low crushing/ grinding work index because crushing and grinding causes a sample to fail under compression, like a UCS test (Doll *et al*., 2001). The plot of the fitted linear regression shows serpentinite is the cause of the negative relationship, because of its disproportionately high BWI but low UCS (Figure 8.6). A strong relationship was identified between PLI Is_{50} and BWI, showing the greater the point load strength index of a rock type the less energy is required to break down the rock (correlation coefficient = -0.89 and R^2 = 0.80). The negative relationship is similar to that between UCS and BWI and again is counter intuitive. Either serpentinite or pyroxenite could be distorting the results (Figure 8.7). However, in chapter 5 it was identified that the pyroxenite PLI Is_{50} was unusual, therefore it is possible that serpentinite is again distorting the results.

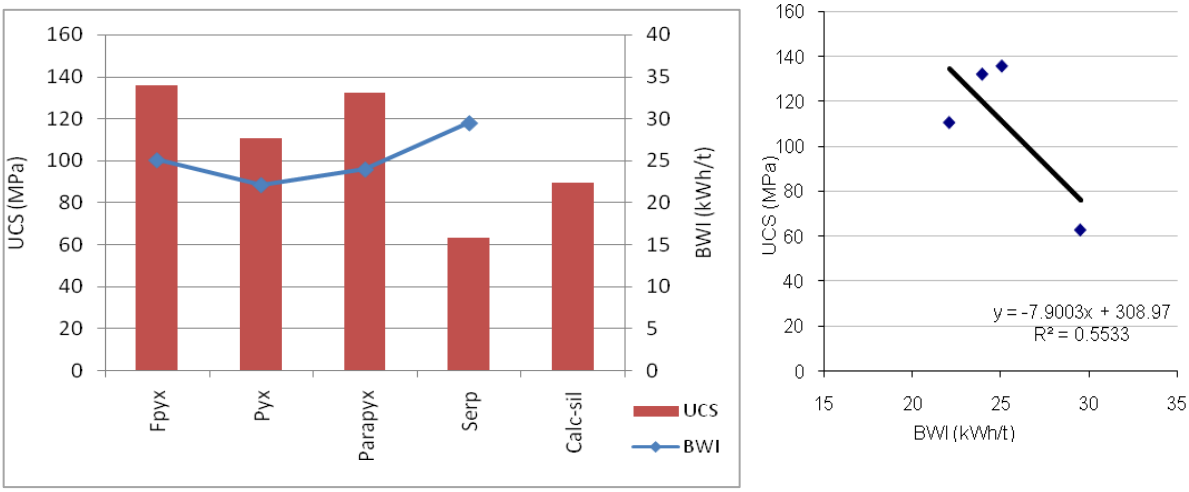

Figure 8.6 Comparison between UCS and BWI, bar graph and scatter plot showing the line of fitted linear regression.

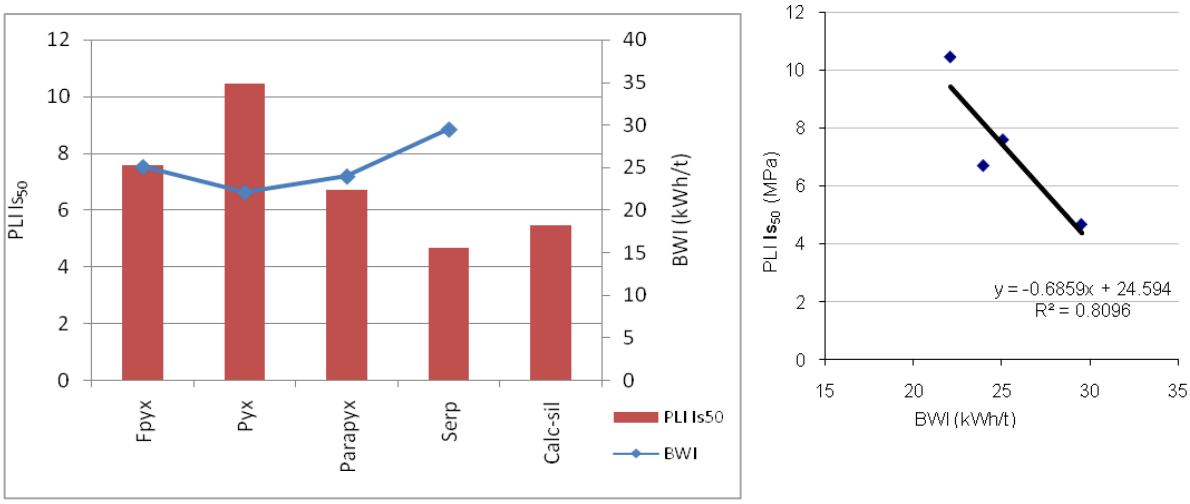

Figure 8.7 Comparison between PLI Is_{50} and BWI, bar graph and scatter plot showing the line of fitted linear regression.

Looking at indirect tensile strength as well as density and ultrasonic velocity in relation to the metallurgical strengths revealed several good and moderate relationships as well as some properties that could not be related. Density related well to BWI, with a correlation coefficient of -0.96 and an R^2 value of 0.93 (Figure 8.8). This indicates that rock types with lower densities, e.g. serpentinite, are more difficult to crush and grind and therefore require more energy to be broken up. Density related moderately to DWT, with a correlation coefficient of 0.84 and R^2 = 0.71 (Figure 8.9). This indicates the higher the density the more susceptible the rock type is to impact breakage. Density also related moderately to *ta*, with a correlation coefficient = 0.87 and R^2 = 0.77, indicating the higher the density of a rock the more susceptible it is to abrasion breakage (Figure 8.10).

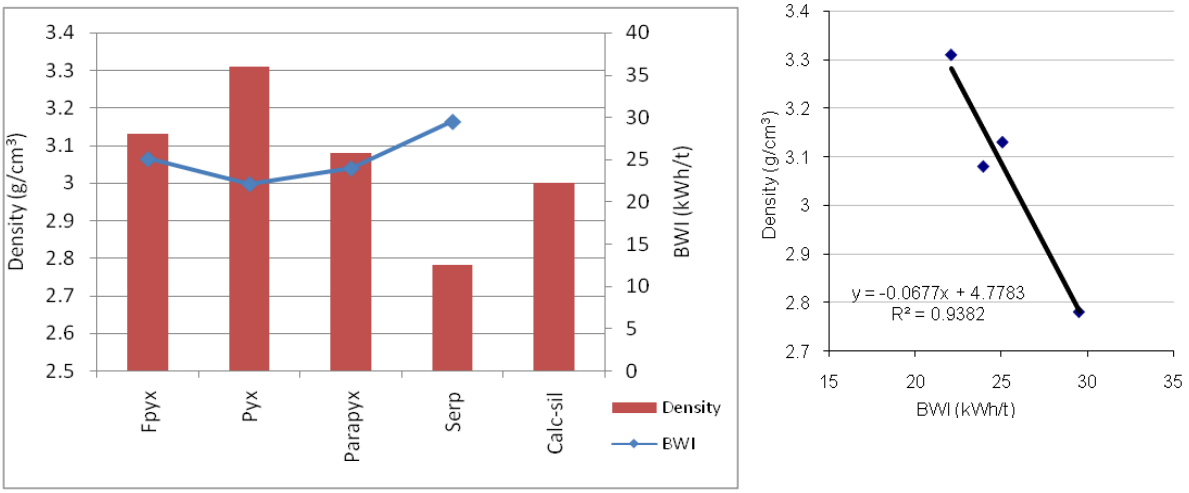

Figure 8.8 Comparison between density and BWI, bar graph and scatter plot showing the line of fitted linear regression.

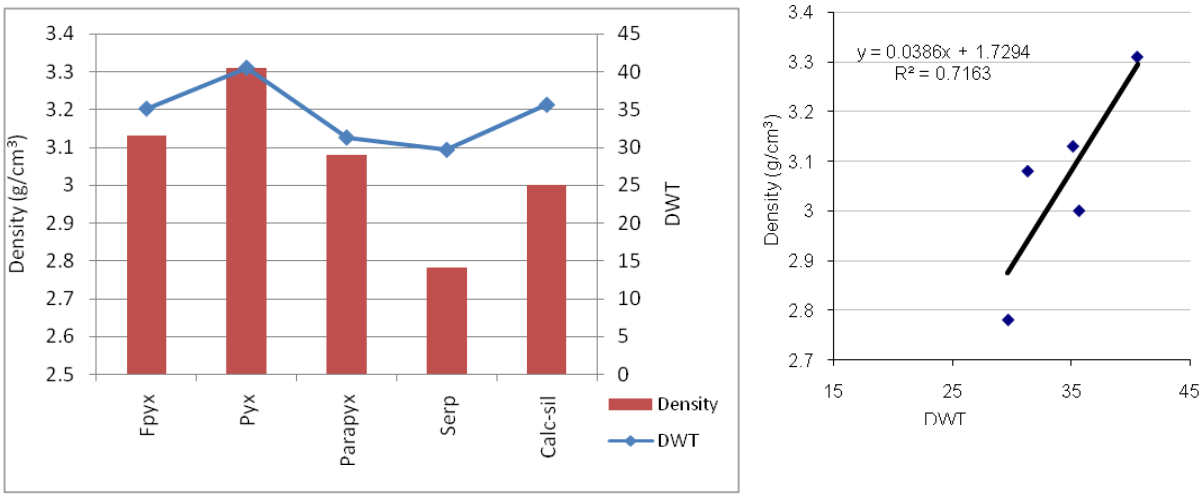

Figure 8.9 Comparison between density and DWT, bar graph and scatter plot showing the line of fitted linear regression.

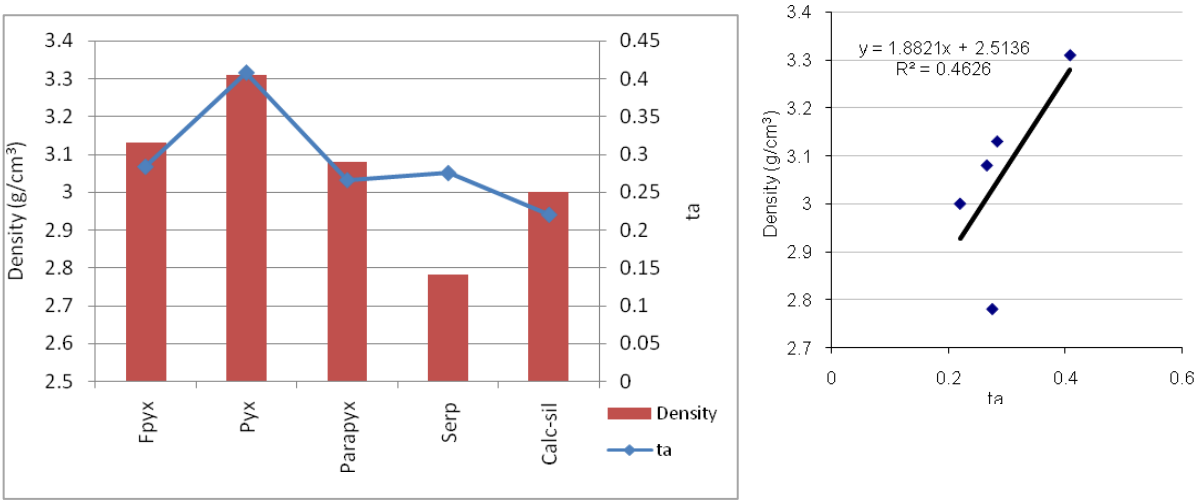

Figure 8.10 Comparison between density and *ta*, bar graph and scatter plot showing the line of fitted linear regression.

Ultrasonic velocity was compared with *ta*, DWI and BWI but only showed a strong relationship with BWI. A strong inverse relationship was identified between the two, with a correlation coefficient = -0.98 and R^2 = 0.95 (Figure 8.11). This indicated a rock with lower ultrasonic velocity required more energy to break up that rock type.

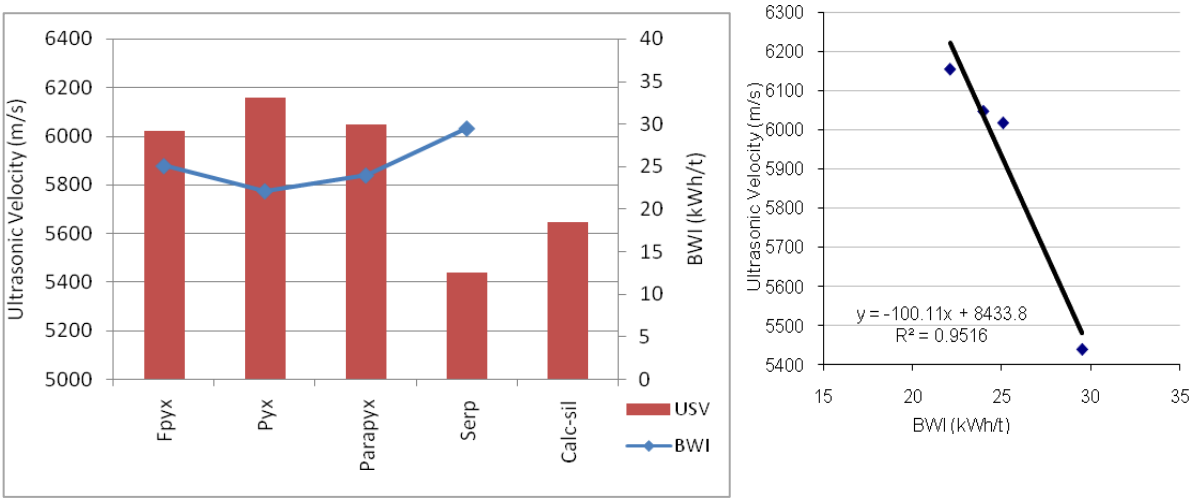

Figure 8.11 Comparison between ultrasonic velocity and BWI, bar graph and scatter plot showing the line of fitted linear regression.

Indirect tensile strength did not relate well to the metallurgical strengths. The highest correlation coefficient was with BWI at -0.51 with a R^2 = 0.26, thereafter the relationships became weaker with correlation coefficient of -0.31 and -0.05 for DWT and *ta*, respectively.

Considering all the data, ultrasonic velocity and indirect tensile strength did not relate well to the metallurgical strength. UCS related moderately, and density and PLI Is_{50} showed the strongest relationships. Although serpentinite seemed to stand out, when comparing geotechnical strengths and metallurgical strengths, the comparisons indicate that the higher the strength of the rock the less susceptible to impact and abrasion breakage it was and therefore more difficult to mill. It was shown that with a decrease in density and ultrasonic velocity there was a decrease in breakage therefore grindability and milling performance of a rock is a combination of its strength, density and ultrasonic velocity/ elasticity.

8.4 Metallurgical and Geochemical Relationships

The metallurgical strength results were compared to the geochemical results to determine if the distribution and relationship of certain elements with the rock types could help characterise the metallurgical strengths, assisting in the characterisation of the orebody for mine-to-mill purposes. A literature search yielded many papers on the links between metallurgy and geochemistry, commonly used in the prospecting for new ore deposits. However, no papers could be located linking the metallurgical strengths and resulting processing parameters to geochemistry predictability. Therefore this study will have made a start to contributing to this field. However, the results must at this stage be seen as significant on for this particular mining operation.

Correlations and linear regressions between metallurgical strengths and geochemical composition revealed that there were strong relationships of significance between BWI and the oxide elements FeO, CaO and TiO_2. The correlation coefficients and R^2 values are detailed in Table 8.2 and the trends are represented graphically in Figures 8.12, 8.13 and 8.14. BWI and FeO show a positive, normal relationship. With an increase in the concentration of FeO in a sample the difficulty in crushing and grinding that sample will increase. CaO and TiO_2 are inversely related to BWI. With an increase in the concentration of either of these two oxides the crushing and grinding of the sample is predicted to be easier.

Table 8.2 Correlation coefficients and R^2 values for the comparison of geochemical composition against metallurgical strength properties.

Properties	Correlation Coefficient	R^2	Description
BWI vs. FeO	0.96	0.92	Strong
BWI vs. CaO	-0.96	0.93	Strong
BWI vs. TiO_2	-0.98	0.96	Strong
DWT vs. V	0.83	0.69	Moderate
BWI vs. Ir	-0.95	0.91	Strong
BWI vs. Os	-0.98	0.97	Strong
BWI vs. Pt	-0.96	0.92	Strong
BWI vs. Ru	-0.88	0.77	Moderate

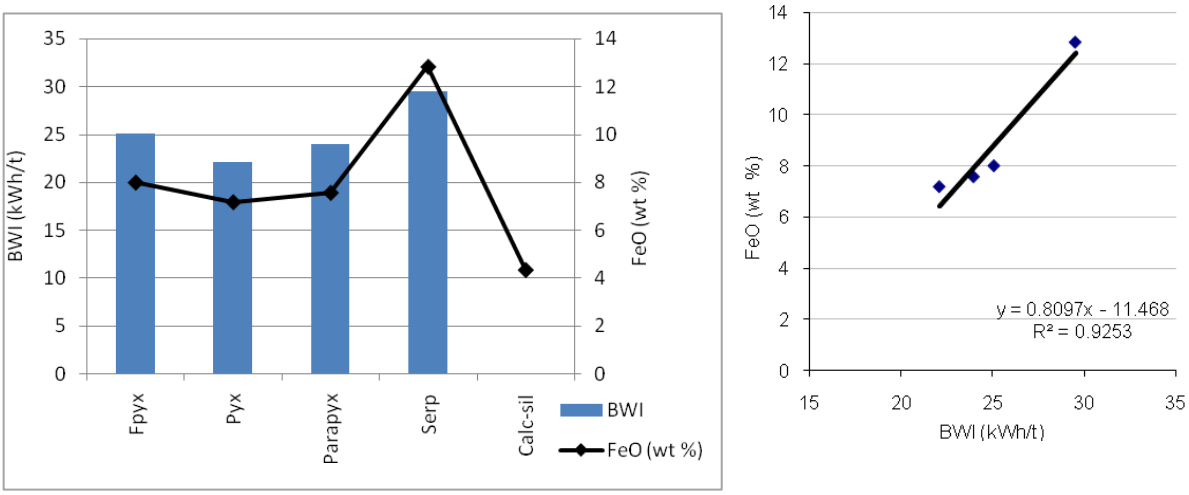

Figure 8.12 Comparison between FeO (wt %) and BWI, bar graph and scatter plot showing the line of fitted linear regression.

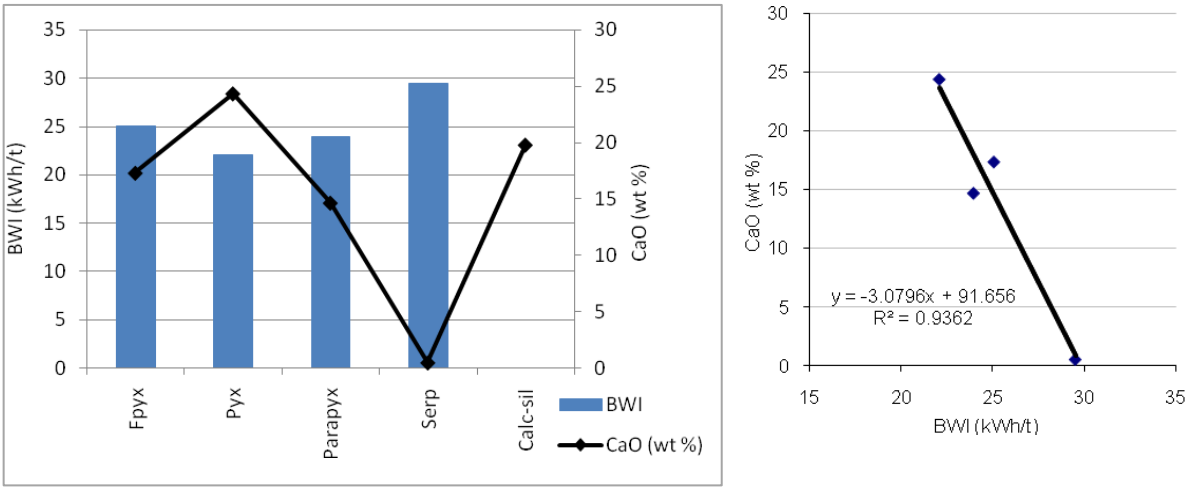

Figure 8.13 Comparison between CaO (wt %) and BWI, bar graph and scatter plot showing the line of fitted linear regression.

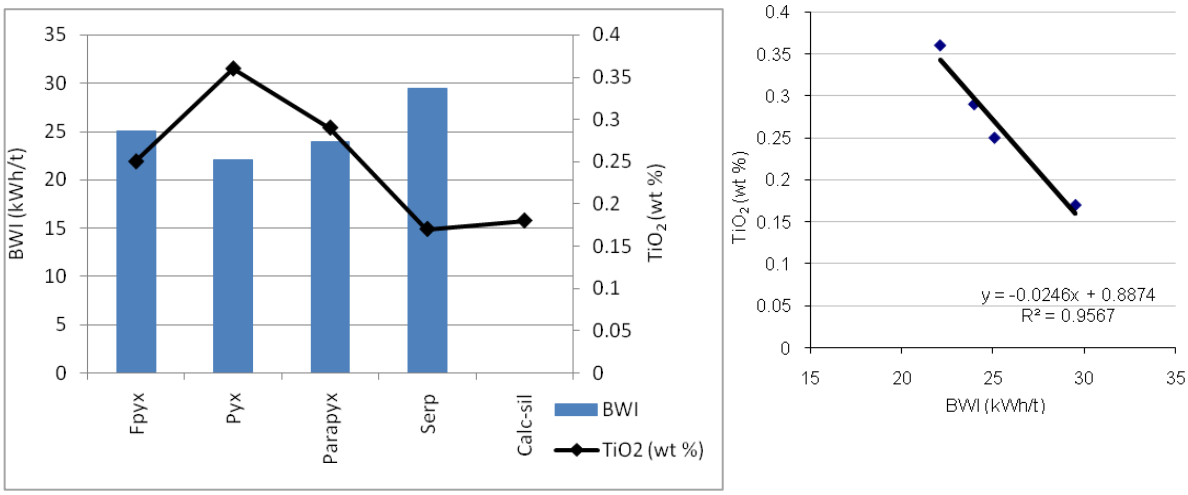

Figure 8.14 Comparison between TiO_2 (wt %) and BWI, bar graph and scatter plot showing the line of fitted linear regression.

Of the base metals, only V related to a metallurgical strength. V showed a moderate positive relationship to DWT (Table 8.2). Therefore as the concentration of V increases in a sample the less resistance it will have against impact breakage – the higher the DWT value the less resistant to impact abrasion – (Figure 8.15).

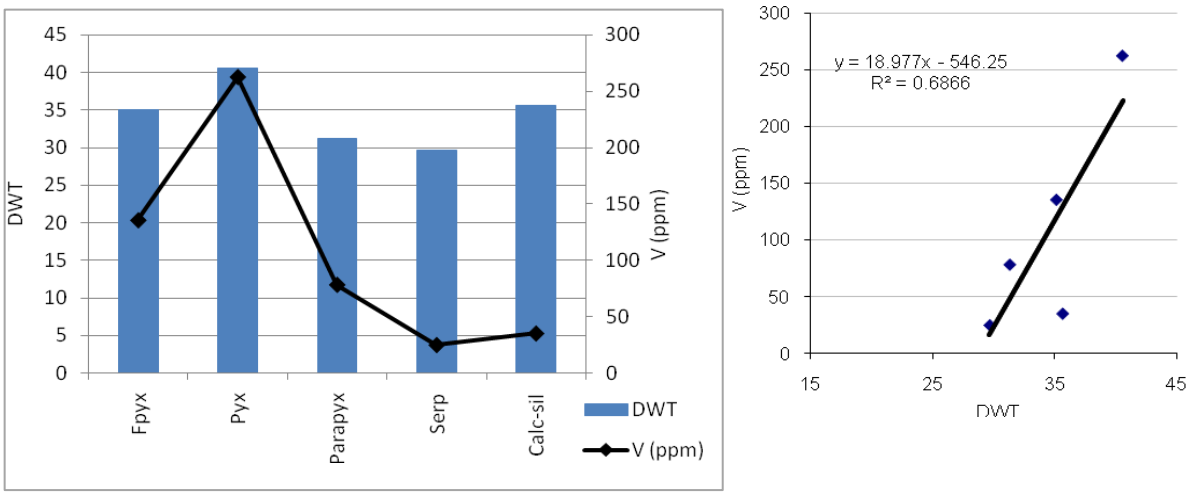

Figure 8.15 Comparison between V (ppm) and DWT, bar graph and scatter plot showing the line of fitted linear regression.

In the comparison of the metallurgical strengths to the platinum group elements (PGEs), the major commodity at Sandsloot mine, three out of six PGEs showed strong inverse relationships with BWI and a fourth showed a moderate inverse relationship with BWI (Table 8.2). These relationships show that with an increase in the concentration of Ir, Os, Pt and Ru in a sample

there will be a decrease in the resistance to crushing and grinding (Figure 8.16 to 8.19). Therefore the higher the grade of the material being processed the less the energy required to break it up.

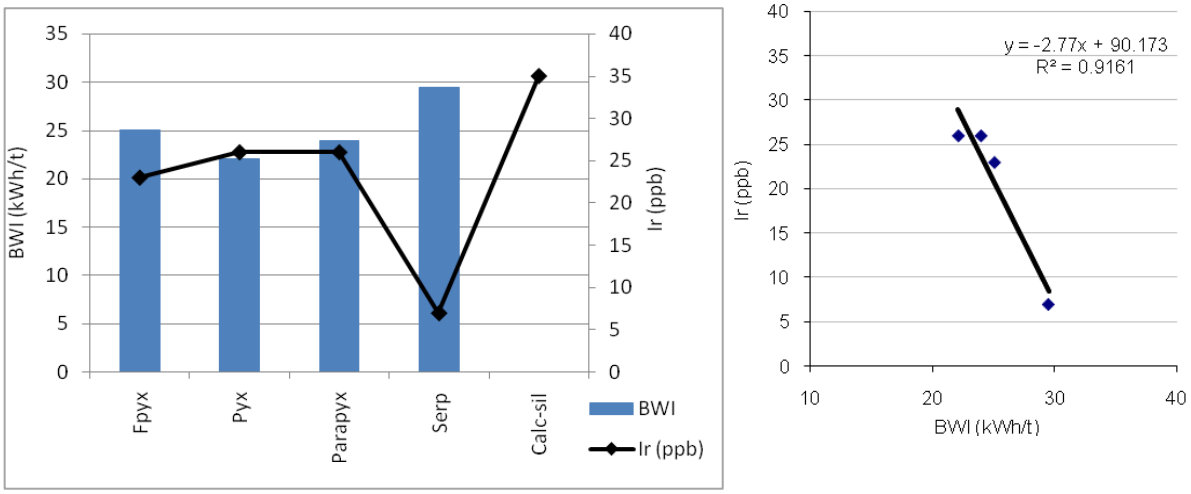

Figure 8.16 Comparison between Ir (ppb) and BWI, bar graph and scatter plot showing the line of fitted linear regression.

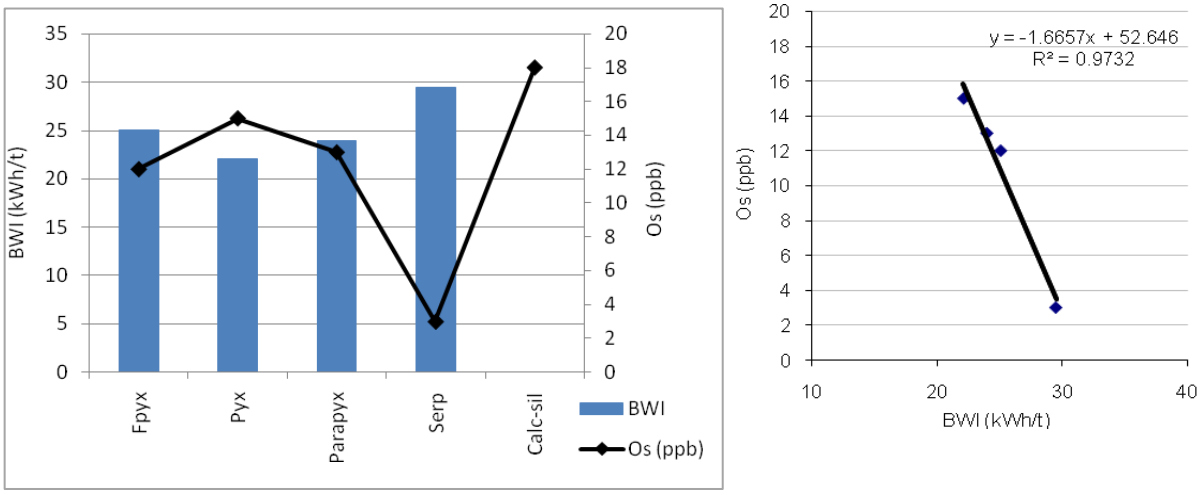

Figure 8.17 Comparison between Os (ppb) and BWI, bar graph and scatter plot showing the line of fitted linear regression.

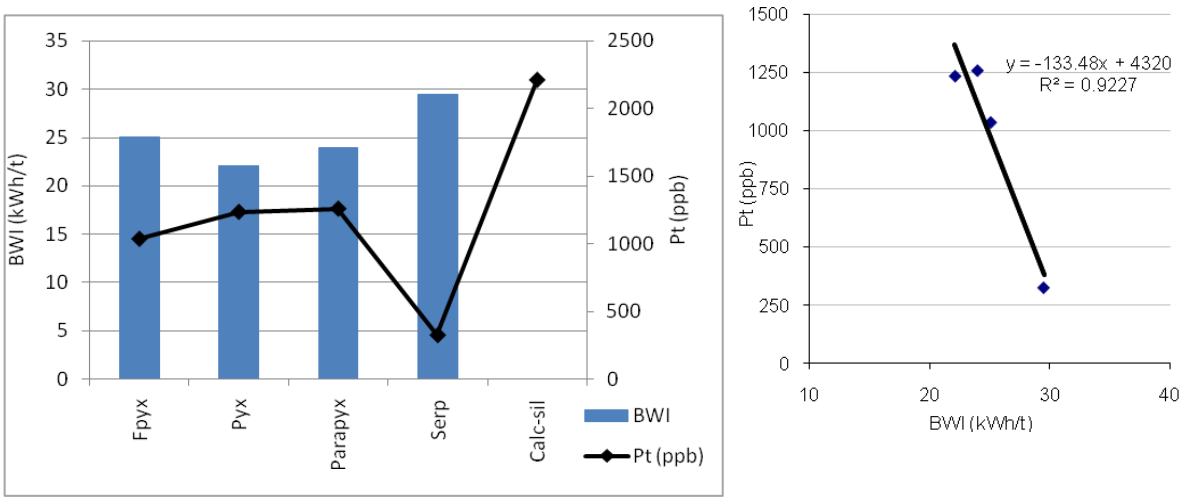

Figure 8.18 Comparison between Pt (ppb) and BWI, bar graph and scatter plot showing the line of fitted linear regression.

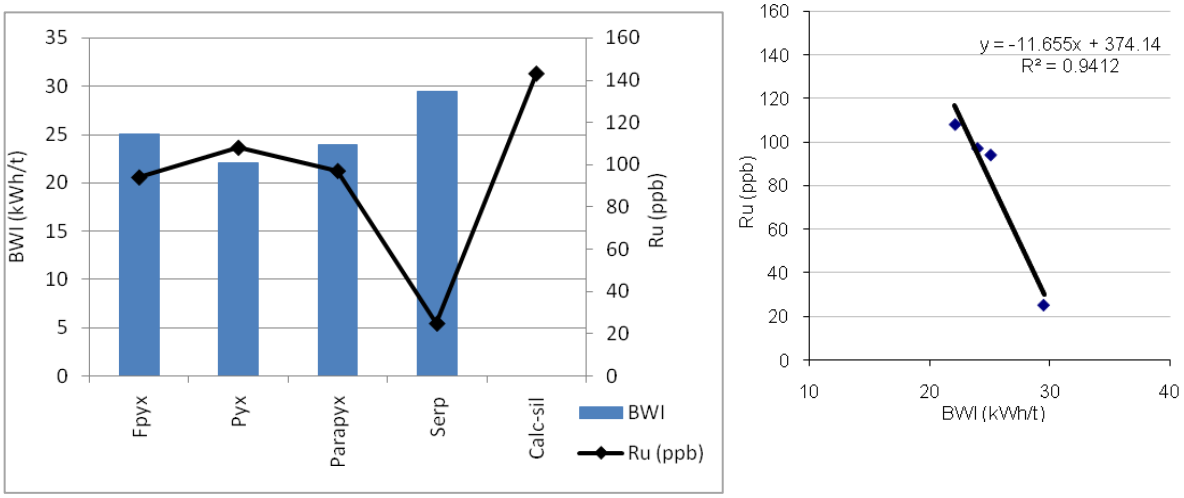

Figure 8.19 Comparison between Ru (ppb) and BWI, bar graph and scatter plot showing the line of fitted linear regression.

The remaining oxides, base metals and PGEs, as well as all the alkali and alkali earth elements, the incompatible elements and the rare earth elements did not relate to the metallurgical strengths with any significance. Overall, few of the geochemical elements analysed related to the metallurgical strengths, but those that related showed strong associations.

Chapter 9

CONCLUSIONS

Research has shown that effective and successful improvement in a mine relies on a holistic approach using mine-to-mill optimisation. Essential to this is the thorough understanding of the materials being mined. An accurately characterised orebody will refine the prediction of the material properties, variability and performance in each of the steps between converting orebody rock mass into a concentrate /marketable product. It will improve the assessment of the mining conditions and consequently will allow for forward planning and proactive adjustment of mining practices for optimum results.

The research in this thesis focused on improving the knowledge of the Platreef orebody being mined, transported and processed at Sandsloot open pit. The materials comprise numerous rock types of varied geological origins and strongly contrasting physical properties. These properties affect blasting, milling and processing operations and the extent of the variability makes predicting mining and milling conditions difficult.

The purpose of this study, as described in the introduction, was to characterise the range of rock types in the ore zone from all aspects of the physical and chemical properties and to determine if these properties could be identified using a few, relatively simple tests. This was achieved through:

- Developing and executing a rigorous testing programme.
- Compilation, management and manipulation of an extensive database of petrographic, geotechnical, geochemical and metallurgical information.
- Characterisation of each orebody rock type using statistical tests to define and assess each studied property for population distributions, descriptives and variability.
- Comparison between rock types for each property and thereafter quantifying the significance of the similarities and differences in resulting rock type behaviour, statistically.
- Defining the associations and correlations within and between the studies of petrography, geotechnical properties, geochemistry and metallurgical strength for the range of orebody rock types.

The body of characterised and distinguished rock properties in this thesis may be used for improving functionality and productivity of Sandsloot open pit mine operations. As mining progresses and the operations expand, this knowledge of the subsurface ground, the orebody properties and performance in the processing plant may be used as a basis for comparison with the rock properties in to adjacent PPRust mining lease areas. It may be used to assist with the processing plant design and in understanding the expected performance of PPRust North material in the current plant.

The following sections summarise the results and conclusions of the research, and end with a discussion of further work and future research suggestions.

9.1 Geological and Data Processing Considerations

Chapters 2 and 3 familiarised the reader with the geological setting and mining operations at Sandsloot open pit mine. The regional geology of the Bushveld Complex magmatic province, its stratigraphy and emplacement were described. It placed into context the setting of the local geology of the Northern Potgietersrus Limb and in-pit geology of Sandsloot open pit mine. An account of the in-pit stratigraphy and varied Platreef lithologies was given and the associated structural features that affect mining, such as faulting, veining, shearing, jointing and groundwater were defined.

An important part of the research was the potential application of results in the development of appropriate and cost effective mining and processing practices of Sandsloot open pit mine. The history of mining on the Northern Potgietersrus Limb and the development of Sandsloot open pit were therefore summarised. Thereafter the reader was provided with a thorough knowledge of the open pit and processing plant design and machinery at Sandsloot, as well as a description of the path for the ore from rock mass to concentrate.

The research focussed on the characterisation of the orebody materials through investigation of the geotechnical properties, geochemistry and the metallurgical strengths. The systematic identification and classification of the orebody rock types through a petrography study was also required. One of the challenges was the handling of the significant number of results collected. The large sets of data required careful assembling into databases, grouping together corresponding samples within and across the different studies. The selection and positioning of the samples was important for relating of properties between analyses. The statistical package,

Statgraphics Centurion XV, was used to analyse and evaluate the numerous variables in the databases. However, before the data could be assessed the understanding of the unique factors that influenced the population distributions in each of the studies was essential. The software package, together with the databases proved to be a powerful tool. Together, multi-level queries and interrogation the results within and between test type, lithology, collection method or sample location and corresponding geotechnical, geochemical and metallurgical results was achieved. The data was modelled, relationships and correlations identified. In turn this was used to distinguish rock types for the prediction of mining properties with statistical robustness and significance.

9.2 Petrographic Considerations

A study of the petrography revealed that the names used to describe the rock types were not petrologically correct. If the rock types were defined according to international standards and conventions the names would highlight the complex geological origins of the orebody material and possible implications for geotechnical and metallurgical strengths as well as milling and plant throughput. Both thin section analysis and XRD analysis revealed characteristics upon which the rock types were differentiated. Each of the rock types showed distinctively different compositions and mineral abundances. However, similarities in composition, grain size, texture and degree of alteration grouped feldspathic pyroxenite, pyroxenite and parapyroxenite as similar to each other. Serpentinite and calc-silicate were distinguished by their degree of alteration and presence of a weak fabric. Parapyroxenite was distinguished due to its variability in composition, alteration and irregular presence of fabric. Texture was the only property that did not distinguish any of the rock types. XRD analysis was identified as an effective gauge of the mineral composition for the general purpose of rock type prediction. But it does not have the benefit of distinguishing similarities and differences between rock types based on properties other than composition. Thin section analysis provides a check on the accuracy of the XRD results and distinguishes properties that have the potential to influence mining and processing properties of the orebody. Thin section analysis should be undertaken on a regular basis for existing operations and on for new mining areas.

9.3 Geotechnical Considerations

In the geotechnical investigation the properties of rock type density, ultrasonic velocity and strength were assessed for predictability in mining. The various strengths that were considered included point load index strength (PLI Is_{50}), tensile strength and compressive strength. For each of the orebody rock types the characteristic values and variability for each property was identified. The study revealed feldspathic pyroxenite, pyroxenite and parapyroxenite typically had the highest density, ultrasonic velocity and strengths, with pyroxenite commonly having the highest value for each of these properties. Serpentinite had the lowest values for strengths, density and ultrasonic velocity, whilst calc-silicate frequently had the second lowest values for these geotechnical properties.

The assessment of statistically significant similarities and differences between rock types for each property frequently distinguished feldspathic pyroxenite, pyroxenite and parapyroxenite as similar to each other, different to serpentinite and calc-silicate and distinguished differences between serpentinite and calc-silicate. This analysis identified the properties of density and ultrasonic velocity clearly distinguished between the rock types as a 95% C.I. It identified feldspathic pyroxenite and parapyroxenite were statistically indistinct from each other and were the most variable rock types in the orebody. Furthermore, parapyroxenite was recognised as the least distinguishable of the orebody rock types, geotechnically.

Comparison of the results between properties for directly and indirectly paired samples produced overlaps between rock type populations, similar to those identified in the statistical assessment of individual properties. The overlaps and scatter clouded the trends and relationships, indicating that complicated relationships between geotechnical properties of the rock types of Sandsloot orebody may exist. It is believed that these arise from the similarity of geological origin and varying degrees of alteration between the rock types, which cause the statistical populations to overlap. A study of the average values between properties for each rock type revealed the properties were commonly characterised by moderate to strong positive relationships. Density and ultrasonic velocity were identified as effective gauges of UCS and PLI Is_{50} and ultrasonic velocity was identified as a good gauge of density. Tensile strength cannot be estimated from density or ultrasonic velocity. Pyroxenite was distinguished as having a disproportionately high PLI Is_{50} and low tensile strength. This caused weakened correlations between these and other geotechnical properties. Density and ultrasonic velocity are valuable in combination with each other, as reasonable estimates of UCS. These properties model UCS

results with a 96% accuracy (95% C.I.) and therefore may be used to predict intact strengths with confidence where tests cannot be performed. The relationship between UCS and PLI Is_{50} was determined to be weak, indicating PLI Is_{50} did not model the UCS results well. Nonetheless, a comparison between the two was undertaken, and for each of the orebody rock types the PLI Is_{50}:UCS ratio used to estimate UCS was less than that used currently for Sandsloot open pit and similar to those used for PPRust operations as a whole.

9.4 Geochemical Considerations

The geochemical investigation of the rock types in Sandsloot orebody used XRF and ICP-MS analysis to determine whole-rock major and trace element abundance and PGE concentration. The elements were split into major element oxides, base metal group elements, PGEs, alkali and alkali earth elements, incompatible elements and rare earth elements for ease of handling the data. The study looked at the individual descriptive properties for each element but the focus fell on identifying which elements could be used either singularly or in combination to predict rock types and potentially mining properties.

Statistical assessment of 41 elements concentrations revealed four of the five orebody rock types can be distinguished on the basis of a single element concentration. Na_2O, Cr_2O_3 or Cr and V distinguish feldspathic pyroxenite, Cu and V distinguish pyroxenite, SiO_2, CaO, FeO, L.O.I. and REE count distinguish serpentinite and FeO distinguishes calc-silicate. Parapyroxenite cannot be distinguished using the geochemical concentration of any of the studied oxides or elements. The range in concentration of each oxide and element for each rock type showed pyroxenite followed by serpentinite typically had the narrowest ranges. Geochemically, they are the least variable rock types in the orebody and their concentrations are therefore expected to be the most predictable. Parapyroxenite, feldspathic pyroxenite and calc-silicate have the widest ranges for most of the oxide and element concentrations. The concentrations in these rock types are expected to be least predictable. However, parapyroxenite will typically be the most variable.

An analysis of the rock type geochemical variability between drill holes indicates feldspathic pyroxenite followed by parapyroxenite and then serpentinite would be the most variable spatially. Predictability is expected to follow this order, however, it is expected that parapyroxenite would have a higher degree of variability compared to the other rock types, when it does vary. The concentration of PGEs, followed by major element oxides and base

metal group elements would be expected to vary spatially more than any other groups of elements.

A comparison study, between the major element oxides that are relatable to rock type mineralogy, identified SiO_2, CaO, MgO, MnO and L.O.I. in combination with each other exhibit good distinction between the rock types. The elements show strongly positive and negative relationships with narrow, discrete or diffuse dispersion and clearly separated groups of major element oxides according to origin/ rock type.

A statistically robust model, using major element oxides to categorize and thereafter predict rock types in the Sandsloot open pit orebody was identified with discriminant analysis (95% C.I.). The model, comprising a pair of vertical and horizontal linear functions, fitted approximately 95% of observed variability displayed by the major element oxides. It showed good visual separation of the rock types and allowed the influence of the oxide variables to be assessed in the collective determination of the different populations/ rock types. The functions were applied to geochemical data from published studies of rock types from the Sandsloot open pit and the results showed good agreement between predicted versus observed rock type classification. The functions may used to classify rock types from other PPRust open pits and predict their geochemical characteristics provided the database is expanded.

9.5 Metallurgical Considerations

The metallurgical investigation studied the Sandsloot orebody rock types for prediction of milling properties in the processing plant. The study looked at the resistance of each rock type to tumbling and impact breakage and the resistance to crushing and grinding in terms of energy input for fragment breakdown. The range in rock strengths gauged by the metallurgical testing is narrow. All of the Sandsloot orebody rock types are classed as moderately hard, hard or very hard rock and may be expected to be relatively difficult to crush, grind and mill, requiring high energy input for breakdown. Results from the two drop weight tests and the Bond ball mill Work Index (BWI) were comparable. They indicate pyroxenite has the lowest metallurgical strengths, performing the best under semi autogenous milling conditions. Serpentinite will typically have higher strengths, performing more poorly than the other orebody rock types. Feldspathic pyroxenite, parapyroxenite and the composite-material will have strengths which range between pyroxenite and serpentinite.

An assessment of the statistically significant similarities and differences between rock types for the same property indicated little differentiation between rock types for metallurgical strengths. Serpentinite was identified as singularly different for BWI, requiring significantly a higher input of energy into the plant circuit to break down the rock fragments, due to high resistance to crushing and grinding. Pyroxenite was identified as more susceptible to abrasion breakage than parapyroxenite, calc-silicate and the composite material, whilst it was identified as more susceptible to impact breakage compared to serpentinite and parapyroxenite. The remaining rock types showed statistical overlaps in properties and therefore will share similar characteristics when milled.

Variability in milling properties between rock types and between different sample locations indicated there were significant differences. Parapyroxenite, feldspathic pyroxenite and pyroxenite are predicted to vary depending on the position in the pit and sample collection method. Petrographic properties and the impact of blasting were highlighted as possible factors that could influence the milling performance of the rock type.

9.6 Comparison of Properties

A Study relating the geotechnical, geochemical and metallurgical properties to one another, drawing comparisons and contrasts between the findings and conclusions was undertaken. Relating some of these properties has not been common practice therefore the research in this thesis represents an important contribution to these fields.

The general similarities, differences and relationships distinguished in the petrography study were reflected in the geotechnical, geochemical and metallurgical trends and relationships between rock types. The grouping of the orebody rock types based on petrographic properties of composition, grain size, alteration and presence of a fabric were reflected well in the similar grouping of rock types according to geotechnical properties of density, ultrasonic velocity and strength. Composition was reflected in density and the presence of a fabric or microscopic features, such as veinlets, were reflected in the ultrasonic velocity, strength and failure modes of the rock types. Furthermore, the degree of alteration was reflected in density and ultrasonic velocity. A comparison of similarities and differences between the geochemical composition of major element oxides and mineral composition for each rock type distinguished similar relationships between the orebody rock types. However, the geochemical assessment distinguished subtle differences and similarities based on element oxide that were not major

components of the rock type. For example, parapyroxenite was distinguished from feldspathic pyroxenite and similarities between parapyroxenite and calc-silicate were identified. The comparison between metallurgical strengths and petrography indicated mineralogy and possibly textures influence milling performance of the rock material. The study identified changes to petrographic properties of grain size, degree of alteration or serpentinisation and the feldspar content affected the resistance of the Sandsloot orebody rock types to abrasion and impact breakages and their resistance to crushing and grinding.

The geochemistry of the orebody rock types was compared to directly paired geotechnical data to determine if, on the basis of specific chemical analysis, mining conditions as derived from density, ultrasonic velocity and UCS could be predicted with any certainty. SiO_2, FeO, V and Sc showed moderate positive relationships to density and MgO showed a moderate positive relationship with ultrasonic velocity. MgO, CaO and L.O.I. showed strong positive relationships with density, with good differentiation between pyroxenite and serpentinite but overlapping populations for parapyroxenite, feldspathic pyroxenite and calc-silicate. None of the elements geochemically analysed showed moderate or strong relationships with UCS.

Relating geotechnical properties to metallurgical strengths revealed UCS and PLI Is_{50} strengths are comparable to *ta* and DWT. In both cases the strength indices indicated are similar, however the correlations were weak or moderate. The poor statistical relation is likely because of the different strengths measured by geotechnical and metallurgical testing, with the former measuring a rock's initial strength to first failure and the latter measuring the strength or resistance of a rock to break down to a final fragment size for processing. BWI related to UCS and PLI Is_{50} results with moderate and strong inverse relationships, respectively. Serpentinite was distinguished as distorting the results and causing an apparent inverse relationship where a positive correlation would have been more intuitive. Density related with positive moderate correlations to *ta* and DWT and related with a strong positive correlation to BWI. Ultrasonic velocity related to BWI with a strong inverse relationship. Tensile strength did not relate well to any of the metallurgical measures of strength. Overall, comparisons indicated that for the Sandsloot orebody materials the higher the strength the more resistance the rock type was to impact and abrasion breakage and therefore more difficult to mill. Furthermore, decreases in density and ultrasonic velocity typically resulted in an increase in metallurgical strength and difficulty in milling.

The metallurgical strengths were compared to geochemical analyses for each of the rock types. FeO related to BWI with a strong positive correlation, indicating an increase in the FeO concentration would increase the resistance of the rock to crushing and grinding, therefore requiring greater input of energy to break the material down. CaO and TiO_2 related to BWI with strong inverse correlations, therefore with an increase in the concentration of these elements the susceptibility of the rock types to crushing and grinding would increase. Strong inverse correlations were identified for Ir, Os and Pt, whilst Ru related with a moderate inverse correlation. This is significant as it indicates that for the orebody rock types at Sandsloot an increase in the grade of the material being processed correlates with the decrease input of energy required to crush and grind the material.

9.7 Further Work and Research Suggestions

The ore zone material properties, their variability and the relationships between them have applications in the prediction of mined material from the orebody at Sandsloot open pit. The physical properties of each mining block, depending on the variety and quantity of each rock type present, can be assessed prior to mining, which will allow forward planning and proactive adjustment of mining practices for optimum blasting, transporting and milling results. In addition, knowledge of these relationships and their effectiveness in determining particular properties may be used to predict mining conditions where some or most of the data is either missing or is difficult to assess.

The database, upon which the relationships and statistical functions in this study are derived, should be expanded to increase sample numbers for serpentinite and calc-silicate rock types. This is necessary for geotechnical, geochemical and metallurgical testing. These results would fill in missing information in the database due to low number of samples or no tests on that rock type. It would increase the statistical robustness of the results, clear up distortions and improve prediction limits.

Further research into the effects of recrystalisation on the propagation of micro-fractures and resulting geotechnical and metallurgical strengths would be beneficial for the characterisation of these materials. In association, the research into the effect of blasting on metallurgical strengths, by comparing pre- and post-blast strengths in samples, would be valuable.

The properties and their characteristics distinguished in this research can be used in the assessment of material types between Sandsloot open pit and future PPRust operations, especially material from PPRust-North pit. The expansion of the database to include rock type properties from other PPRust operations would allow the models and correlations, derived in this research, to predict material properties and variability for rock types in the other operations. A compare and contrast style study of the similarities or differences would assist with the optimum design of the PPRust plant expansion and provide an understanding of the expected performance of the PPRust-North pit material in the current plant.

A study relating the characteristics and relationships identified in this research to the processing plant production figures from a single mining/ blast block would enable improvements in prediction of mining conditions to be quantified financially. A suggested mining block upon which the study could be undertaken is ‘blast 138 – 055’, which represents blast number 55 on bench 38 in Sandsloot open pit (pit 1). This block is chosen because many of the results in this database are from this and neighbouring mining blocks.

REFERENCES

Anon. 1979. Classification of soils and rocks for engineering geological mapping. Part 1 Rock and soils materials, *Bulletin International Association of Engineering Geologists*, **19**, 364 – 371

Anon. 1970. Working party report on the logging of cores for engineering purposes, *Quarterly Journal of Engineering Geology*, **3**, 1 – 24.

Armitage, P. E. B., McDonald, I., Edwards, S. J. and Manby, G. M. 2002. PGE mineralisation in the Platreef and Calc-silicate footwall at Sandsloot, Potgietersrus District, South Africa. *Transactions of the Institute of Mining and Metallurgy*, **111**, January – April 2002.

Arndt, N., Jenner, G., Ohnenstetter, M., Deloule, E. and Wilson, A. H. 2005. Trace elements in the Merensky Reef and adjacent norites Bushveld Complex South Africa. *Mineralium Deposita*, **40**, 550 – 575.

Barton, J. M., Cawthorn, R. G. and White, J. 1986. The role of contamination in the evolution of the Platreef of the Bushveld Complex. *Economic Geology,* **81**, 1096 – 1104.

Battey, M. H. 1981. *Mineralogy for Students*. Second Edition, Essex, Longman Group UK Limited, 355pp.

Bell, F. G. 1992. *Engineering in Rock Masses*, Oxford, Butterworth-Heinemann Ltd. 580pp.

Bell, F. G. 1993. *Engineering Geology*, London, Blackwell Scientific Publications. 359pp.

Bieniawski, Z. T. 1975. The Point Load Test in Geotechnical Practice. *Engineering Geology,* **9**, 1 – 11.

Bieniawski, Z. T. 1989. *Engineering Rock Mass Classifications: a Complete Manual for Engineers and Geologists in Mining, Civil and Petroleum Engineering,* New York, John Wiley & Sons. 251pp.

Bond, F. C. 1961. *Crushing and Grinding Calculations*. Unpublished Allis-Chalmers Manufacturing Company Internal Paper for the Processing Machinery Department. Wisconsin, USA, 14pp.

Brace, W. F. 1961. Dependence of fracture strength of rocks on grain size. *Bulletin of Industrial Minerals*, **76**, 99 – 103.

Buchanan, D. L. 1988. Platinum group element exploration. *Developments in Economic Geology*, **26**. Elsevier, Amsterdam, 185pp.

Buchanan, D. L., Nolan, J., Suddaby, P., Rouse, J. E., Viljoen, M. J., and Davenport, J. W. J. 1981. The genesis of sulfide mineralisation in a portion of the Potgietersrus lobe of the Bushveld Complex. *Economic Geology,* **76**, 568 – 579.

Button, A. 1976. Stratigraphy and relations of the Bushveld floor in the Eastern Transvaal. *Transactions of the Geological Society of South Africa*, **79**, 3 – 12.

Bye, A. R. 2003. *The Development and Application of a 3D Geoteechnical Model for Mining Optimisation, Sandsloot Open Pit Platinum Mine, South Africa*. Unpublised Ph.D – Engineering Geology, University of Natal, Durban, South Africa. 203pp.

Bye, A. R. and Bell, F. G. 2001. Stability Assessment and Slope Design at Sandsloot Open Pit, South Africa. *International Journal of Rock Mechanics and Mining Sciences*, **38,** 449 – 466.

Bye, A. R., Jermy. C. A. and Bell, F. G. 1998. Using Geotechnical Methods as Production and Planning Tools in an Open Pit Environment. *8th International IAEG Congress*, Balkema, Rotterdam., 2995 – 3003.

Bye, A. R. and Hansmann, K. 2004. *PPRust North Geotechnical Study*. Unpublished Anglo Platinum Internal Report. MGS-001-09, Potgietersrus, South Africa. 22pp.

Cawthorn, R. G., Barton, J. M., and Viljoen, M. J. 1985. Interactions of floor rocks with Platreef on Overysel, Potgietersrus, Northern Transvaal. *Economic Geology*, **80**, 988 – 1006.

Cheney, E. S. and Twist, D. 1991. The conformable emplacement of the Bushveld mafic rocks along a regional unconformity in the Transvaal succession of South Africa. *Precamb. Res*. **52**, 115 – 132.

Chitombo, G. 2003. *An Independent Review of Current Drilling and Blasting Practices at the Potgietersrus Platinum Ltd, Sandsloot Open Pit Operations*. Unpublished Anglo Platinum Internal Report by JKTech – JKMRC Commercial Division, Potgietersrus, South Africa. 19pp.

Core Logging committee of the South Africa Section of The Association of Engineering Geologists. 1979. A guide to core logging for rock engineering, *Proceedings of the Symposium for Rock Engineering*, 71 – 87.

Davis, J. C. 1986. *Statistics and data analysis in geology*. Second edition, Chapter 2, 10 – 103, Singapore, John Wiley and Sons, 646pp.

Deer, W. A., Howie, R. A. and Zussman, J. 1992. *An Introduction to Rock-Forming Minerals*. Second Edition, Essex, Longman Group UK Limited, 696pp.

de Vaux, D. and Schouwstra, R. 2006. *Hardness data (UCS and BMI) on a suite of rocks from the Potgietersrus area*. Unpublished Anglo Platinum Internal Report. MPM/38/06, Potgietersrus, South Africa. 11pp.

Doll, A., Barratt, D. and Wood, K. 2001. *Comparison of UCS to Bond Work Indicies*. Unpublished AGD Consulting Ltd. Internal Report, Edmonton, Cananda. 10pp.

Eales, H. V. and Cawthorn, R. G. 1996. *The Bushveld Complex*. In: Cawthorn, R. G. (ed.), Layered Intrusions. Elsevier Sciences. 531pp.

Friese, A. E. W. 2004 a. *The tectono-sedimetary evolution of the southerm Free State Goldfields within the Witwatersrand Basin, with implications for the development of the Kaapvaal Craton*, South Africa. Unpublised PhD Thesis, University of the Witwatersrand, Johannesburg, South Africa.

Friese, A. E. W. 2004 b. *Geology and tectono-magmatic evolution of PPL concession area, Villa Nora-Potgietersrus Limb, Bushveld Complex – Geological Visitors Guide*. Unpublished Anglo Platinum Internal Report, Potgietersrus, South Africa. 67pp.

Good, N. 1999. *Structural and thermal control on basinal fluid flow and mineralisation beneath the Bushveld Complex and along the adjacent Thabazimbi-Murchison lineament; Kaapvaal Craton, South Africa*. Unpublished PhD Thesis, University of Cape Town, South Africa.

Goodman, R. E. 1989. *Rock Mechanics*, New York, John Wiley and Sons. 562pp.

Hamilton, W. 1970. Bushveld Complex, product of impact? *Special Publication of the Geological Society of South Africa*, **1**, 367 – 379.

Harris, C. and Chaumba, J. B. 2001. Crustal contamination and fluid – rock interaction during the formation of the Platreef, Northern Limb of the Bushveld Complex, South Africa. *Journal of Petrology*, **42**, no. 7, 1321 – 1347.

Hatton, C. J. 1995. Primary magmas in the Ventersdorp and Bushveld Igneous Provinces: magma extraction from a lower mantle plume. Extended Abstracts, *Centennial Geocongress* 1995, Geological Society of South Africa, Rand Afrikaans University, **1**, 520 – 521.

Hochreiter, R. C., Kennedy, D.C., Muir, W. and Woods, A. I. 1985. Platinum in South Africa. J. *S. Afr. Inst. Min. Metall*., **85,** 6. 165-185.

Hoek, E. 1965. Rock fracture under static stress conditions. *National Mechanical Engineering Division*, **106**, 1013 – 1035.

Holwell, D. A. and Jordaan, A. 2006. Three-dimensional mapping of the Platreef at the Zwartfontein South mine: implications for the timing of magmatic events in the northern limb of the Bushveld Complex, South Africa, *Transactions of the Institute of Mining and Metallurgy,* **115**, *B*

Imrie, C. J. O. 1998. Ore Flow Optimisation – Mine to Mill. *The Australasian Institute of Mining and Metallurgy Proceedings for Mine to Mill 1998 Conference*. Brisbane, Australia, October, 1998/04, 248pp.

International Society of Rock Mechanics (ISRM). 1981. ED. Brown, E. T. *Rock Classification Testing and Monitoring (ISRM suggested methods)*. Third Edition, Pergamun Press. 211pp.

Jankovic, A., and Valery, Jnr. W. 2002. Mine to Mill Optimisation for Conventional Grinding Circuits – a Scoping Study. *Journal of Mining and Metallurgy*, **38 (1-4) A**, 49 – 66.

JKTech Pty. Limited. 2008 a. *Comminution Testing*. http://www.jktech.com.au/ (accessed June 20, 2008).

JKTech Pty. Limited. 2008 b. *Mine-to-mill optimisation study*. http://www.jktech.com.au/ (accessed June 20, 2008).

JKTech Pty. Limited. 2008 c. *Photographs of laboratory test apparatus*. JKTech Laboratories, Brisbane, Australia.

Kinnaird, J. A., Hutchinson, D., Schurmann, L., Nex, P. A. M., and de Lange, R. 2005. Petrology and mineralisation of the southern Platreef: northern limb of the Bushveld Complex, South Africa. *Mineralium Deposita*, **40**, 576 – 597.

Kruger, J. F. 2005. Filling the Bushveld Complex magma chamber: lateral expansion, roof and floor iteraction, magmatic unconformities, and the formation of giant chromitite, PGE and Ti-V-magnetite deposits. *Mineralium Deposita*, **40**, 451 – 472.

Lapidus, D. F., Coats, D. R., Winstanley, I., MacDonald, J., and Burton, C. 2003. *Collins Geology Dictionary*. HarperCollins Publishers, Great Britian, 480pp.

Laubscher, D. H. 1990. A Geomechanics Classification System for the Rating of Rock Mass in Mine Design. *J. S. Afri. Inst. Min. Metall*., **90**:10., 257 – 273.

Le Maitre, R. W. 1989. *A classification of igneous rocks and glossary of terms – Recommendations of the International Union of Geological Sciences Subcommision on the Systematics of Igneous Rocks*. Oxford, Blackwell Scientific Publications, 193pp.

Lilly, P.A. 1986. An empirical method of assessing rock mass blastability. *The Australian Institute of Mining and Metallurgy Proceedings of Large Open pit Planning Conference*. Parkville, Victoria, October, 1986, 89–92.

Little, M. 2006. *Datamine ® image output.* PPRust Sandsloot Mine, Geotechnical Engineering Department.

McDonald, I., Holwell, D. A. and Armitage, P. E. B. 2005. Geochemistry and mineralogy of the Platreef and "Critical Zone" of the northern lobe of the Bushveld Complex, South Africa: implications for Bushveld stratigraphy and the development of PGE mineralisation. *Mineralium Deposita*, **40**, 526 – 549.

Morrell, S. and Valery, Jnr. W. 2001. Influence of feed size on AG/SAG Mill Performance. *The Third International Conference on Autogenous and Semi-autogenous Grinding Technology*. Vancouver, Canada, September, 2001/1, 203 – 214

Mostert, A. B. 1982. The mineralogy, petrology and sulphide mineralization of the Plat Reef northwest of Potgietersrus, Transvaal, Republic of South Africa. *South African geological Survey Bulletin*, **72**, 48pp.

Nell, J. 1985. The Bushveld metamorphic aureole in the Potgietersus area: evidence for a two-stage metamorphic event. *Economic Geology* **80**, 1129–1152.

Nickson, S., Ecobichon, D., Leclerc, M., and Cote, E. 1996. A methodology for rock mechanics feasibility studies. *CIM Bulletin*, **89**, 120-125

Pease, J. D., Young, M. F., Johnson, M, Clark, A. and Tucker, G., 1998. Lessons from Manufacturing – Integrating mining and milling for a complex orebody. *The Australasian Institute of Mining and Metallurgy Proceedings for Mine to Mill 1998 Conference*. Brisbane, Australia, October, 1998/04, 248pp.

Reimann, C. and Filzmoser, P. 2000. Normal and lognormal data distribution in geochemistry: Consequences for the statistical treatment of geochemical and environmental data, *Environmental Geology*, **39**, 1001 – 1014.

Rollinson, H. 1995. *Using geochemical data: evaluation, presentation, interpretation*. Singapore, Longman Singapore Publishers, 352pp.

Schweitzer, J. K., Hatton, C.J., and de Waal, S.A. 1995. Regional litho-chemical stratigraphy of the Rooiberg Group, upper Transvaal group: A proposed new subdivision. *South African Journal of Geology.* **98** (3): 245-255.

Simkus, R and Dance, A., 1998. Tracking hardness and size: Measuring and monitoring ROM ore properties at Highland Valley Copper. *Australasian Institute of Mining and*

Metallurgy Proceedings for Mine to Mill 1998 Conference. Brisbane, Australia, October, 1998/04, 248pp.

Sjöberg, J., 1996. *Large Scale Sloping Stability in Open Pit Mining – A Review*. Lulea University of Technology, Sweden. 215pp.

Statpoint, Inc., 2005. The user's guide to STATGRAPHICS® Centurion XV. United States of America, 295pp.

Stimpson, B. 1981. A suggested technique for determining the basic friction angle of rock surfaces using core. *Journal of Rock Mech. Min. Sci. & Geomech.,* **18**. 63 – 65.

Swan, A. R. H. and Sandilands, M. 1995. *Introduction to geological data analysis*. Great Britian, Blackwell Science Limited, 466pp.

Valery Jnr., W., Morrell, S., Kojovic, T, Kanchibotla, S. and Thornton, D. 2001. Modelling and simulation techniques applied for optimisation of mine to mill operations and case studies. *The Proceedings for the VI Southern Hemisphere Conference on Minerals Technology*. Rio de Janerio, Brazil, May, 2001. 107 – 116.

Valery, Jnr., W., La Rosa, D., Jankovic, A. 2004. Mining and Milling Process Intergration and Optimisation. *Annual Society for Mining, Metallurgy and Exploration (SME) Conference.* Denver, Colorado, February, 2004.

van der Merwe, M. J. 1976. The layered sequence of the Potgietersrus Limb of the Bushveld Complex. *Economic Geology*, **71**, 1337 – 1351.

Von Gruenewaldt, G., Hulbert, L. J. and Naldrett, A. J. 1989. Contrasting platinum-group element concentrations in cumulates of the Bushveld Complex. *Mineralium Deposita*, **24**, 219 – 229.

Walraven, F., Armstrong, R. A. and Kruger, F. J. 1990. A chronostratigraphic framework for the north-central Kaapvaal craton, the Bushveld Complex and the Vredefort structure. *Tectonophysics*, **171**, 23 – 48.

Wilson, A. H., Jermy, C. A., Ridgeway, M. and Chunnett, G. 2005. Rock strength and physical properties of Norites of the Merensky and Bastard Units, western Bushveld Complex. *South African Journal of Geology*, **108**, 525 – 540.

White, J. A., 1994. The Potgietersrus prospect – geology and exploration history. *XVth CMMI Congress, SIAMM, Johannesburg*. **3**, 173 – 181.

APPENDIX - A

Core Photographs and Diamond Drill Hole Logs

Diamond Drill Hole SSMET3 (0 - 60.07m)

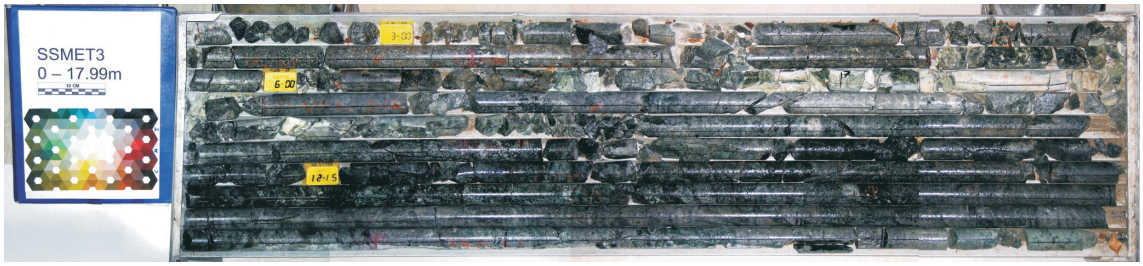

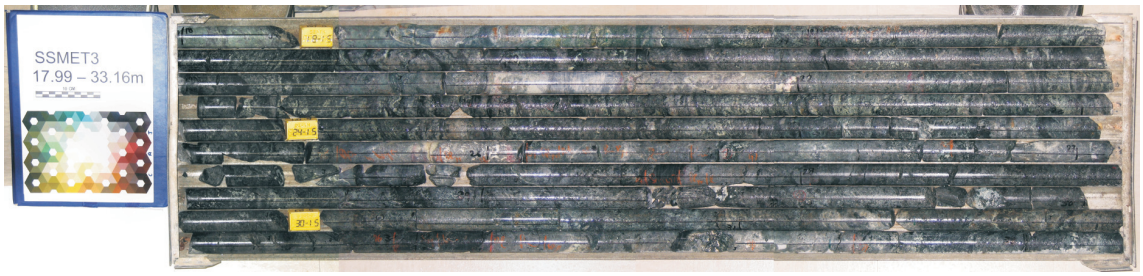

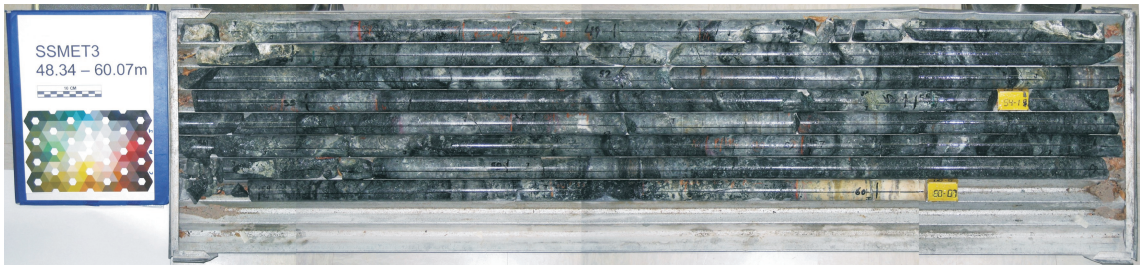

Diamond Drill Hole SSMET4 (0 - 30.13m)

Diamond Drill Hole SSMET5 (0 - 30.36m)

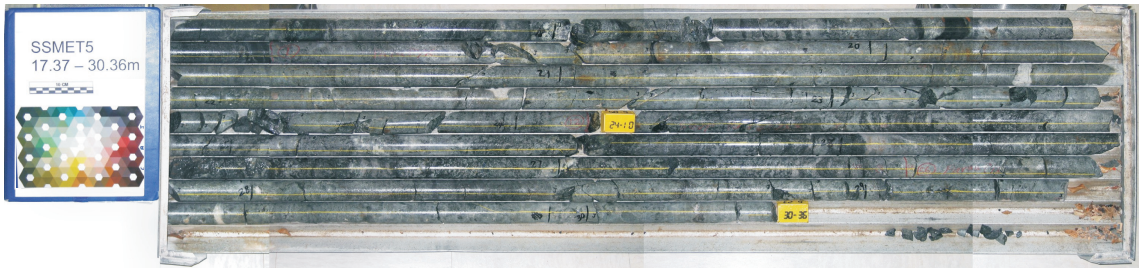

Diamond Drill Hole SSPit149 (0 - 45m)

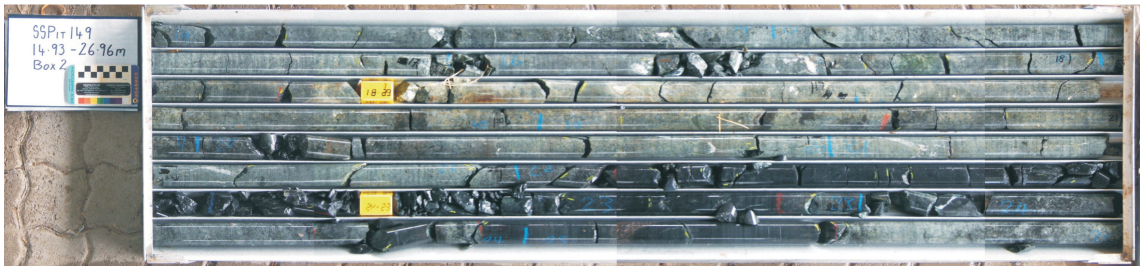

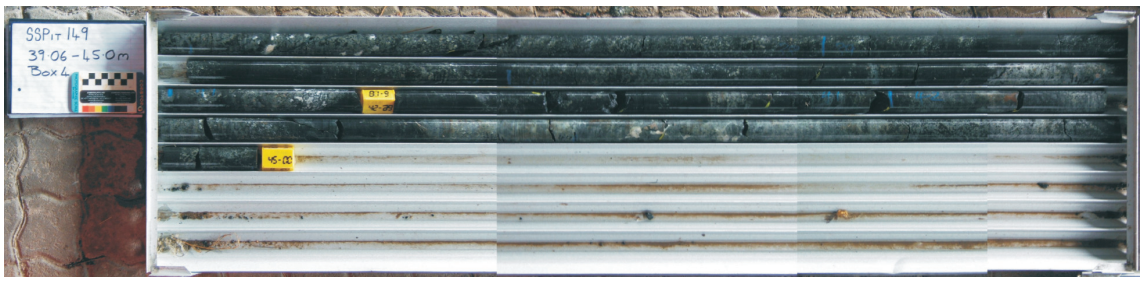

Diamond Drill Hole SSPit150 (0 - 63.30m)

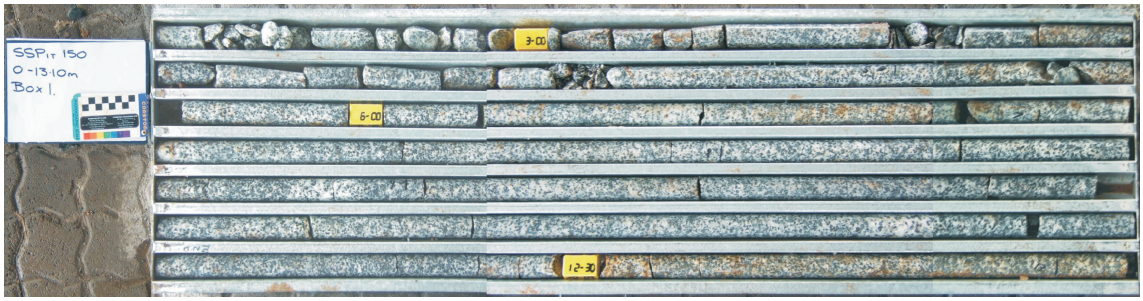

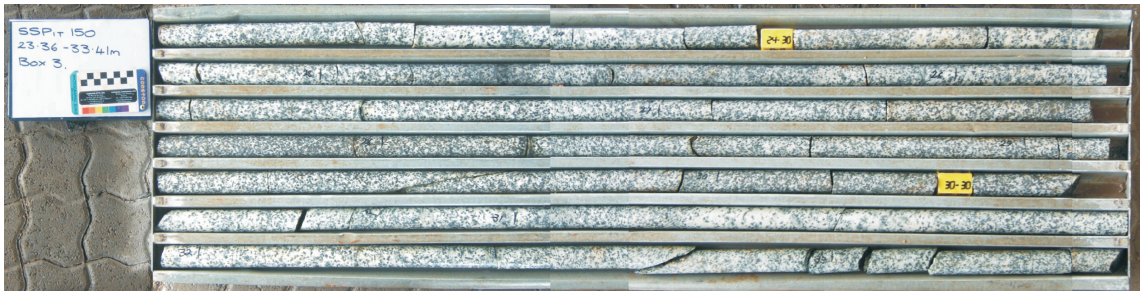

Diamond Drill Hole SSPit154 (0 - 56.60m)

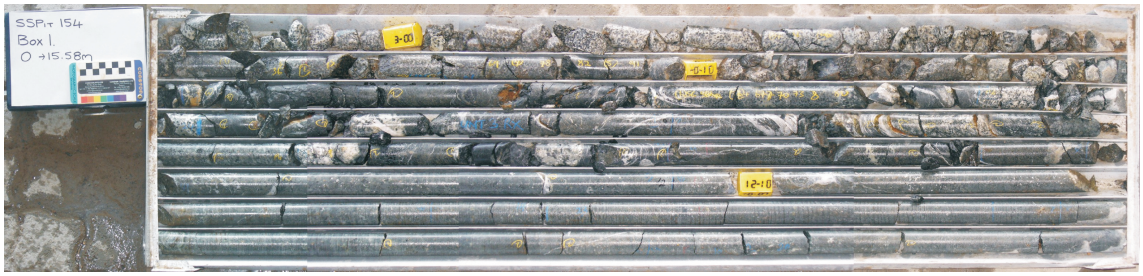

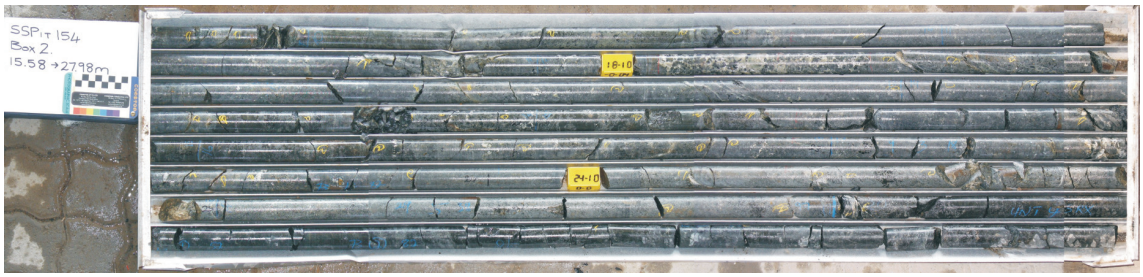

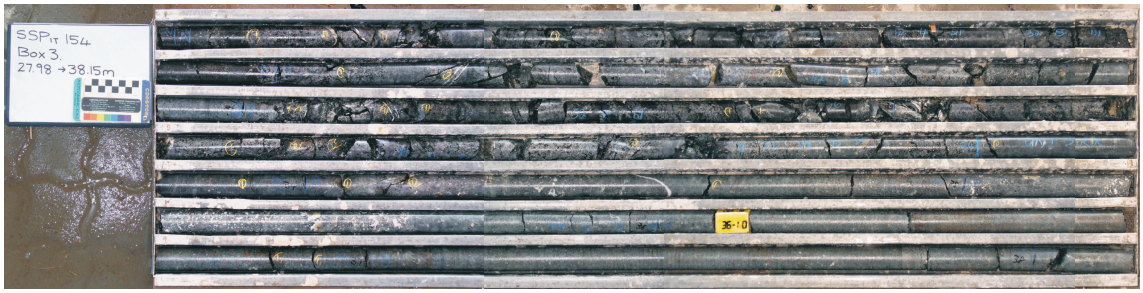

Diamond Drill Hole SSPit158 (0 - 23m)

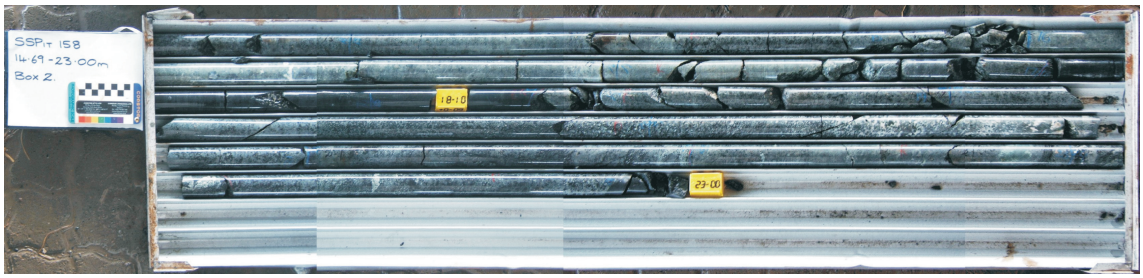

Diamond Drill Hole SSPit159 (0 - 45.10m)

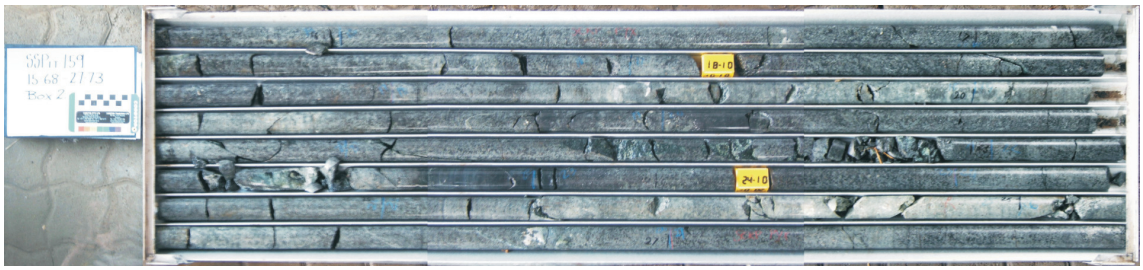

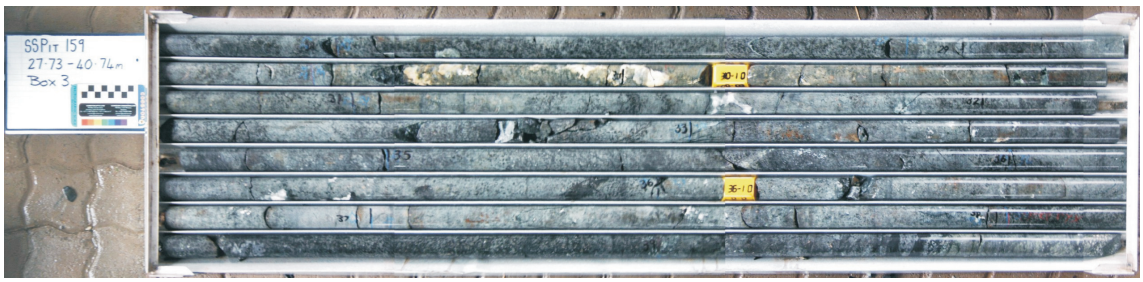

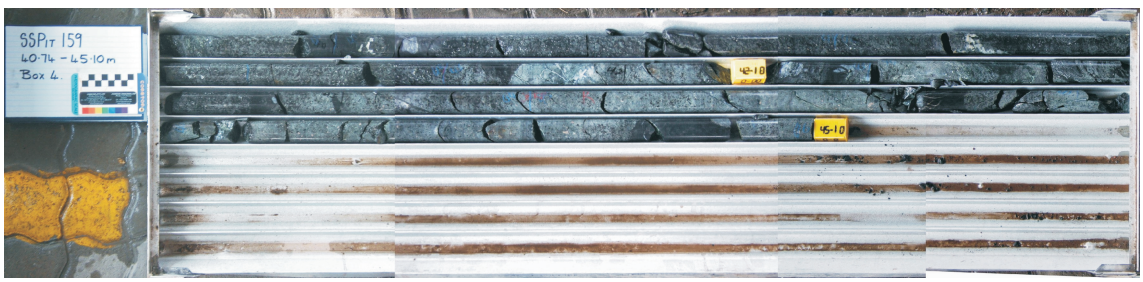

Diamond Drill Hole SSPit160 (0 - 45.02m)

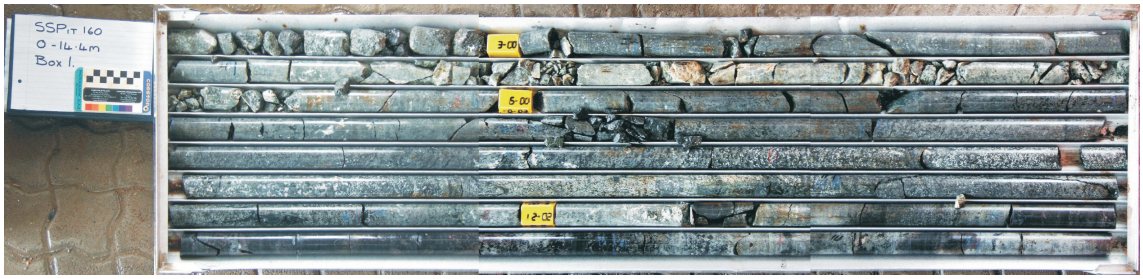

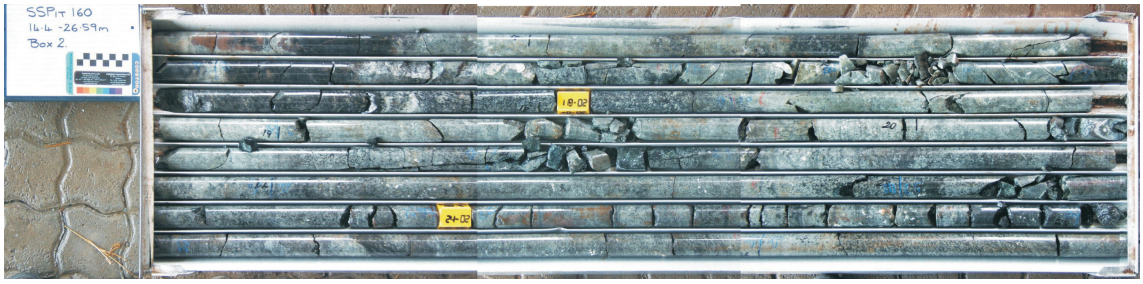

Diamond Drill Hole SSPit161 (0 - 45.02m)

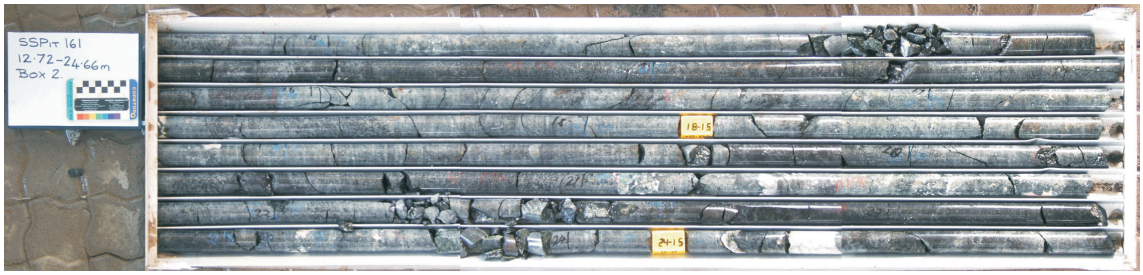

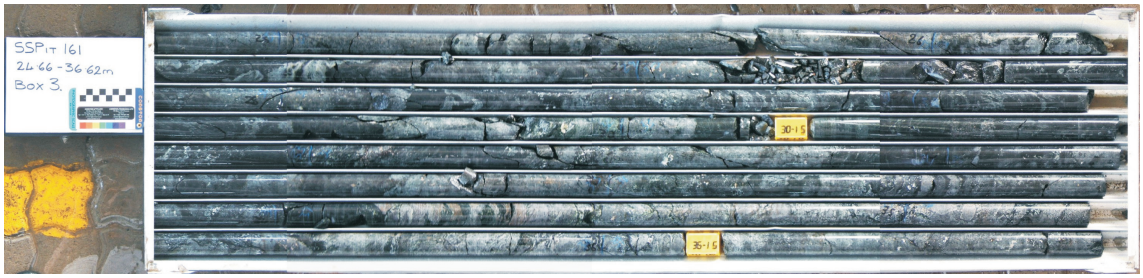

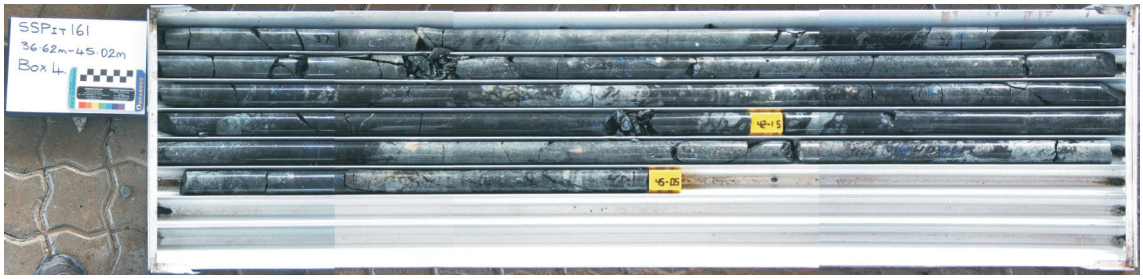

Simplified Drill Hole logs

Drill Hole SSMET1 - Logged by PPRust Personnel

FROM (m)	TO (m)	Rock type	Recovery (%)	RQD (%)	FF/m	Estimated strength	Weathering
0	4.12	N	100.00	0.00	-	R5	W1
4.12	15.6	FPYX	100.00	70.73	-	R5	W2
15.6	17.34	PEGFPYX	100.00	99.43	-	R5	W1
17.34	25.8	PARAPYX	100.00	75.53	-	R5	W2
25.8	34.99	PARAPYX	100.00	94.67	-	R5	W1
34.99	41.39	PARAPYX	100.00	80.16	-	R5	W1
41.39	45.51	PARAPYX	100.00	84.71	-	R5	W2
45.51	47.15	SERP	100.00	96.95	-	R5	W2
47.15	54.31	CALCSIL	100.00	78.07	-	R5	W2
54.31	60	PARAPYX	100.00	80.32	-	R5	W1

Drill Hole SSMET2 - Logged by PPRust Personnel

FROM (m)	TO (m)	Rock type	Recovery (%)	RQD (%)	FF/m	Estimated strength	Weathering
2.4	3	N	100.00	0.00	-	R5	W1
3	5.07	N	100.00	70.05	-	R5	W1
5.07	10.53	FPYX	83.33	46.15	-	R5	W1
10.53	25.7	FPYX	98.22	88.59	-	R5	W1
25.7	37.38	SPARAPYX	100.00	90.75	-	R5	W1
37.38	45.68	SERP	100.00	84.94	-	R5	W1
45.68	51.53	CALCSIL	100.00	95.73	-	R4	W1
51.53	60.25	PARAPYX	100.00	66.51	-	R5	W1

Drill Hole SSMET3

FROM (m)	TO (m)	Rock type	Recovery (%)	RQD (%)	FF/m	Estimated strength	Weathering
0	3	NCOR	0.00	0.00	0.00	R0	0
3	6.58	Fpyx	70.67	51.40	0.00	R5	1
6.58	7.53	Qzfs	26.84	20.00	0.00	R4	3
7.53	13.65	Parapyx	85.70	79.25	2.94	R5	1
13.65	14.44	Parapyx	97.47	88.61	3.80	R5	1
14.44	18.58	Parapyx	99.03	97.34	2.42	R5	1
18.58	23.9	Parapyx	96.99	96.05	0.94	R5	1
23.9	31.27	Parapyx	94.17	92.13	2.85	R5	1
31.27	32.67	Parapyx	98.57	73.57	7.86	R5	1
32.67	34.6	Parapyx	88.08	88.08	1.55	R5	1
34.6	37.11	Parapyx	87.25	84.46	3.19	R5	1
37.11	40.6	Parapyx	97.13	91.98	6.02	R5	1
40.6	43.91	Calcsil	96.98	90.18	3.93	R4	2
43.91	45.36	Parapyx	100.00	100.00	3.45	R5	2
45.36	47.4	Calcsil	100.00	100.00	0.49	R4	2
47.4	50.04	Parapyx	93.56	88.64	5.68	R5	2
50.04	53.3	Parapyx	98.47	95.40	1.53	R5	1
53.3	54.04	Parapyx	100.00	78.08	8.22	R5	1
54.04	60.15	Parapyx	93.30	93.30	2.12	R5	1

Drill Hole SSMET4

FROM (m)	TO (m)	Rock type	Recovery (%)	RQD (%)	FF/m	Estimated strength	Weathering
0	3	NCOR	0	0	0	R0	0
3	5.55	Parapyx	79.61	63.53	4.71	R5	1
5.55	9.52	Parapyx	92.44	89.42	5.04	R5	1
9.52	12.05	Parapyx	100.40	100.40	1.58	R5	1
12.05	12.4	Parapyx	91.43	0.00	20	R5	2
12.4	13.34	Parapyx	103.19	103.19	2.13	R5	1
13.34	15.8	Parapyx	98.98	80.89	8.13	R5	1
15.8	19.8	Parapyx	99.00	98.00	3	R5	1
19.8	26.15	Parapyx	95.12	92.36	1.73	R5	1
26.15	27.8	Parapyx	90.91	66.67	10.90	R5	1
27.8	30.15	Parapyx	90.21	85.53	2.98	R5	1

Drill Hole SSMET5

FROM (m)	TO (m)	Rock type	Recovery (%)	RQD (%)	FF/m	Estimated strength	Weathering
0	3	NCOR	0.00	0.00	0.00	R0	0
3	5.87	Parapyx	86.15	81.29	4.32	R5	1
5.87	6.78	Parapyx	93.96	71.98	13.19	R5	1
6.78	10.16	Parapyx	93.64	89.20	3.85	R5	1
10.16	12.08	Parapyx	98.96	79.95	10.42	R5	1
12.08	15.7	Parapyx	95.30	90.47	5.52	R5	1
15.7	17.99	Parapyx	90.17	90.17	1.31	R5	1
17.99	22.55	Parapyx	97.37	89.91	4.39	R5	1
22.55	24.4	Parapyx	92.97	54.32	10.81	R5	1
24.4	30.3	Parapyx	99.66	96.95	2.71	R5	1

Drill Hole SSMET6 - Logged by PPRust Personnel

FROM (m)	TO (m)	Rock type	Recovery (%)	RQD (%)	FF/m	Estimated strength	Weathering
0	1.23	NCOR	100.00	100.00	-	R0	0
1.23	3.74	N	100.00	100.00	-	R5	1
3.74	26.83	N	100.00	97.06	-	R5	1
26.83	50.46	SPARAPYX	100.00	99.28	-	R5	1

Drill Hole SSMET7 - Logged by PPRust Personnel

FROM (m)	TO (m)	Rock type	Recovery (%)	RQD (%)	FF/m	Estimated strength	Weathering
0	0.55	NCOR	100.00	100.00	-	R0	0
0.55	4.35	PYX	100.00	76.84	-	R4	1
4.35	10.48	PEGFPYX	100.00	95.11	-	R5	1
10.48	22.4	SPARAPYX	100.00	96.64	-	R5	1
22.4	32.49	CALCSIL	100.00	98.22	-	R5	1
32.49	50.44	SPARAPYX	100.00	98.16	-	R5	1

Drill Hole SSMET8 - Logged by PPRust Personnel

FROM (m)	TO (m)	Rock type	Recovery (%)	RQD (%)	FF/m	Estimated strength	Weathering
0	1.24	NCOR	100.00	100.00	-	R0	0
1.24	2.3	N	100.00	100.00	-	R5	1
2.3	11.74	N	100.00	99.15	-	R5	1
11.74	23.41	SPARAPYX	100.00	95.72	-	R5	1
23.41	49.9	CALCSIL	100.00	98.19	-	R5	1
49.9	51.88	SPARAPYX	100.00	100.00	-	R5	1

Drill Hole SSPIT149

FROM (m)	TO (m)	Rock type	Recovery (%)	RQD (%)	FF/m	Estimated strength	Weathering
0	3	NCOR	0.00	0.00	0.00	R0	0
3	6.32	Parapyx (Serp)	83.67	33.00	6.66	R5	1
6.32	7.12	Parapyx	87.67	68.00	4.66	R5	1
7.12	9.4	Parapyx (Serp)	87.67	68.00	4.66	R5	1
9.4	11.65	Parapyx	92.00	64.00	5.33	R5	1
11.65	14.93	Parapyx (Serp)	95.33	87.00	4.33	R5	1
14.93	18.09	Parapyx	86.33	79.60	3.66	R5	1
18.09	20.64	Parapyx	99.33	93.33	3.00	R5	1
20.64	23.18	Parapyx	90.83	84.60	5.33	R5	1
23.18	24.89	SERP	83.33	82.45	5.84	R4	1
24.89	25.95	Parapyx	83.33	95.00	4.00	R5	1
25.95	27.23	SERP	83.33	89.00	5.47	R4	1
27.23	31.81	Parapyx	87.00	61.30	5.66	R5	1
31.81	33.9	Fpyx	92.67	84.30	3.33	R5	1
33.9	36.1	Parapyx (Serp)	95.00	98.00	0.66	R5	1
36.1	40.05	Fpyx	96.33	75.00	3.00	R5	1
40.05	45	Parapyx	95.00	96.60	3.00	R5	1

Drill Hole SSPIT150

FROM (m)	TO (m)	Rock type	Recovery (%)	RQD (%)	FF/m	Estimated strength	Weathering
0	3.46	NCOR	0	0	0	R0	0
3.46	46.96	N	100	98.37	0.92	R5	1
46.96	52.38	Fpyx	100	98.37	0.92	R5	1
52.38	54.61	PARAPYX	100	97.80	1.37	R5	1
54.61	55.87	Fpyx	100	97.80	1.37	R5	1
55.87	63.38	PARAPYX	100	97.80	1.37	R5	1

Drill Hole SSPIT154

FROM (m)	TO (m)	Rock type	Recovery (%)	RQD (%)	FF/m	Estimated strength	Weathering
0	2.62	NCOR	0.00	0.00	0.00	R0	0
2.62	11	N	100.00	96.98	1.07	R5	1
11	18.1	Pyx	100.00	95.09	3.11	R5	1
18.1	18.5	Pyx	100.00	95.09	3.11	R5	1
18.5	26.12	Pyx	100.00	95.09	3.11	R5	1
26.12	33.87	Ppyx	99.60	96.95	2.32	R5	1
33.87	42.76	Pyx	100.00	97.57	1.10	R5	1
42.76	44.27	Fpyx	100.00	97.57	1.10	R5	1
44.27	48.89	Pyx	100.00	97.57	1.10	R5	1
48.89	49.56	Fpyx	100.00	97.57	1.10	R5	1
49.56	51.96	Pyx	100.00	97.57	1.10	R5	1
51.96	52.66	Fpyx	100.00	97.57	1.10	R5	1
52.66	54.17	Pyx	100.00	97.57	1.10	R5	1
54.17	55.49	Ppyx	100.00	97.57	1.10	R5	1
55.49	56.66	Calc	100.00	97.57	1.10	R5	1

Drill Hole SSPIT158

FROM (m)	TO (m)	Rock type	Recovery (%)	RQD (%)	FF/m	Estimated strength	Weathering
0	3	NCOR	0.00	0.00	0.00	R0	0
3	7.2	Ppyx (serp)	100.00	96.29	2.15	R5	1
7.2	7.64	Serp	100.00	94.33	2.29	R5	1
7.64	8.71	Ppyx (serp)	100.00	96.29	2.15	R5	1
8.71	10	Ppyx	100.00	94.33	2.29	R5	1
10	16.15	Ppyx (serp)	100.00	96.29	2.15	R5	1
16.15	17.7	Ppyx	100.00	96.29	2.15	R5	1
17.7	18.21	Serp	100.00	94.33	2.29	R5	1
18.21	19.71	Ppyx (serp)	100.00	96.29	2.15	R5	1
19.71	20.65	Fpyx	100.00	94.33	2.29	R5	1
20.65	21.54	Ppyx (serp)	100.00	96.29	2.15	R5	1
21.54	22.12	Ppyx	100.00	96.29	2.15	R5	1
22.12	23	Ppyx (serp)	100.00	96.29	2.15	R5	1

Drill Hole SSPIT159

FROM (m)	TO (m)	Rock type	Recovery (%)	RQD (%)	FF/m	Estimated strength	Weathering
0	3	NCOR	0.00	0.00	0.00	R0	0
3	9.4	Pyx (serp)	70.94	59.06	2.50	R5	1
9.4	13.1	Fpyx (serp)	100.00	81.08	0.81	R5	1
13.1	19.08	Pyx (serp)	99.33	96.91	2.68	R5	1
19.08	20.5	Ppyx	95.00	90.07	4.23	R5	1
20.5	25.12	Pyx (serp)	93.38	89.05	2.81	R5	1
25.12	26.41	Ppyx	91.47	78.29	4.65	R5	1
26.41	35.06	Pyx (serp)	99.36	95.43	3.12	R5	1
35.06	38.05	Ppyx	99.67	93.65	2.68	R5	1
38.05	45.1	Pyx (serp)	98.72	84.68	4.40	R5	1

Drill Hole SSPIT160

FROM (m)	TO (m)	Rock type	Recovery (%)	RQD (%)	FF/m	Estimated strength	Weathering
0	3	NCOR	0.00	0.00	0.00	R0	0
3	4.21	Ppyx	100.00	52.35	4.71	R5	1
4.21	5.69	Calc	100.00	52.35	4.71	R5	1
5.69	8.93	Ppyx	100.00	94.49	3.53	R5	1
8.93	11.5	Fpyx	100.00	94.49	3.53	R5	1
11.5	12.75	Ppyx	100.00	94.49	3.53	R5	1
12.75	13.4	Serp	100.00	94.49	3.53	R5	1
13.4	34.5	Ppyx	100.00	94.49	3.53	R5	1
34.5	35.59	Fpyx	100.00	94.49	3.53	R5	1
35.59	42.57	Ppyx	100.00	92.31	5.59	R5	1
42.57	43.67	Fpyx	100.00	90.14	4.84	R5	1
43.67	44.4	Serp	100.00	90.14	4.84	R5	1
44.4	45.1	Fpyx	100.00	90.14	4.84	R5	1

Drill Hole SSPIT161

FROM (m)	TO (m)	Rock type	Recovery (%)	RQD (%)	FF/m	Estimated strength	Weathering
0	0.8	NCOR	0.00	0.00	0.00	R0	0
0.8	4.19	Fpyx	100.00	42.43	4.45	R5	1
4.19	8.65	Ppys (serp)	94.93	82.92	3.65	R5	1
8.65	9.65	Fpyx	100.00	81.18	1.65	R5	1
9.65	21.06	Ppys (serp)	100.00	75.88	5.85	R5	1
21.06	21.78	Fpyx	100.00	81.18	1.65	R5	1
21.78	24.29	Ppys (serp)	100.00	92.99	4.63	R5	1
24.29	24.38	Qzfs	100.00	100.00	0.00	R5	1
24.38	31.83	Ppys (serp)	100.00	92.99	4.63	R5	1
31.83	32.04	Serp	100.00	92.99	4.63	R4	1
32.04	41.55	Ppys (serp)	100.00	92.99	4.63	R5	1
41.55	42.09	Serp	100.00	92.99	4.63	R4	1
42.09	45.05	Ppys (serp)	100.00	92.99	4.63	R5	1

DRILLHOLE: SSMet 3
Joint Condition Description

Geotech Unit no.	Joint name	Set no.	Depth	Separation	Infill	Infill name	Roughness	Slickensides	S/s dir.	Fracture condition	Dip	Reletive dip direction	Dip direction	Quantity	Comment
3.03	jt1	1	8.35	vn	f	24	sm	y	30	2	30	110	250	1	
3.03	jt2	1	9.13	n	f	22a	sr			3	0	170	190	1	
3.03	jt3	2	10.39	vn	f	17	sr			2	55	45	315	1	
3.03	jt4	1	11.72	vn	f	34	sr			2	30	195	165	1	
3.03	jt5	1	11.98	n	f	22a	sr			2	1	140	220	1	
3.03	jt6	1	13.08	n	f	a6	sr			3	10	52	308	1	
3.04	jt7	1	14.2	vn	f	22	mr			3	30	230	130	1	
3.05	jt8	1	15.13	n	f	4	sr			2	10	125	235	1	
3.05	jt9	1	16.28	vn	f	3	sr			2	30	110	250	2	
3.05	jt10	1	17.26	n	f	22a	sr			3	10	98	262	3	
3.05	jt11	1	17.32	n	f	22a	sr			3	10	260	100	1	
3.05	jt12	1	18.17	missing	f	4	sr			3	30	314	46	1	
3.06	jt13	2	21.34	vn	f	4	sr			2	55	224	136	1	
3.06	jt14	1	22.64	n	f	24	sr			2	17.5	270	90	1	
3.07	jt15	1	25.18	vn	f	2a	sr			3	20	200	160	1	
3.07	jt16	3	26.06	n	f	2a	sr			3	80	125	235	1	
3.07	jt17	2	27.16	missing	f	3	sr			2	45	340	20	2	
3.07	jt18	1	27.88	vn	f	17	sr			2	15	150	210	1	
3.07	jt19	1	28.79	vn	f	17	mr			2	30	22	338	2	
3.07	jt20	1	30.64	vn	f	a19	sr			2&3	5	390	-30	1	
3.08	jt21	2	31.5	vn	f	11a	mr			2	55	300	60	2	
3.08	jt22	2	31.81	vn	f	19	sr			1&2	40	150	210	1	
3.08	jt23	1	32.05	vn	f	24	sr			2	20	290	70	1	
3.09	jt24	3	32.68	vn	f	24	mr			2	65	104	256	2	
3.09	jt25	2	33.65	vn	cl		sr			1	52.5	126	234	3	
3.10	jt26	1	35.16	vn	f	17	sr			2	20	320	40	2	
3.10	jt27	1	36.04	vn	f	32	sr			2	15	166	194	1	
3.10	jt28	2	36.45	vn	f	24	sm	y	45	2	55	320	40	4	
3.11	jt29	2	37.58	vn	f	11a	sr			1&2	60	238	122	2	
3.11	jt30	1	38.05	vn	f	22a	sr			3	30	260	100	3	
3.11	jt31	1	38.84	vn	f	17	sr			2	25	20	340	1	
3.11	jt32	2	39.77	vn	f	17	sr			2	45	40	320	2	
3.11	jt33	3	40	n	f	17	sr			2	70	30	330	1	
3.11	jt34	1	40.33	vn	f	11a	sr			2	27.5	24	336	2	
3.12	jt35	1	41.19	vn	f	17	sr			2	10	208	152	1	
3.12	jt36	1	41.6	vn	f	17	sr			1&2	25	76	284	3	
3.12	jt37	1	42.88	vn	f	4	sr			1&2	20	87	273	2	
3.12	jt38	2	43.32	vn	f	17	sr			2	35	86	274	2	

3.13	jt39	2	44.09	vn	f	2a	sr		2	35	12	348	1
3.13	jt40	2	44.825	vn	f	17	sr		2	55	6	354	1
3.14	jt41	2	47.24	vn	f	4	sr		2	55	170	190	1
3.15	jt42	1	47.61	vn	f	a41	sr		3	30	354	6	2
3.15	jt43	1	48.23	n	f	2a	sr		2	20	176	184	1
3.15	jt44	1	48.85	vn	f	22a	sr		2&3	20	210	150	2
3.15	jt45	1	49.79	n	f	a44	sr		3	15	328	32	3
3.16	jt46	1	50.5	n	f	a45	mr		3	25	290	70	3
3.17	jt47	3	53.54	vn	f	17	sr		1&2	70	342	18	1
3.18	jt48	2	54.56	vn	f	4	sr		2	40	68	292	1
3.18	jt49	3	55.24	vn	f	17	mr		2	70	288	72	1
3.18	jt50	2	55.82	vn	f	32	mr		2	35	300	60	3
3.18	jt51	2	56.58	vn	f	19	sr		1&2	35	130	230	1
3.18	jt52	1	58.05	vn	f	24	sr		2	10	88	272	3
3.18	jt53	3	59.99	n	f	45	sr		2	72.5	136	224	1

DRILLHOLE: SSMet 3
Corrected dip and dip direction

Geotech Unit no.	Joint name	Set no.	Dip (corrected)	Dip direction (corrected)	Quantity
3.03	jt1	1	60	250	1
3.03	jt2	1	90	190	1
3.03	jt3	2	35	315	1
3.03	jt4	1	60	165	1
3.03	jt5	1	89	220	1
3.03	jt6	1	80	308	1
3.04	jt7	1	60	130	1
3.05	jt8	1	80	235	1
3.05	jt9	1	60	250	2
3.05	jt10	1	80	262	3
3.05	jt11	1	80	100	1
3.05	jt12	1	60	46	1
3.06	jt13	2	35	136	1
3.06	jt14	1	72.5	90	1
3.07	jt15	1	70	160	1
3.07	jt16	3	10	235	1
3.07	jt17	2	45	20	2
3.07	jt18	1	75	210	1
3.07	jt19	1	60	338	2
3.07	jt20	1	85	-30	1
3.08	jt21	2	35	60	2
3.08	jt22	2	50	210	1
3.08	jt23	1	70	70	1
3.09	jt24	3	25	256	2
3.09	jt25	2	37.5	234	3
3.10	jt26	1	70	40	2
3.10	jt27	1	75	194	1
3.10	jt28	2	35	40	4
3.11	jt29	2	30	122	2
3.11	jt30	1	60	100	3
3.11	jt31	1	65	340	1
3.11	jt32	2	45	320	2
3.11	jt33	3	20	330	1
3.11	jt34	1	62.5	336	2
3.12	jt35	1	80	152	1
3.12	jt36	1	65	284	3
3.12	jt37	1	70	273	2
3.12	jt38	2	55	274	2
3.13	jt39	2	55	348	1
3.13	jt40	2	35	354	1
3.14	jt41	2	35	190	1
3.15	jt42	1	60	6	2
3.15	jt43	1	70	184	1
3.15	jt44	1	70	150	2
3.15	jt45	1	75	32	3
3.16	jt46	1	65	70	3
3.17	jt47	3	20	18	1
3.18	jt48	2	50	292	1
3.18	jt49	3	20	72	1
3.18	jt50	2	55	60	3
3.18	jt51	2	55	230	1
3.18	jt52	1	80	272	3
3.18	jt53	3	17.5	224	1

DRILLHOLE: SSMet 4
Joint Condition Description

Geotech Unit no.	Joint name	Set no.	Depth	Separation	Infill	Infill name	Roughness	Slickensides	S/s dir.	Fracture condition	Dip	Reletive dip direction	Dip direction	Quantity	Comment
4.01	jt1	2	4.3	vn	f	2a	sr			2	40	240	120	1	
4.01	jt2	2	4.88	vn	f	17	sr			1&2	35	40	320	1	
4.01	jt3	2	5.13	vn	f	2a	sr			2	40	31	329	1	
4.02	jt4	1	5.69	n	f	17	sr			2	30	350	10	3	
4.02	jt5	2	5.98	vn	f	2a	sr			2	55	230	130	1	
4.02	jt6	2	6.43	vn	f	17	mr			1&2	50	20	340	1	
4.02	jt7	2	6.83	vn	f	17	sr			2	40	165	195	2	
4.02	jt8	1	7.37	n	f	17	sr			2&3	25	206	154	1	soapy
4.02	jt9	2	8.14	vn	f	17	mr			1&2	45	166	194	1	
4.02	jt10	2	8.57	n	f	17	sm	y	40	1&2	35	25	335	1	possible frabric
4.02	jt11	2	9.2	n	f	17	sr			1	40	18	342	1	
4.02	jt12	3	9.495	vn	f	40	sr			2	75	236	124	1	
4.03	jt13	1	10.3	vn	f	40	sr			1&2	25	210	150	1	
4.03	jt14	2	11.68	n	f	17	sr			1&2	42.5	174	186	1	
4.03	jt15	3	11.89	n	f	15a	mr			2	75	334	26	1	
4.04	jt16	2	12.11	n	f	3	sm	y	45	2	40	20	340	1	
4.04	jt17	2	12.17	n	f	3	sm	y	2	2	40	340	20	2	possible frabric
4.04	jt18	1	12.18	missing	f	40	sm	y	20	2	25	190	170	1	
4.04	jt19	3	12.26	vn	f	3	mr			2	80	176	184	1	
4.04	jt20	2	12.31	n	f	11a	sr			2	50	20	340	1	
4.05	jt21	3	12.6695	n	f	24a	mr			2	85	197	163	1	
4.05	jt22	2	12.85	vn	f	11a	sr			2	60	0	360	1	
4.06	jt23	2	13.72	vn	f	2a	mr			2	40	6	354	2	
4.06	jt24	3	13.83	n	f	2a	mr			2&3	85	110	250	1	
4.06	jt25	1	13.99	n	f	22a	sr			2&3	22.5	340	20	3	
4.06	jt26	2	14.28	n	f	17	sr			2	40	345	15	1	
4.06	jt27	2	14.91	n	f	24a	sr			2	35	140	220	1	
4.06	jt28	2	15.63	vn	f	2a	mr			2	60	90	270	2	
4.07	jt29	1	16.05	n	f	2a	sr			2	25	95	265	3	
4.07	jt30	2	17.52	vn	f	17	sr			2	40	60	300	2	
4.07	jt31	3	18.59	n	f	17	sr			1&2	75	24	336	2	
4.08	jt32	2	21.16	vn	cl		sr			1&2	50	110	250	1	
4.08	jt33	3	22.27	vn	f	35	mr			2	67.5	182	178	1	
4.08	jt34	1	23.06	vn	s	17	sr			1&2	2	25	335	1	
4.08	jt35	1	24.11	missing	f	2a	mr			2	22.5	150	210	1	
4.08	jt36	1	25.66	n	f	34	sr			2	15	90	270	1	
4.09	jt37	1	26.36	vn	f	24	sr			2	25	280	80	1	
4.09	jt38	2	26.66	missing	f	3	sm	y	20	2	40	350	10	1	

4.09	jt39	1	26.81	vn	f	2a	sr			2	30	20	340	2
4.09	jt40	3	26.865	vn	f	15a	mr			2	65	214	146	1
4.09	jt41	2	27.05	vn	f	19	sr			1&2	45	246	114	3
4.09	jt42	3	27.15	vn	f	17	sr			2	62.5	28	332	1
4.09	jt43	2	27.35	n	cl		sm	y	10	1	35	40	320	2
4.09	jt44	1	27.8	vn	f	15a	sr			2	30	10	350	1
4.10	jt45	1	28.81	n	f	2a	sr			2	20	170	190	3
4.10	jt46	2	28.97	missing	f	3	mr			2	32.5	6	354	1

DRILLHOLE: SSMet 4
Corrected dip and dip direction

Geotech Unit no.	Joint name	Set no.	Dip (corrected)	Dip direction (corrected)	Quantity
4.01	jt1	2	50	120	1
4.01	jt2	2	55	320	1
4.01	jt3	2	50	329	1
4.02	jt4	1	60	10	3
4.02	jt5	2	35	130	1
4.02	jt6	2	40	340	1
4.02	jt7	2	50	195	2
4.02	jt8	1	65	154	1
4.02	jt9	2	45	194	1
4.02	jt10	2	55	335	1
4.02	jt11	2	50	342	1
4.02	jt12	3	15	124	1
4.03	jt13	1	65	150	1
4.03	jt14	2	47.5	186	1
4.03	jt15	3	15	26	1
4.04	jt16	2	50	340	1
4.04	jt17	2	50	20	2
4.04	jt18	1	65	170	1
4.04	jt19	3	10	184	1
4.04	jt20	2	40	340	1
4.05	jt21	3	5	163	1
4.05	jt22	2	30	360	1
4.06	jt23	2	50	354	2
4.06	jt24	3	5	250	1
4.06	jt25	1	67.5	20	3
4.06	jt26	2	50	15	1
4.06	jt27	2	55	220	1
4.06	jt28	2	30	270	2
4.07	jt29	1	65	265	3
4.07	jt30	2	50	300	2
4.07	jt31	3	15	336	2
4.08	jt32	2	40	250	1
4.08	jt33	3	22.5	178	1
4.08	jt34	1	88	335	1
4.08	jt35	1	67.5	210	1
4.08	jt36	1	75	270	1
4.09	jt37	1	65	80	1
4.09	jt38	2	50	10	1
4.09	jt39	1	60	340	2
4.09	jt40	3	25	146	1
4.09	jt41	2	45	114	3
4.09	jt42	3	27.5	332	1
4.09	jt43	2	55	320	2
4.09	jt44	1	60	350	1
4.10	jt45	1	70	190	3
4.10	jt46	2	57.5	354	1

DRILLHOLE: SSMet 5
Joint Condition Description

Geotech Unit no.	Joint name	Set no.	Depth	Separation	Infill	Infill name	Roughness	Slickensides	S/s dir.	Fracture condition	Dip	Reletive dip direction	Dip direction	Quantity	Comment
5.01	jt1	2	3.4	c	cl		sr			1	45	274	86	1	
5.01	jt2	2	3.56	c	cl		sr			1	40	300	60	1	
5.01	jt3	1	3.87	vn	f	cal	mr			2	25	342	18	1	
5.01	jt4	1	4.3	vn	f	c&s	mr			3	5	30	330	1	
5.01	jt5	1	4.56	n	f	3	sr			2	20	8	352	1	
5.01	jt6	1	4.63	n	f	3	mr			2	22.5	264	96	1	
5.01	jt7	1	4.88	vn	f	3	sr			2	30	150	210	1	
5.01	jt8	1	5.05	vn	f	3	mr			2	22.5	12	348	1	
5.01	jt9	1	5.062	w	f	3	sr			3	25	26	334	1	
5.01	jt10	1	5.64	n	f	3	sr			2	25	26	334	1	
5.01	jt11	1	5.66	n	f	3	sr			2	25	26	334	1	
5.02	jt12	1	5.93	n	f	3	sr			2	17.5	68	292	1	
5.02	jt13	1	5.96	n	f	3	sr			2	30	324	36	1	
5.02	jt14	1	6	vn	f		mr			1	30	18	342	1	
5.02	jt15	1	6.1	vn	f	17	sm	y	60	2	20	44	316	1	possible fabric
5.02	jt16	1	6.18	vn	f	18	mr			2	22.5	24	336	1	
5.02	jt17	1	6.36	n	f	17	sr			2	20	42	318	1	
5.02	jt18	2	6.48	vn	cl		mr			1	40	28	332	1	
5.02	jt19	1	6.58	vn	s&f	22	r			2	20	210	150	1	
5.02	jt20	2	6.65	missing	f	17	sm	y	40	2	45	126	234	3	
5.03	jt21	3	7.88	vn	f	24	sm	y	55	3	75	180	180	3	
5.03	jt22	1	8.46	vn	f	17	mr			1	25	88	272	1	
5.03	jt23	3	8.6	vn	f	3	sm			2	90	250	110	1	
5.03	jt24	2	9.06	n	f	22a	sr			3	35	180	180	1	
5.03	jt25	2	9.145	vn	f	3	sr			2	37.5	4	356	1	
5.03	jt26	1	9.34	vn	f	17	sr			2	25	320	40	1	
5.03	jt27	2	9.74	n	f	22a	mr			3	33	80	280	1	
5.04	jt28	2	10.77	n	f	3	mr			2	35	32	328	2	
5.04	jt29	1	11.03	vn	f	17	sr			2	88	180	180	1	
5.04	jt30	2	11.04	vn	cl		sr			2	35	192	168	1	
5.04	jt31	1	11.27	vn	f	34	sm	y	2.5	2	15	176	184	2	
5.04	jt32	3	11.89	vn	f	35	sr			2	65	98	262	6	
5.05	jt33	1	13.93	vn	f	3	sr			2	10	188	172	1	
5.05	jt34	1	14.19	w	f	24	sm	y	15	3	30	205	155	2	
5.05	jt35	3	14.59	vn	f	24a	mr			2	70	300	60	1	
5.05	jt36	1	14.82	vn	f	3	sm	y	12.5	2	20	306	54	1	

DRILLHOLE: SSMet 5
Joint Condition Description

Geotech Unit no.	Joint name	Set no.	Depth	Separation	Infill	Infill name	Roughness	Slickensides	S/s dir.	Fracture condition	Dip	Reletive dip direction	Dip direction	Quantity	Comment
5.05	jt37	3	15.3	vn	f	17	sr			2	87.5	65	295	1	
5.05	jt38	2	15.68	vn	f	19	sm	y	65	1	42.5	352	8	1	possible fabric
5.06	jt39	2	17.05	vn	f	34	sr			2	45	165	195	1	
5.07	jt40	1	18.02	vn	f	4	mr			3	10	22	338	1	
5.07	jt41	3	18.98	vn	f	40	sm			2	72.5	308	52	1	
5.07	jt42	2	19.49	vn	f	3	sr			2	40	250	110	1	
5.07	jt43	1	20.87	n	f	24	sr			3	30	76	284	1	
5.07	jt44	2	21.44	vn	f	34	sr			2	35	56	304	1	
5.07	jt45	3	21.75	vn	f	22	sr			2	65	66	294	3	
5.08	jt46	1	22.7	w	f	24	sr			3	30	276	84	3	
5.08	jt47	3	22.79	vn	f	17	sr			2	62.5	96	264	2	
5.08	jt48	1	22.91	n	f	18	sr			2&3	0	0	360	1	
5.08	jt49	2	22.97	vn	f	17	sm	y	55	2	50	140	220	3	possible fabric
5.08	jt50	1	23.13	vn	f	3	sr			2	17.5	276	84	1	
5.08	jt51	3	23.51	n	f	17	sr			2	65	67	293	1	
5.08	jt52	1	23.64	vn	f	22	mr			2	20	340	20	1	
5.08	jt53	2	24.13	missing	f	34	sm	y	25	2	50	12	348	2	
5.09	jt54	1	25.58	missing	f	19	sm	y	35	2	15	146	214	2	possible fabric
5.09	jt55	1	26.38	vn	f	4	sr			1&2	17.5	150	210	1	
5.09	jt56	1	27.75	vn	f	34	sm	y	10	2	25	335	25	1	
5.09	jt57	2	27.87	vn	f	17	sr			2	50	218	142	1	
5.09	jt58	1	28.55	vn	f	24	sr			2	20	40	320	1	
5.09	jt59	3	28.92	vn	f	17	sr			1&2	75	214	146	3	
5.09	jt60	2	29.31	vn	f	35	sr			1	40	335	25	1	
5.09	jt61	3	30.1	vn	f	19	sr			1&2	70	260	100	1	

DRILLHOLE: SSMet 5
Corrected dip and dip direction

Geotech Unit no.	Joint name	Set no.	Dip (corrected)	Dip direction (corrected)	Quantity
5.01	jt1	2	45	86	1
5.01	jt2	2	50	60	1
5.01	jt3	1	65	18	1
5.01	jt4	1	85	330	1
5.01	jt5	1	70	352	1
5.01	jt6	1	67.5	96	1
5.01	jt7	1	60	210	1
5.01	jt8	1	67.5	348	1
5.01	jt9	1	65	334	1
5.01	jt10	1	65	334	1
5.01	jt11	1	65	334	1
5.02	jt12	1	72.5	292	1
5.02	jt13	1	60	36	1
5.02	jt14	1	60	342	1
5.02	jt15	1	70	316	1
5.02	jt16	1	67.5	336	1
5.02	jt17	1	70	318	1
5.02	jt18	2	50	332	1
5.02	jt19	1	70	150	1
5.02	jt20	2	45	234	3
5.03	jt21	3	15	180	3
5.03	jt22	1	65	272	1
5.03	jt23	3	0	110	1
5.03	jt24	2	55	180	1
5.03	jt25	2	52.5	356	1
5.03	jt26	1	65	40	1
5.03	jt27	2	57	280	1
5.04	jt28	2	55	328	2
5.04	jt29	1	2	180	1
5.04	jt30	2	55	168	1
5.04	jt31	1	75	184	2
5.04	jt32	3	25	262	6
5.05	jt33	1	80	172	1
5.05	jt34	1	60	155	2
5.05	jt35	3	20	60	1
5.05	jt36	1	70	54	1
5.05	jt37	3	2.5	295	1
5.05	jt38	2	47.5	8	1
5.06	jt39	2	45	195	1
5.07	jt40	1	80	338	1
5.07	jt41	3	17.5	52	1
5.07	jt42	2	50	110	1
5.07	jt43	1	60	284	1
5.07	jt44	2	55	304	1
5.07	jt45	3	25	294	3
5.08	jt46	1	60	84	3
5.08	jt47	3	27.5	264	2
5.08	jt48	1	90	360	1
5.08	jt49	2	40	220	3
5.08	jt50	1	72.5	84	1
5.08	jt51	3	25	293	1

DRILLHOLE: SSMet 5
Corrected dip and dip direction

Geotech Unit no.	Joint name	Set no.	Dip (corrected)	Dip direction (corrected)	Quantity
5.08	jt52	1	70	20	1
5.08	jt53	2	40	348	2
5.09	jt54	1	75	214	2
5.09	jt55	1	72.5	210	1
5.09	jt56	1	65	25	1
5.09	jt57	2	40	142	1
5.09	jt58	1	70	320	1
5.09	jt59	3	15	146	3
5.09	jt60	2	50	25	1
5.09	jt61	3	20	100	1

SSMet 3 - RMR calculations (Bieniawski, 1989), uncorrected

Geotech Unit		Str. of intact rock (MPa)			RQD		Spacing of discont.		Condition of discont.		Ground water				RMR
no.	Depth (m)	C(act) Avg.	PI Avg.	Rating	(%)	Rating	Avg. (mm)	Rating		Rating	Inflow/10m etc.	Jt.H2O pres/σ	Gen. condit.	Rating	Total Rating
1	3.0 - 6.58		5.2	12	51.40	13	Little intact core, no distinguishable joints				None	0	Complet. Dry	15	
2	6.58 - 7.53	no str. tests possible			20.00	3	Little intact core, no distinguishable joints				None	0	Complet. Dry	15	
3	7.53 - 13.65		5.1	12	79.25	17	0.20 - 0.60	10	2;0;3;2;5	12	None	0	Complet. Dry	15	66
4	13.65 - 14.44	97.89		7	88.61	17	0.06 - 0.20	8	2;0;3;2;6	13	None	0	Complet. Dry	15	60
5	14.44 - 18.58	104.02		12	97.34	20	0.20 - 0.60	10	2;0;3;4;5;	14	None	0	Complet. Dry	15	71
6	18.58 - 23.9	118.35		12	96.05	20	0.60 - 2	15	2;0;3;2;3	10	None	0	Complet. Dry	15	72
7	23.9 - 31.27	138.00		12	92.13	20	0.20 - 0.60	10	2;0;3;2;5	12	None	0	Complet. Dry	15	69
8	31.27 - 32.67	195.42		12	73.57	13	0.06 - 0.20	8	2;0;3;2;5	12	None	0	Complet. Dry	15	60
9	32.67 - 34.6	140.23		12	88.08	17	0.60 - 2	15	2;0;3;6;6	17	None	0	Complet. Dry	15	76
10	34.6 - 37.11	99.53		7	84.46	17	0.06 - 0.20	8	2;0;3;2;5	12	None	0	Complet. Dry	15	59
11	37.11 - 40.6	141.86		12	91.98	20	0.06 - 0.20	8	2;0;3;2;5	12	None	0	Complet. Dry	15	67
12	40.6 - 43.91	119.84		12	90.18	20	0.06 - 0.20	8	2;0;3;2;5	12	None	0	Complet. Dry	15	67
13	43.91 - 45.36	146.52		12	100.00	20	0.20 - 0.60	10	2;0;3;2;5	12	None	0	Complet. Dry	15	69
14	45.36 - 47.4	98.20		7	100.00	20	0.60 - 2	15	2;0;3;2;5	12	None	0	Complet. Dry	15	69
15	47.4 - 50.04	105.27		12	88.64	17	0.20 - 0.60	10	2;0;3;2;3	10	None	0	Complet. Dry	15	64
16	50.04 - 53.3	125.99		12	95.40	20	0.20 - 0.60	10	2;0;3;2;3	10	None	0	Complet. Dry	15	67
17	53.3 - 54.03	182.85		12	78.08	17	0.06 - 0.20	8	2;0;3;2;5	12	None	0	Complet. Dry	15	64
18	54.03 - 60.15	110.45		12	93.30	20	0.20 - 0.60	10	2;0;3;2;3	10	None	0	Complet. Dry	15	67

SSMet 4 - RMR calculations (Bieniawski, 1989), uncorrected

Geotech Unit		Str. of intact rock (MPa)			RQD		Spacing of discont.		Condition of discont.		Ground water				RMR
no.	Depth (m)	C(act) Avg.	PI Avg.	Rating	(%)	Rating	Avg. (mm)	Rating		Rating	Inflow/10m etc.	Jt.H2O pres/σ	Gen. condit.	Rating	Total Rating
1	3 - 5.55	126.72		12	63.53	13	0.2 - 0.6	10	2;0;3;4;5	14	none	0	Dry	15	64
2	5.55 - 9.52	130.85		12	89.42	17	0.06 - 0.2	8	2;0;3;2;5	12	none	0	Dry	15	64
3	9.52 - 12.05	112.2		12	100.4	20	0.2 - 0.6	10	2;0;3;4;5	14	none	0	Dry	15	71
4	12.05 - 12.4		1.88	4	0	3	<0.06	5	2;0;1;2;5	10	none	0	Dry	15	37
5	12.4 - 13.34	127.35		12	103.19	20	0.2 - 0.6	10	2;0;3;2;5	12	none	0	Dry	15	69
6	13.34 - 15.8	136.43		12	80.89	17	0.06 - 0.2	8	2;0;3;2;5	12	none	0	Dry	15	64
7	15.8 - 19.8	169.37		12	98	20	0.2 - 0.6	10	2;0;3;2;5	12	none	0	Dry	15	69
8	19.8 - 26.15	169.14		12	92.36	20	0.2 - 0.6	10	2;0;3;6;6	17	none	0	Dry	15	74
9	26.15 - 27.8	70.72		7	66.67	13	<0.06	5	2;0;1;2;5	10	none	0	Dry	15	50
10	27.8 - 30.15	169.08		12	85.53	17	0.06 - 0.2	8	2;0;3;4;5	14	none	0	Dry	15	66

SSMet 5 - RMR calculations (Bieniawski, 1989), uncorrected

Geotech Unit		Str. of intact rock (MPa)			RQD		Spacing of discont.		Condition of discont.		Ground water				RMR
no.	Depth (m)	C(act) Avg.	PI Avg.	Rating	(%)	Rating	Avg. (mm)	Rating		Rating	Inflow/10m etc.	Jt.H2O pres/σ	Gen. condit.	Rating	Total Rating
1	3 - 5.87		3	7	81.29	17	0.2 - 0.6	10	2;0;3;2;5	12	None	0	Complet. Dry	15	**61**
2	5.87 - 6.78		3.8	7	71.98	13	0.06 - 0.2	8	2;0;3;2;5	12	None	0	Complet. Dry	15	**55**
3	6.78 - 10.16	105.3		12	89.2	17	0.06 - 0.2	8	2;0;3;4;3	12	None	0	Complet. Dry	15	**64**
4	10.16 - 12.08	80.86		7	79.95	17	<0.06	5	2;0;3;2;5	12	None	0	Complet. Dry	15	**56**
5	12.08 - 15.7	94.99		7	90.47	20	0.06 - 0.2	8	2;0;1;2;5	10	None	0	Complet. Dry	15	**60**
6	15.7 - 17.99	121.5		12	90.17	20	0.2 - 0.6	10	2;0;3;2;5	12	None	0	Complet. Dry	15	**69**
7	17.99 - 22.55	157.42		12	89.91	17	0.2 - 0.6	10	2;0;3;2;6	13	None	0	Complet. Dry	15	**67**
8	22.55 - 24.4		2.31	7	54.32	13	0.06 - 0.2	8	2;0;3;2;5	12	None	0	Complet. Dry	15	**55**
9	24.4 - 30.3	130.48		12	96.66	20	0.2 - 0.6	10	2;0;1;2;5	10	None	0	Complet. Dry	15	**67**

APPENDIX - B

Petrography Appendix

Sample Preparation for geochemical analysis

The shattered or sheared UCS specimens were collected after each test and bagged. The bagged specimens were crushed in a low molybdenum carbon steel jaw crusher to fragmentation of <1cm. The crushed specimen was then milled three times, first to a coarse grade, after which the specimen was split using the cone and quarter technique. Half the sample was bagged and saved. 100g of the coarse grade specimen was milled a second time for one minute down to normal grade. Again the sample was coned, quartered and bagged. Finally 20g of normal grade was milled a third time, for 45 seconds, to a fine grade and bagged. At all stages between crushing and milling care was taken to prevent contamination by brushing off excess specimen powder on the apparatus, wiping clean apparatus with acetone and in some cases vacuuming the apparatus. Preparation was performed in a ventilation-controlled environment and the bags in which specimens were stored were unused.

XRD Sample Preparation and Equipment Specifications

Fine grade powder was backpacked into an aluminum container with an imposed near random orientation. Analysis using a Philips PW 1710 diffractometer with a CoKα radiation source and with a graphite monochromator; long line focus was performed. The tension and the current of the generator were set at 40 kV and 30 mA respectively and a scan speed of 0.020˚2θ was used with a one second time interval per step.

Eva software, provided by PPRust Operations, was used to filter the raw data files and thus determine which minerals were present in the samples. The filters used by the mine were used in this analysis for consistency.

Detailed Thin Section Analyses

Detailed thin section analysis of SSMet 3/18.

Mineralogy			Textures	
			Grain shape	**Grain Size**
Essential Minerals		**%**		**Rock average:** coarse
Plagioclase		15	Interstitial	**Rock range:** fine - coarse
Orthopyroxene		63	anhedral - subhedral	**Description:** The pyroxene minerals were coarse
Clinopyroxene		22	subhedral	grained, clinopyroxene were more coarse than ortho-
				pyroxene. Plagioclase was interstitial and all other
Total		100		minerals present were fine to very fine grained.
Accessory Minerals		**No. observed**	**Common textures**	
Biotite		7	This rock had a poikilitic texture as plagioclase and biotite were enclosed	
Amphibole		4	within pyroxene. Plagioclase was present as interstitial crystals. All the plagio-	
Garnet		2	clase crystals showed an exsolution texture.	
Opaque minerals		6	**Alteration** (layers of weaker material)	
Olivine		2	Plagioclase was highly altered, showing break down to clay minerals (talc).	
Total		21	Alteration of the plagioclase varied from uniform and extensive to spotted,	
Modal Composition			generally within the centre of the minerals. The pyroxenes showed alteration	
		Recalc.	to amphibole, chlorite and some serpentine preferentially along cleavage	
P =	15	15	planes and fractures. Orthopyroxene had a higher degree of alteration com-	
Ol =	0	0	pared to clinopyroxene.	
Opx =	63	63	**Degree of Alteration**	50% moderate
Cpx =	22	22	**Microfracturing**	
Hbl =	0	0	**Following grain boundaries**	No
Total	100	100	**Across crystals**	Yes
IUGS name	Clinopyroxene norite		**Fabric**	
Colour Index	Melanocratic		There was a granular, coarse grained texture.	

Detailed thin section analysis of SSMet 3/276.

Mineralogy			Textures	
			Grain shape	**Grain Size**
Essential Minerals		**%**		**Rock average:** coarse
Orthopyroxene		85	subhedral - euhedral	**Rock range:** very fine - coarse
Clinopyroxene		5	subhedral	**Description:** Orthopyroxene minerals were
Olivine		3	subhedral	present at either coarse euhedral grains or
Calcite		4	subhedral - euhedral	as medium subhedral grains. The calcite and
Garnet		3	subhedral	olivine were medium grained with the rest
				of the material being fine grained
Total		100	**Common textures**	
Accessory Minerals		**No. observed**	A subpoikilitic texture was present with olivine partially enclosed by	
Amphibole		7	pyroxene, orthopyroxene and clinopyroxene showed recrystalisation	
Biotite		<20	around the olivine and calcite crystals. Biotite was concentrated	
			around the calcite and was kinked. This thinsection showed a large	
			number of veins cross cutting all the minerals, some the length of the	
			thinsection. Infilling consisted of two materials, a carbonate material	
			and serpentine with a highly fiberous appearance, possibly lizardite	
			These materials were present together and as individual veins.	
			Alteration (layers of weaker material)	
Total		27	Olivine was completely serpentinised showing a mesh testure. Ortho-	
Modal Composition			pyroxene and clinopyroxene were altered with a dusty fine-grained	
		Recalc.	appearance to chlorite and possible talc. The pyroxenes on the	
P =	0	0.0	boundaries of the calcite showed greater alteration at the points of	
Ol =	3	3.2	contact.	
Opx =	85	91.4	**Degree of Alteration**	70% high
Cpx =	5	5.4	**Microfracturing**	
Hbl =	0	0.0	**Following grain boundaries**	Yes
Total	93	100	**Across crystals**	Yes
IUGS name	Orthopyroxenite		**Fabric**	
Colour Index	Ultramafic		The veins had a perfered orientation parallel to the length of the bore-	
			hole core.	

Detailed thin section analysis of SSMet 3/390.

Mineralogy			Textures	
			Grain shape	**Grain Size**
Essential Minerals		**%**		**Rock average:** medium
Othopyroxene		25	anhedral	**Rock range:** fine - medium
Clinopyroxene		15	andhedral	**Description:** The pyroxene minerals were
Olivine		50	subhedral	larger than the olivines and the opaque
Opaque minerals		10	andhedral	minerals
Total		100		
Accessory Minerals		**No. observed**	**Common textures**	
Biotite		9	Olivine was enclosed by orthopyroxene, there were olivine and pyroxene	
Carbonate mineral		3	intergrowths. The carbonate material present within the fractures of	
			the olivine and also present as indiviual minerals. Veins of	
			fine grained carbonate material was present. The orthopyroxene	
			showed zoned extinction. The opaque minerals form lacy networks and	
Total		12	indervidual minerals	
Modal Composition			**Alteration** (layers of weaker material)	
		Recalc.	Olivine was completely serpentinised, orthopyroxene and clinopyroxene	
P =	0	0	were serpentinised, clinopyroxene to a lesser degree. Orthopyroxene	
Ol =	50	56	also showed alteration into chlorite.	
Opx =	25	28	**Degree of Alteration**	high - estimated 80 %
Cpx =	15	16	**Microfracturing**	
Hbl =	0	0	**Following grain boundaries**	Yes
Total	90	100	**Across crystals**	Yes
IUGS name	Iherzolite		**Fabric**	
Colour Index	Ultramafic		The opaque minerals showed an general perfered orientation.	

Detailed thin section analysis of SSMet 3/408.

Mineralogy			Textures	
			Grain shape	**Grain Size**
Essential Minerals		**%**		**Rock average:** medium
Olivine		25	subhedral	**Rock range:** fine - coarse
Orthopyroxene		40	anhedral - subhedral	**Description:** Olivine is finer than pyroxene,
Clinopyroxene		25	anhedral - subhedral	the opaque minerals are very fine grained.
Calcite		3	anhedral	Orthopyroxene and clinopyroxene are equal
Opaque minerals		3	bleby	in size are the coarses grained minerals
Garnet		4	subhedral - irregular	present ranging from medium to coarse grained.
	Total	100	**Common textures**	
Accessory Minerals		**No. observed**	There was a poikilitic texture with the opaque minerals enclosing calcite, garnet and olivine were enclosed by the pyroxene. Olivine was present as individual grains as well as an aggregate. The pyroxenes were highly fractured and insome places appeared to have an exsolution texture, some orthopyroxene minerals had zoned extinction. Veins of serpentine were present with small amount of calcite within them.	
Brown mineral		1		
Biotite		4		
	Total	5	**Alteration** (layers of weaker material)	
Modal Composition			Olivine was completely serpentinised however opaque mineralisation does not appear connected with the serpentinisation. A mesh texture was present in all the olivine minerals. Orthopyroxene and clinopyroxene appeared dusty and showed alteration to a fine grained mass of chlorite and talc. Alteration of the pyroxenes was highest around contact with olivine minerals and where opaque mineralisation occured. Clinopyroxene was altered preferentially along cleavage plains and fractures. A mesh texture in the olivine was due to the alteration to serpentine.	
		Recalc.		
P =	0	0.0		
Ol =	25	27.8	**Degree of Alteration**	70% high
Opx =	40	44.4	**Microfracturing**	
Cpx =	25	27.8	**Following grain boundaries**	Yes
Hbl =	0	0.0	**Across crystals**	Yes
Total	90	100	**Fabric**	
IUGS name	Olivine websterite		Veins within the thinsection as well as fractures in the pyroxenes run perpendicular to the length of the borehole core	
Colour Index	Ultramafic			

Detailed thin section analysis of SSMet 3/525.

Mineralogy			Textures	
			Grain shape	**Grain Size**
Essential Minerals		**%**		**Rock average:** fine
Orthopyroxene		15	anhedral	**Rock range:** fine - medium
Clinopyroxene		10	anhedral	**Description:** The thinsection was dominated
Spinel		3	euhedral	by fine grained alteration material, olivine was
Olivine		32	subhedral	medium grained, opaques were fine to med-
Calcite		15	anhedral - euhedral	ium grained. Could not see original grain
Milky white/yellow mineral		15	not possible to tell	boundaries for most crystals
Opaque minerals		10	anhedral	
			Common textures	
			Opaque minerals were present within the olivine, calcite was ringed	
Total		100	by fine grained serpentinite and chlorite	
Accessory Minerals		**No. observed**	**Alteration** (layers of weaker material)	
Biotite		5	Olivine was completely serpentinised and only the remnants of the	
Garnet		<15	crystals could be seen. Orthopyroxene and clinopyroxene were altered	
			to chlorite as well as amphibole. Carbonate material was replacing the	
			olivine. Precipitation of calcite and opaque minerasl into fractures of	
			olivine, due to serpentinisation.	
			Degree of Alteration	95% High
			Microfracturing	
			Following grain boundaries	No
Total		20	**Across crystals**	Yes
Rock type: Metamorphic			**Fabric**	
Compositionally defined name	Spinel-olivine garnet-bearing calc-silicate		Fractures in olivine where serpentinisation occurred showed a prefered orientation perpendicular to the long axis of the borehole	
Protolith	dolomite		core.	

Detailed thin section analysis of SSMet 3/532.

Mineralogy			Textures	
			Grain shape	**Grain Size**
Essential Minerals		**%**		**Rock average:** fine
Calcite		10	anhedral	**Rock range:** fine - medium
Olivine		10	anhedral	**Description:** Olivine and pyroxene were
Garnet		2	subhedral	fine grained. The milky material was very
Orthopyroxene		25	anhedral	fine grained, forming a matrix type material
Clinopyroxene		5	anhedral	about the crystals. Calcite was medium
Opaque minerals		10	not possible to tell	grained and garnet was very fine grained.
Milky white/yellow material		38	not possible to tell	
			Common textures	
			All the minerals were heavily fractured, precipitation of the opaques and milky material occurred along fractures and cleavages. The calcite	
	Total	100	crystals were ringed by serpentine.	
Accessory Minerals		**No. observed**	**Alteration (layers of weaker material)**	
Biottie		4	Olivine was completely serpentinised, only the remnant shape of the	
Prehnite		2	original crystals could be seen. Amphibole and muscovite alteration	
Spinel		<10	material were present around the olivine crystals. Pyroxene showed	
			a high degree of alteration to chlorite	
			Degree of Alteration	95% High
			Microfracturing	
			Following grain boundaries	No
	Total	16	**Across crystals**	Yes
Rock type: Metamorphic			**Fabric**	
Compositionally defined name	Garnet-olivine spinel-bearing calc-silicate		Bands of orthopyroxene rich and orthopyroxene poor layers of approx. 1 cm were observed. Layers which were orthopyroxene poor tended to be concentrated in the milky minerals	
Protolith	dolomite			

Detailed thin section analysis of SSMet 4/15.

Mineralogy			Textures	
			Grain shape	**Grain Size**
Essential Minerals		**%**		**Rock average:** medium
Olivine		55	subhedral	**Rock range:** fine - medium
orothopyroxene		30	anhedral	**Description:** The pyroxene minerals were
Clinopyroxene		10	anhedral	larger than olivine minerals present. Olivine
Opaque minerals		5	anhedral - euhedral	minerals were larger than biotie minerals. The
				Opaque minerals were present in two distinct
				sizes, coarse and fine. The majority were
				fine grained.
	Total	100	**Common textures**	
Accessory Minerals		**No. observed**	A poikilitic texture was present with olivine and amphibole enclosed by	
Garnet		5	pyroxene. Orthopyroxene was enclosed and sometimes ringed by	
Amphibole		2	clinopyroxene. Pyroxene was also present as interstitial minerals.	
			Zoned extinction was present in the orthopyroxene. The olivine had	
			a mesh testure as a result of the serpentinisation.	
			Alteration (layers of weaker material)	
			Olivine completely altered to serpentinite, carbonate material, talc	
			and amphibole. Pyroxene appeared speckled and dusty showing	
			alteration to chlorite. Orthopyroxene was more altered cf. clino-	
	Total	7	pyroxene.	
Modal Composition			**Degree of Alteration**	85% high
		Recalc.	**Microfracturing**	
P =	0	0.0	**Following grain boundaries**	Yes
Ol =	55	57.9	**Across crystals**	Yes
Opx =	30	31.6	**Fabric**	
Cpx =	10	10.5	Thinsection appeared to be banded with layers which were greater in	
Hbl =	0	0.0	serpentine and olivine. Heavy minerals were concentrated into	
Total	95	100	these bands too. The opaque minerals showed a prefered orientation	
IUGS name	Iherzolite		parallel with the fractures in the olivine and perpendicular to the length	
Colour Index	Ultramafic		of the borehole core.	

Detailed thin section analysis of SSMet 4/166.

Mineralogy			Textures	
			Grain shape	**Grain size**
Essential Minerals		**%**		**Rock average:** medium
Olivine		45	subhedral - euhedral	**Rock range:** fine - medium
Clinopyroxene		10	subhedral	**Description:** The pyroxene minerals were
Orthopyroxene		35	subhedral	much the largest with olivine uniform in size
Biotite		2	subhedral	and the biotie minerals were fine grained.
Opaque Minerals		5	string like appearance	
Chrlorite		3	subherdral - euhedral	
	Total	100	**Common textures**	
Accessory Minerals		**No. observed**	Poikilitic texture with pyroxene enclosing olivine and biotite. Clinopyroxene was present as interstitial minerals. Irregular grain-boundaries show recrystalisation. Opaque minerals were present mostly in the olivine minerals. Veins of opaque minerals were also present.	
Brown unidentified		1		
Garnet		5		
	Total	6	**Alteration** (layers of weaker material)	
Modal Composition			Olivine completely altered to serpentine. Both orthopyroxene (opx) and clinopyroxene (cpx) were altered showing a dusty appearance with opx showing a greater degree of alteration cf. cpx. Cpx showed alteration mainly along the cleavage. Chlorite was present as an alteration product of the pyroxene.	
		Recalc.	**Degree of Alteration**	50% moderate
P =	0	0.0	**Microfracturing**	
Ol =	45	50.0	**Following grain boundaries**	Yes
Opx =	35	38.9	**Across crystals**	Yes
Cpx =	10	11.1	**Fabric**	
Hbl =	0	0	Bands of olivine rich and olivine poor layers were present resulting in bands of high opaque mineral content and zones of high alteration. The fracturing within the olivine and the opaque minerals showed a perfered orientation perpendicular to the length of the borehole core.	
Total	90	100		
IUGS name	Iherzolite			
Colour Index	Ultramafic			

Detailed thin section analysis of SSMet 5/119.

Mineralogy			Textures	
			Grain shape	**Grain Size**
Essential Minerals		**%**		**Rock average:** medium
Boitite		5	subhedral	**Rock range:** fine - medium
Olivine		65	subhedral	**Description:** Clinopyroxene minerals were the largest,
Orthopyroxene		20	anhedral	followed by othropyroxene, olivine and amphibole.
Clinopyroxene		5	anhedral	The amphibole was present within the olivine
Opaque minerals		2	variable	
Amphibole		3	subhedral	
	Total	100	**Common textures**	
Accessory Minerals		**No. observed**	Biotite, orthopyroxene and clinopyroxene all present as interstitial minerals. Biotite enclosed in olivine and clinopyroxene. Veins of serpentine and carbonate material, generally the serpentine lines the outer contact of the vein with the carbonate material inside. Opaque minerals within veins, orthopyroxene and clinopyroxene. Olivine shows a distinct meshing testure of serpentinisation. The olivine is present as individual crystals and as an aggregate.	
Garnet		4	**Alteration** (layers of weaker material)	
	Total	4	Olivine was altered entirely into serpentinite, with serpentinisation occuring along the grain boundaries and within the mineral along fractures. Alteration of the pyroxenes to chlorite was variable with some minerals being extensively replaced and others remaining unweathered. The orthopyroxene had a higher degree of alteration compared to the clinopyroxene. Talc was present as an alteration product of the pyroxenes and olivine.The serpentinisation suggests hydrothermal alteration.	
Modal Composition			**Degree of Alteration**	80% High
		Recalc.	**Microfracturing**	
P =	0	0	**Following grain boundaries**	Yes
Ol =	65	72.2	**Across crystals**	Yes
Opx =	20	22.2	**Fabric**	
Cpx =	5	5.6	The fractures along which the majority of the alteration occures showed a prefered orientation across the olivine and orthopyroxene. This suggests the fractures aligned to a local stress in the area. Bands of dominantly serpentinised minerals and less serpentised minerals were present. These bands were roughly 3mm in thickness.	
Hbl =	0	0		
Total	90	100.0		
IUGS name	Iherzolite			
Colour Index	Ultramafic			

Detailed thin section analysis of SSMet 5/291.

Mineralogy			Textures	
			Grain shape	**Grain Size**
Essential Minerals		**%**		**Rock average**: medium
Olivine		40	anhedral - subhedral	**Rock range:** fine - coarse
Orthopyroxene		20	anhedral - subhedral	**Description:** The opaque minerals take their
Clinopyroxene		25	subhedral	shape of the fractures in the olivine. The
Tremolite		3	subhedral - euhedral	thinsection was dominated by medium grained
Opaque minerals		12	irregular	olivine and pyroxene, pyroxene was also present as coarse grains. The opaque minerals were fine grained
Total		100		
Accessory Minerals		**No. observed**	**Common textures**	
Biotite		2	Olivine showed mesh and hour glass textures due to serpentinisation. The opaque minerals were present mainly within the fractures of the olivine. A poikilitic texture is present with olivine enclosed by pyroxene and a subpoikilitic texture was shown by orthopyroxene partially enclosed by clinopyroxene. Irregular grain boundaries show there had been a degree of recrystalisation. Veins of serpentinite and carbonatious material were present.	
Total		2	**Alteration** (layers of weaker material)	
Modal Composition			Olivine was completely serpentinised, the pyroxene minerals have a dusty, speckled appearance due to extensive and uniform alteration to chlorite and talc. Clinopyroxene was altered along its cleavage.	
		Recalc.		
P =	0	0.0		
Ol =	40	47.1	**Degree of Alteration**	85% high
Opx =	20	23.5	**Microfracturing**	
Cpx =	25	29.4	**Following grain boundaries**	Yes
Hbl =	0	0.0	**Across crystals**	Yes
Total	85	100	**Fabric**	
IUGS name	Iherzolite		The opaque minerals show a perfered orientation perpendicular to the length of the borehole core.	
Colour Index	Ultramafic			

Detailed thin section analysis of SSPit 149/7.

Mineralogy			Textures	
			Grain shape	**Grain Size**
Essential Minerals		**%**		**Rock average:** very fine
Opaque minerals		45	massive, lath-like	**Rock range:** very fine - fine
Pyroxene (cant distinguish apart)		30	anhedral	**Description:** The olivine crystals were very
Olivine		24	subhedral	fine grained with the pyroxenes slightly
Calcite		1	na	larger in size, the opaque minerals were very
				fine grained and the calcite crystal size could
				not be determined as it was present only in
	Total	100		veins.
Accessory Minerals		**No. observed**	**Common textures**	
Amphibole		1	The opaque minerals were present within the olivine but also enclosed	
Garnet		3	the olivines and pyroxenes. There was an hourglass and mesh texture	
			which has resulted from the serpentinisation of the olivine.	
			Alteration (layers of weaker material)	
			Serpentinisation of the olivine has resulted in the precipitation of magnetite following the substitution of Fe2+ for Mg, the serpentine shows a small degree of alteration to talc. The pyroxenes have been altered to chlorite and have a dusty appearance. The alteration within this thinsection is extremely high.	
			Degree of Alteration	95% high
	Total	4	**Microfracturing**	
Rock type: Metamorphic			**Following grain boundaries**	No
Compositionally defined name	Garnet and amphibole-bearing serpentinite		**Across crystals**	Yes
			Fabric	
Protolith	pyroxenite		The veins all run perpendicular to the length of the borehole core.	

Detailed thin section analysis of SSPit 150/16.

Mineralogy			Textures	
			Grain shape	**Grain Size**
Essential Minerals		**%**		**Rock average:** medium
Orthopyroxene		45	anhedral	**Rock range:** fine - coarse
Clinopyroxene		40	anhedral	**Description:** Pyroxene crystals dominated the thinsection with a range in size from medium to coarse. Plagioclase is interstitial and was present as fine crystals of a subhedral shape. The opaque minerals were irregular in shape and size
Plagioclase		10	interstitial - subhedral	
Calcite		2	anhedral - euhedral	
Opaque minerals		3	bleby	
Total		100	**Common textures**	
Accessory Minerals		**No. observed**	There is a poikilitic texture present with olivine enclosed within pyroxene, plagioclase within the opaque minerals and within pyroxene. Plagioclase shows an exsolution texture and irregular grain boundaries show there has been a dregree of recrystalisation. Veins of a fibrous serpentinite are present, possibly lizardite.	
Garnet		4		
Olivine		2		
Total		6	**Alteration** (layers of weaker material)	
Modal Composition			Both types of pyroxene were altered to chlorite and talc, with a dusty spotted appearance, however orthopyroxene was more weathered than clinopyroxene (cpx) and cpx showed preferential alteration to amphibole along its cleavage planes. Plagioclase was extensively altered uniformally or starting in the centre of the mineral. Alteration around the carbonate material was much higher and some carbonate material was present as an alteration product.	
		Recalc.		
P =	10	10.5		
Ol =	0	0.0		
Opx =	45	47.4	**Degree of Alteration**	50% moderate
Cpx =	40	42.1	**Microfracturing**	
Hbl =	0	0.0	**Following grain boundaries**	Yes
Total	95	100	**Across crystals**	No
IUGS name	Gabbronorite		**Fabric**	
Colour Index	Melanocratic		Coarse grained and granular	

Detailed thin section analysis of SSPit 154/40.

Mineralogy			Textures	
			Grain shape	**Grain Size**
Essential Minerals		**%**		**Rock average:** coarse
Orthopyroxene		88	subhedral	**Rock range:** fine - coarse
Clinopyroxene		5	subhedral	**Description:** The pyroxenes were dominantly
Opaque minerals		3	subhedral	coarse grained with calcite, prehnite and
Calcite		2	anhedral	opaque minerals were all fine grained.
Prehnite		2	anhedral	
Total		100	**Common textures**	
Accessory Minerals		**No. observed**	Prehnite was present as a randomly orientated aggregate of crystals	
Biotite		4	which display a wavy/ complicated extinction. There was a poikilitic	
Garnet		<10	texture orthopyroxene, calcite and opaque minerals ringed by prehnite.	
Olivine		2	Veins of carbonate material was present.	
			Alteration (layers of weaker material)	
Total		16	Othopyroxene showed greater alteration compared to clinopyroxene.	
Modal Composition			Both were altered to chlorite, amphibole (tremolite) and possibly talc.	
		Recalc.	Olivine had a moderate degree of replacement by serpentine.	
P =	0	0.0	**Degree of Alteration**	20% low
Ol =	0	0.0	**Microfracturing**	
Opx =	88	94.6	**Following grain boundaries**	Yes
Cpx =	5	5.4	**Across crystals**	Yes
Hbl =	0	0.0	**Fabric**	
Total	93	100	The thinsection was dominated by pyroxene crystals which were coarse	
IUGS name	Orthopyroxenite		grained and granular. There was a slight preferred orientation of the	
Colour Index	Ultramafic		opaque minerals.	

Detailed thin section analysis of SSPit 157/17.

Mineralogy			Textures	
			Grain shape	**Grain Size**
Essential Minerals		**%**		**Rock average:** coarse
Clinopyroxene		15	subhedral	**Rock range:** fine - coarse
Orthopyroxene		80	subhedral	**Description:** The pyroxenes were coarse with
Opaque minerals		5	anhedral - euhedral	orthopyroxene crystals on average greater in size than clinopyroxene. The opaque minerals were all fine grained.
Total		100	**Common textures**	
Accessory Minerals		**No. observed**	There was a poikilitic texture with the opaque minerals enclosed within proxene and a subpoikilitic texture with prehnite partially enclosing calcite. Some of the orthopyroxene showed zoned extinction. Prehnite exhibited a wavy almost radial extinction. Veins of prehnite and calcite were present, occasionally the two were present within the same vein.	
Olivine		2		
Garnet		4		
Biotite		3		
Calcite		<15		
Muscovite		2		
			Alteration (layers of weaker material)	
Total		26	Orthopyroxene and clinopyroxene showed alteration to chlorite with a dusty speckled appearance. Amphibole was also present as an alteration product within the pyroxenes. It is possibly tremolite. The veins of prehnite were cause by alteration in low grade metamorphic processes.	
Modal Composition				
		Recalc.		
P =	0	0.0		
Ol =	0	0.0	**Degree of Alteration**	50% moderate
Opx =	80	84.2	**Microfracturing**	
Cpx =	15	15.8	**Following grain boundaries**	Yes
Hbl =	0	0.0	**Across crystals**	Yes
Total	95	100	**Fabric**	
IUGS name	Olivine websterite		Most of the grains were granular to slightly columnar. The opaque minerals show no apparent preferred orientation.	
Colour Index	Ultramafic			

Detailed thin section analysis of SSPit 158/9.

Mineralogy			Textures	
			Grain shape	**Grain Size**
Essential Minerals		**%**		**Rock average:** fine
Opaque minerals (magnitite)		15	lath-like	**Rock range:** very fine -fine
Clinopyroxene		15	anhedral - interstitial	**Description:** Very fine grained mass of olivine
Orthopyroxene		25	anhedral	with fine grained pyroxene, interstitial pyrox-
Olivine		45	subhedral	ene and opaque minerals.
			Common textures	
			There was a poikilitic texture with olivine enclosed in orthopyroxene. Olivine was present as an aggregate and as individual grains. Opaque minerals appeared lath like and were present within minerals (mainly olivine) and along grain boundaries. Olivine showed a mesh and hourglass texture as a result of the serpentinisation.	
Total		100		
Accessory Minerals		**No. observed**	**Alteration (layers of weaker material)**	
Rutile		2	Olivine has been serpentinised extensively during which there has been substution of Fe^{2}+ for Mg and the resulting spare Fe^{2}+ has been incorporated into magnetite. The serpentine is altering to talc. Pyroxene crystals have been heavily altered to chlorite. Prehnite is present as an alteration product.	
Calcite		< 20		
Amphibole		5		
Garnet		< 5		
			Degree of Alteration	95% high
			Microfracturing	
			Following grain boundaries	no microfracturing
			Across crystals	no microfracturing
			Fabric	
Total		< 32	Preferential orientation of opaque minerals perpendicular to the length of the borehole. This could be a result of the fractures in the olivine (in which the opaques were mineralised) were formed in response to a local stress. There was a slight layering with 'opaque-rich' and opaque-poor' layers.	
Rock type: Metamorphic				
Compositionally defined name	Garnet and amphibole-bearing serpentinite			
Protolith	pyroxenite			

Detailed thin section analysis of SSPit 161/12.

Mineralogy			Textures	
			Grain shape	**Grain Size**
Essential Minerals		**%**		**Rock average:** medium
Orthopyroxene		60	subhdral	**Rock range:** medium - coarse
Clinopyroxene		25	subhdral	**Description:** The pyroxenes were medium to coarse grained with the altered plagioclase present as interstitial crystals. Some fine grained crystals of plagioclase were observed as well as fine opaque minerals, biotite and amphibole.
Plagioclase		15	interstitial - subhedral	
Total		100		
Accessory Minerals		**No. observed**	**Common textures**	
Biotite		5	There was a granular texture as the thinsection was dominated by pyroxene minerals which appear equidimentional. Olivine was partially enclosed by chlorite laths. The crystals of the alteration product prehnite were randomly orientated in a crystal aggregate.	
Opaque minerals		6		
Olivine		1		
Amphibole		3		
			Alteration (layers of weaker material)	
			Prehnite is present as a late stage replacement product of feldspar, replacenment of pyroxene with prehnite has started. This replacement was extensive. Pyroxene was completely altered in some crystals and in others was only slightly altered. Alteration to chlorite and talc was common and the crystals therefore had a dusty spotted appearance.	
Total		15		
Modal Composition				
		Recalc.		
P =	15	15	**Degree of Alteration**	30% low, plagioclase was almost completely replaced
Ol =	0	0		
Opx =	60	60	**Microfracturing**	
Cpx =	25	25	**Following grain boundaries**	No
Hbl =	0	0	**Across crystals**	No
Total	100	100	**Fabric**	
IUGS name	Clinopyroxene norite		The crystals were medium to coarse and granular in shape, no fabric was present.	
Colour Index	Melanocratic			

Summarised analyses for thin sections SS3/63 – SS4/245.

Sample Name	Rock Type	Mineralogy		Estimated Avg. grain size	Alteration		Degree of Alteration	Notes
		Fits XRD	Essential		Serp.	Chlor.		
SS3/63	Parapyx	Y	Ol,Pyx,Om,Am	F - M	Y	Y	High	Green spinel present as accessory, rounded grains,prefered orientation of opaque minerals
SS3/72	Parapyx	Y	Pyx,Ol	M - VC	Y	Y	Low	Green spinel being altered itself, calcite present, olivine grains fine and rounded
SS3/81	Parapyx	Y	Ol,Pyx, Gr	M - C	Y	Y	High	Green spinel showing alteration, veins of carbonate material
SS3/101	Parapyx	Y	Ol,Pyx,Om,Am	F - M	Y	Y	High	Fractures in pyroxene radiating outward from olivine minerals that are enclosed
SS3/154	Parapyx	Y	Ol,Pyx,Om	F - M	Y	Y	High	high & low alteration bands corrispond with olivine or pyroxene rich zones respectively
SS3/181	Parapyx	Y	Ol,Pyx,Gr	VF - M	Y	Y	High	Green spinel present as essential mineral(altered), banding of olivine rich and poor zones
SS3/236	Parapyx	Y	Ol,Pyx,Am,Om	F - M	Y	Y	High	Opaque minerals mainly in veins & in pyroxene, intergrowth texture pyx and vesuvianite
SS3/318	Parapyx	Y	Ol,Pyx	F	Y	Y	Very High	Orthopyroxene dominant, steal blue birefringence for chlorite, garnet ringed by hydrogrossular
SS3/327	Parapyx	Y	Ol,Pyx,Om,Am	F - M	Y	Y	Moderate	Pyroxenes highly fractured, carbonate material present in veins
SS3/349	Parapyx	Y	Ol,Pyx,Sp,Om	C	Y	Y	Moderate	Green fractured and altered spinel present as an essential mineral, calcite present
SS3/367	Parapyx	Y	Ol,Pyx,Om	M	Y	Y	High	Accessory green spinel, olivine enclosed by pyroxene less altered, olivine rich & poor zones
SS3/427	Parapyx	Y	Ol,Pyx,Am,Om	F	Y	Y	High	Pyroxenes highly fractured, intergrowth textures present in pyroxenes
SS3/487	Parapyx	Y	Ol,Pyx	F - M	Y	Y	Moderate	Minor serpentinisation, opaque minerals present in accessory abundences
SS3/518	Parapyx	Y	Ol,Pyx	M	N	Y	Low	Clinopyroxene is interstitial, almost completely altered green spinel present, ringed by pyroxenes
SS3/559	Parapyx	Y	Pyx	M	N	Y	Low	Almost completely composed of pyroxene, orthopyroxene shows zoned extinction
SS3/586	Parapyx	Y	Pyx,Ol	F	Y	Y	High	Hydrogrossular present, olivine rich & poor zones with corrisponding alteration high zones
SS3/608	Parapyx	Y	Pyx,Ol	M - C	Y	Y	Moderate	Pyroxene highly fractured, fine grained olivine completely rounded with irregular crystal shapes
SS3/638	Parapyx	Y	Pyx,Ol,Am	M	N	Y	Low	No opaque minerals, veins of serpentine which are parellel to the long axis of the borehole core
SS3/663	Parapyx	Y	Pyx,Ol	F - M	Y	Y	High	Bands of olivine rich & poor zones, olivine is fine grained whilst pyroxene is medium grained
SS3/684	Parapyx	Y	Ol,Pyx,Am,Gr	M	Y	Y	High	Reaction rings of intergrown tremolite and phlogopite
SS4/37	Parapyx	Y	Pyx,Ol	F	Y	Y	High	Olivine irregular in shape and anhedral, pyroxene interstitial
SS4/56	Parapyx	Y	Ol,Pyx,Am	M	Y	Y	High	Heavy alteration along cleavages
SS4/88	Parapyx	Y	Ol,Pyx,Om,Am	M	Y	Y	High	Garnet and opaque minerals present in veins which cut across all minerals
SS4/92	Parapyx	Y	Pyx,Ol	F	Y	Y	High	Banded with three distinct zones of olivine, pyroxene and a very fine grained material present
SS4/188	Parapyx	Y	Ol,Pyx,Om	F - M	Y	Y	High	Banding of fine grained rounded crystals of olivine. Green spinel and vesuvianite present.
SS4/208	Parapyx	Y	Ol,Pyx	F	Y	Y	High	Green spinel present. Large reaction ring of pyroxene surrounded by highly altered olivine
SS4/239	Fpyx	Y	Pyx,Plg,Am,Ol	M	N	Y	Moderate	Plagioclase is interstitial and heavily altered. Tremolite laths.
SS4/245	Fpyx	Y	Pyx,Plg,Am,Ol	F - M	Y	Y	High	Banding of olivine and opaque minerals. Amphibole is coarse grained

Summarised analyses for thin sections SS4/254 – SSP159/7.

Sample Name	Rock Type	Mineralogy		Estimated Avg. grain size	Alteration		Degree of Alteration	Notes
		Fits XRD	Essential		Serp.	Chlor.		
SS4/254	Parapyx	Y	Ol,Pyx,Am,Gr	F - M	Y	Y	High	Plagioclase not present. Opaque minerals enclosing olivine and as an alteration product.
SS4/283	Parapyx	Y	Pyx	M - C	N	Y	Low	Few opaques, olivine and amphible in small amounts. Rounded grain boundies and intergrowths
SS4/291	Parapyx	Y	Pyx	F	N	Y	High	Orthopyroxene completely altered to chlorite, bands of alteration to tremolite and phlogopite
SS4/322	Parapyx	Y	Pyx,Am,Bio,Ol	M	N	Y	Moderate	Small amount of olivine. Opaques only in olivine
SS5/22	Parapyx	Y	Ol,Pyx,Ves	F	Y	Y	High	Intergrown pyroxene and vesuvianite, low amounts of opaques not precipitating out of olivine
SS5/42	Parapyx	Y	Ol,Pyx	F - M	Y	Y	High	Low amounts of opaques, some very coarse(12mm), alteration of crystals along cleavage
SS5/68	Parapyx	Y	Pyx,Ves	C	N	Y	Moderate	Low amounts of opaques, calcite in veins, intergrowths of pyroxene and vesuvianite
SS5/90	Parapyx	Y	Pyx,Am,Bio	C	N	Y	High	Dominated by pyroxene, very coarse grained, highly fractured, all fractures run in one direction
SS5/181	Parapyx	Y	Ol,Pyx,Gr,Am	F	Y	Y	High	Poikilitic texture. Opaque minerals have a perfered orientation parallel to length of borehole core
SS5/189	Parapyx	Y	Ol,Pyx,Pm,Am	F - M	Y	Y	High	Pyroxene coarse, fractures withincontain serpentine. bands of olivine rich zones, very fractures
SS5/223	Parapyx	Y	Ol,Pyx,Cal,Am	F - M	Y	Y	High	Calcite in veins, pyroxene exhibits unusual undulatory extinction. Banding of olivine with alteation
SS5/264	Parapyx	Y	Pyx,Pm,Bio,Am	M	Y	Y	Moderate	Veins of serpentinite (lizardite). Alteration on pyroxene uniform and spotted
SS5/305	Parapyx	Y	Ol,Pyx,Sp	F - M	Y	Y	High	Green spinel, very fine grained and subhedral. Concentrated where alteration is highest
SS5/315	Parapyx	Y	Pyx,Cal,Am,Ol	F - M	Y	Y	High	Medium grained spinel, recrystalised amphibole, chlorite alteration heavy on grain boundaries
SS5342	Parapyx	Y	Pyx,Cal	M - C	Y	Y	Moderate	Accessory olivine, elongate rounded opaques, alteration concentrated into zones
SSP159/7	Fpyx	Y	Py,Plg,Am,Ol	M	Y	Y	High	Plagiocalse completely altered, medium grained opaque, olivine altered to serpintine and chlorite

SSMet 3 Photomicrographs

SSMet 3/18 PPL field of view 7 mm

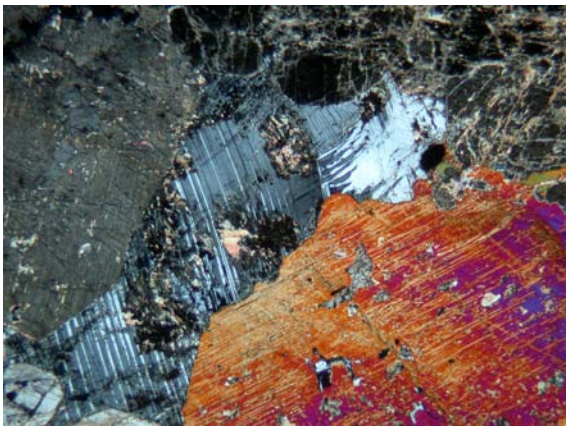

SSMet 3/18 XPL field of view 7 mm

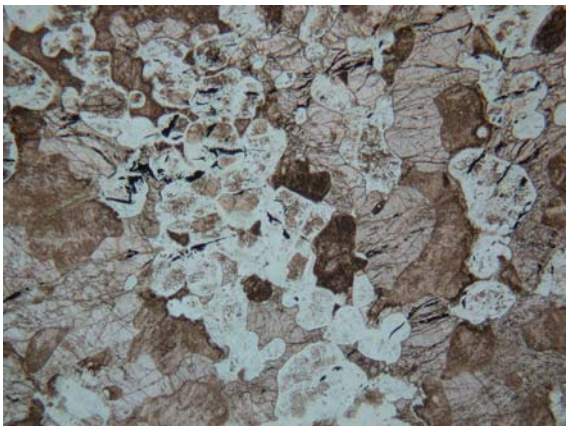

SSMet 3/763 PPL field of view 7 mm

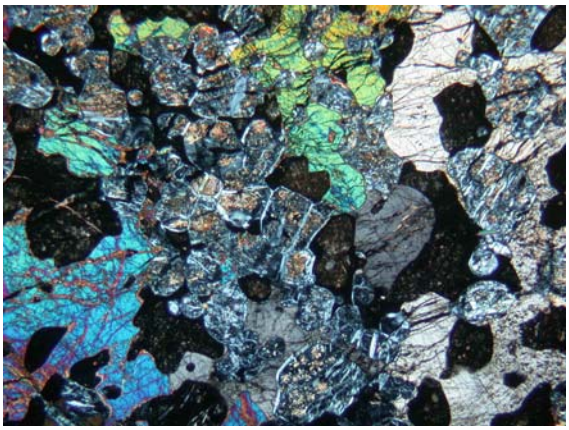

SSMet 3/63 XPL file of view 7 mm

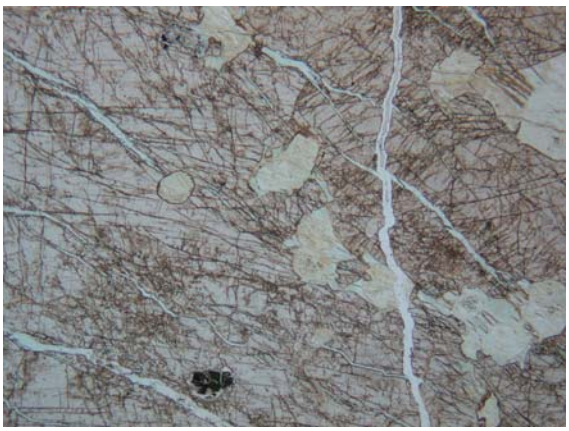

SSMet 3/72 PPL field of view 7 mm

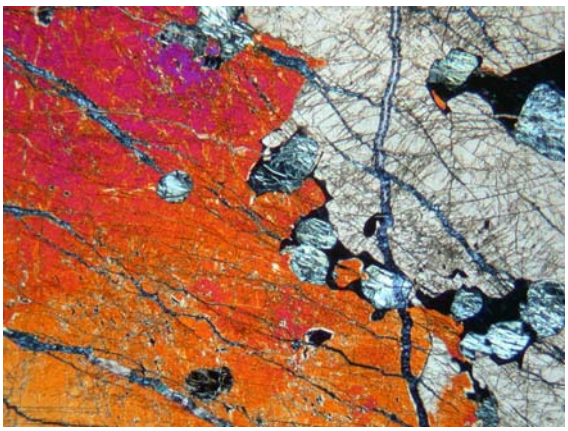

SSMet 3/72 XPL field of view 7 mm

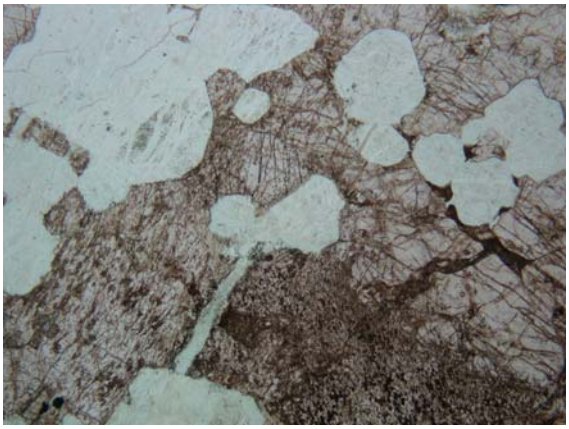

SSMet 3/81 PPL field of view 7 mm

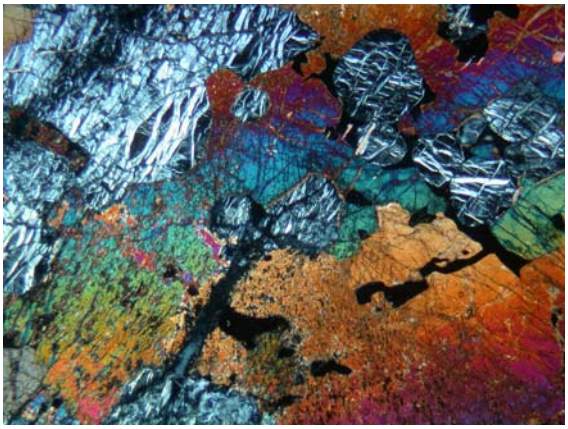

SSMet 3/81 XPL field of view 7 mm

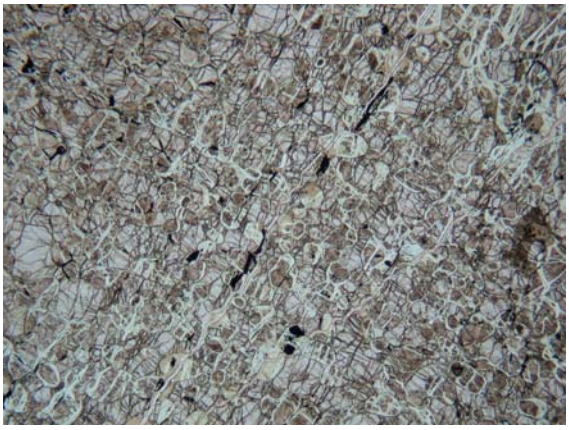

SSMet 3/101 PPL field of view 7 mm

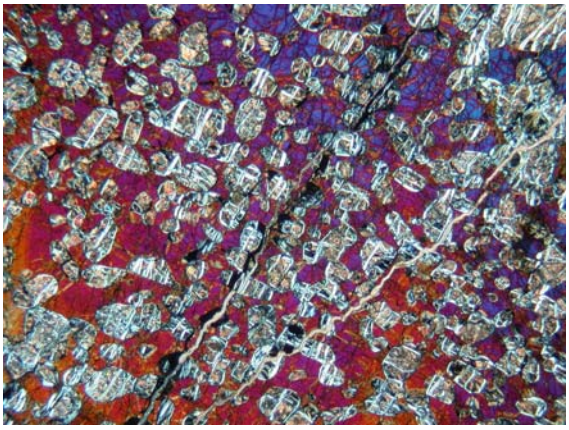

SSMet 3/101 XPL field of view 7 mm

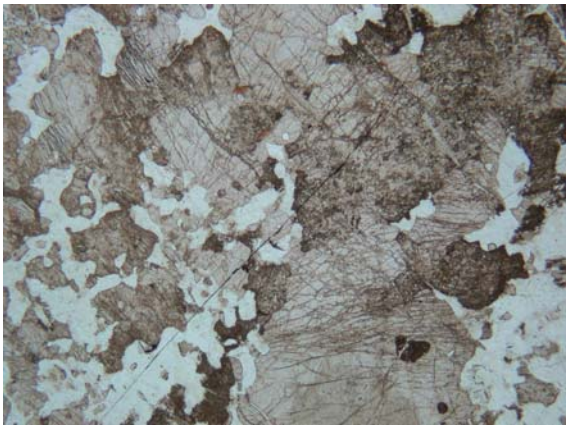

SSMet 3/154 PPL field of view 7 mm

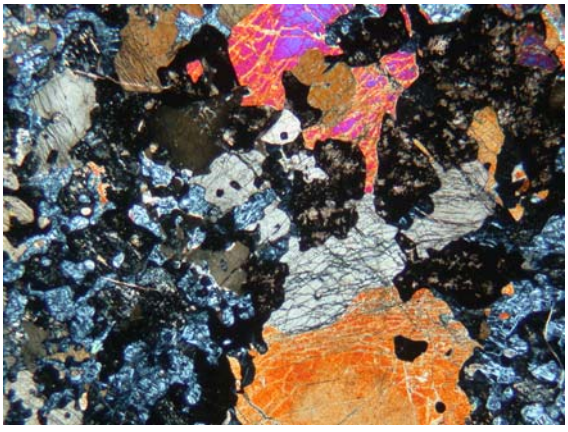

SSMet 3/154 XPL field of view 7 mm

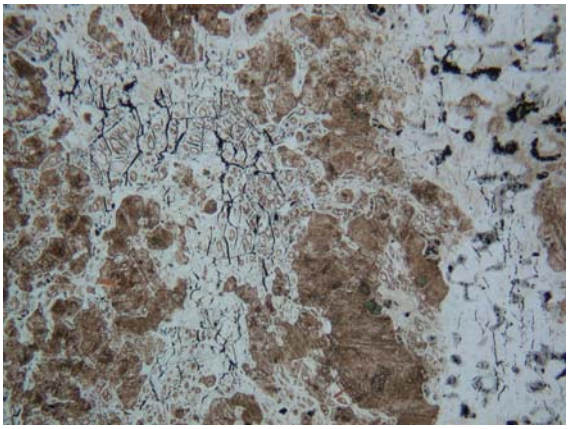

SSMet 3/181 PPL field of view 7 mm

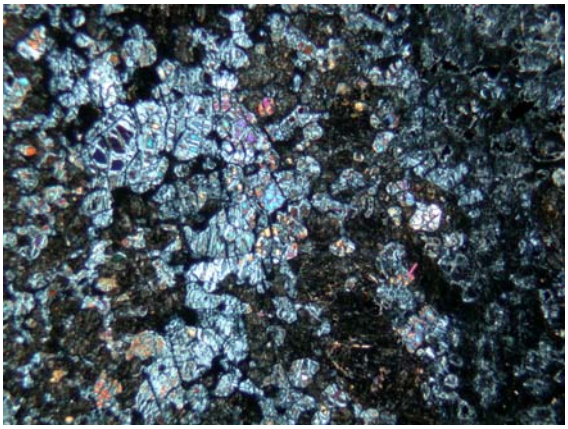

SSMet 3/181 XPL field of view 7 mm

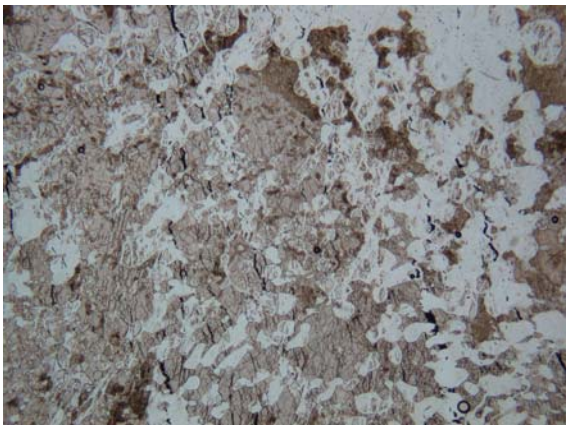

SSMet 3/236 PPL field of view 7 mm

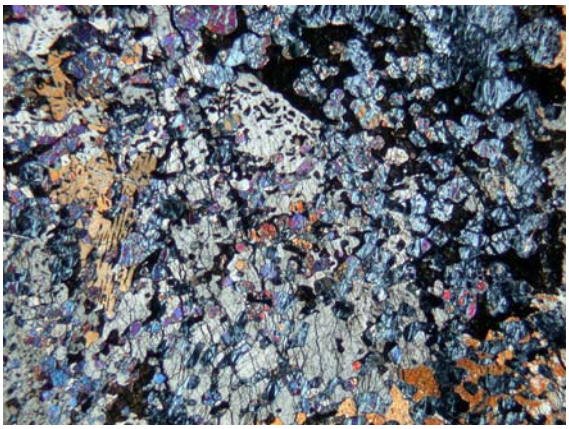

SSMet 3/236 XPL field of view 7 mm

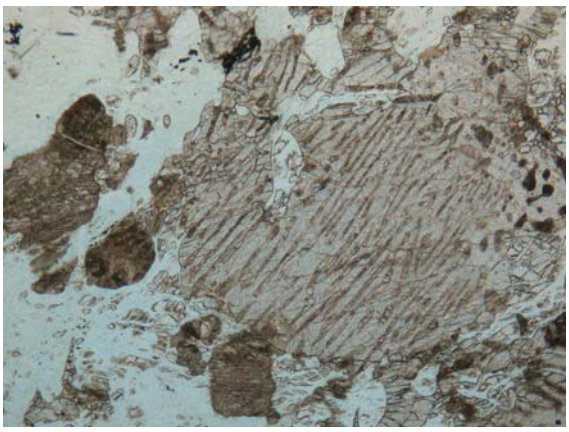

SSMet 3/236 PPL field of view 3 mm

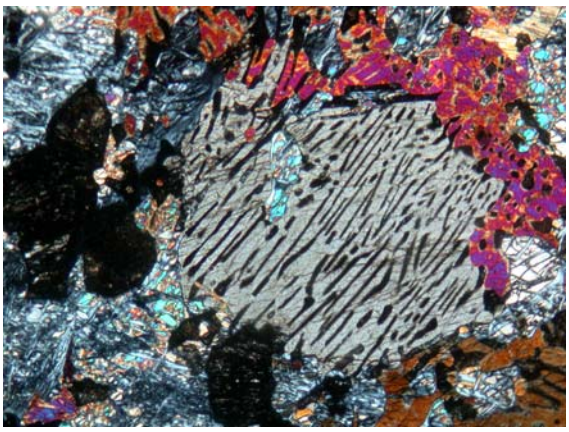

SSMet 3/236 field of view 3 mm

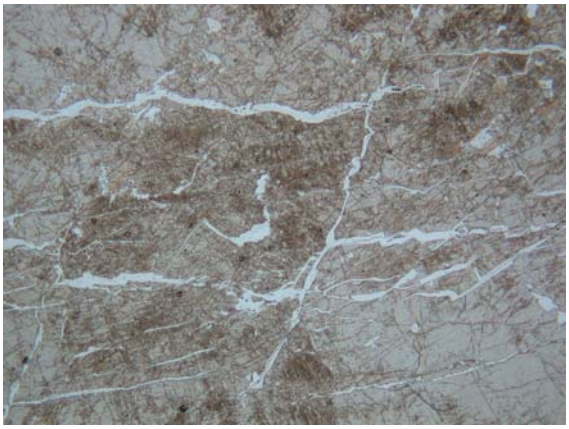

SSMet 3/276 PPL field of view 7 mm

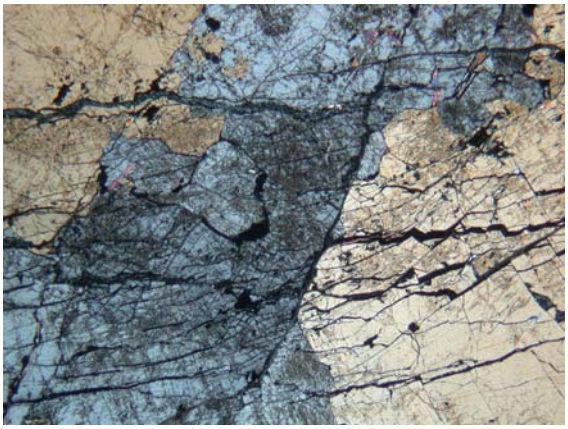

SSMet 3/276 XPL field of view 7 mm

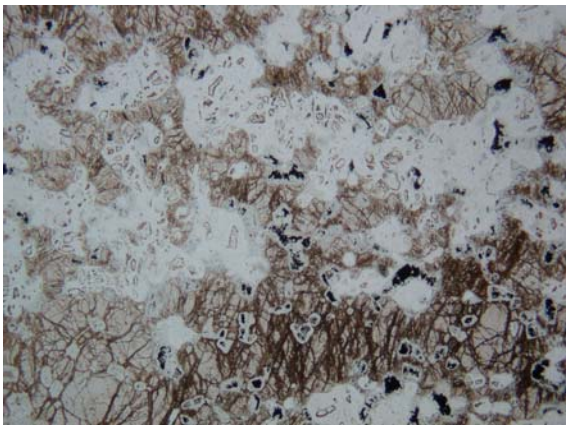

SSMet 3/318 PPL field of view 7 mm

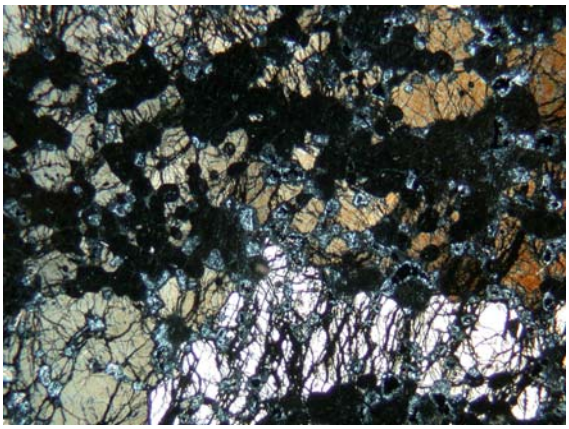

SSMet 3/318 XPL field of view 7 mm

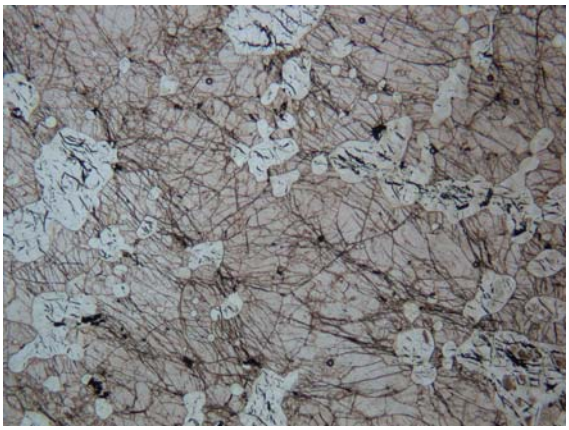

SSMet 3/327 PPL field of view 7 mm

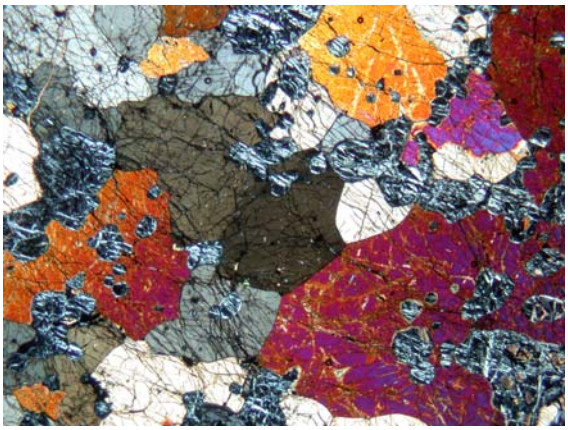

SSMet 3/327 XPL field of view 7 mm

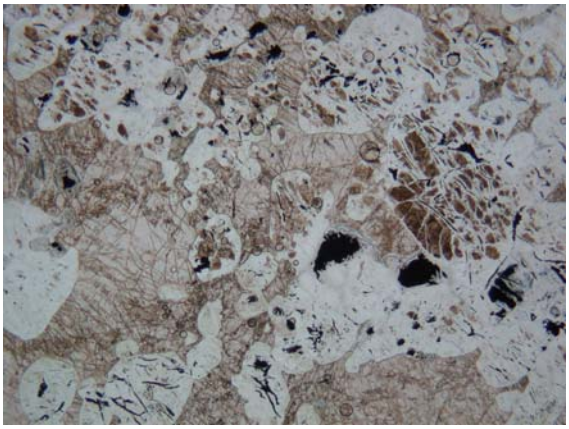

SSMet 3/349 PPL field of view 7 mm

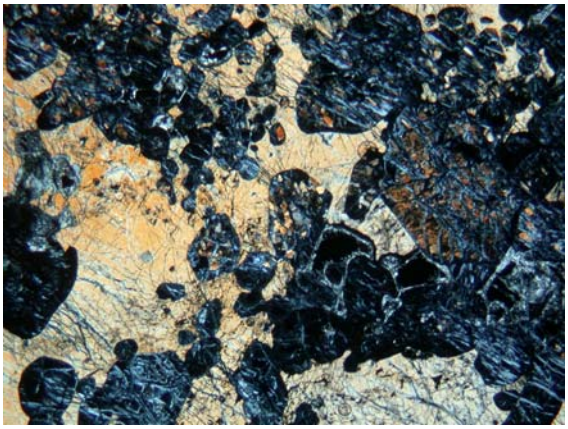

SSMet 3/349 field of view 7 mm

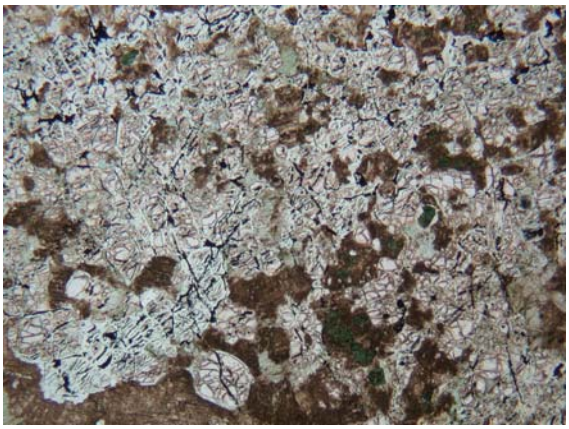

SSMet 3/367 PPL field of view 7 mm

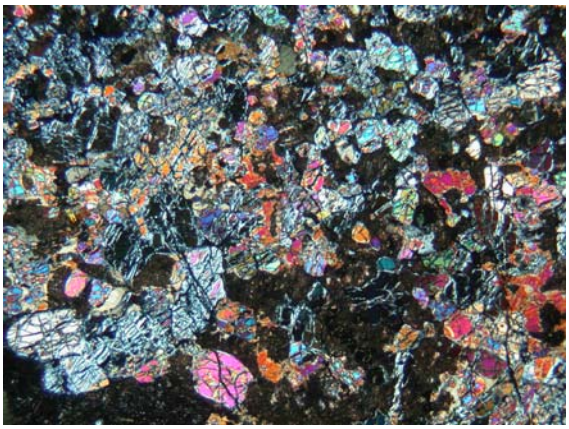

SSMet 3/367 XPL field of view 7 mm

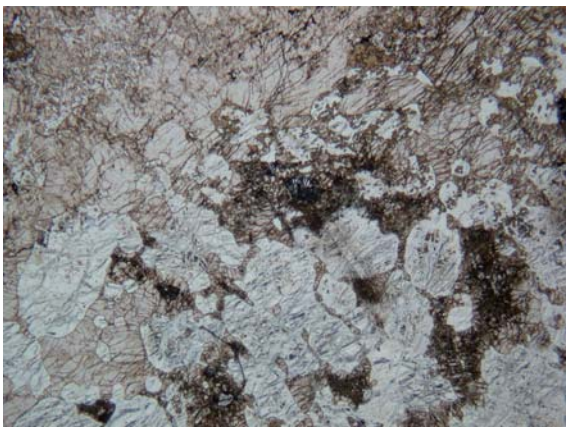

SSMet 3/408 PPL field of view 7 mm

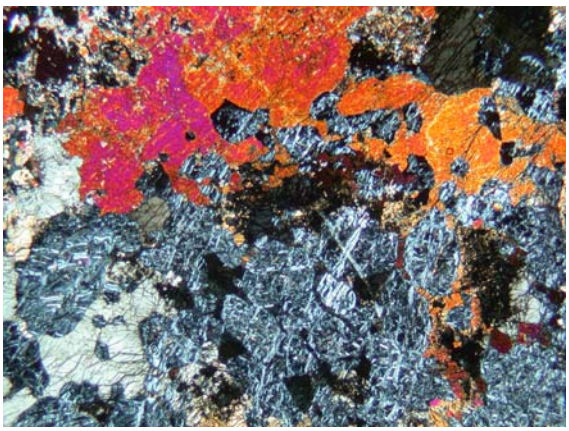

SSMet 3/408 XPL field of view 7 mm

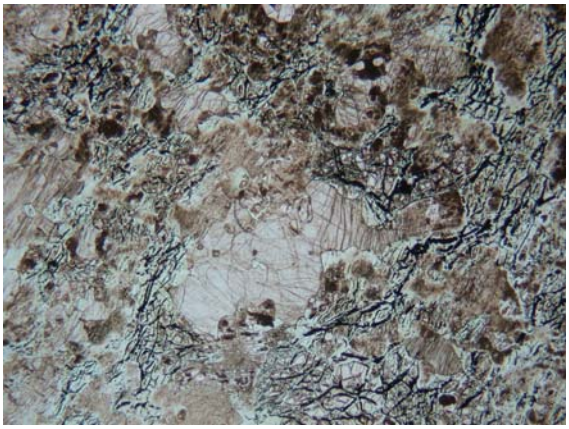

SSMet 3/427 PPL field of view 7 mm

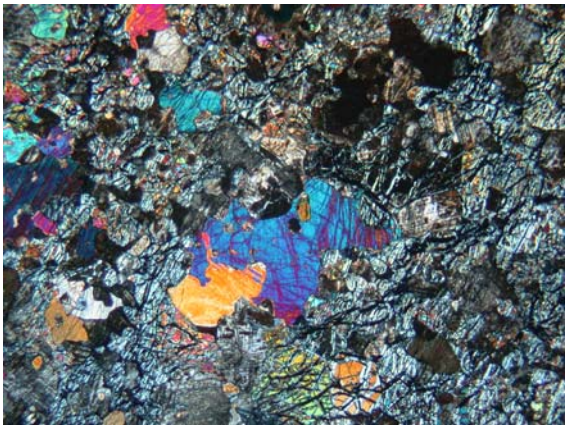

SSMet 3/427 XPL field of view 7 mm

SSMet 3/470 PPL field of view 7 mm

SSMet 3/470 XPL field of view 7 mm

SSMet 3/487 PPL field of view 7 mm

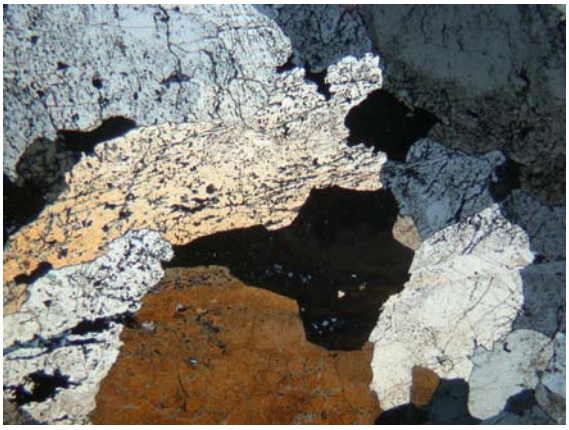

SSMet 3/487 XPL field of view 7 mm

SSMet 3/518 PPL field of view 7 mm

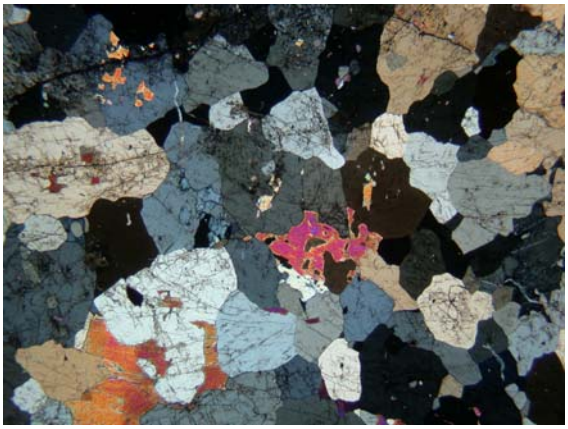

SSMet 3/518 XPL field of view 7 mm

SSMet 3/524a PPL field of view 7 mm

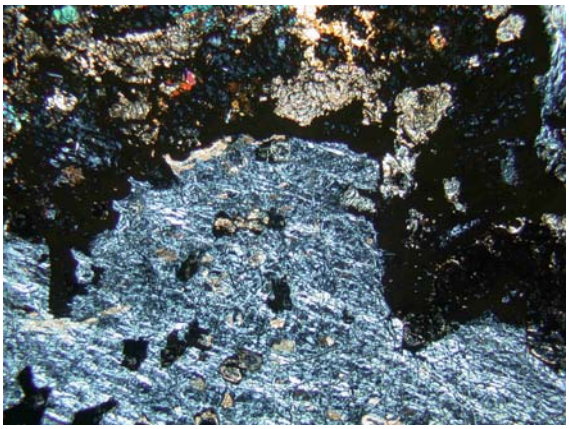

SSMet 3/524a XPL field of view 7 mm

SSMet 3/532 PPL field of view 7 mm

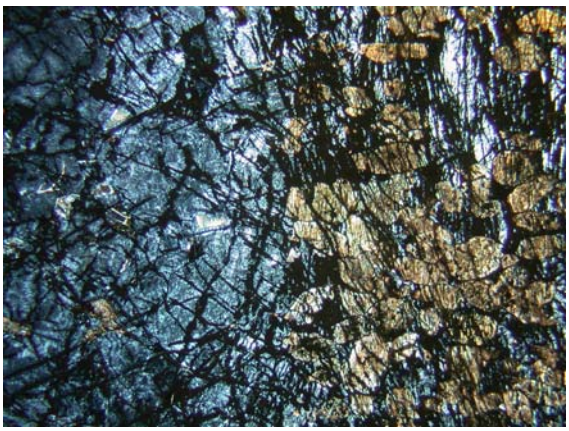

SSMet 3/532 field of view 7 mm

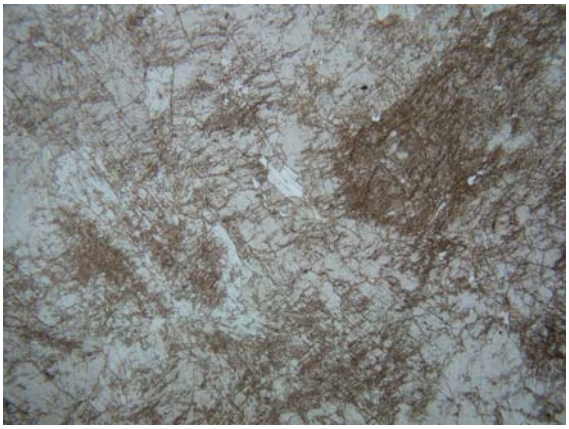

SSMet 3/559 PPL field of view 7 mm

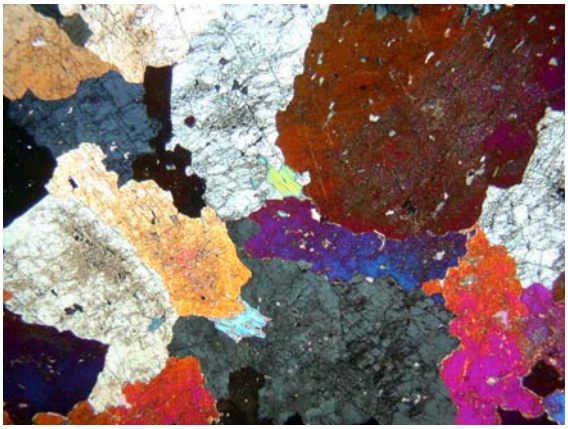

SSMet 3/559 XPL field of view 7 mm

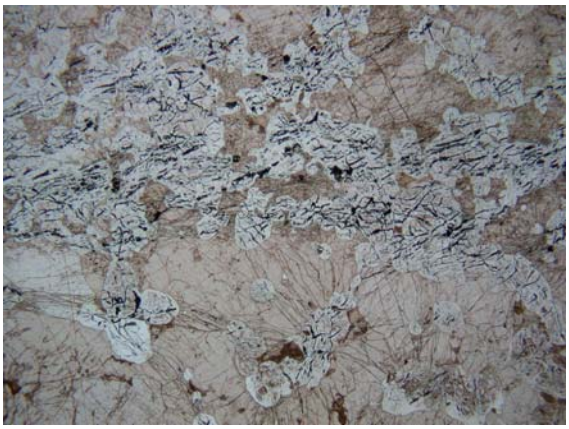

SSMet 3/586 PPL field of view 7 mm

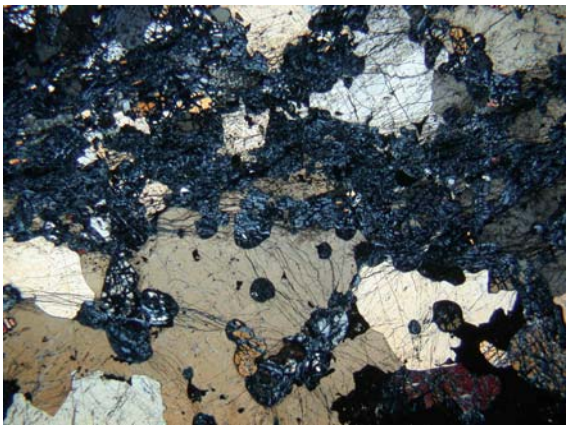

SSMet 3/586 XPL field of view 7 mm

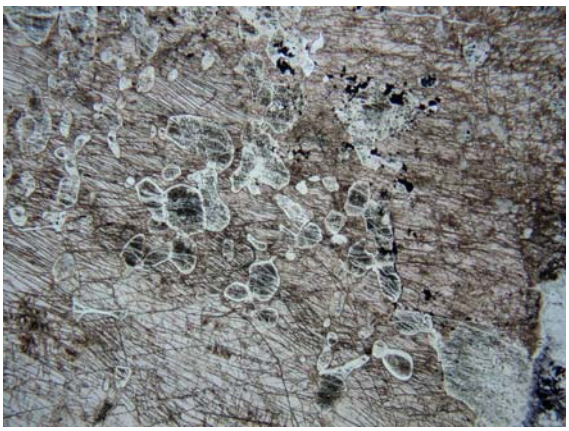

SSMet 3/608 PPL field of view 7 mm

SSMet 3/608 XPL field of view 7 mm

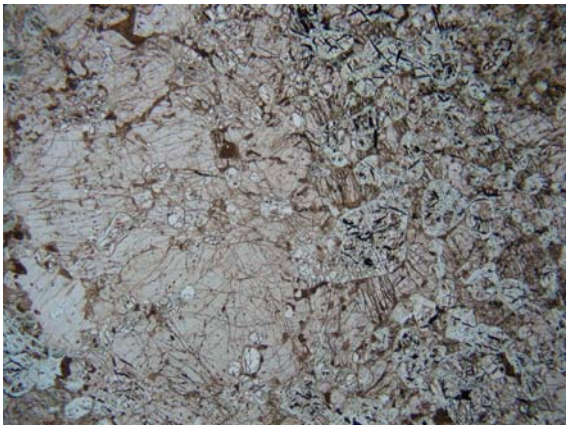

SSMet 3/663 PPL field of view 7 mm

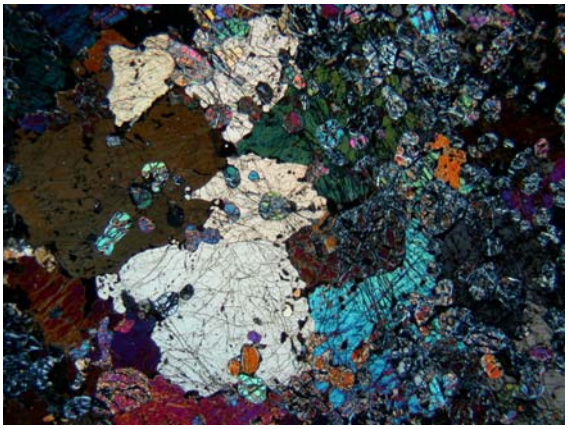

SSMet 3/663 XPL field of view 7 mm

SSMet 3/684 PPL field of view 7 mm

SSMet 3/684 XPL field of view 7 mm

SSMet 4 Photomicrographs

SSMet 4/15 PPL field of view 7 mm

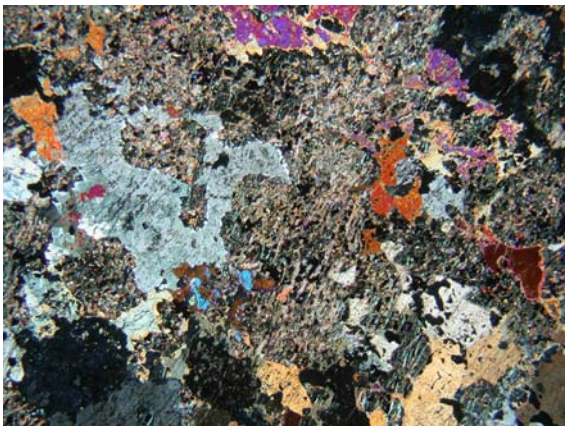

SSMet 4/15 XPL field of view 7 mm

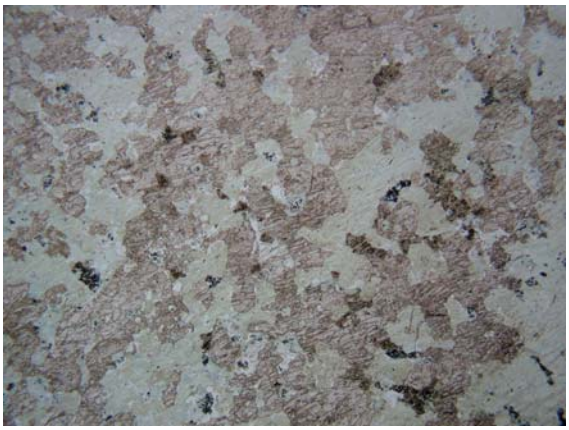

SSMet 4/37 PPL field of view 7 mm

SSMet 4/37 XPL field of view 7 mm

SSMet 4/57 PPL field of view 7 mm

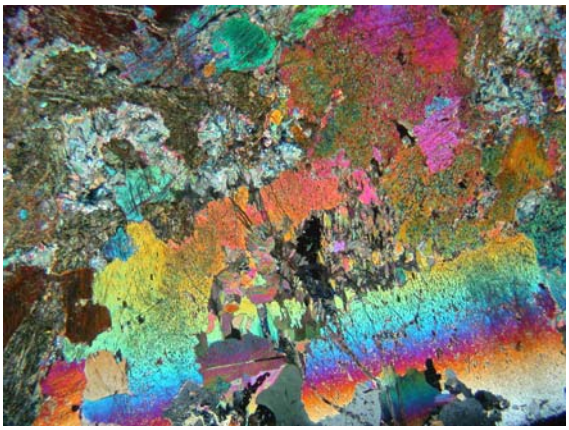

SSMet 4/57 XPL field of view 7 mm

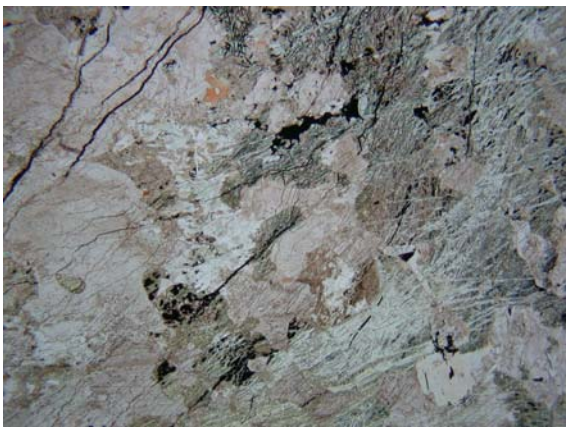

SSMet 4/88 PPL field of view 7 mm

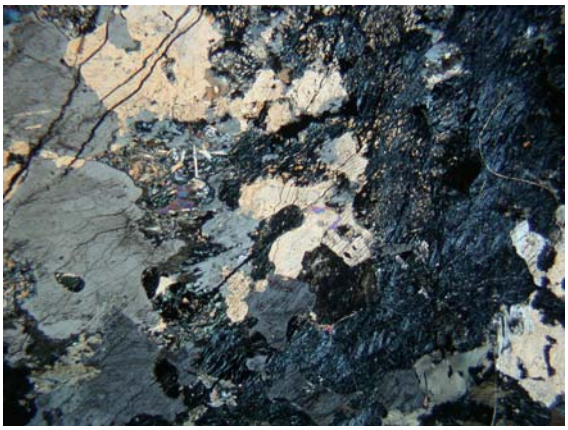

SSMet 4/88 XPL field of view 7 mm

SSMet 4/92 PPL field of view 7 mm

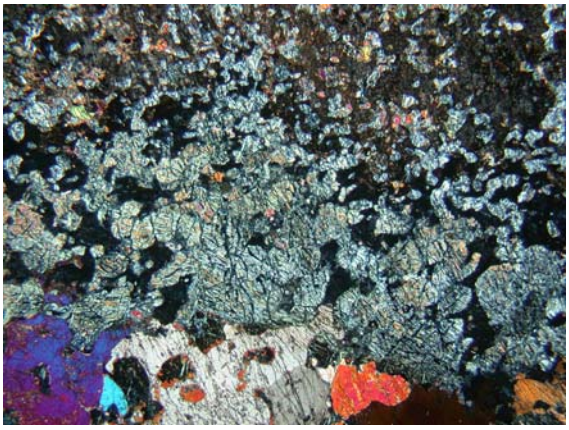

SSMet 4/92 XPL field of view 7 mm

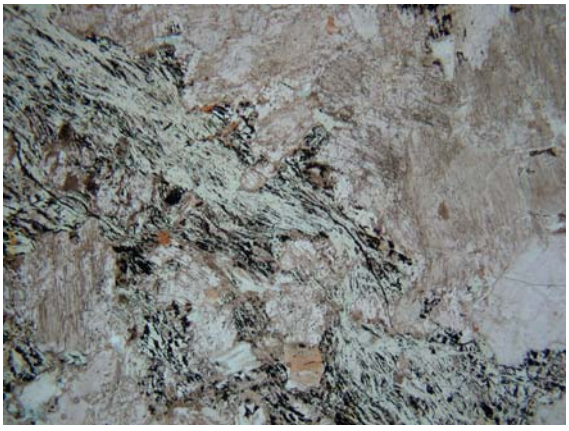

SSMet 4/166 PPL field of view

SSMet 4/166 XPL field of view 7 mm

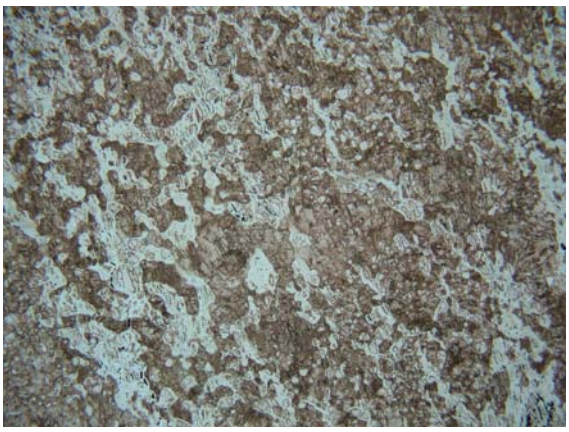

SSMet 4/188 PPL field of view 7 mm

SSMet 4/188 XPL field of view 7 mm

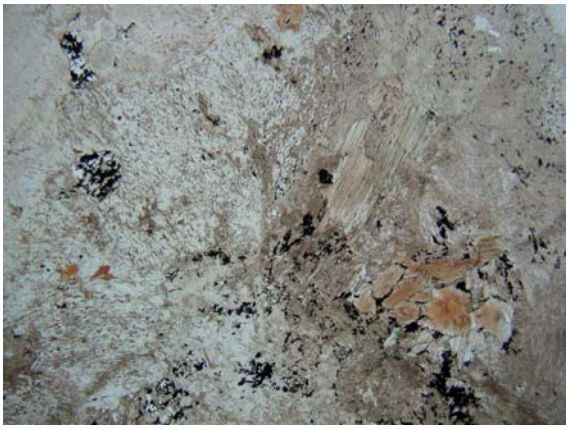

SSMet 4/222 PPL field of view 7 mm

SSMet 4/222 XPL field of view 7 mm

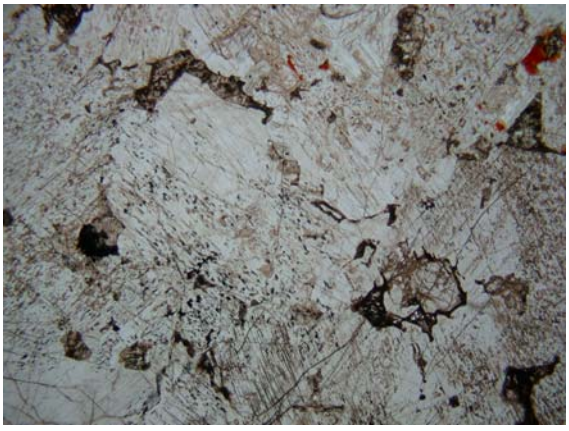

SSMet 4/239 PPL field of view 7 mm

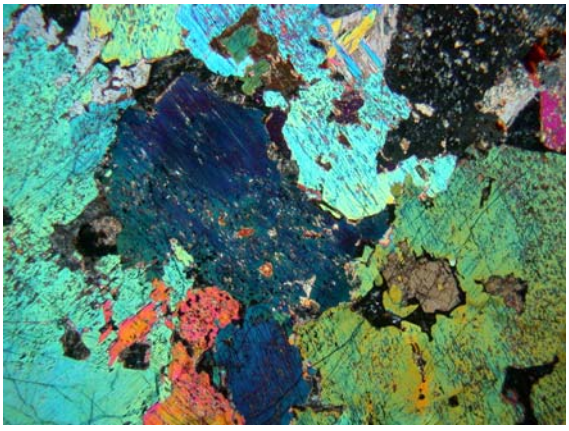

SSMet 4/239 XPL field of view 7 mm

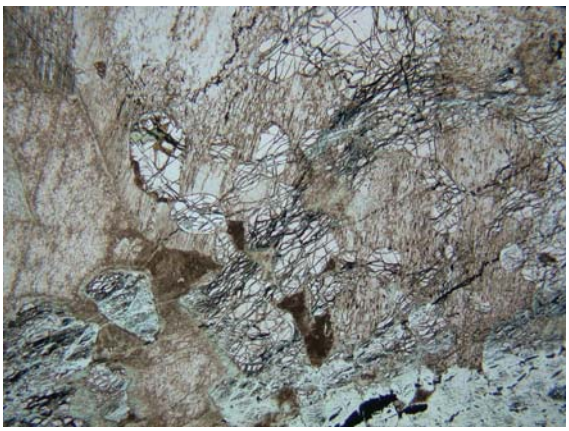

SSMet 4/245 PPL field of view 7 mm

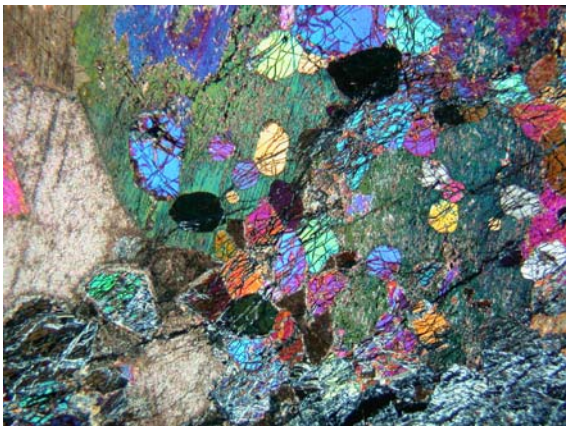

SSMet 4/245 XPL field of view 7 mm

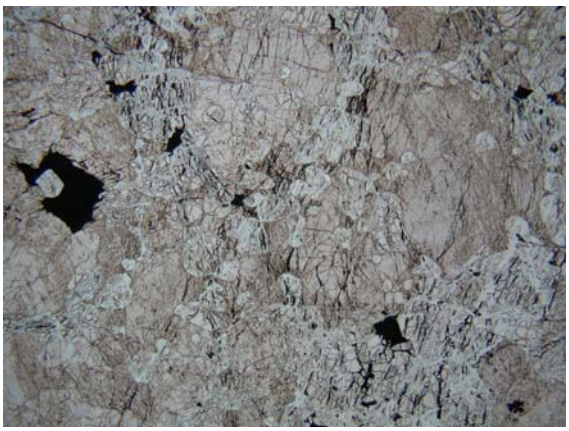

SSMet 4/254 PPL field of view 7 mm

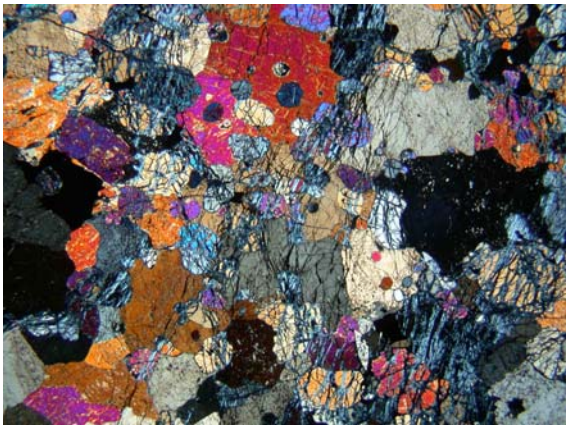

SSMet 4/254 XPL field of view 7 mm

SSMet 4/283 PPL field of view 7 mm

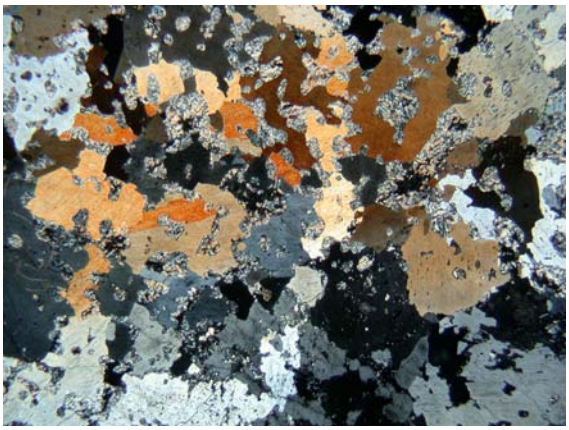

SSMet 4/283 XPL field of view 7 mm

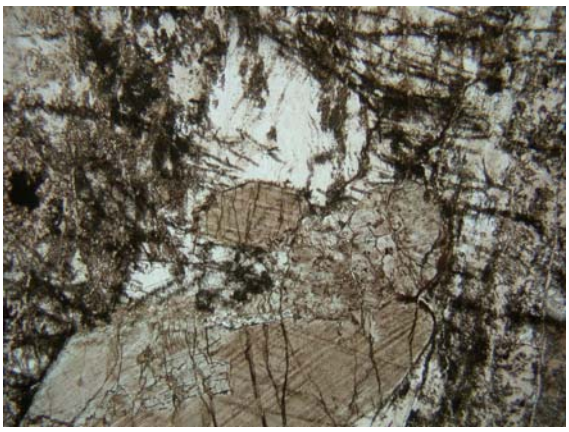

SSMet 4/291 PPL field of view 7 mm

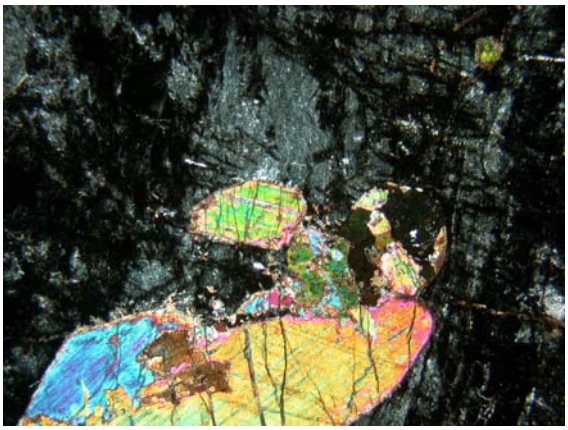

SSMet 4/291 XPL field of view 7 mm

SSMet 5 Photomicrographs

SSMet 5/22 PPL field of view 7 mm

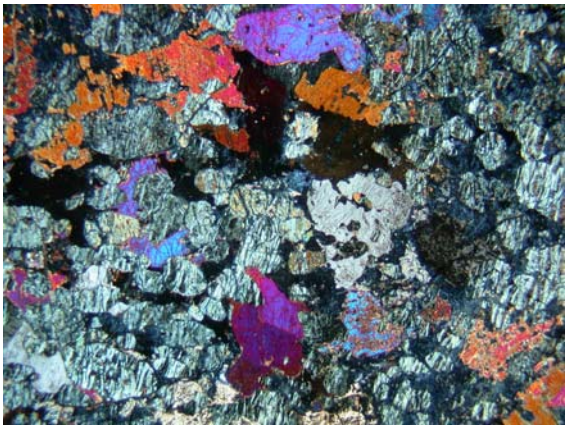

SSMet 5/22 XPL field of view 7 mm

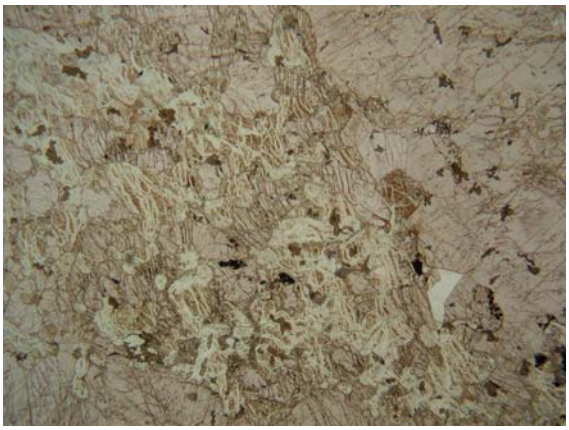

SSMet 5/42 PPL field of view 7 mm

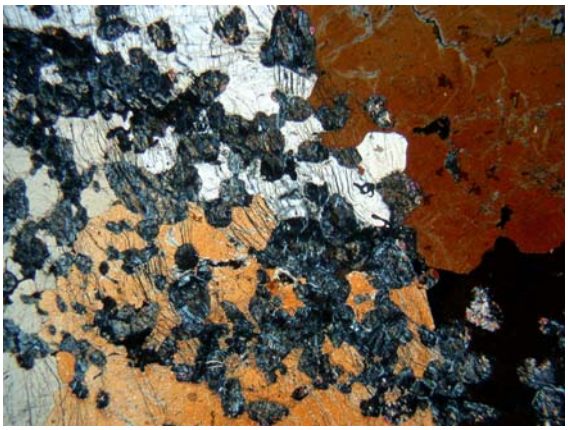

SSMet 5/42 XPL field of view 7 mm

SSMet 5/68 PPL field of view 7 mm

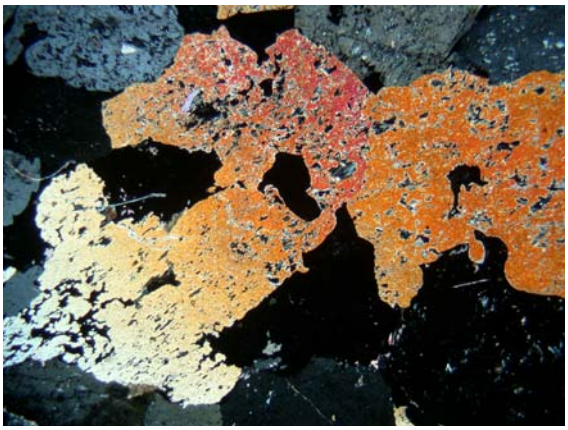

SSMet 5/68 XPL field of view 7 mm

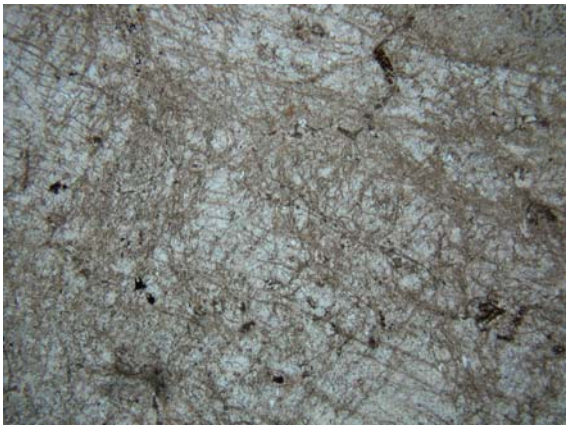

SSMet 5/96 PPL field of view 7 mm

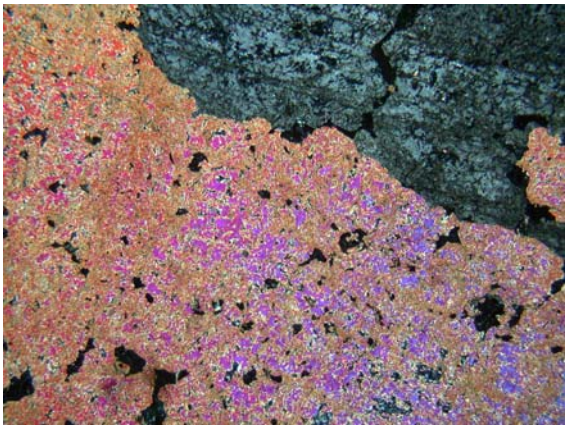

SSMet 5/96 XPL field of view 7 mm

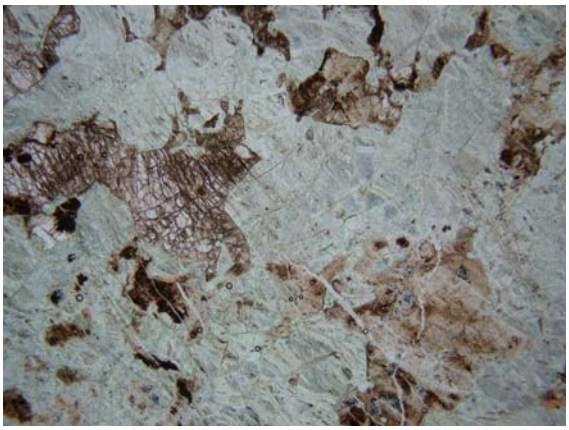

SSMet 5/119 PPL field of view 7 mm

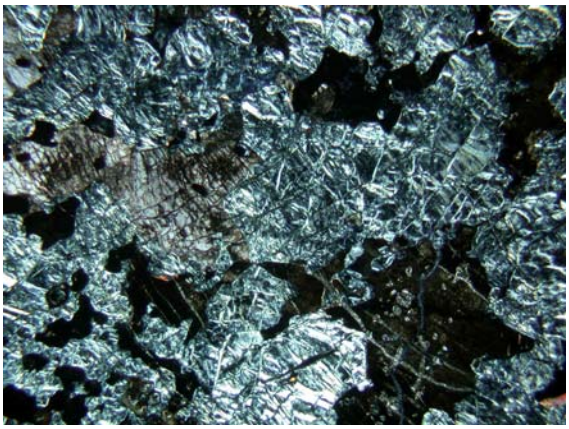

SSMet 5/119 XPL field of view 7 mm

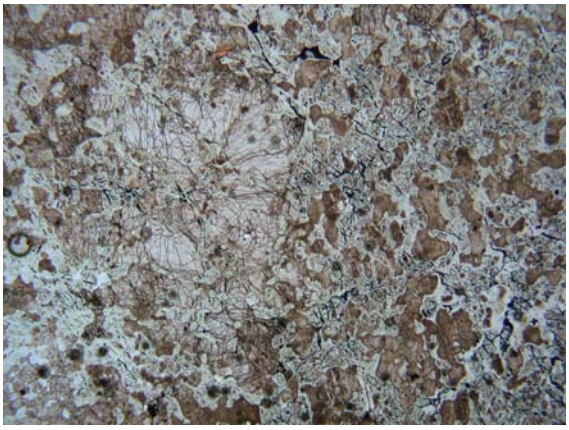

SSMet 5/181 PPL field of view 7 mm

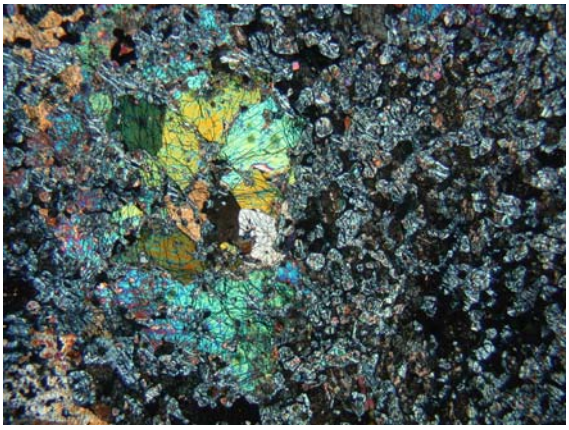

SSMet 5/181 XPL field of view 7 mm

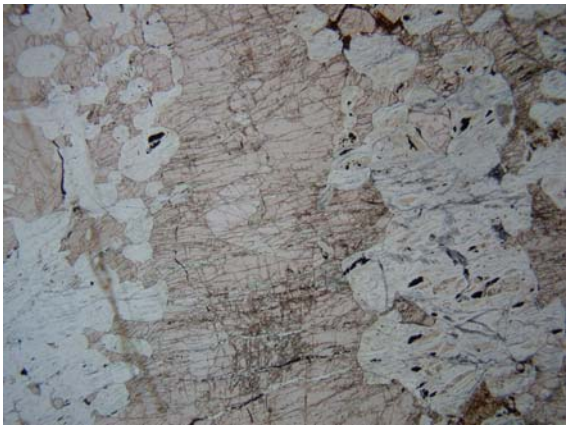

SSMet 5/198 PPL field of view 7 mm

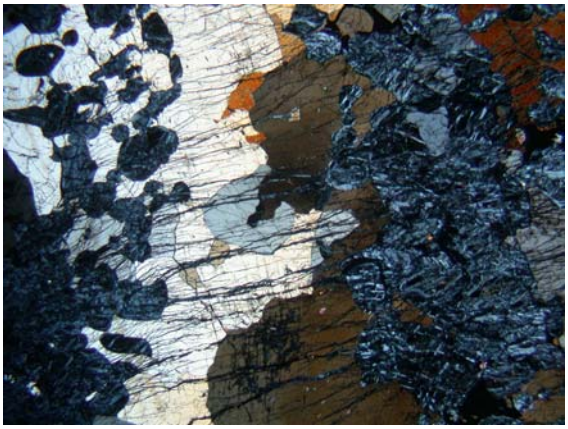

SSMet 5/198 XPL field of view 7 mm

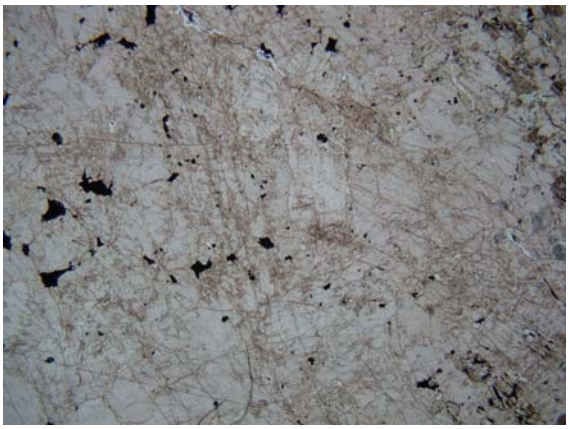

SSMet 5/223 PPL field of view 7 mm

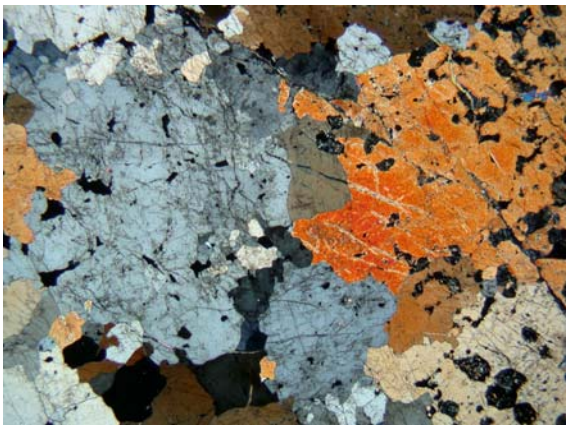

SSMet 5/223 XPL field of view 7 mm

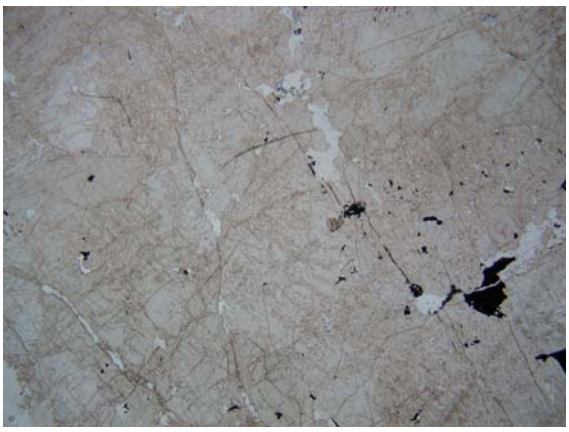

SSMet 5/264 PPL field of view 7 mm

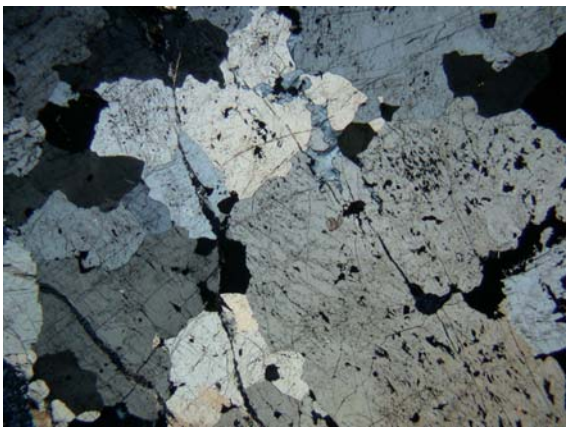

SSMet 5/264 XPL field of view 7 mm

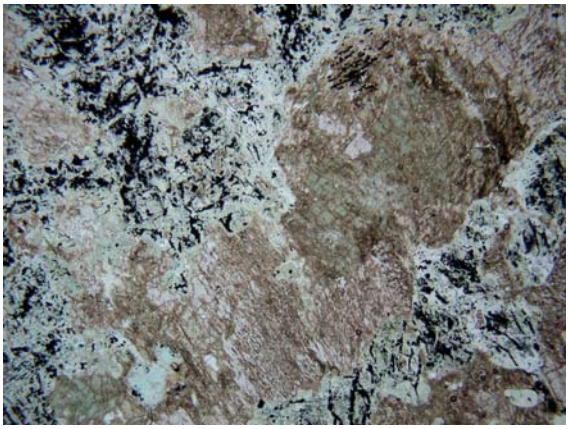

SSMet 5/291 PPL field of view 7 mm

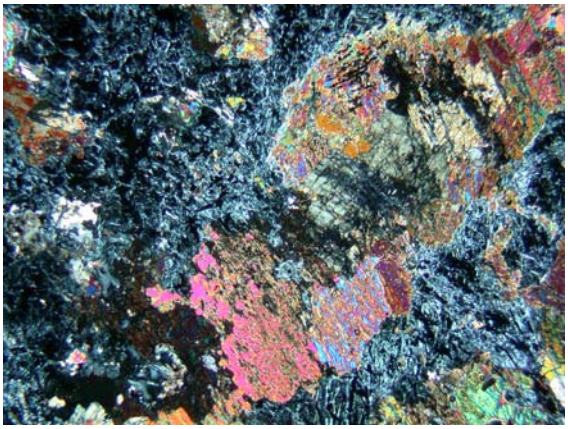

SSMet 5/291 XPL field of view 7 mm

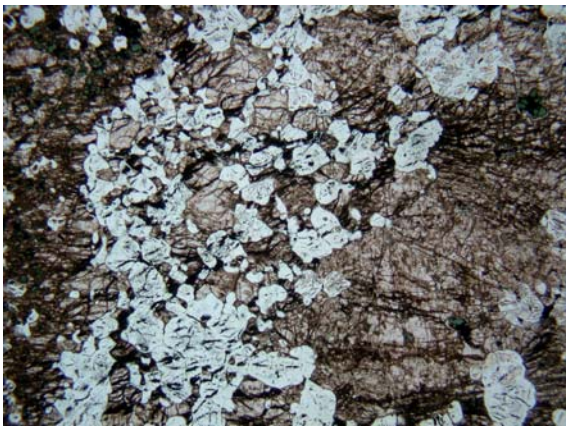

SSMet 5/305 PPL field of view 7 mm

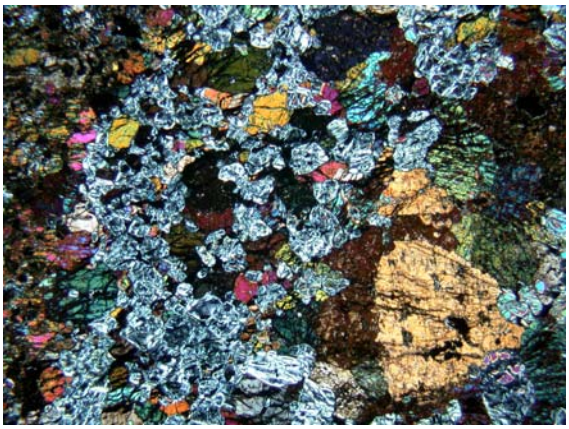

SSMet 5/305 XPL field of view 7 mm

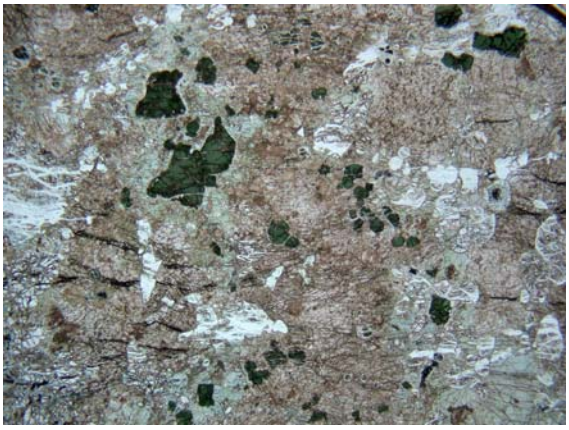

SSMet 5/315 PPL field of view 7 mm

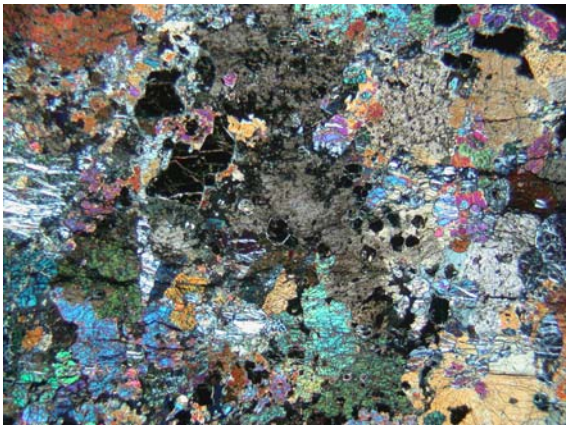

SSMet 5/315 XPL field of view 7 mm

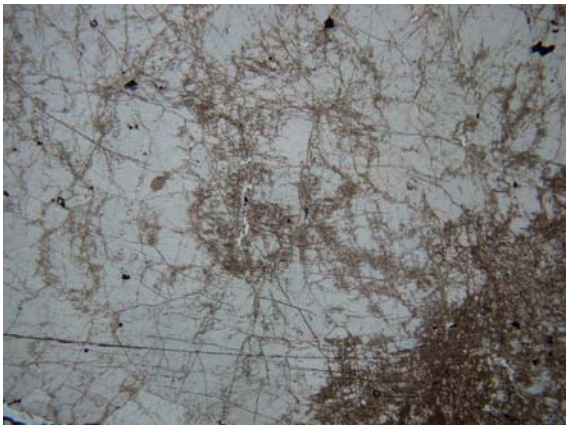

SSMet 5/342 PPL field of view 7 mm

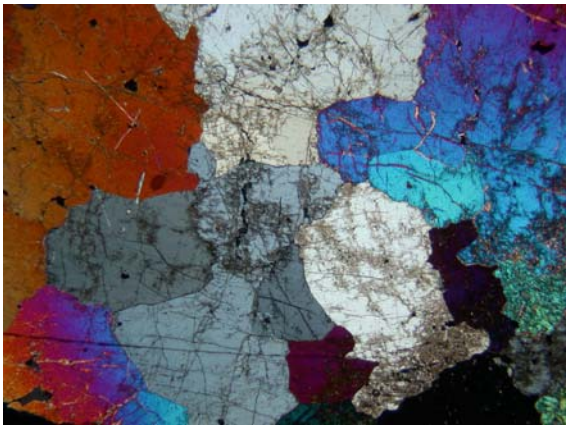

SSMet 5/342 XPL field of view 7 mm

SSPit 149 Photomicrographs

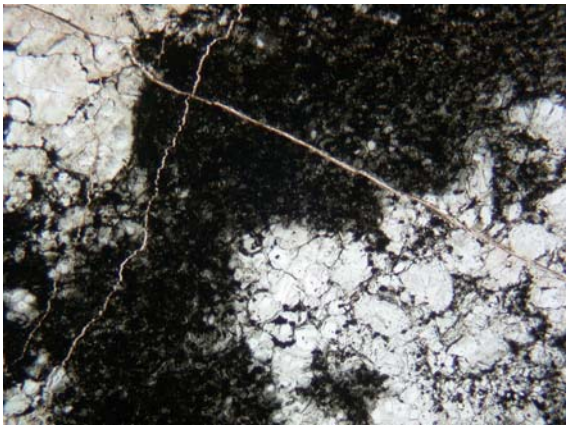

SSPit 149/7 PPL field of view 7 mm

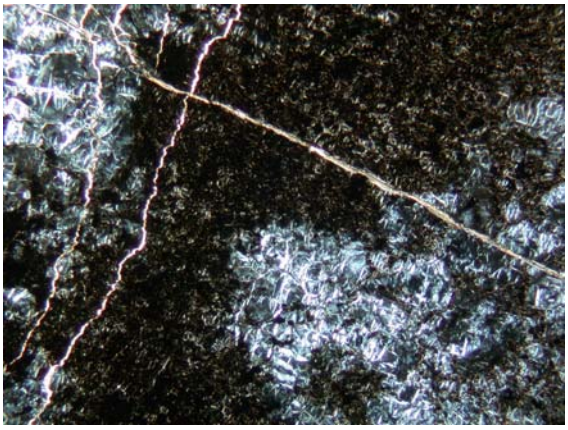

SSPit 149/7 XPL field of view 7 mm

SSPit 150 Photomicrographs

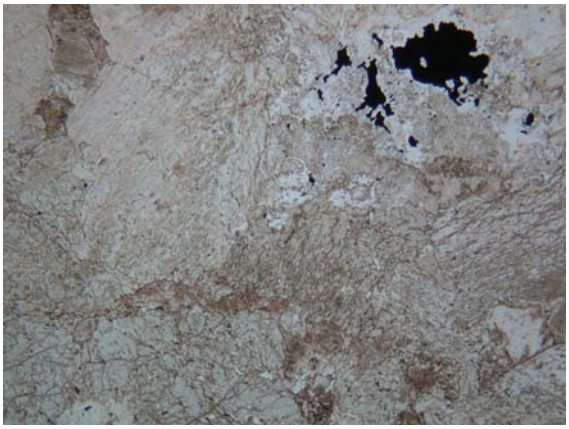

SSPit 150/16 PPL field of view 7 mm

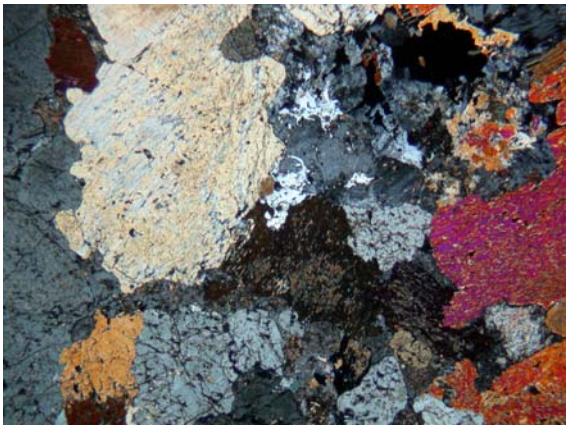

SSPit 150/16 XPL field of view 7 mm

SSPit 154 Photomicrographs

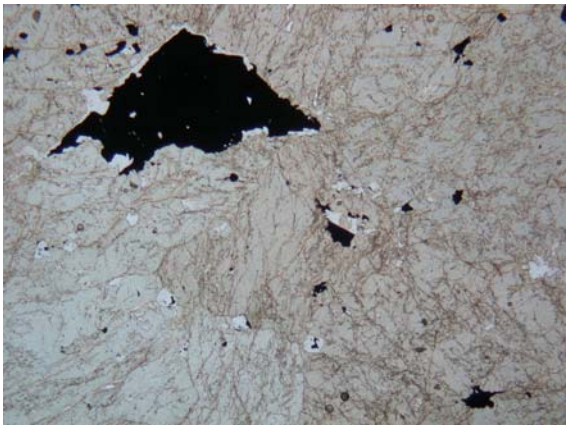

SSPit 154/17 PPL field of view 7 mm

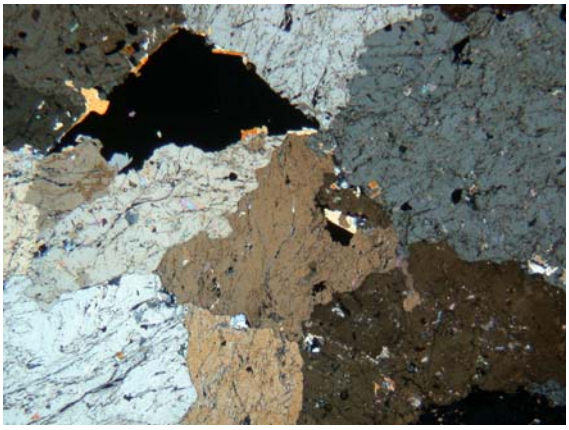

SSPit 154/17 XPL field of view 7 mm

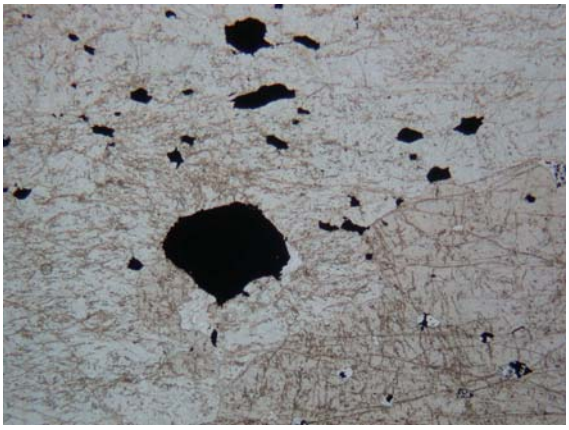

SSPit 154/40 PPL field of view 7 mm

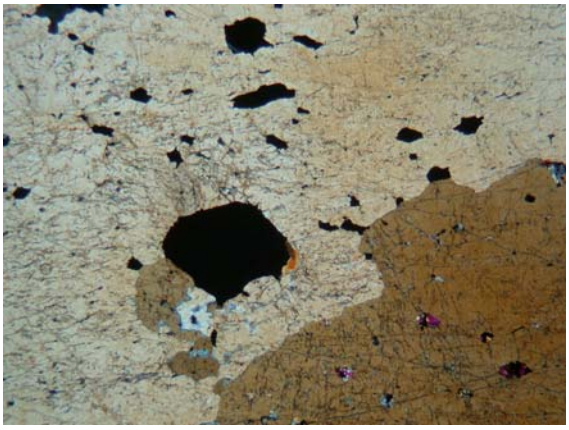

SSPit 154/40 XPL field of view 7 mm

SSPit 158 Photomicrographs

SSPit 158/8 PPL field of view 7 mm

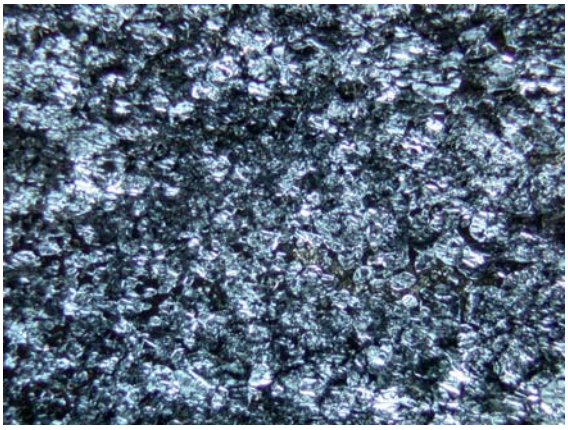

SSPit 158/8 XPL field if view 7 mm

SSPit 159 Photomicrographs

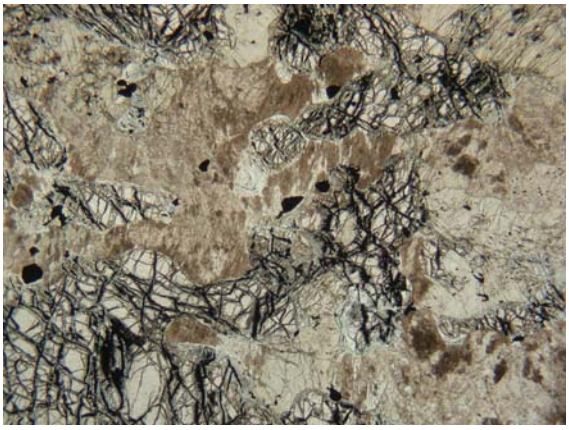

SSPit 159/42 PPL field of view 7 mm

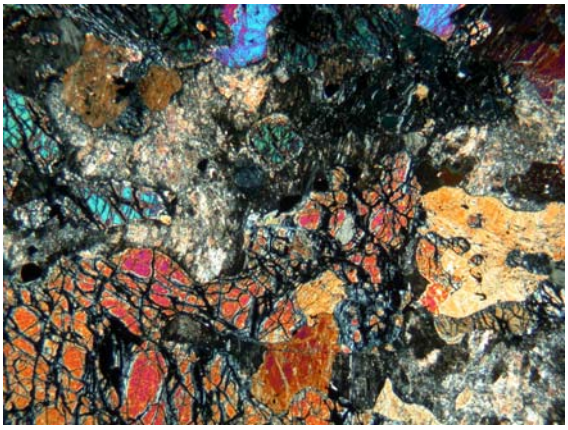

SSPit 159/42 XPL field of view 7 mm

SSPit 161 Photomicrographs

SSPit 161/12 PPL field of view 7 mm

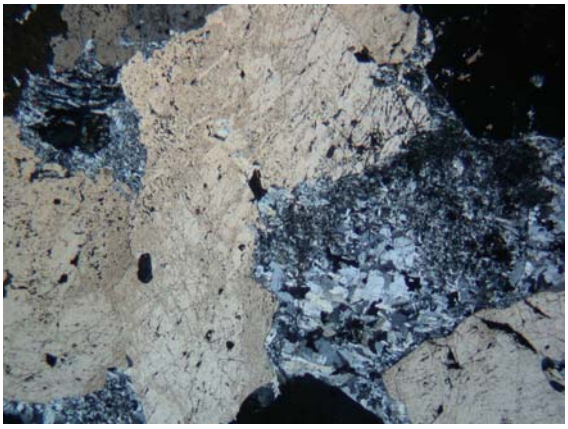

SSPit 161/12 XPL field of view 7 mm

APPENDIX - C

Geotechnical Appendix

In-house Procedures for Geotechnical Testing

Density

Apparatus:

(a) A scale, measuring to two decimal places.

(b) Two (how many liter buckets), one containing nothing and the other containing water up to a marked level.

(c) Fishermen's line connected to the underneath of the scale with an adjustable loop to fix around specimens securely.

(d) A plank of wood, set up on trellis legs, with a circle of wood cut out beneath the center of the scale, where the Fisherman's line is tied.

Procedure:

(a) A dried specimen was fixed to the fishermen's line beneath the scale and placed in the bucket containing nothing but air. The bucket served as an environment control, to prevent drafts of wind from affecting the readings.

(b) Once the specimen was no longer moving a reading of its weight in air (g) was taken thereafter the sample was removed.

(c) Steps a – b were repeated a second time using the bucket filled with water, recording the weight of the specimen in water (g) was recorded.

(d) After ten specimens had been weighed a control test was performed in which a specimen of known weight was weighed to ensure the readings were precise and accurate.

Calculations

(a) The density of the specimen was calculated by dividing the dry weight of a sample by the difference between its weight in air and its mass in water.

Density = (weight in air (g))/ (weight in air (g) – weight in water (g))

Ultrasonic Velocity

Apparatus

(a) A Portable Ultrasonic Non-destructive Digital Indicating Tester (PUNDIT) pulse generator unit with a transmitter, a receiver and an electronic counter to measure the time interval between the pulse being transmitted and then received was used.

(b) Vaseline

Procedure

(a) Specimens were prepared in accordance with the specifications set out in ISRM (1981)
(b) Vaseline was applied to both ends of the specimen to improve conduction of the pulse
(c) The pulse generator unit was calibrated to 26 micro-seconds
(d) The transmitter and receiver were placed on opposing ends of the core and the results were recorded.
(e) The Vaseline was removed from the ends of the specimen using first paper toweling and then acetone.
(f) The pulse generator was calibrated to 26 micro-seconds after every ten specimens tested.

Calculations

(a) The velocity of the wave moving through the core was calculated by dividing the length of the specimen, in meters, by the time, in seconds, it took for the pulse to be transmitted and then received.
Velocity (m/s) = length (m) / time (s)

Point Load Index Strength

Apparatus

(a) Carbide platon tip, hydraulic pump loading device.

Sample Geometry

(a) Core of diameter BQ (36 mm) was used.
(b) The length to diameter ratio of 0.5:1 was used for axial testing
(c) The length to diameter ratio of 1:1 was used for diametrical testing.

Procedure

(a) All specimens tested were taken from boreholes with a zero deflection therefore direction of axial loading was orientated perpendicular to possible anisotropy due to layering of the igneous intrusion and the diametrical loading was orientated parallel.

Brazilian Disc Indirect Tensile Strength

Apparatus

(a) Steel jaws of proportions consistent to the dimensions detailed in the ISRM (1981) were made for the project by the Chief technician of Geology, University of KwaZulu-Natal, Howard College.

(b) The Relsma Universal Compression – Tension soft-strain machine, as described under the Uniaxial Compressive Strength apparatus outline, was used for Brazilian disc testing.

(c) Markings indicating the centre of the spherical seat of the Relsma were drawn to ensure the loading was uniform over the sample

Sample Geometry

(a) Core of diameter BQ (36 mm) was used.

(b) The length to diameter ratio was 0.5:1

Procedure

(a) All specimens tested were taken from boreholes with a zero deflection therefore direction of loading was orientated parallel to possible anisotropy due to layering of the igneous intrusion

Uniaxial Compressive Strength

Apparatus

(a) A Relsma Universal Compression – Tension soft-strain machine was used for testing

(b) Two platens, conforming to the specifications in ISRM (1981), were designed and made to fit the 36mm diameter core.

Sample Geometry

(a) Core of diameter BQ (36mm) was used.

(b) The length to diameter ratio was 2:1

Procedure

(a) The procedure followed that set out in ISRM (1981)

(b) Markings to indicate the centre of the spherical seat of the Relsma equipment were drawn ensuring the load was applied at right angles to the length of the specimen and uniformly.

Sandsloot Database of Point Load Results

Drill hole ID	From	To	Rock Type	Tes type	Strength (kN)	Core diam. (mm)	Is (MPa)	F	Is_{50} (IMPa)
SS242	161.60		CALCSIL	PLI - diam	0.5	37	0.37	0.87	0.32
SS242	161.00		CALCSIL	PLI - diam	1.9	37	1.39	0.87	1.21
SS242	160.50		CALCSIL	PLI - diam	3.8	37	2.78	0.87	2.43
SS242	313.60		CALCSIL	PLI - diam	4.8	37	3.51	0.87	3.07
SS242	159.80		CALCSIL	PLI - diam	5.3	37	3.87	0.87	3.38
SS242	307.70		CALCSIL	PLI - diam	6.6	37	4.82	0.87	4.21
SS242	317.70		CALCSIL	PLI - diam	7	37	5.11	0.87	4.46
SS242	338.90		CALCSIL	PLI - diam	8.2	37	5.99	0.87	5.23
SS242	310.30		CALCSIL	PLI - diam	9.5	37	6.94	0.87	6.06
SS242	334.70		CALCSIL	PLI - diam	10.2	37	7.45	0.87	6.51
SS242	340.00		CALCSIL	PLI - diam	14.4	37	10.52	0.87	9.19
SS242	320.70		CALCSIL	PLI - diam	15	37	10.96	0.87	9.57
SS242	162.00		CALCSIL	PLI - diam	16	37	11.69	0.87	10.21
SS242	343.00		CALCSIL	PLI - diam	20	37	14.61	0.87	12.76
SS242	159.20		CALCSIL	PLI - diam	27.2	37	19.87	0.87	17.35
SS242	330.00		PARAPYX	PLI - diam	18.1	37	13.22	0.87	11.54
SS242	323.50		PARAPYX	PLI - diam	20.3	37	14.83	0.87	12.95
SS242	327.80		PARAPYX	PLI - diam	57.9	37	42.29	0.87	36.93
SS242	286.40		PYX	PLI - diam	11.7	37	8.55	0.87	7.47
SS242	285.90		PYX	PLI - diam	19.1	37	13.95	0.87	12.18
SS242	291.90		PYX	PLI - diam	23	37	16.80	0.87	14.67
SS242	299.00		PYX	PLI - diam	36	37	26.30	0.87	22.97
SS242	289.00		PYX	PLI - diam	53.5	37	39.08	0.87	34.13
SS242	301.30		SERP	PLI - diam	11.4	37	8.33	0.87	7.27
SS247	285.50		CALCSIL	PLI - diam	3	37	2.19	0.87	1.91
SS247	288.50		CALCSIL	PLI - diam	10	37	7.30	0.87	6.37
SS247	291.80		CALCSIL	PLI - diam	10	37	7.30	0.87	6.37
SS247	299.50		CALCSIL	PLI - diam	12	37	8.76	0.87	7.65
SS257	372.75		CALCSIL	PLI - diam	10	37	7.30	0.87	6.37
SS257	371.50		CALCSIL	PLI - diam	20.9	37	15.27	0.87	13.34
SS257	358.04		PARAPYX	PLI - diam	7.1	37	5.19	0.87	4.53
SS257	274.04		PARAPYX	PLI - diam	7.2	37	5.26	0.87	4.59
SS257	367.10		PARAPYX	PLI - diam	7.5	37	5.48	0.87	4.79
SS257	361.20		PARAPYX	PLI - diam	11.5	37	8.40	0.87	7.34
SS257	266.80		PARAPYX	PLI - diam	13.1	37	9.57	0.87	8.36
SS257	311.00		PARAPYX	PLI - diam	13.2	37	9.64	0.87	8.42
SS257	342.80		PARAPYX	PLI - diam	13.2	37	9.64	0.87	8.42
SS257	277.10		PARAPYX	PLI - diam	13.9	37	10.15	0.87	8.86
SS257	309.50		PARAPYX	PLI - diam	14	37	10.23	0.87	8.93
SS257	257.50		PARAPYX	PLI - diam	14.1	37	10.30	0.87	8.99
SS257	351.85		PARAPYX	PLI - diam	14.2	37	10.37	0.87	9.06
SS257	341.50		PARAPYX	PLI - diam	14.9	37	10.88	0.87	9.50
SS257	328.04		PARAPYX	PLI - diam	16	37	11.69	0.87	10.21
SS257	288.70		PARAPYX	PLI - diam	16.2	37	11.83	0.87	10.33
SS257	265.30		PARAPYX	PLI - diam	17	37	12.42	0.87	10.85
SS257	292.04		PYX	PLI - diam	8.2	37	5.99	0.87	5.23
SS257	280.15		PYX	PLI - diam	10.2	37	7.45	0.87	6.51
SS257	242.20		PYX	PLI - diam	11.9	37	8.69	0.87	7.59
SS257	257.90		PYX	PLI - diam	13.5	37	9.86	0.87	8.61
SS257	252.90		PYX	PLI - diam	14.1	37	10.30	0.87	8.99
SS257	324.00		PYX	PLI - diam	14.8	37	10.81	0.87	9.44
SS257	306.00		PYX	PLI - diam	15.2	37	11.10	0.87	9.69
SS257	307.04		PYX	PLI - diam	16.1	37	11.76	0.87	10.27
SS257	241.15		PYX	PLI - diam	18.2	37	13.29	0.87	11.61
SS257	293.50		PYX	PLI - diam	18.9	37	13.81	0.87	12.06
SS257	321.60		PYX	PLI - diam	19.1	37	13.95	0.87	12.18
SS257	239.20		PYX	PLI - diam	19.8	37	14.46	0.87	12.63

Drill hole ID	From	To	Rock Type	Tes type	Strength (kN)	Core diam. (mm)	Is (MPa)	F	Is_{50} (IMPa)
SS257	254.00		PYX	PLI - diam	19.8	37	14.46	0.87	12.63
SS257	315.00		SERP	PLI - diam	6	37	4.38	0.87	3.82
SS257	272.40		SERP	PLI - diam	6.9	37	5.04	0.87	4.40
SS257	284.50		SERP	PLI - diam	9	37	6.57	0.87	5.74
SS257	284.20		SERP	PLI - diam	10.1	37	7.38	0.87	6.44
SS258	374.70		CALCSIL	PLI - diam	10.1	37	7.00	0.87	6.11
SS258	365.50		CALCSIL	PLI - diam	12.9	37	9.00	0.87	7.86
SS258	366.90		CALCSIL	PLI - diam	11.8	37	9.00	0.87	7.86
SS258	371.00		CALCSIL	PLI - diam	13.3	37	10.00	0.87	8.73
SS258	281.70		FPYX	PLI - diam	6.1	37	4.00	0.87	3.49
SS258	282.00		FPYX	PLI - diam	13	37	9.00	0.87	7.86
SS258	280.10		PARAPYX	PLI - diam	9.8	37	7.00	0.87	6.11
SS258	337.20		PARAPYX	PLI - diam	9	37	7.00	0.87	6.11
SS258	294.50		PARAPYX	PLI - diam	10.8	37	8.00	0.87	6.99
SS258	322.15		PARAPYX	PLI - diam	11.5	37	8.00	0.87	6.99
SS258	297.85		PARAPYX	PLI - diam	12.9	37	9.00	0.87	7.86
SS258	345.95		PARAPYX	PLI - diam	13.9	37	10.00	0.87	8.73
SS258	352.30		PARAPYX	PLI - diam	13.2	37	10.00	0.87	8.73
SS258	301.20		PARAPYX	PLI - diam	15.5	37	11.00	0.87	9.61
SS258	317.60		PARAPYX	PLI - diam	15	37	11.00	0.87	9.61
SS258	332.75		PARAPYX	PLI - diam	16.1	37	12.00	0.87	10.48
SS258	310.10		PARAPYX	PLI - diam	18.1	37	13.00	0.87	11.35
SS258	327.90		PARAPYX	PLI - diam	22.4	37	16.00	0.87	13.97
SS258	357.60		PARAPYX	PLI - diam	22.5	37	16.00	0.87	13.97
SS258	268.70		PYX	PLI - diam	2.5	37	2.00	0.87	1.75
SS258	272.30		PYX	PLI - diam	6.1	37	4.00	0.87	3.49
SS258	265.10		PYX	PLI - diam	6.9	37	5.00	0.87	4.37
SS258	277.15		PYX	PLI - diam	8.1	37	6.00	0.87	5.24
SS258	286.20		PYX	PLI - diam	12	37	9.00	0.87	7.86
SS258	288.80		PYX	PLI - diam	13.9	37	10.00	0.87	8.73
SS258	305.50		PYX	PLI - diam	16.2	37	12.00	0.87	10.48
SS258	312.70		PYX	PLI - diam	17	37	12.00	0.87	10.48
SS259	386.05		CALCSIL	PLI - diam	9.9	37	7.23	0.87	6.31
SS259	373.45		CALCSIL	PLI - diam	11.5	37	8.40	0.87	7.34
SS259	380.35		CALCSIL	PLI - diam	14.9	37	10.88	0.87	9.50
SS259	349.50		CALCSIL	PLI - diam	17.1	37	12.49	0.87	10.91
SS259	360.50		PARAPYX	PLI - diam	13.1	37	9.57	0.87	8.36
SS259	364.70		PARAPYX	PLI - diam	13.9	37	10.15	0.87	8.86
SS259	341.30		PARAPYX	PLI - diam	18.8	37	13.73	0.87	11.99
SS259	335.00		PARAPYX	PLI - diam	20.4	37	14.90	0.87	13.01
SS259	344.20		PARAPYX	PLI - diam	22	37	16.07	0.87	14.03
SS259	322.70		PYX	PLI - diam	17	37	12.42	0.87	10.85
SS259	328.90		PYX	PLI - diam	32	37	23.37	0.87	20.41
SS259	330.00		PYX	PLI - diam	33.1	37	24.18	0.87	21.12
SS303	241.26	241.48	CALCSIL	PLI - diam	4	35	2.78	0.85	2.37
SS303	280.19	280.39	CALCSIL	PLI - diam	4	35	2.78	0.85	2.37
SS303	251.16	251.31	CALCSIL	PLI - diam	5	35	3.48	0.85	2.96
SS303	246.75	246.99	CALCSIL	PLI - diam	6	35	4.17	0.85	3.55
SS303	235.68	235.80	CALCSIL	PLI - diam	6.2	35	4.31	0.85	3.67
SS303	230.22	230.44	CALCSIL	PLI - diam	6.3	35	4.38	0.85	3.73
SS303	261.09	261.24	CALCSIL	PLI - diam	6.3	35	4.38	0.85	3.73
SS303	256.15	256.40	CALCSIL	PLI - diam	7	35	4.87	0.85	4.15
SS303	266.11	266.30	CALCSIL	PLI - diam	7	35	4.87	0.85	4.15
SS303	524.38	524.50	CALCSIL	PLI - diam	8	35	5.56	0.85	4.74
SS303	643.79	643.96	FPYX	PLI - diam	7	35	4.87	0.85	4.15
SS303	451.14	451.35	FPYX	PLI - diam	8	35	5.56	0.85	4.74
SS303	655.24	655.48	FPYX	PLI - diam	8.2	35	5.70	0.85	4.86
SS303	608.44	608.59	FPYX	PLI - diam	9	35	6.26	0.85	5.33
SS303	630.01	630.15	FPYX	PLI - diam	9	35	6.26	0.85	5.33

Drill hole ID	From	To	Rock Type	Tes type	Strength (kN)	Core diam. (mm)	Is (MPa)	F	Is_{50} (IMPa)
SS303	552.71	552.88	FPYX	PLI - diam	10	35	6.95	0.85	5.92
SS303	619.70	619.93	FPYX	PLI - diam	10	35	6.95	0.85	5.92
SS303	679.76	679.97	FPYX	PLI - diam	11.2	35	7.79	0.85	6.63
SS303	557.30	557.54	FPYX	PLI - diam	12.2	35	8.48	0.85	7.22
SS303	496.28	496.50	FPYX	PLI - diam	12.3	35	8.55	0.85	7.28
SS303	439.01	439.17	FPYX	PLI - diam	13	35	9.04	0.85	7.70
SS303	598.85	598.99	FPYX	PLI - diam	13	35	9.04	0.85	7.70
SS303	149.26	149.51	FPYX	PLI - diam	13.3	35	9.25	0.85	7.88
SS303	460.24	460.42	FPYX	PLI - diam	14	35	9.73	0.85	8.29
SS303	166.29	166.47	FPYX	PLI - diam	15	35	10.43	0.85	8.88
SS303	445.21	445.31	FPYX	PLI - diam	15	35	10.43	0.85	8.88
SS303	666.26	666.40	FPYX	PLI - diam	15	35	10.43	0.85	8.88
SS303	131.12	131.34	FPYX	PLI - diam	15.3	35	10.64	0.85	9.06
SS303	516.09	516.31	FPYX	PLI - diam	20	35	13.91	0.85	11.84
SS303	685.07	685.27	FPYX	PLI - diam	20	35	13.91	0.85	11.84
SS303	218.66	218.84	PARAPYX	PLI - diam	4.3	35	2.99	0.85	2.55
SS303	204.50	204.67	PARAPYX	PLI - diam	8.3	35	5.77	0.85	4.92
SS303	505.09	505.23	PARAPYX	PLI - diam	9	35	6.26	0.85	5.33
SS303	190.19	190.34	PARAPYX	PLI - diam	10.3	35	7.16	0.85	6.10
SS303	423.08	423.28	PARAPYX	PLI - diam	10.3	35	7.16	0.85	6.10
SS303	530.21	530.39	PARAPYX	PLI - diam	13.2	35	9.18	0.85	7.82
SS303	181.53	181.72	PARAPYX	PLI - diam	14.2	35	9.87	0.85	8.41
SS303	401.74	401.93	PARAPYX	PLI - diam	14.2	35	9.87	0.85	8.41
SS303	382.42	382.63	PARAPYX	PLI - diam	16	35	11.12	0.85	9.47
SS303	549.13	549.43	PARAPYX	PLI - diam	16	35	11.12	0.85	9.47
SS303	112.03	112.12	PYX	PLI - diam	8	35	5.56	0.85	4.74
SS303	100.12	100.25	PYX	PLI - diam	9.3	35	6.47	0.85	5.51
SS303	88.68	88.86	PYX	PLI - diam	10	35	6.95	0.85	5.92
SS303	116.12	116.29	PYX	PLI - diam	10	35	6.95	0.85	5.92
SS303	104.09	104.25	PYX	PLI - diam	11.2	35	7.79	0.85	6.63
SS303	96.28	96.42	PYX	PLI - diam	15	35	10.43	0.85	8.88
SS303	108.53	108.75	PYX	PLI - diam	15.3	35	10.64	0.85	9.06
SS303	92.09	92.28	PYX	PLI - diam	18	35	12.51	0.85	10.66
SS303	154.69	154.91	PYX	PLI - diam	18	35	12.51	0.85	10.66
SS303	156.32	156.47	PYX	PLI - diam	20.2	35	14.04	0.85	11.96
SS303	151.44	151.55	SERP	PLI - diam	3	35	2.09	0.85	1.78
SS303	152.78	152.95	SERP	PLI - diam	5	35	3.48	0.85	2.96
SS303	153.06	153.18	SERP	PLI - diam	6	35	4.17	0.85	3.55
SS303	151.65	151.86	SERP	PLI - diam	7	35	4.87	0.85	4.15
SS303	153.46	153.62	SERP	PLI - diam	7.3	35	5.08	0.85	4.32
SS303	153.34	153.44	SERP	PLI - diam	8	35	5.56	0.85	4.74
SS303	151.04	151.20	SERP	PLI - diam	9	35	6.26	0.85	5.33
SS303	153.65	153.87	SERP	PLI - diam	9	35	6.26	0.85	5.33
SS303	153.19	153.29	SERP	PLI - diam	9.2	35	6.40	0.85	5.45
SSMET2	46.68	46.78	CALCSIL	PLI - diam	2	32	1.60	0.82	1.31
SSMET2	48.41	48.53	CALCSIL	PLI - diam	2	32	1.60	0.82	1.31
SSMET2	50.47	50.62	CALCSIL	PLI - diam	2	32	1.60	0.82	1.31
SSMET2	49.37	49.47	CALCSIL	PLI - diam	3	32	2.40	0.82	1.96
SSMET2	45.84	45.98	CALCSIL	PLI - diam	4	32	3.20	0.82	2.61
SSMET2	47.01	47.13	CALCSIL	PLI - diam	4	32	3.20	0.82	2.61
SSMET2	47.57	47.68	CALCSIL	PLI - diam	4	32	3.20	0.82	2.61
SSMET2	48.17	48.30	CALCSIL	PLI - diam	4	32	3.20	0.82	2.61
SSMET2	50.13	50.25	CALCSIL	PLI - diam	5	32	3.99	0.82	3.27
SSMET2	50.62	50.76	CALCSIL	PLI - diam	5	32	3.99	0.82	3.27
SSMET2	25.09	25.19	FPYX	PLI - diam	2	32	1.60	0.82	1.31
SSMET2	24.43	24.60	FPYX	PLI - diam	6	32	4.79	0.82	3.92
SSMET2	7.64	7.75	FPYX	PLI - diam	8	32	6.39	0.82	5.23
SSMET2	10.05	10.15	FPYX	PLI - diam	9	32	7.19	0.82	5.88
SSMET2	13.88	14.00	FPYX	PLI - diam	11	32	8.79	0.82	7.19

Drill hole ID	From	To	Rock Type	Tes type	Strength (kN)	Core diam. (mm)	Is (MPa)	F	Is_{50} (IMPa)
SSMET2	22.36	22.47	FPYX	PLI - diam	11	32	8.79	0.82	7.19
SSMET2	21.58	21.68	FPYX	PLI - diam	12	32	9.59	0.82	7.84
SSMET2	18.47	18.59	FPYX	PLI - diam	14	32	11.18	0.82	9.15
SSMET2	23.21	23.35	FPYX	PLI - diam	16	32	12.78	0.82	10.46
SSMET2	19.89	19.98	FPYX	PLI - diam	25	32	19.97	0.82	16.34
SSMET2	41.18	41.35	PARAPYX	PLI - diam	2	32	1.60	0.82	1.31
SSMET2	53.77	53.87	PARAPYX	PLI - diam	4	32	3.20	0.82	2.61
SSMET2	59.75	59.87	PARAPYX	PLI - diam	4	32	3.20	0.82	2.61
SSMET2	26.22	26.33	PARAPYX	PLI - diam	5	32	3.99	0.82	3.27
SSMET2	44.68	44.80	PARAPYX	PLI - diam	5	32	3.99	0.82	3.27
SSMET2	38.38	38.50	PARAPYX	PLI - diam	6	32	4.79	0.82	3.92
SSMET2	31.33	31.43	PARAPYX	PLI - diam	7	32	5.59	0.82	4.57
SSMET2	34.14	34.26	PARAPYX	PLI - diam	8	32	6.39	0.82	5.23
SSMET2	55.36	55.48	PARAPYX	PLI - diam	10	32	7.99	0.82	6.54
SSMET2	52.74	52.84	PARAPYX	PLI - diam	13	32	10.39	0.82	8.50
SSMET3	40.48	40.62	CALCSIL	PLI - diam	2	32	1.60	0.82	1.31
SSMET3	41.55	41.72	CALCSIL	PLI - diam	2	32	1.60	0.82	1.31
SSMET3	44.08	44.21	CALCSIL	PLI - diam	2	32	1.60	0.82	1.31
SSMET3	46.64	46.74	CALCSIL	PLI - diam	3	32	2.40	0.82	1.96
SSMET3	43.41	43.53	CALCSIL	PLI - diam	4	32	3.20	0.82	2.61
SSMET3	44.83	44.95	CALCSIL	PLI - diam	4	32	3.20	0.82	2.61
SSMET3	39.06	39.17	CALCSIL	PLI - diam	8	32	6.39	0.82	5.23
SSMET3	47.10	47.24	CALCSIL	PLI - diam	8	32	6.39	0.82	5.23
SSMET3	46.88	47.04	CALCSIL	PLI - diam	12	32	9.59	0.82	7.84
SSMET3	42.14	42.27	CALCSIL	PLI - diam	15	32	11.98	0.82	9.80
SSMET3	12.38	12.50	PARAPYX	PLI - diam	2	32	1.60	0.82	1.31
SSMET3	20.50	20.63	PARAPYX	PLI - diam	2	32	1.60	0.82	1.31
SSMET3	24.07	24.18	PARAPYX	PLI - diam	2	32	1.60	0.82	1.31
SSMET3	26.35	26.47	PARAPYX	PLI - diam	2	32	1.60	0.82	1.31
SSMET3	14.71	14.82	PARAPYX	PLI - diam	5	32	3.99	0.82	3.27
SSMET3	19.75	19.88	PARAPYX	PLI - diam	5	32	3.99	0.82	3.27
SSMET3	13.81	13.92	PARAPYX	PLI - diam	6	32	4.79	0.82	3.92
SSMET3	37.60	37.70	PARAPYX	PLI - diam	6	32	4.79	0.82	3.92
SSMET3	29.45	29.55	PARAPYX	PLI - diam	8	32	6.39	0.82	5.23
SSMET3	30.35	30.47	PARAPYX	PLI - diam	10	32	7.99	0.82	6.54
SSMET4	9.52	9.65	PARAPYX	PLI - diam	2	32	1.60	0.82	1.31
SSMET4	16.79	16.89	PARAPYX	PLI - diam	2	32	1.60	0.82	1.31
SSMET4	25.95	26.09	PARAPYX	PLI - diam	2	32	1.60	0.82	1.31
SSMET4	4.69	4.79	PARAPYX	PLI - diam	3	32	2.40	0.82	1.96
SSMET4	18.44	18.54	PARAPYX	PLI - diam	3	32	2.40	0.82	1.96
SSMET4	24.36	24.46	PARAPYX	PLI - diam	3	32	2.40	0.82	1.96
SSMET4	19.77	19.89	PARAPYX	PLI - diam	5	32	3.99	0.82	3.27
SSMET4	11.32	11.43	PARAPYX	PLI - diam	6	32	4.79	0.82	3.92
SSMET4	12.72	12.84	PARAPYX	PLI - diam	7	32	5.59	0.82	4.57
SSMET4	29.27	29.37	PARAPYX	PLI - diam	7	32	5.59	0.82	4.57
SSMET5	6.27	6.37	PARAPYX	PLI - diam	2	32	1.60	0.82	1.31
SSMET5	7.63	7.80	PARAPYX	PLI - diam	2	32	1.60	0.82	1.31
SSMET5	19.53	19.65	PARAPYX	PLI - diam	2	32	1.60	0.82	1.31
SSMET5	21.46	21.59	PARAPYX	PLI - diam	2	32	1.60	0.82	1.31
SSMET5	13.16	13.26	PARAPYX	PLI - diam	3	32	2.40	0.82	1.96
SSMET5	29.27	29.37	PARAPYX	PLI - diam	4	32	3.20	0.82	2.61
SSMET5	15.55	15.65	PARAPYX	PLI - diam	5	32	3.99	0.82	3.27
SSMET5	16.89	17.05	PARAPYX	PLI - diam	9	32	7.19	0.82	5.88
SSMET5	24.36	24.50	PARAPYX	PLI - diam	11	32	8.79	0.82	7.19
SSMET5	27.47	27.57	PARAPYX	PLI - diam	12	32	9.59	0.82	7.84
SSP256	402.00		CALCSIL	PLI - diam	7.9	37	5.77	0.87	5.04
SSP256	394.00		CALCSIL	PLI - diam	12	37	8.77	0.87	7.66
SSP256	363.15		CALCSIL	PLI - diam	16.3	37	11.91	0.87	10.40
SSP256	265.65		CALCSIL	PLI - diam	19.1	37	13.95	0.87	12.18

Drill hole ID	From	To	Rock Type	Tes type	Strength (kN)	Core diam. (mm)	Is (MPa)	F	Is_{50} (IMPa)
SSP256	273.30		CALCSIL	PLI - diam	21.1	37	15.41	0.87	13.46
SSP256	346.04		FPYX	PLI - diam	12.8	37	9.35	0.87	8.17
SSP256	263.80		FPYX	PLI - diam	24.2	37	17.68	0.87	15.44
SSP256	295.70		PARAPYX	PLI - diam	8	37	5.84	0.87	5.10
SSP256	399.10		PARAPYX	PLI - diam	9.9	37	7.23	0.87	6.31
SSP256	438.74		PARAPYX	PLI - diam	12.3	37	8.98	0.87	7.84
SSP256	285.15		PARAPYX	PLI - diam	13.2	37	9.64	0.87	8.42
SSP256	437.50		PARAPYX	PLI - diam	14.1	37	10.30	0.87	8.99
SSP256	428.10		PARAPYX	PLI - diam	15.3	37	11.18	0.87	9.76
SSP256	278.50		PARAPYX	PLI - diam	20.4	37	14.90	0.87	13.01
SSP256	303.55		PYX	PLI - diam	12.1	37	8.84	0.87	7.72
SSP256	413.00		PYX	PLI - diam	13	37	9.50	0.87	8.30
SSP256	416.00		PYX	PLI - diam	14.4	37	10.52	0.87	9.19
SSP256	384.40		PYX	PLI - diam	16.2	37	11.83	0.87	10.33
SSP256	313.35		PYX	PLI - diam	18.9	37	13.81	0.87	12.06
SSP256	373.95		PYX	PLI - diam	19	37	13.88	0.87	12.12
SSP256	337.20		PYX	PLI - diam	20.2	37	14.76	0.87	12.89
SSP256	432.05		PYX	PLI - diam	23.1	37	16.87	0.87	14.73

Sandsloot Open Pit Rock Testing Database

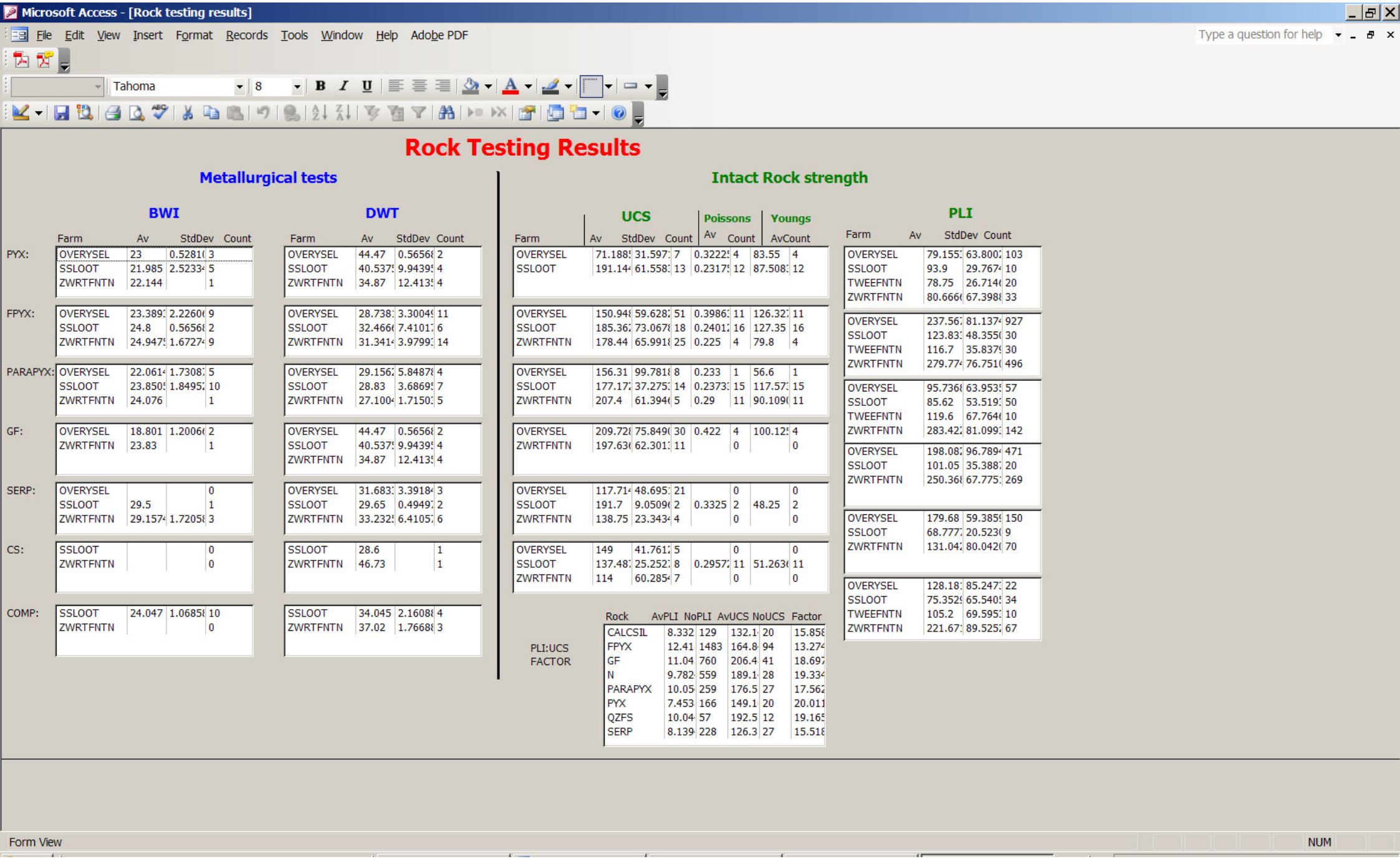

Microsoft Access - [Rock testing results]

File Edit View Insert Format Records Tools Window Help Adobe PDF

Type a question for help

Tahoma 8

Rock Testing Results

Metallurgical tests

BWI

	Farm	Av	StdDev	Count
PYX:	OVERYSEL	23	0.5281	3
	SSLOOT	21.985	2.5233	5
	ZWRTFNTN	22.144		1
FPYX:	OVERYSEL	23.389	2.2260	9
	SSLOOT	24.8	0.5656	2
	ZWRTFNTN	24.947	1.6727	9
PARAPYX:	OVERYSEL	22.061	1.7308	5
	SSLOOT	23.850	1.8495	10
	ZWRTFNTN	24.076		1
GF:	OVERYSEL	18.801	1.2006	2
	ZWRTFNTN	23.83		1
SERP:	OVERYSEL			0
	SSLOOT	29.5		1
	ZWRTFNTN	29.157	1.7205	3
CS:	SSLOOT			0
	ZWRTFNTN			0
COMP:	SSLOOT	24.047	1.0685	10
	ZWRTFNTN			0

DWT

Farm	Av	StdDev	Count
OVERYSEL	44.47	0.5656	2
SSLOOT	40.537	9.9439	4
ZWRTFNTN	34.87	12.413	4
OVERYSEL	28.738	3.3004	11
SSLOOT	32.466	7.4101	6
ZWRTFNTN	31.341	3.9799	14
OVERYSEL	29.156	5.8487	4
SSLOOT	28.83	3.6869	7
ZWRTFNTN	27.100	1.7150	5
OVERYSEL	44.47	0.5656	2
SSLOOT	40.537	9.9439	4
ZWRTFNTN	34.87	12.413	4
OVERYSEL	31.683	3.3918	3
SSLOOT	29.65	0.4949	2
ZWRTFNTN	33.232	6.4105	6
SSLOOT	28.6		1
ZWRTFNTN	46.73		1
SSLOOT	34.045	2.1608	4
ZWRTFNTN	37.02	1.7668	3

Intact Rock strength

UCS / Poissons / Youngs

Farm	UCS Av	UCS StdDev	UCS Count	Poissons Av	Poissons Count	Youngs AvCount
OVERYSEL	71.188	31.597	7	0.3222	4	83.55 4
SSLOOT	191.14	61.558	13	0.2317	12	87.508 12
OVERYSEL	150.94	59.628	51	0.3986	11	126.32 11
SSLOOT	185.36	73.067	18	0.2401	16	127.35 16
ZWRTFNTN	178.44	65.991	25	0.225	4	79.8 4
OVERYSEL	156.31	99.781	8	0.233	1	56.6 1
SSLOOT	177.17	37.275	14	0.2373	15	117.57 15
ZWRTFNTN	207.4	61.394	5	0.29	11	90.109 11
OVERYSEL	209.72	75.849	30	0.422	4	100.12 4
ZWRTFNTN	197.63	62.301	11		0	0
OVERYSEL	117.71	48.695	21		0	0
SSLOOT	191.7	9.0509	2	0.3325	2	48.25 2
ZWRTFNTN	138.75	23.343	4		0	0
OVERYSEL	149	41.761	5		0	0
SSLOOT	137.48	25.252	8	0.2957	11	51.263 11
ZWRTFNTN	114	60.285	7		0	0

PLI

Farm	Av	StdDev	Count
OVERYSEL	79.155	63.800	103
SSLOOT	93.9	29.767	10
TWEEFNTN	78.75	26.714	20
ZWRTFNTN	80.666	67.398	33
OVERYSEL	237.56	81.137	927
SSLOOT	123.83	48.355	30
TWEEFNTN	116.7	35.837	30
ZWRTFNTN	279.77	76.751	496
OVERYSEL	95.736	63.953	57
SSLOOT	85.62	53.519	50
TWEEFNTN	119.6	67.764	10
ZWRTFNTN	283.42	81.099	142
OVERYSEL	198.08	96.789	471
SSLOOT	101.05	35.388	20
ZWRTFNTN	250.36	67.775	269
OVERYSEL	179.68	59.385	150
SSLOOT	68.777	20.523	9
ZWRTFNTN	131.04	80.042	70
OVERYSEL	128.18	85.247	22
SSLOOT	75.352	65.540	34
TWEEFNTN	105.2	69.595	10
ZWRTFNTN	221.67	89.525	67

PLI:UCS FACTOR

Rock	AvPLI	NoPLI	AvUCS	NoUCS	Factor
CALCSIL	8.332	129	132.1	20	15.858
FPYX	12.41	1483	164.8	94	13.274
GF	11.04	760	206.4	41	18.697
N	9.782	559	189.1	28	19.334
PARAPYX	10.05	259	176.5	27	17.562
PYX	7.453	166	149.1	20	20.011
QZFS	10.04	57	192.5	12	19.165
SERP	8.139	228	126.3	27	15.518

Form View NUM

APPENDIX - D

Geochemical Appendix

Sample Preparation for geochemical analysis

The shattered or sheared UCS specimens were collected after each test and bagged. The bagged specimens were crushed in a low molybdenum carbon steel jaw crusher to fragmentation of <1cm. The crushed specimen was then milled three times, first to a coarse grade, after which the specimen was split using the cone and quarter technique. Half the sample was bagged and saved. 100g of the coarse grade specimen was milled a second time for one minute down to normal grade. Again the sample was coned, quartered and bagged. Finally 20g of normal grade was milled a third time, for 45 seconds, to a fine grade and bagged. At all stages between crushing and milling care was taken to prevent contamination by brushing off excess specimen powder on the apparatus, wiping clean apparatus with acetone and in some cases vacuuming the apparatus. Preparation was performed in a ventilation-controlled environment and the bags in which specimens were stored were unused.

XRF Sample Preparation

Pressed Powder Pellets for (Major/trace) Analysis

9 - 10 grams of fine grade powder was used. To this roughly 0.6 ml of Mowiol binder was added and the two were ground together with an agate pestle and mortar until a paste like consistency was achieved. The paste was pressed into a pellet using a pellet dye and approximately 8 to 10 tons of pressure. There after the pellets were dried at 110˚C for 6 – 8 hours.

Norrish Fusion Discs for (Major/trace) Analysis

Approximately 0.5g of fine grade powder was weighed into a silica crucible and placed into a furnace at 1000˚C for 4 hours, after which the ashed sample was removed and allowed to cool in a desiccator. To make the fusion discs approximately 0.4g of the ashed sample was added to the Johnson Matthey Spectroflux 105, which previously had been heated in a Pt crucible. The ratio to which the flux was added to the sample was 1:2.2. The flux and sample were fused together at 1000˚C and the product cast in a brass dye which was maintained at a temperature of 250˚C.The

discs were allowed to anneal for 3 hours on a heated asbestos plate and there after allowed to cool.

ICP-MS Sample Preparation

Approximately 50g of fine grade sample powder was digested with HF and HNO_3. The solution was evaporated down to a solid on a hot plate at approximately 70˚- 80˚ over a 48 hour period. 100 µl of pure nitric acid was added to the remaining solid. Finally the product was dissolved in 5% concentrate nitric acid. The sample was analysed in solution form with a total procedural blank (TPB) to monitor the process and a standard solution of dilution 50ppm as a reference. Between each analysis the instruments were flushed clean with 5% concentrate nitric acid.

PGE Sample Preparation

Approximately 26g of normal grade powder sample was weighed into envelope, double packed and freighted to Genalysis Laboratories in Perth, Australia for analysis. The power was then mixed with sulphur, sodium metabisulohite, sodium carbonate and nickel oxide powder, thereafter fused as 1000 ˚C in a ceramic pot for eight hours in a gas-fired furnace. The pot was removed from the furnace and allowed to cool. When cool, the pot was broken and a small Ni-sulphide bead or prill was recovered. The prill containing the PGEs and Au extracted from the sample was returned to the University of KwaZulu-Natal for ICP-MS analysis. Analysis was carried out in duplicate by measuring the solutions twice in each run. The final result is the average of the two runs.

International Standards

ATTENTION MRSL TURNER
MINEMET

FAX NO. 031 - 7014323.

Element	Tube	kV	Ma	Analytical Line	Analysing Crystal	Collimator	Counter	Peak 2 θ	Count Time Sec.	Background 2 θ	Count Time Sec.	Standard	Blanks	Detection Limits	Analytical Accuracy
* SiO_2	Cr	50	50	Ka	Pet	Coarse	Flow	109.165	60	106.000	30	SiO_2 100% NIMD 37.02%		0.004%	0.2%
* Al_2O_3	Cr	50	50	Ka	"	"	"	145.040	60	139.160	30	NIML 13.90%	SiO_2	0.005%	0.5%
* Fe_2O_3	Au	50	50	Ka	Lif200	Fine	"	57.525	40	Blank standards used to calibrate		NIML 10.28%	SiO_2 and $60CaO{\cdot}40SiO_2$	0.001%	0.5%
* MnO	Au	50	50	Ka	Lif200	"	"	62.990	40	background.		NIML 0.78%	SiO_2 and $60CaO{\cdot}40SiO_2$	0.001%	0.5%
* MgO	Cr	50	50	Ka	PX-1	Coarse	"	23.300	60	25.300	30	W-1 6.55%	SiO_2	0.011%	0.3%
* CaO	Cr	50	50	Ka	pet	Fine	"	45.240	40	Blank standards		NIML 3.32%	SiO_2 and $40Fe_2O_3{\cdot}60SiO_2$	0.0003%	0.2%
* K_2O	Cr	50	50	Ka	Pet	"	"	50.720	40	used to calibrate		W-1 0.65%	SiO_2 and $60CaO{\cdot}40SiO_2$	0.0003%	0.2%
* TiO_2	Cr	50	50	Ka	Pet	"	"	36.720	40	background	30	W-1 1.05%	SiO_2 and $60CaO{\cdot}40SiO_2$	0.0004%	0.2%
* P_2O_5	Cr	50	50	Ka	Ge	Coarse	"	141.040	60	138.000 143.000	30	BR 1.10%	SiO_2	0.001%	0.2%
* Na_2O	Cr	50	50	Ka	PX-1	Fine	"	28.170	60	30.000	30	BR 3.12%	SiO_2	0.018%	2%
Sc	Cr	50	50	Ka	Lif200	"	"	97.730	60	95.850 98.555	30	BCR 33 ppm	SiO_2 and $CaCO_3$	0.3 ppm	10%
Ba	Cr	50	50	La	Lif220	"	"	115.275	60	114.500 116.500	30	W-1 160 ppm	SiO_2 and MgO	1 ppm	± 20%
* Zn	Au	50	50	Ka	Lif200	"	"	41.795	60	39.65 46.70	30	NIMP 100 ppm	SiO_2 and $CaCO_3$	0.3 ppm	± 10%
* Cu	Au	50	50	Ka	Lif200	"	"	45.040	60	39.65 46.70	30	UU-4 110 ppm	SiO_2 and $CaCO_3$	0.2 ppm	± 10%
* Ni	Au	50	50	Ka	Lif200	"	"	48.690	60	46.70 50.00	30	BR 260 ppm	SiO_2 and $CaCO_3$	0.1 ppm	± 10%
Cr	Au	50	50	Ka	Lif200	"	"	69.375	60	68.10 70.80	30	JB1 400 ppm	SiO_2	0.6 ppm	10%
V	Au	50	50	Ka	Lif220	"	"	123.220	60	117.10 123.80	30	W-1 260 ppm	SiO_2	0.5 ppm	± 10%
La	Au	50	50	Ka	Lif220	"	"	138.920	60	132.60 141.80	30	BR 80 ppm	SiO_2	1.5 ppm	15%
* Zr	Rh	50	50	Ka	Lif220	"	Scint	32.045	60	29.30 34.89	30	AGV 230 ppm	SiO_2	0.3 ppm	3%
* Sr	Rh	50	50	Ka	Lif220	"	"	35.830	60	34.89 36.90	30	W-1 190 ppm	SiO_2	0.2 ppm	3%
Nb	Rh	50	50	Ka	Lif220	"	"	30.420	60	29.45 34.80	30	GSP 23 ppm	SiO_2	0.1 ppm	3%
Y	Rh	50	50	Ka	Lif220	"	"	33.855	60	29.45 34.80	30	NIMG 145 ppm	SiO_2	0.3 ppm	3%
Rb	Rh	50	50	Ka	Lif220	"	"	37.960	60	34.80 41.10	30	NIMG 320 ppm	SiO_2	0.4 ppm	2%
U	Rh	50	50	Ka	Lif220	"	"	37.300	100	36.90 41.10	30	NIMG 15 ppm	SiO_2	0.1 ppm	20%
Th	Rh	50	50	Ka	Lif220	"	"	39.250	100	36.90 41.10	30	GSP 105 ppm	SiO_2	0.5 ppm	20%
Pb	Au	50	50	Ka	Lif220	"	Flow/ Scint	40.225	60	39.80 41.50	30	GSP 54 ppm	SiO_2	1 ppm	± 10%
Ga	Au	50	50	Ka	Lif220	"	"	56.165	60	55.50 57.20	30	GSP 23 ppm	SiO_2	0.2 ppm	10%
Co	Au	50	50	Ka	Lif220	"	"	77.890	60	77.40 79.00	30	NIMD 210 ppm	SiO_2	1 ppm	± 10%

12 May 1989
/br

Statistical Summary Descriptives for all Geochemical Elements Analysed

Major Element Oxides

Summary statistics for SiO_2 (weight %) per a rock type.

Rock Type	Count	Avg.	Median	Standard dev.	Min	Max	Range	Interquartile range
Fpyx	13	48.602	49.150	3.427	41.460	52.790	11.330	1.690
Pyx	10	46.413	46.340	0.360	45.770	47.080	1.3100	0.380
Parapyx	54	44.683	44.705	2.944	38.410	51.000	12.590	4.140
Serp	7	37.995	36.760	3.066	34.600	41.400	6.800	5.910
Calc-sil	3	46.613	45.980	7.609	39.340	54.520	15.180	15.180
Total	87	44.996	45.500	3.916	34.600	54.520	19.920	4.990

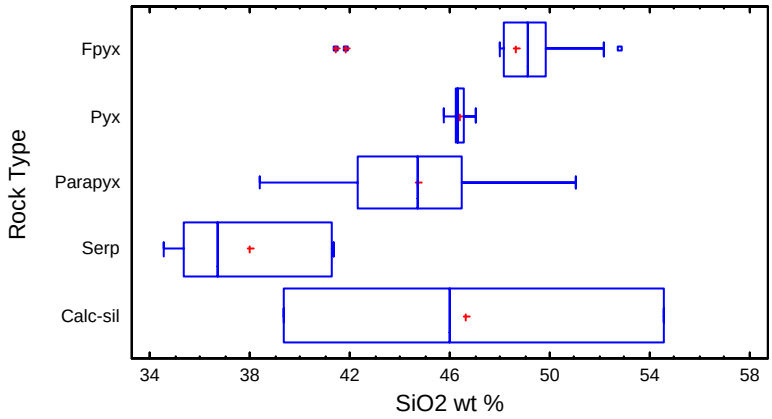

Summary statistics for Al_2O_3 (weight %) per a rock type.

Rock Type	Count	Avg.	Median	Standard dev.	Min	Max	Range	Interquartile range
Fpyx	13	7.046	6.380	1.666	5.160	10.900	5.740	2.360
Pyx	10	5.844	5.775	0.169	5.690	6.110	0.420	0.340
Parapyx	54	7.846	7.210	3.445	0.910	16.360	15.450	4.960
Serp	7	6.348	7.710	3.585	0.670	10.250	9.580	6.440
Calc-sil	3	4.926	3.330	5.763	0.130	11.320	11.190	11.190
Total	87	7.275	6.410	3.176	0.130	16.360	16.230	4.190

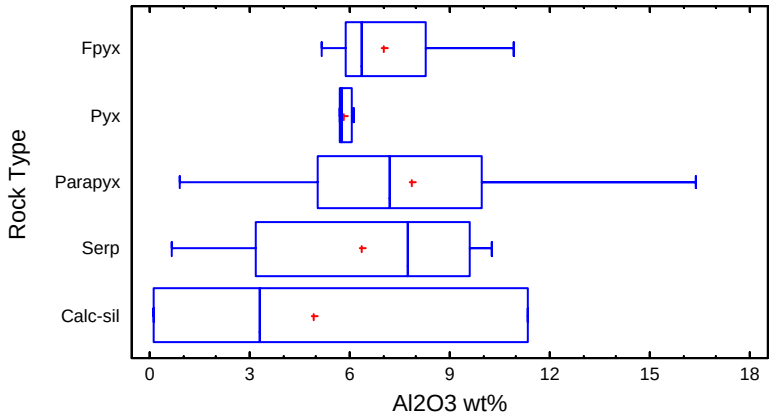

Summary statistics for FeO (weight %) per a rock type.

Rock Type	Count	Average.	Median	Standard dev.	Min	Max	Range	Interquartile range
Fpyx	13	8.001	7.240	2.429	4.460	12.960	8.500	2.100
Pyx	10	7.184	7.115	0.316	6.820	7.730	0.910	0.430
Parapyx	54	7.575	7.345	1.635	3.840	12.260	8.420	1.610
Serp	7	12.847	13.560	1.876	10.210	15.160	4.950	3.450
Calc-sil	3	4.340	5.530	2.904	1.030	6.460	5.430	5.430
Total	87	7.906	7.320	2.342	1.030	15.160	14.130	1.970

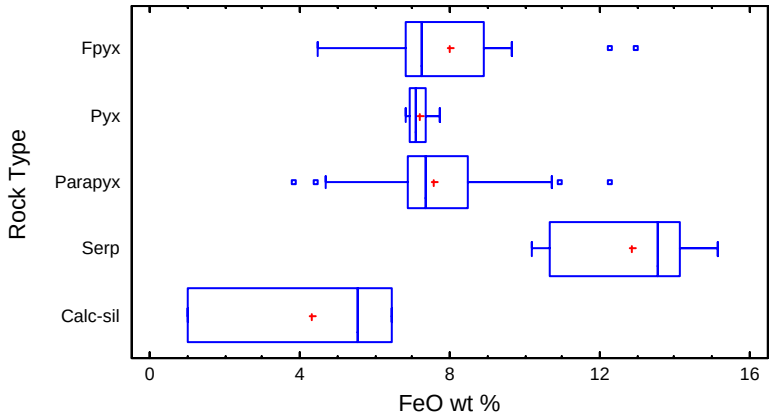

Summary statistics for MnO (weight %) per a rock type.

Rock Type	Count	Avg.	Median	Standard dev.	Min	Max	Range	Interquartile range
Fpyx	13	0.310	0.237	0.138	0.177	0.608	0.431	0.134
Pyx	10	0.282	0.284	0.007	0.264	0.293	0.029	0.004
Parapyx	54	0.449	0.454	0.126	0.260	0.891	0.630	0.123
Serp	7	0.277	0.303	0.090	0.148	0.389	0.241	0.168
Calc-sil	3	0.517	0.496	0.099	0.429	0.625	0.196	0.196
Total	87	0.398	0.383	0.139	0.148	0.891	0.743	0.191

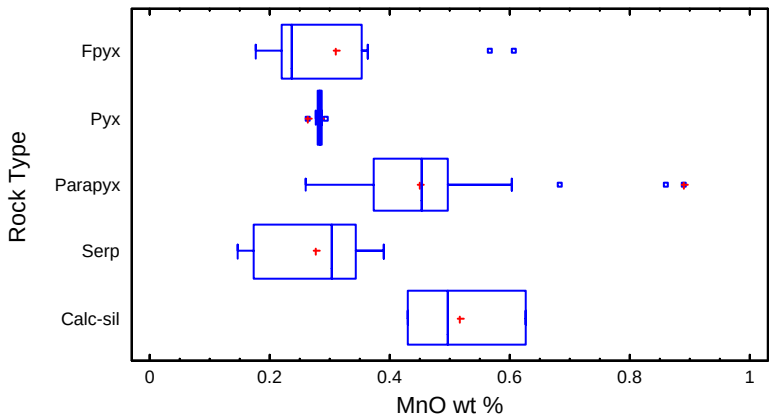

Summary statistics for MgO (weight %) per a rock type.

Rock Type	Count	Avg.	Median	Standard dev.	Min	Max	Range	Interquartile range
Fpyx	13	15.533	14.140	3.944	10.530	22.690	12.160	3.170
Pyx	10	13.037	13.050	0.148	12.770	13.230	0.460	0.160
Parapyx	54	23.167	24.255	5.009	11.470	32.530	21.060	7.990
Serp	7	39.324	38.110	2.486	36.610	42.900	6.290	4.910
Calc-sil	3	23.160	21.430	6.490	17.710	30.340	12.630	12.630
Total	87	22.162	22.640	7.747	10.530	42.900	32.370	12.310

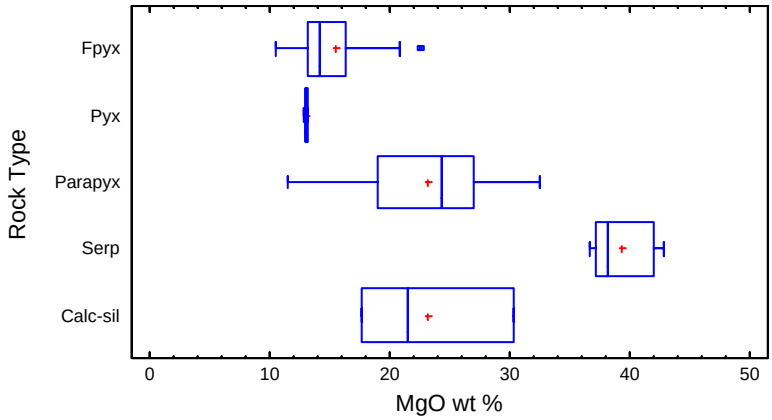

Summary statistics for CaO(weight %) per a rock type.

Rock Type	Count	Avg.	Median	Standard dev.	Min	Max	Range	Interquartile range
Fpyx	13	17.301	19.000	4.962	5.510	22.530	17.020	4.730
Pyx	10	24.350	24.355	0.105	24.140	24.550	0.410	0.080
Parapyx	54	14.650	13.215	5.097	5.180	26.760	21.580	7.240
Serp	7	0.4842	0.300	0.445	0.110	1.350	1.240	0.620
Calc-sil	3	19.806	21.250	6.968	12.230	25.940	13.710	13.710
Total	87	15.199	14.100	7.039	0.110	26.760	26.650	9.820

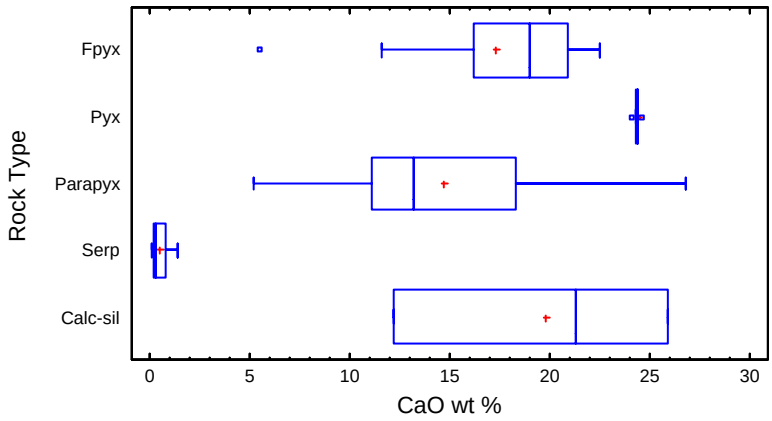

Summary statistics for Na_2O (weight %) per a rock type.

Rock Type	Count	Avg.	Median	Standard dev.	Min	Max	Range	Interquartile range
Fpyx	13	0.893	0.540	0.796	0.130	2.450	2.320	1.140
Pyx	10	0.107	0.110	0.044	0.040	0.170	0.130	0.060
Parapyx	54	0.185	0.170	0.126	0.000	0.560	0.560	0.150
Serp	7	0.031	0.000	0.045	0.000	0.120	0.120	0.060
Calc-sil	3	0.023	0.000	0.040	0.000	0.070	0.070	0.070
Total	87	0.263	0.150	0.414	0.000	2.450	2.450	0.180

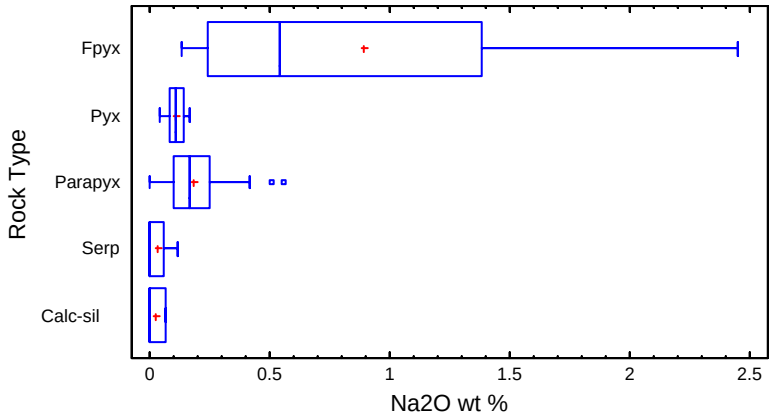

Summary statistics for K_2O (weight %) per a rock type.

Rock Type	Count	Avg.	Median	Standard dev.	Min	Max	Range	Interquartile range
Fpyx	13	0.159	0.080	0.156	0.010	0.400	0.390	0.310
Pyx	10	0.010	0.010	0.000	0.010	0.010	0.000	0.000
Parapyx	54	0.133	0.070	0.166	0.010	0.830	0.820	0.150
Serp	7	0.011	0.010	0.008	0.000	0.020	0.020	0.020
Calc-sil	3	0.010	0.010	0.000	0.010	0.010	0.000	0.000
Total	87	0.108	0.040	0.153	0.000	0.830	0.830	0.120

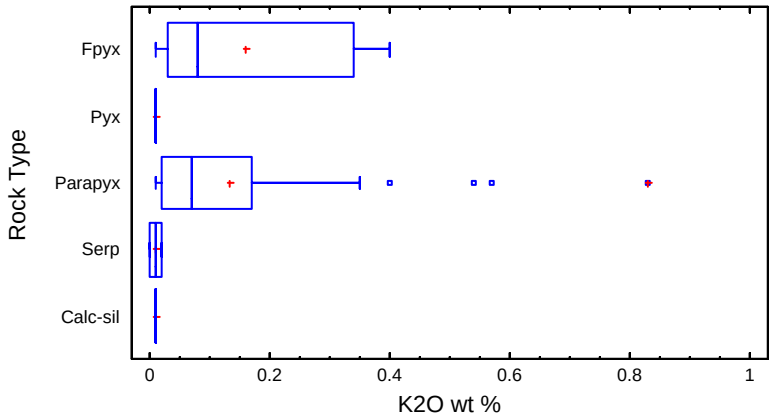

Summary statistics for TiO_2 (weight %) per a rock type.

Rock Type	Count	Avg.	Median	Standard dev.	Min	Max	Range	Interquartile range
Fpyx	13	0.258	0.249	0.072	0.144	0.390	0.246	0.094
Pyx	10	0.368	0.367	0.005	0.360	0.378	0.017	0.009
Parapyx	54	0.295	0.286	0.128	0.098	0.852	0.754	0.167
Serp	7	0.172	0.190	0.108	0.024	0.327	0.302	0.209
Calc-sil	3	0.182	0.091	0.215	0.027	0.429	0.402	0.402
Total	87	0.284	0.284	0.123	0.024	0.852	0.828	0.167

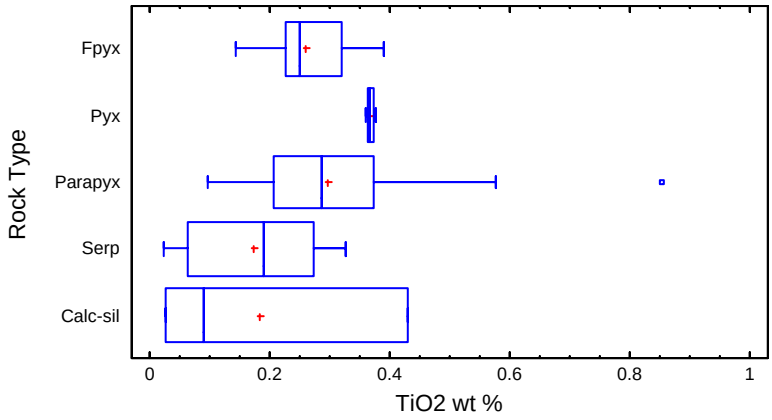

Summary statistics for P_2O_5 (weight %) per a rock type.

Rock Type	Count	Avg.	Median	Standard dev.	Min	Max	Range	Interquartile range
Fpyx	13	0.026	0.020	0.013	0.010	0.050	0.040	0.020
Pyx	10	0.012	0.010	0.004	0.010	0.020	0.010	0.000
Parapyx	54	0.014	0.010	0.016	0.000	0.120	0.120	0.010
Serp	7	0.008	0.010	0.003	0.000	0.010	0.010	0.000
Calc-sil	3	0.006	0.010	0.005	0.000	0.010	0.010	0.010
Total	87	0.015	0.010	0.015	0.000	0.120	0.120	0.010

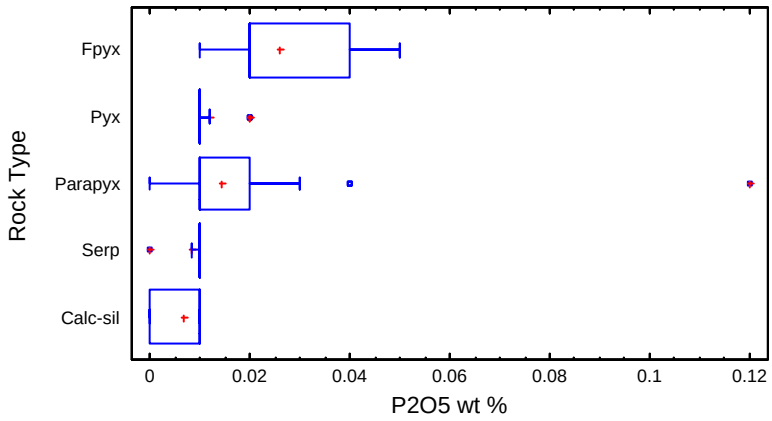

Summary statistics for Cr_2O_3 (weight %) per a rock type.

Rock Type	Count	Avg.	Median	Standard dev.	Min	Max	Range	Interquartile range
Fpyx	13	0.144	0.180	0.137	0.000	0.371	0.371	0.197
Pyx	10	0.027	0.029	0.007	0.013	0.035	0.021	0.010
Parapyx	54	0.017	0.001	0.048	-0.014	0.243	0.257	0.010
Serp	7	0.027	0.022	0.028	0.001	0.078	0.077	0.048
Calc-sil	3	0.011	0.011	0.011	0.000	0.023	0.023	0.023
Total	87	0.038	0.008	0.078	-0.014	0.371	0.386	0.026

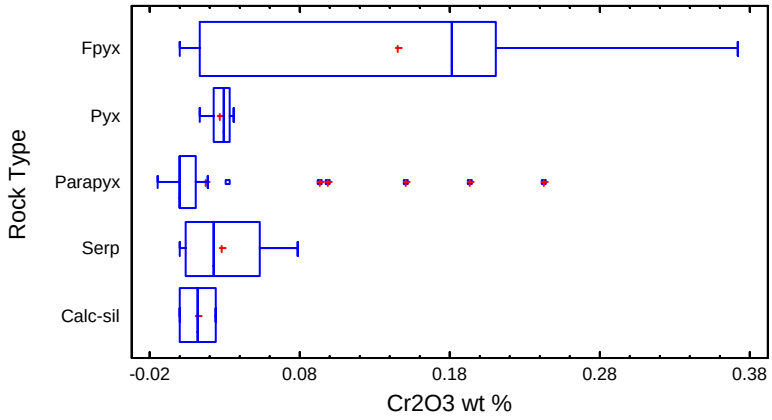

Summary statistics for NiO (weight %) per a rock type.

Rock Type	Count	Avg.	Median	Standard dev.	Min	Max	Range	Interquartile range
Fpyx	13	0.247	0.261	0.126	0.011	0.472	0.460	0.135
Pyx	10	0.377	0.367	0.049	0.320	0.486	0.166	0.033
Parapyx	54	0.108	0.049	0.136	0.003	0.609	0.605	0.118
Serp	7	0.235	0.159	0.307	0.014	0.910	0.895	0.171
Calc-sil	3	0.074	0.106	0.064	0.001	0.116	0.115	0.115
Total	87	0.169	0.108	0.172	0.001	0.910	0.909	0.253

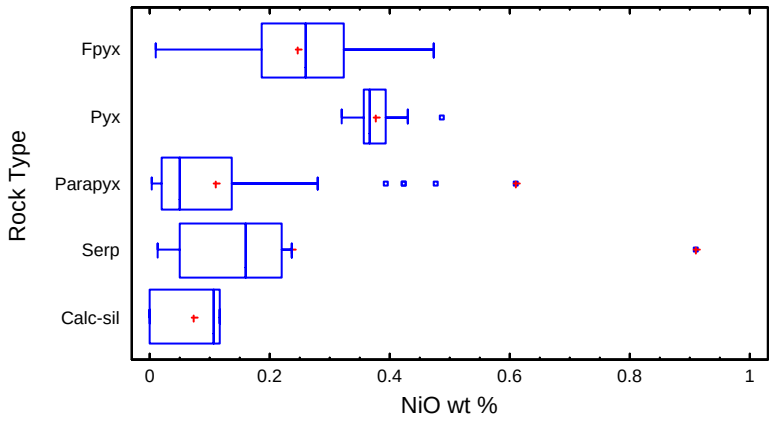

Summary statistics for loss on ignition (LOI) (weight %) per a rock type.

Rock Type	Count	Avg.	Median	Standard dev.	Min	Max	Range	Interquartile range
Fpyx	13	2.806	2.420	1.597	1.230	6.240	5.010	1.390
Pyx	10	0.924	0.890	0.160	0.670	1.140	0.470	0.260
Parapyx	54	6.049	6.380	2.258	1.100	10.930	9.830	3.090
Serp	7	12.484	12.380	0.621	11.880	13.550	1.670	0.930
Calc-sil	3	5.970	5.880	5.055	0.960	11.070	10.110	10.110
Total	87	5.490	5.760	3.438	0.670	13.550	12.880	5.200

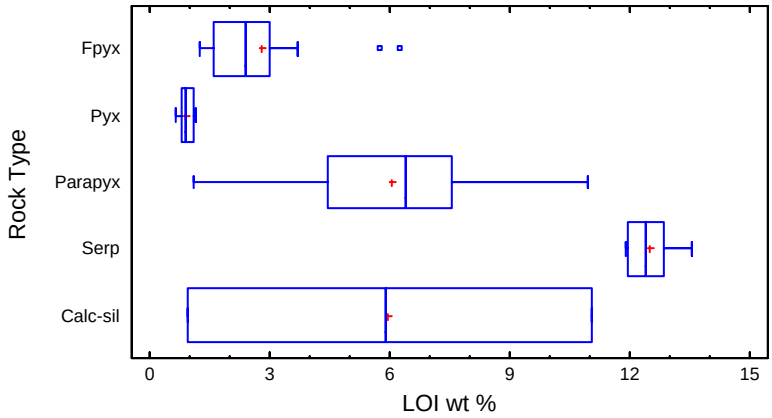

Base Metal Elements

Summary statistics for Ni (ppm) per a rock type.

Rock Type	Count	Avg.	Median	Standard dev.	Min	Max	Range	Interquartile range
Fpyx	13	1821.220	1899.130	904.533	92.699	3325.370	3232.670	1174.840
Pyx	10	2852.580	2814.010	308.289	2339.760	3432.050	1092.290	266.704
Parapyx	54	779.846	348.215	1023.860	26.604	4959.220	4932.620	923.430
Serp	7	1577.260	975.249	2143.120	95.009	6309.320	6214.310	1173.080
Calc-sil	3	551.150	765.497	470.743	11.379	876.575	865.196	865.196
Total	87	1229.970	765.497	1268.010	11.379	6309.320	6297.940	1821.140

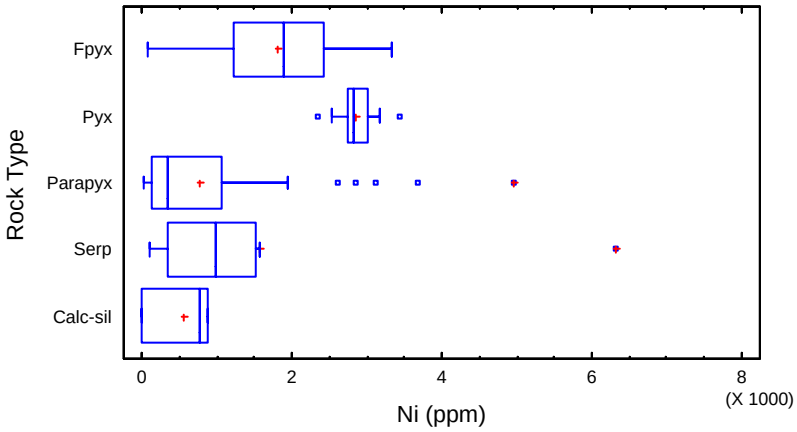

Summary statistics for Cu (ppm) per a rock type.

Rock Type	Count	Avg.	Median	Standard dev.	Min	Max	Range	Interquartile range
Fpyx	13	1085.350	1051.140	695.936	25.962	2407.330	2381.360	977.646
Pyx	10	1853.920	1819.640	194.257	1515.960	2214.130	698.175	145.425
Parapyx	54	392.609	103.534	591.929	3.738	2879.850	2876.120	632.339
Serp	7	893.436	561.228	985.219	156.266	2958.430	2802.160	993.539
Calc-sil	3	307.159	135.496	418.588	1.69114	784.289	782.598	782.598
Total	87	701.439	324.008	777.361	1.69114	2958.430	2956.740	1167.460

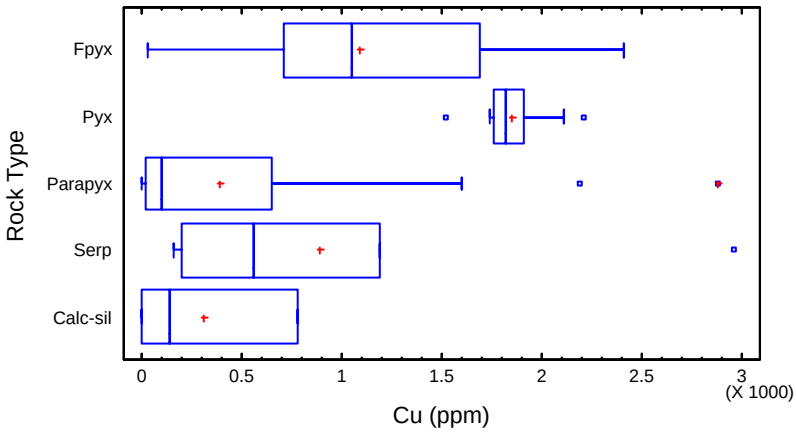

Summary statistics for S (ppm) per a rock type.

Rock Type	Count	Avg.	Median	Standard dev.	Min	Max	Range	Interquartile range
Fpyx	13	5751.410	5328.900	4509.690	70.800	17068.300	16997.500	4146.400
Pyx	10	22770.500	22124.200	2887.050	18822.000	27766.800	8944.800	2411.500
Parapyx	54	4748.370	1568.950	8292.960	54.400	52590.700	52536.300	5410.000
Serp	7	16514.900	21264.900	9402.670	2009.900	25272.900	23263.000	18099.500
Calc-sil	3	1679.070	1733.500	1652.520	0.000	3303.700	3303.700	3303.700
Total	87	7810.660	4696.700	9610.200	0.000	52590.700	52590.700	10733.400

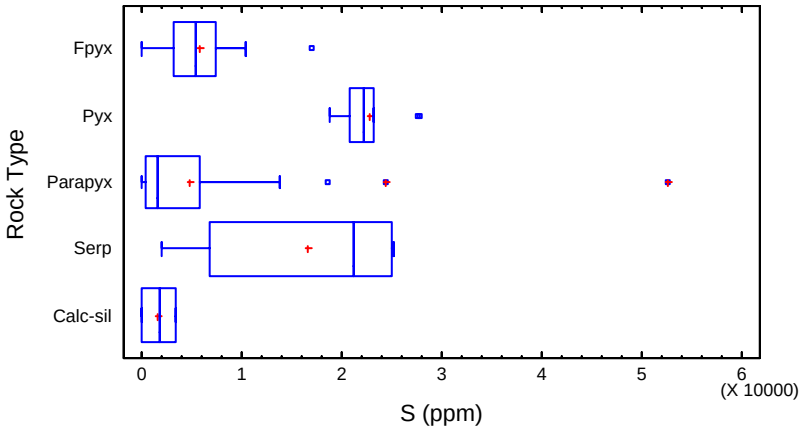

Summary statistics for Co (ppm) per a rock type.

Rock Type	Count	Avg.	Median	Standard dev.	Min	Max	Range	Interquartile range
Fpyx	13	76.096	73.508	28.422	25.517	139.920	114.403	19.820
Pyx	10	83.711	83.044	7.629	67.867	96.544	28.677	8.986
Parapyx	54	40.857	33.605	23.988	7.852	133.194	125.342	25.900
Serp	7	94.205	70.653	73.062	47.089	255.207	208.117	42.821
Calc-sil	3	26.551	23.510	25.271	2.937	53.205	50.267	50.267
Total	87	54.847	47.193	36.093	2.937	255.207	252.269	47.965

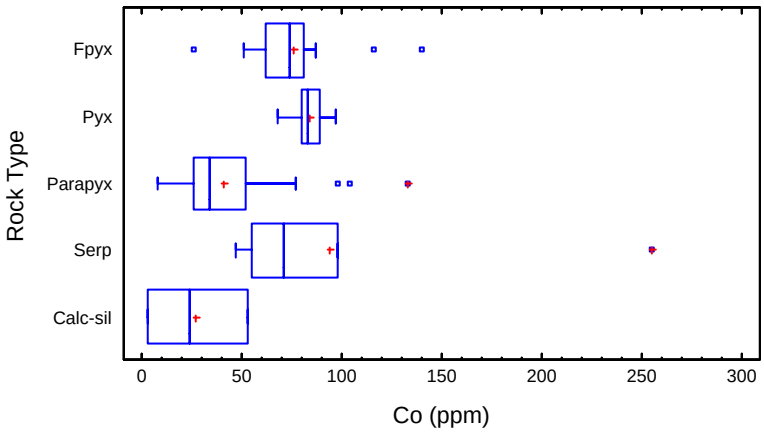

Summary statistics for V (ppm) per a rock type.

Rock Type	Count	Avg.	Median	Standard dev.	Min	Max	Range	Interquartile range
Fpyx	13	135.740	128.500	62.288	43.488	269.972	226.484	76.141
Pyx	10	262.791	252.761	34.480	223.798	324.718	100.920	52.900
Parapyx	54	78.591	65.122	47.429	9.696	228.000	218.303	35.532
Serp	7	25.194	25.709	12.851	9.121	45.542	36.421	24.262
Calc-sil	3	35.365	14.393	43.663	6.145	85.558	79.413	79.413
Total	87	102.516	72.182	79.153	6.145	324.718	318.573	77.618

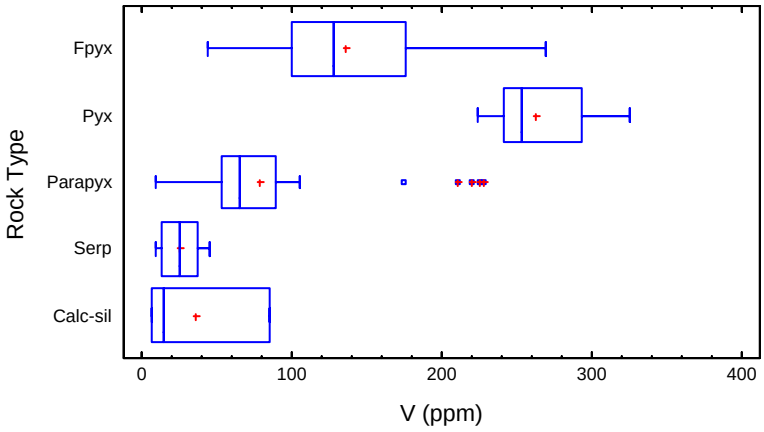

Summary statistics for As (ppm) per a rock type.

Rock Type	Count	Avg.	Median	Standard dev.	Min	Max	Range	Interquartile range
Fpyx	13	0.958	0.457	1.332	0.223	5.148	4.925	0.535
Pyx	10	0.710	0.689	0.091	0.583	0.868	0.284	0.153
Parapyx	54	0.458	0.294	0.418	0.116	1.932	1.816	0.328
Serp	7	0.633	0.526	0.359	0.318	1.288	0.970	0.581
Calc-sil	3	1.448	0.527	1.940	0.139	3.678	3.538	3.538
Total	87	0.610	0.393	0.715	0.116	5.148	5.032	0.433

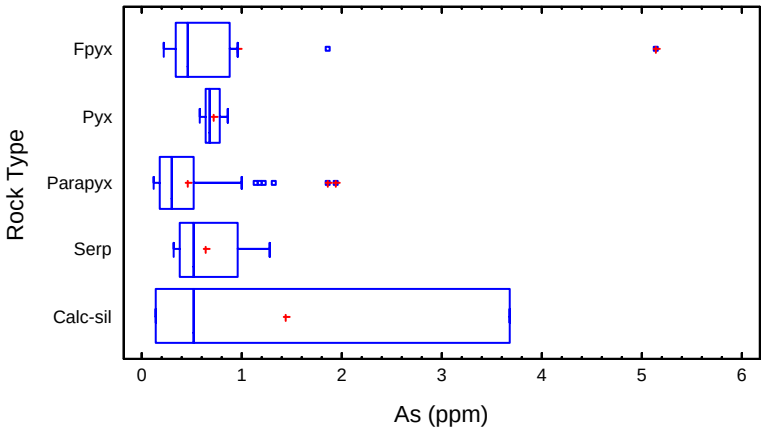

Summary statistics for Sc (ppm) per a rock type.

Rock Type	Count	Avg.	Median	Standard dev.	Min	Max	Range	Interquartile range
Fpyx	13	26.879	25.892	9.682	11.992	49.794	37.802	11.088
Pyx	10	32.085	31.988	4.220	25.411	40.758	15.347	2.164
Parapyx	54	15.630	12.865	9.359	0.663	44.469	43.806	7.882
Serp	7	7.169	9.244	5.260	1.072	12.839	11.767	10.884
Calc-sil	3	6.734	4.766	7.643	0.267	15.169	14.901	14.901
Total	87	18.215	13.783	11.165	0.267	49.794	49.526	15.206

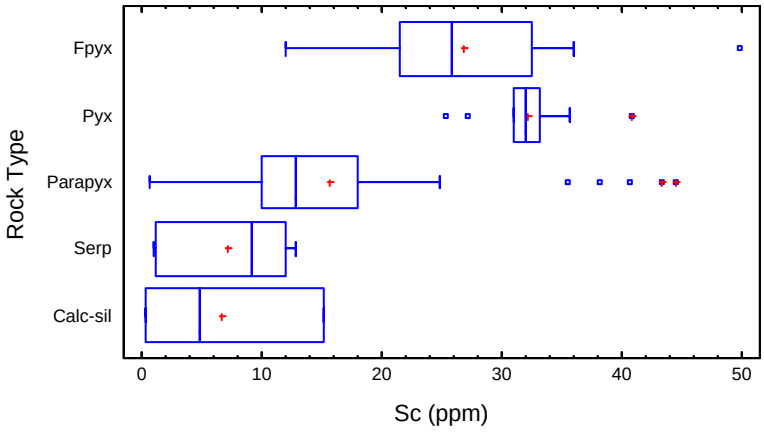

Summary statistics for Pb (ppm) per a rock type.

Rock Type	Count	Avg.	Median	Standard dev.	Min	Max	Range	Interquartile range
Fpyx	13	39.282	14.308	83.023	1.115	310.100	308.984	16.606
Pyx	10	5.211	5.868	1.992	2.035	7.485	5.449	3.520
Parapyx	54	9.368	7.846	7.759	0.763	38.778	38.015	8.863
Serp	7	9.691	7.205	10.220	0.695	30.216	29.520	13.444
Calc-sil	3	111.272	11.834	180.706	2.124	319.858	317.734	317.734
Total	87	16.900	7.281	46.991	0.695	319.858	319.162	9.422

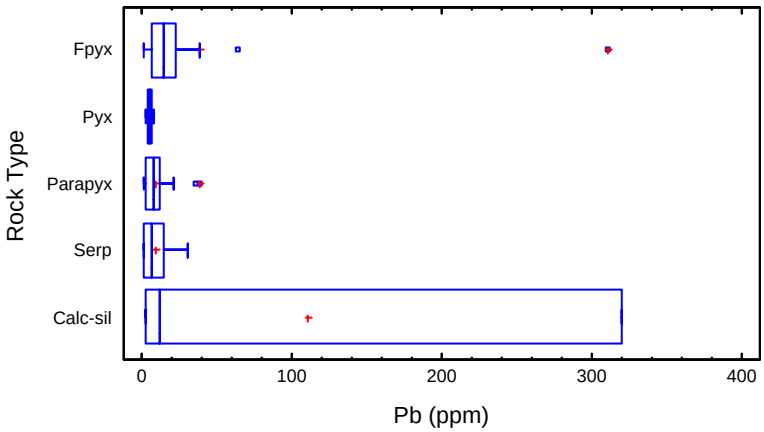

Summary statistics for Cr (ppm) per a rock type.

Rock Type	Count	Avg.	Median	Standard dev.	Min	Max	Range	Interquartile range
Fpyx	13	848.704	1235.690	774.472	23.789	2184.940	2161.150	1190.470
Pyx	10	140.435	139.482	35.203	93.944	185.260	91.315	65.831
Parapyx	54	148.452	45.305	319.548	2.918	1509.810	1506.900	75.346
Serp	7	143.367	83.406	162.892	7.061	421.785	414.723	307.108
Calc-sil	3	84.690	99.900	72.467	5.825	148.345	142.520	142.520
Total	87	249.558	77.953	461.150	2.918	2184.940	2182.020	122.594

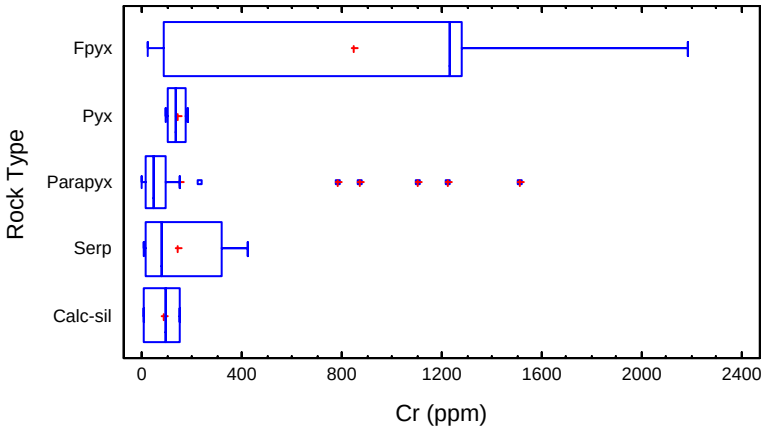

Summary statistics for Zn (ppm) per a rock type.

Rock Type	Count	Avg.	Median	Standard dev.	Min	Max	Range	Interquartile range
Fpyx	13	78.920	52.378	70.648	34.173	270.029	235.856	28.065
Pyx	10	31.511	29.330	5.9465	26.240	43.576	17.335	8.923
Parapyx	54	43.023	38.687	20.249	15.995	107.662	91.667	30.590
Serp	7	51.067	47.178	33.616	14.796	103.743	88.946	67.358
Calc-sil	3	72.662	39.084	87.088	7.3601	171.542	164.181	164.181
Total	87	48.733	39.084	37.698	7.3601	270.029	262.669	27.115

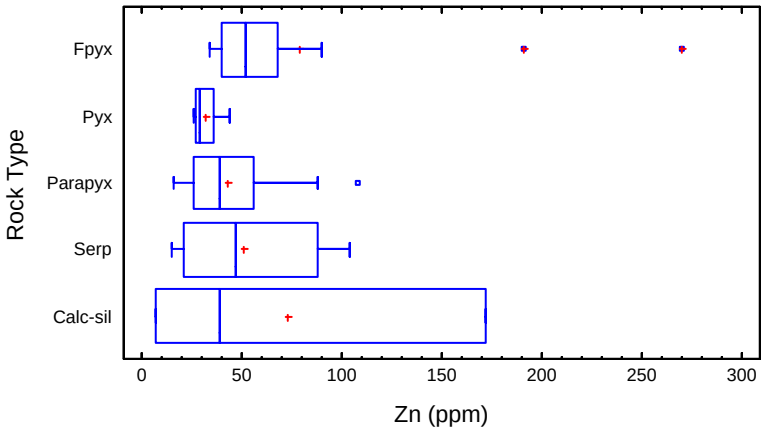

Platinum Group Elements

Summary statistics for Au (ppb) per a rock type.

Rock Type	Count	Avg.	Median	Standard dev.	Min	Max	Range	Interquartile range
Fpyx	13	168.4	199.0	92.5	13.0	300.0	287.0	118.0
Pyx	10	156.8	157.5	25.3	111.0	189.0	78.0	40.0
Parapyx	35	227.1	109.0	271.6	10.0	1306.0	1296.0	290.0
Serp	7	91.0	74.0	104.5	8.0	309.0	301.0	95.0
Calc-sil	3	132.6	47.0	178.6	13.0	338.0	325.0	325.0
Total	68	187.3	145.0	207.6	8.0	1306.0	1298.0	205.5

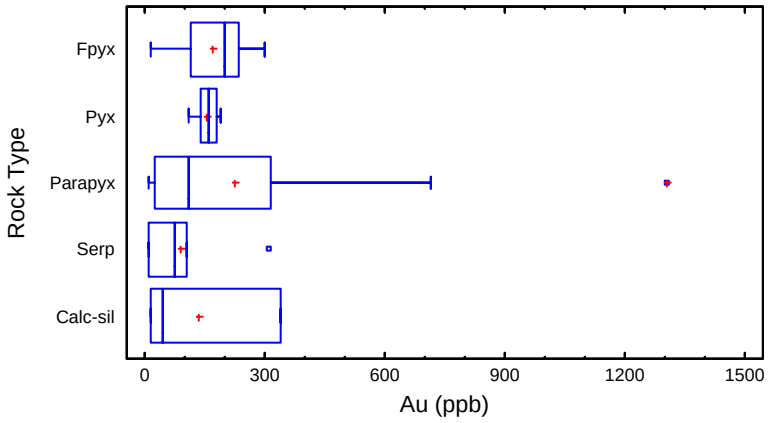

Summary statistics for Ir (ppb) per a rock type.

Rock Type	Count	Avg.	Median	Standard dev.	Min	Max	Range	Interquartile range
Fpyx	13	23.4	20.0	16.1	0.0	62.0	62.0	7.0
Pyx	10	26.1	24.0	6.64	18.0	42.0	24.0	8.0
Parapyx	54	26.7	0.0	50.1	0.0	216.0	216.0	35.0
Serp	7	7.0	3.0	9.0	0.0	22.0	22.0	17.0
Calc-sil	3	35.3	15.0	48.7	0.0	91.0	91.0	91.0
Total	87	24.9	15.0	41.0	0.0	216.0	216.0	26.0

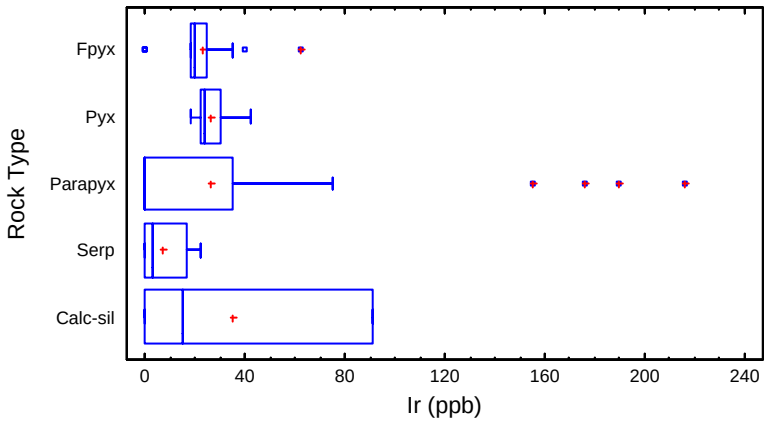

Summary statistics for Os (ppb) per a rock type.

Rock Type	Count	Avg.	Median	Standard dev.	Min	Max	Range	Interquartile range
Fpyx	13	12.2	10.0	8.5	0.0	32.0	32.0	4.0
Pyx	10	15.4	14.0	4.9	9.0	28.0	19.0	4.0
Parapyx	54	13.0	0.0	25.8	0.0	106.0	106.0	17.0
Serp	7	3.5	0.0	4.9	0.0	11.0	11.0	10.0
Calc-sil	3	18.3	7.0	25.9	0.0	48.0	48.0	48.0
Total	87	12.6	8.0	21.2	0.0	106.0	106.0	15.0

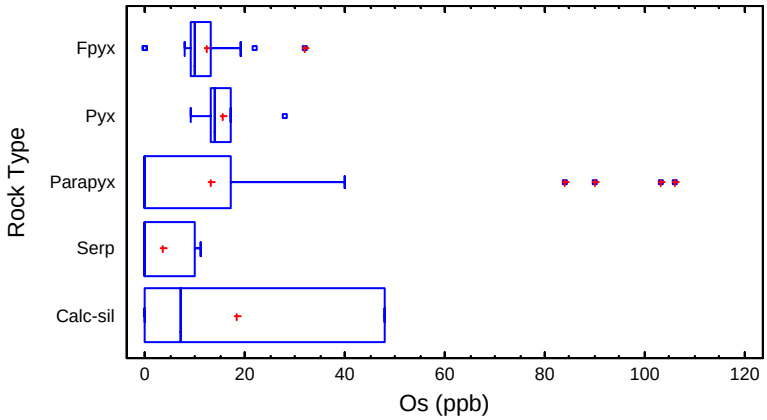

Summary statistics for Pd (ppb) per a rock type.

Rock Type	Count	Avg.	Median	Standard dev.	Min	Max	Range	Interquartile range
Fpyx	13	1308.3	1329.0	783.7	6.0	2632.0	2626.0	619.0
Pyx	10	1332.1	1302.5	179.2	1086.0	1689.0	603.0	160.0
Parapyx	54	1477.3	77.5	2860.6	4.0	15177.0	15173.0	2108.0
Serp	7	546.7	516.0	704.9	9.0	2020.0	2011.0	619.0
Calc-sil	3	1883.0	744.0	2639.7	4.0	4901.0	4897.0	4897.0
Total	87	1374.4	732.0	2324.0	4.0	15177.0	15173.0	1676.0

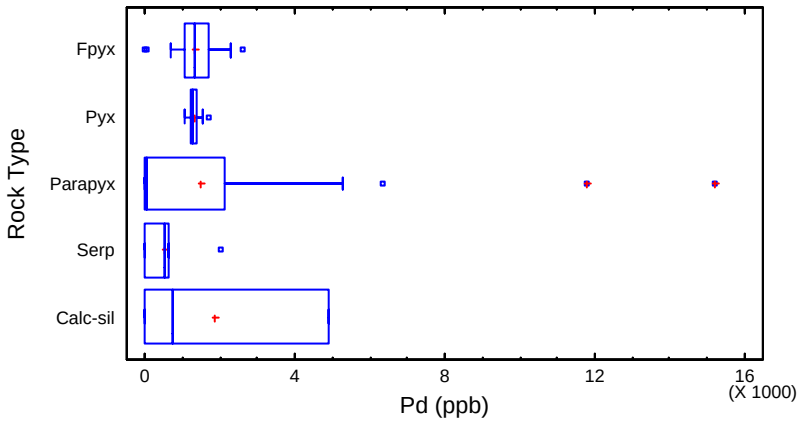

Summary statistics for Pt (ppb) per a rock type.

Rock Type	Count	Avg.	Median	Standard dev.	Min	Max	Range	Interquartile range
Fpyx	13	1035.6	1094.0	611.1	3.0	1957.0	1954.0	386.0
Pyx	10	1234.3	1185.5	149.6	1070.0	1546.0	476.0	145.0
Parapyx	54	1258.8	70.0	2223.0	2.0	11265.0	11263.0	1684.0
Serp	7	324.2	353.0	323.0	7.0	816.0	809.0	634.0
Calc-sil	2	2209.0	2209.0	2170.8	674.0	3744.0	3070.0	3070.0
Total	86	1168.2	704.0	1814.3	2.0	11265.0	11263.0	1418.0

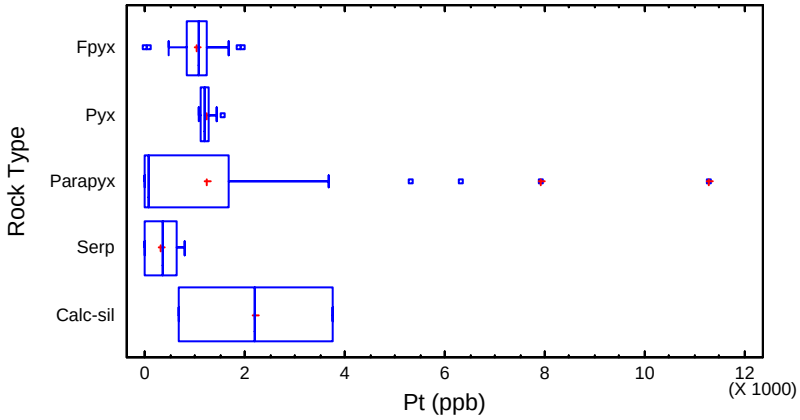

Summary statistics for Rh (ppb) per a rock type.

Rock Type	Count	Avg.	Median	Standard dev.	Min	Max	Range	Interquartile range
Fpyx	13	106.1	102.0	68.4	0.0	267.0	267.0	43.0
Pyx	10	100.8	93.0	22.8	70.0	152.0	82.0	23.0
Parapyx	54	111.8	4.0	210.9	0.0	947.0	947.0	148.0
Serp	7	33.0	23.0	40.1	1.0	100.0	99.0	78.0
Calc-sil	3	154.3	67.0	211.9	0.0	396.0	396.0	396.0
Total	87	104.8	67.0	172.6	0.0	947.0	947.0	117.0

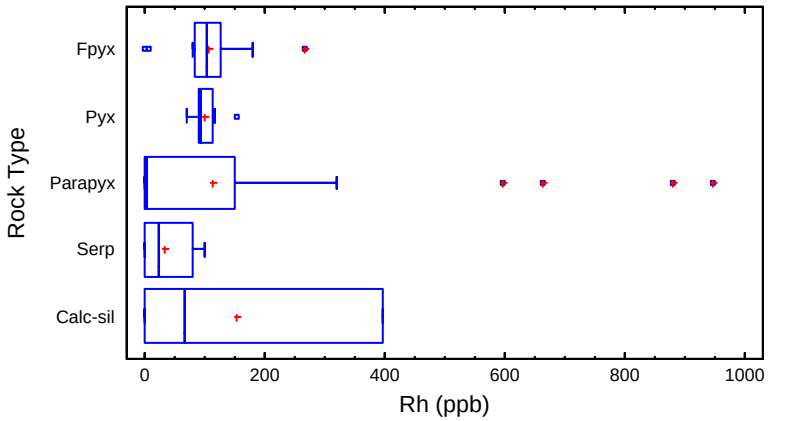

Summary statistics for Ru (ppb) per a rock type.

Rock Type	Count	Avg.	Median	Standard dev.	Min	Max	Range	Interquartile range
Fpyx	13	94.4	79.0	67.8	0.0	258.0	258.0	36.0
Pyx	10	108.5	99.5	35.2	61.0	194.0	133.0	31.0
Parapyx	54	97.5	6.0	186.8	0.0	803.0	803.0	126.0
Serp	7	25.4	11.0	31.5	0.0	71.0	71.0	68.0
Calc-sil	3	143.0	62.0	196.4	0.0	367.0	367.0	367.0
Total	87	94.1	55.0	154.1	0.0	803.0	803.0	108.0

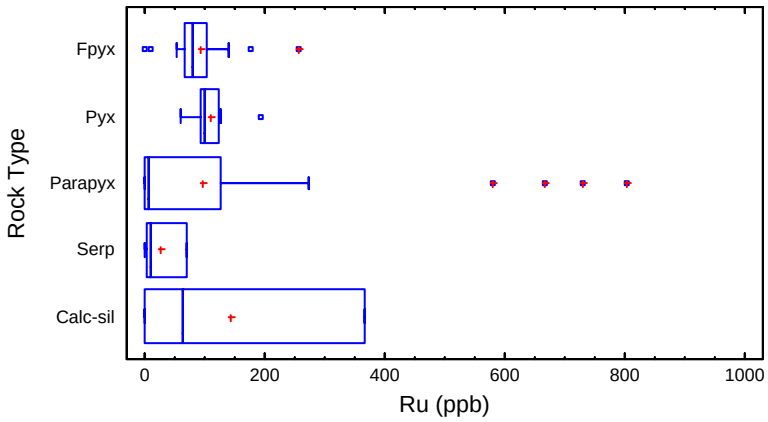

Alkali Earth Elements

Summary statistics for Na2O (weight %) per a rock type.

Rock Type	Count	Avg.	Median	Standard dev.	Min	Max	Range	Interquartile range
Fpyx	13	0.893	0.540	0.796	0.130	2.450	2.320	1.140
Pyx	10	0.107	0.110	0.044	0.040	0.170	0.130	0.060
Parapyx	54	0.185	0.170	0.126	0.000	0.560	0.560	0.150
Serp	7	0.031	0.000	0.045	0.000	0.120	0.120	0.060
Calc-sil	3	0.023	0.000	0.040	0.000	0.070	0.070	0.070
Total	87	0.263	0.150	0.414	0.000	2.450	2.450	0.180

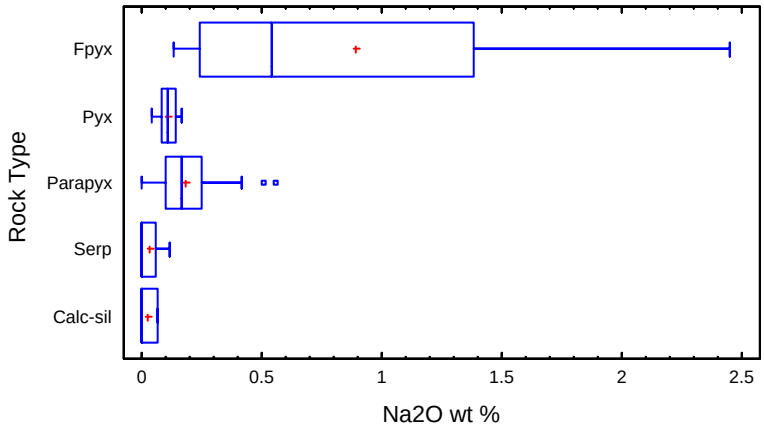

Summary statistics for K2O (weight %) per a rock type.

Rock Type	Count	Avg.	Median	Standard dev.	Min	Max	Range	Interquartile range
Fpyx	13	0.159	0.080	0.156	0.010	0.400	0.390	0.310
Pyx	10	0.010	0.010	0.000	0.010	0.010	0.000	0.000
Parapyx	54	0.133	0.070	0.166	0.010	0.830	0.820	0.150
Serp	7	0.011	0.010	0.008	0.000	0.020	0.020	0.020
Calc-sil	3	0.010	0.010	0.000	0.010	0.010	0.000	0.000
Total	87	0.108	0.040	0.153	0.000	0.830	0.830	0.120

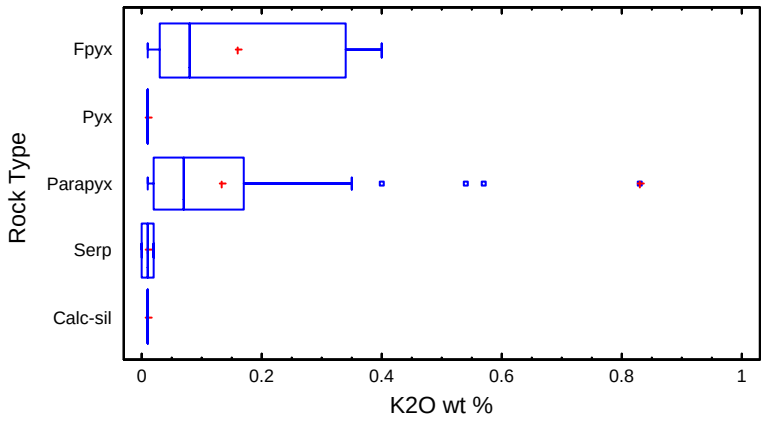

Summary statistics for Sr (ppm) per a rock type.

Rock Type	Count	Avg.	Median	Standard dev.	Min	Max	Range	Interquartile range
Fpyx	13	58.468	40.361	50.111	11.937	155.641	143.703	70.014
Pyx	10	32.113	32.409	3.241	25.889	35.946	10.056	4.434
Parapyx	54	27.325	12.803	32.286	2.103	166.374	164.270	17.864
Serp	7	1.874	1.773	0.716	0.900	3.067	2.166	1.102
Calc-sil	3	10.969	12.290	2.970	7.567	13.049	5.482	5.482
Total	87	29.917	15.029	34.622	0.900	166.374	165.473	24.481

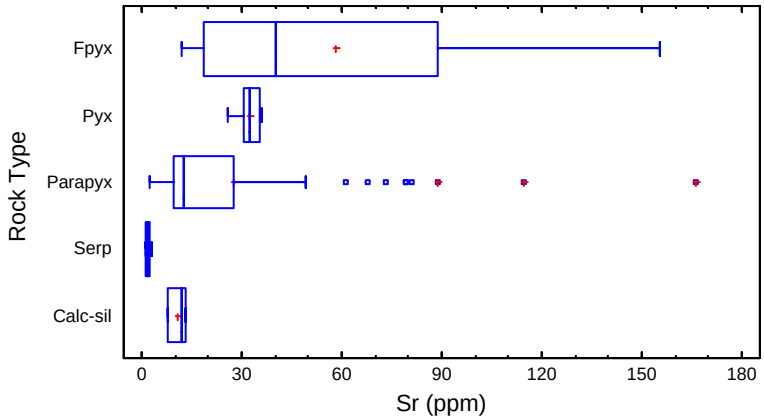

Summary statistics for Rb (ppm) per a rock type.

Rock Type	Count	Avg.	Median	Standard dev.	Min	Max	Range	Interquartile range
Fpyx	13	5.806	1.807	6.489	0.676	17.876	17.200	11.637
Pyx	10	0.157	0.158	0.033	0.115	0.211	0.095	0.056
Parapyx	54	5.543	3.175	7.962	0.049	48.424	48.374	5.086
Serp	7	0.578	0.535	0.465	-0.004	1.355	1.360	0.766
Calc-sil	3	0.170	0.185	0.094	0.068	0.255	0.186	0.186
Total	87	4.378	1.542	7.070	-0.004	48.424	48.428	5.051

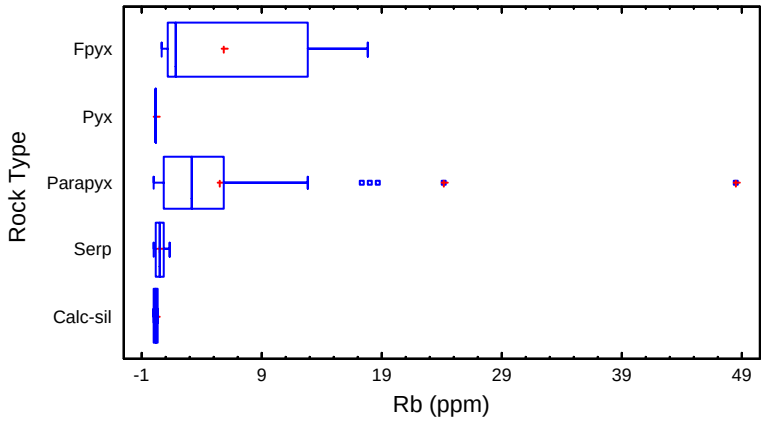

Rare Earth Elements

Summary statistics for Total REE per a rock type.

Rock Type	Count	Avg.	Median	Standard dev.	Min	Max	Range	Interquartile range
Fpyx	13	43.308	39.331	17.996	17.170	66.210	49.040	25.277
Pyx	10	34.781	34.715	3.162	29.884	39.488	9.603	5.496
Parapyx	54	27.539	25.285	11.237	10.409	78.396	67.987	11.431
Serp	7	10.529	11.190	5.384	4.263	18.870	14.607	9.705
Calc-sil	3	43.527	9.895	60.044	7.836	112.851	105.015	105.015
Total	87	29.910	28.097	16.745	4.263	112.851	108.588	15.465

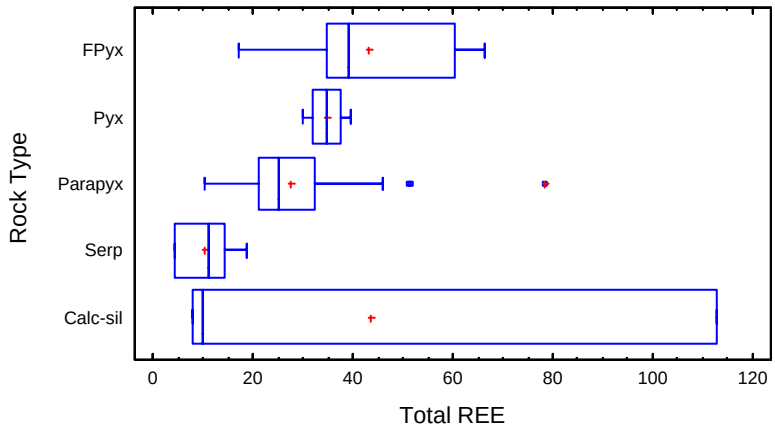

Incompatible Elements

Summary statistics for Ba (ppm) per rock type.

Rock Type	Count	Avg.	Median	Standard dev.	Min	Max	Range	Interquartile range
Fpyx	13	40.319	14.450	63.907	2.757	241.652	238.894	46.238
Pyx	10	2.779	2.359	1.463	1.656	6.75586	5.09937	0.930
Parapyx	54	20.921	9.614	40.586	0.885	265.281	264.396	17.888
Serp	7	2.997	3.127	1.970	0.812	5.537	4.725	3.870
Calc-sil	3	1.389	0.593	1.617	0.324	3.250	2.926	2.926
Total	87	19.619	6.046	41.455	0.324	265.281	264.957	15.804

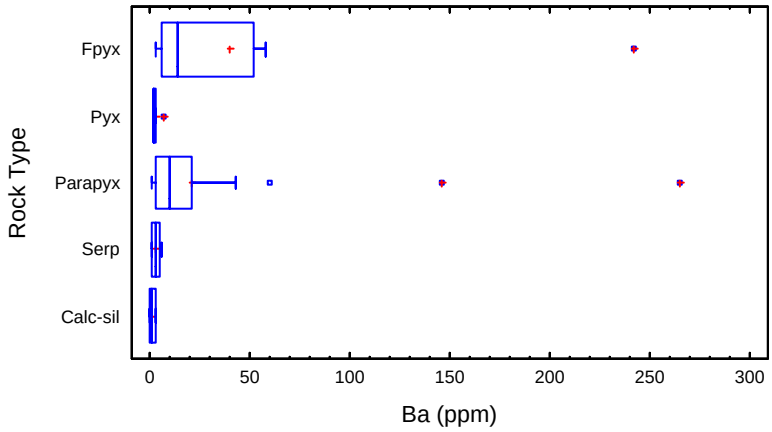

Summary statistics for Th (ppm) per rock type.

Rock Type	Count	Avg.	Median	Standard dev.	Min	Max	Range	Interquartile range
Fpyx	13	0.931	0.788	0.726	0.128	2.640	2.511	0.874
Pyx	10	0.513	0.506	0.083	0.399	0.653	0.254	0.134
Parapyx	54	0.804	0.347	2.590	0.072	19.090	19.017	0.227
Serp	7	0.247	0.150	0.293	0.001	0.853	0.852	0.337
Calc-sil	3	1.424	2.035	1.214	0.025	2.213	2.187	2.187
Total	87	0.766	0.396	2.073	0.001	19.090	19.089	0.386

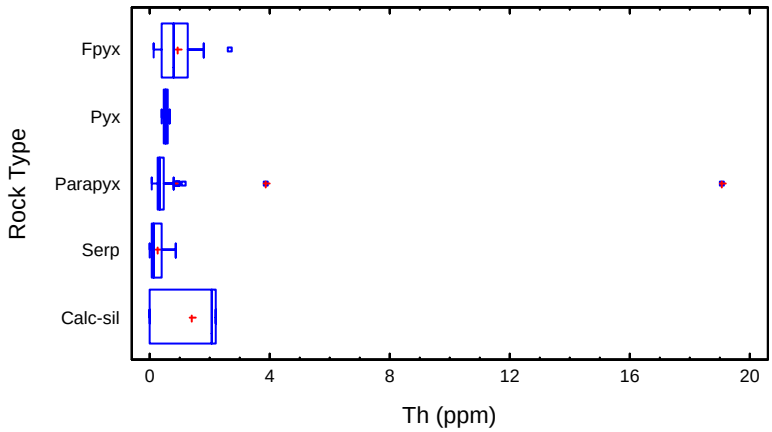

Summary statistics for U (ppm) per rock type.

Rock Type	Count	Avg.	Median	Standard dev.	Min	Max	Range	Interquartile range
Fpyx	13	0.336	0.256	0.239	0.085	0.825	0.740	0.276
Pyx	10	0.227	0.228	0.015	0.201	0.261	0.059	0.011
Parapyx	54	0.202	0.103	0.371	0.033	2.696	2.663	0.140
Serp	7	0.145	0.100	0.146	0.043	0.468	0.424	0.073
Calc-sil	3	0.482	0.150	0.664	0.049	1.247	1.197	1.197
Total	87	0.230	0.147	0.331	0.033	2.696	2.663	0.148

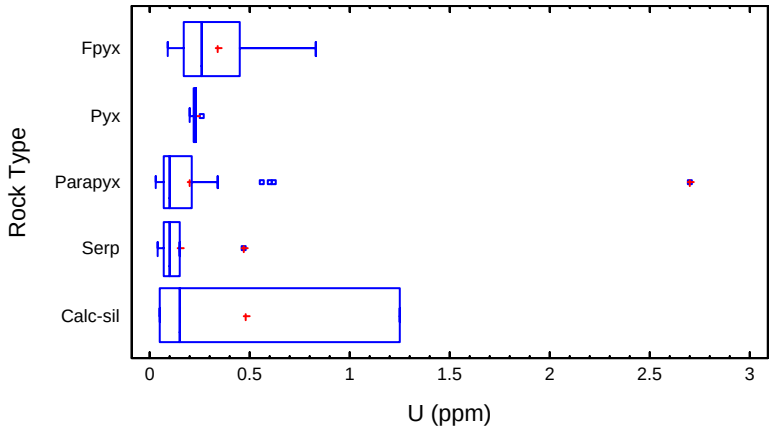

Summary statistics for Ta (ppm) per rock type.

Rock Type	Count	Avg.	Median	Standard dev.	Min	Max	Range	Interquartile range
Fpyx	13	0.077	0.063	0.056	0.014	0.203	0.189	0.061
Pyx	10	0.055	0.054	0.004	0.047	0.064	0.016	0.006
Parapyx	54	0.056	0.038	0.064	0.009	0.422	0.412	0.020
Serp	7	0.046	0.033	0.030	0.014	0.091	0.077	0.056
Calc-sil	3	0.050	0.003	0.081	0.003	0.145	0.141	0.141
Total	87	0.058	0.042	0.057	0.003	0.422	0.419	0.031

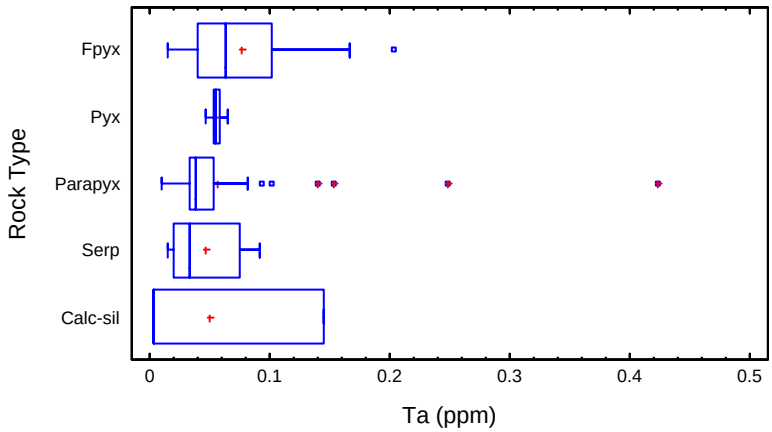

Summary statistics for Zr (ppm) per rock type.

Rock Type	Count	Avg.	Median	Standard dev.	Min	Max	Range	Interquartile range
Fpyx	13	28.288	26.773	11.848	9.272	51.458	42.186	15.662
Pyx	10	42.939	44.732	5.089	33.614	48.130	14.515	7.024
Parapyx	54	32.693	30.025	18.512	7.191	98.162	90.970	27.849
Serp	7	21.524	16.692	18.834	2.549	60.574	58.025	16.758
Calc-sil	3	22.233	2.610	34.707	1.783	62.306	60.523	60.523
Total	87	31.953	31.564	17.743	1.783	98.162	96.379	27.849

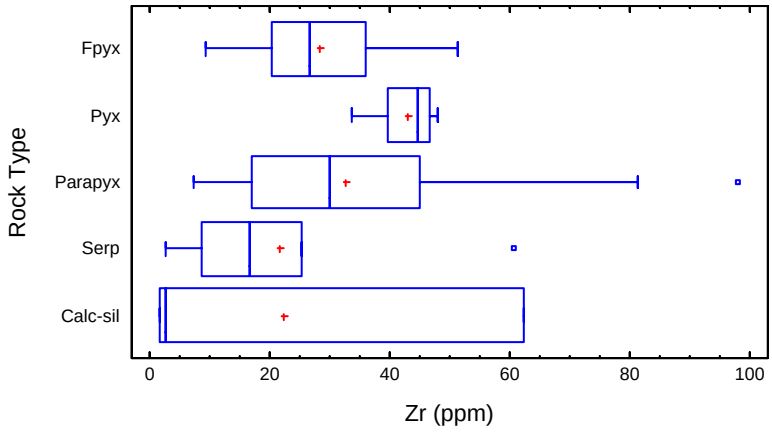

Summary statistics for Nb (ppm) per rock type.

Rock Type	Count	Avg.	Median	Standard dev.	Min	Max	Range	Interquartile range
Fpyx	13	1.181	0.802	0.998	0.145	3.327	3.182	1.079
Pyx	10	0.876	0.889	0.092	0.735	1.032	0.297	0.150
Parapyx	54	0.674	0.411	0.762	0.129	4.623	4.494	0.400
Serp	7	0.354	0.267	0.241	0.110	0.850	0.740	0.230
Calc-sil	3	0.607	0.306	0.712	0.094	1.420	1.325	1.325
Total	87	0.745	0.475	0.749	0.094	4.623	4.528	0.557

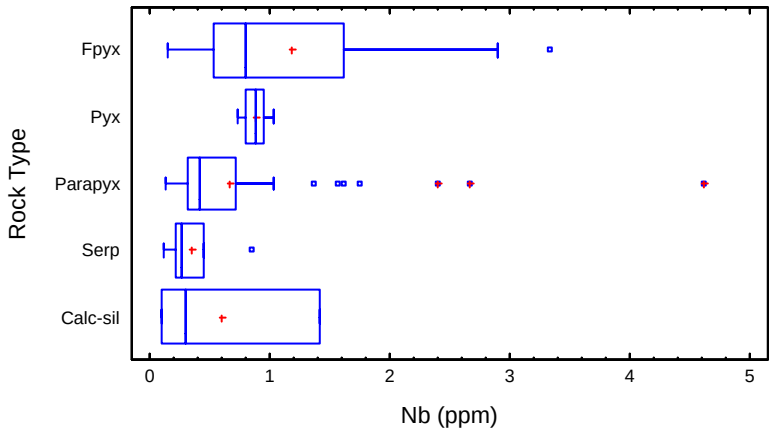

Summary statistics for P (ppm) per rock type.

Rock Type	Count	Avg.	Median	Standard dev.	Min	Max	Range	Interquartile range
Fpyx	13	97.294	81.258	60.179	19.608	195.445	175.836	111.995
Pyx	10	28.550	19.914	16.409	11.473	55.901	44.428	27.075
Parapyx	54	59.433	41.013	74.745	11.898	542.467	530.569	42.372
Serp	7	20.053	16.268	11.516	9.1105	39.179	30.068	21.006
Calc-sil	3	30.686	31.803	15.184	14.974	45.282	30.307	30.307
Total	87	57.381	39.025	66.854	9.110	542.467	533.357	48.918

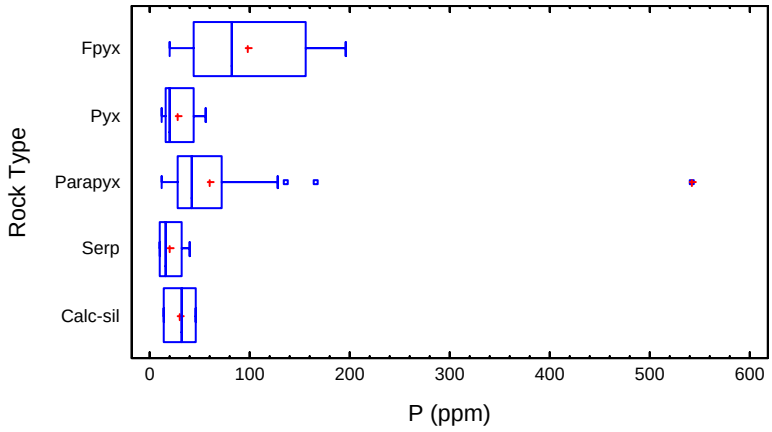

Summary statistics for Hf (ppm) per rock type.

Rock Type	Count	Avg.	Median	Standard dev.	Min	Max	Range	Interquartile range
Fpyx	13	0.942	0.987	0.364	0.291	1.626	1.334	0.461
Pyx	10	1.583	1.644	0.172	1.279	1.753	0.473	0.231
Parapyx	54	1.299	1.269	0.733	0.295	3.230	2.935	1.230
Serp	7	0.833	0.874	0.547	0.073	1.831	1.758	0.521
Calc-sil	3	0.671	0.053	1.077	0.046	1.915	1.868	1.868
Total	87	1.219	1.173	0.674	0.046	3.230	3.184	1.074

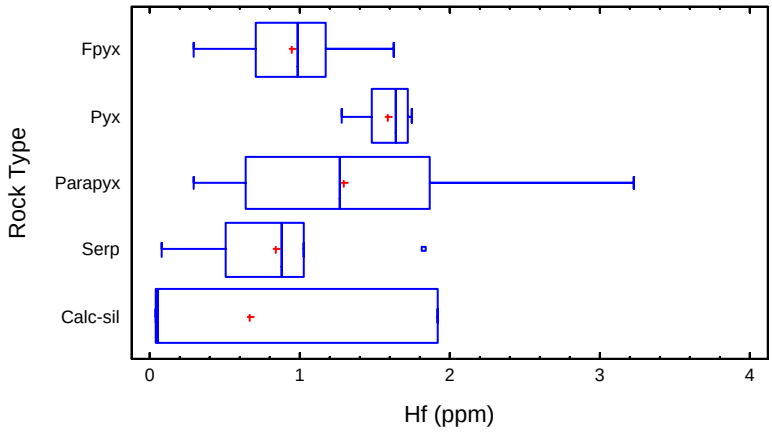

APPENDIX - E

Metallurgical Appendix

Summary statistics for **A**

Rock Type	Count	Avg.	Median	Standard dev.	Min	Max	Range	Interquartile range
Fpyx	11	**65.04**	61.69	9.38	55.80	80.00	24.20	20.07
Pyx	3	**53.53**	61.20	17.42	33.60	65.80	32.20	32.20
Parapyx	10	**61.30**	63.02	4.62	50.63	66.60	15.97	5.40
Serp	2	**58.15**	58.15	0.64	57.70	58.60	0.90	0.90
Calc-sil	5	**64.51**	65.97	2.25	61.95	66.40	4.45	3.91
Comp	3	**62.40**	62.90	1.80	60.40	63.90	3.50	3.50
Total	34	**60.82**	62.16	6.02	53.35	66.88	13.54	11.00

Summary statistics for **b**

Rock Type	Count	Avg.	Median	Standard dev.	Min	Max	Range	Interquartile range
Fpyx	11	**0.56**	0.61	0.17	0.27	0.83	0.56	0.25
Pyx	3	**0.77**	0.53	0.43	0.51	1.26	0.75	0.75
Parapyx	10	**0.51**	0.46	0.16	0.37	0.93	0.56	0.05
Serp	2	**0.51**	0.51	0.01	0.50	0.52	0.02	0.02
Calc-sil	5	**0.55**	0.55	0.09	0.43	0.69	0.26	0.04
Comp	3	**0.53**	0.53	0.03	0.50	0.56	0.06	0.06
Total	34	**0.57**	0.53	0.15	0.43	0.80	0.37	0.20